IN THE UNITED STATES PATENT AND TRADEMARK OFFICE

Appl. No.	: 09/857,000	Confirmation No. 7846
Applicants	: Philippe Clair et al.	
Filed	: September 7, 2001	
TC/A.U.	: 1656	
Examiner	: Kam, Chih Min	
Docket No.	: 03-520	
Customer No.	: 34704	

DECLARATION UNDER 37 C.F.R. §1.132

Mailstop RCE
Commissioner for Patents
P.O. Box 1450
Alexandria, VA 22313

Dear Sir:

I, Cecile Bonnafous, declare as follows:

1. I am presently an R&D Manager at Innate Pharma in Marseille, France. A copy of my Curriculum Vitae is attached and labeled Exhibit A.

2. I have read the claims of the present application as submitted in the response dated November 30, 2006. A copy of the pending claims is attached as Exhibit B.

3. I have also read the pending claims of the response submitted herewith. In the pending claims, claim 9 is cancelled without prejudice, claims 10 and 11 are amended and new claims 12-13 have been added.

4. Presently, the examiner asserts claims 10-11 allegedly lack essential steps in the claim process. Specifically, the examiner asserts these missing steps concern the following: the effective amount of the conjugate being administered, the outcome of the treatment, the diagnosis of the Central Nervous System disease using the conjugate and the end point of the treatment.

5. The examiner also asserts the specification of the above-referenced application allegedly does not

CB

support administering the conjugate to a patient because the specification does not disclose working examples demonstrating the claimed subject matter recited in pending amended claims 10-11.

6. It is my opinion one of ordinary skill in the art can practice the claimed subject matter of amended claims 10-11 without undue experimentation based upon the present specification and claims of the aforementioned application.

7. First, one of ordinary skill in the art recognizes rodent models are now widely used in place of human models. For ethical and experimental reasons, non-human models have to be used to study the molecular basis, the genetic regulatory networks, protein interactions, and physiological alterations during health and disease conditions. Currently, rodent models of the central nervous system (CNS) are regarded as the animal model most closely resembling human models of the CNS.

8. It is my opinion that the alleged absence of working examples dealing with human test subjects does not prevent one of ordinary skill in the art from being able to perform either the treatment step of pending amended claim 10 or the administration step of pending amended claim 11. In fact, there are numerous animal models demonstrating a proven track record of predictability for efficacy in humans. For instance, Bendele indicated, as an example, that the models of arthritis such as rat adjuvant arthritis (Benslay, D.N. et al., *Development of a Rapid Screen for Detecting and Differentiating Immunomodulatory vs. Anti-Inflammatory Compounds in Rats*, Agents and Actions, vol. 34:254-6 (1991) (attached and labeled as Exhibit D)) and rat type II collagen arthritis (Trentham, D. E. et al., *Autoimmunity to Type II Collagen: An Experimental Model of Arthritis*, J Exp Med 146:857-68 (1977) (attached and labeled as Exhibit E)) are known to have the capacity to predict efficacy of agents in humans. Agents currently in the market that are active in these animal models are corticosteroids, methotrexate, NSAIDs and TNF antibodies (See Bendele, J., *Animal Models of Rheumatoid Arthritis*, Musculoskel Neuron Interact. 1(4):377-85 (2001) (attached and labeled as Exhibit C).

9. It is also my opinion that one of ordinary skill in the art knows also that there are pain tests developed in animals that are also used in humans. For example, scientists use the electrical hyperalgesia to assess pain in animals (Ayhan et al., *A New Method for the Rapid Measurement of Analgesic Activity in Rabbits*, Arch Int Pharmacodyn Ther., Apr. 262(2):215-20 (1983) (attached and labeled as Exhibit F)). Interestingly, the same test is carried out in human patients (Peterson-Felix et al., *Psychophysical and Electrophysiological Responses to Experimental Pain May Be Influenced By Sedation: Comparison of the Effects of a Hypnotic (Propofol) and an Analgesic (Alfentanil)*, British Journal of Anaesthesia 77:165-71 (1996) (attached and labeled as Exhibit G)). In the case of cancer, various orthotopic in vivo models were developed that share many characteristics with human cancers. As an example, Howard et al. established a model of lung cancer that replicates the pattern of human lung cancer (Howard et al., *Irradiated Nude Rat Model for Orthotopic Human Lung Cancers*, Cancer Research 51:3274-80 (June 15, 1991) (attached and labeled as Exhibit H)). Similarly, Mohammed et al. used an orthotopic model of human pancreatic cancer in mice to demonstrate the efficacy of chemotherapy (Mohammed et al., *An Orthotopic Model of Human Pancreatic Cancer in Severe Combined Immunodeficient Mice: Potential for Application for Preclinical Studies*, Clinical Cancer Research vol. 4:887-94 (1998) (attached and labeled as Exhibit I)). Similarly, there are numerous studies showing clearly and unambiguously that rodents are currently considered as the preferred animal model for the study of meningitis in humans. For instance, it has long been recognized that adult rodents were used as the model for disease due to the wild strain Ia of Group B streptococcal bacteria (Wennerstom, D.E. et al., *Adult Mice as a Model for Early Onset Group B Streptococcal Disease*, Infection and Immunity 32:41-57 (1978) (attached and labeled as Exhibit J)), but also infant rats are just as suitable in histopathological studies of meningitis (Ferrieri, P. et al., *Production of Bacteremia and Meningitis in Infant Rats with Group B Streptococcal Serotypes*, Infection and Immunity 27(3):1023-32 (1980) (attached and labeled as Exhibit K)).

CB

10. It is further my opinion that when one of ordinary skill in the art is seeking a suitable model for studying meningitis in humans, one of ordinary skill would undoubtedly consider the use of neonatal rodents (5-days old) for studying infections by meningococci as their use is reported as follows: "this neonatal mouse model mimics meningococcal disease as seen in humans and may be useful in studying the initial events in the pathogenesis of meningococcal disease" (Salit, I.E. et al., *Experimental Meningococcal Infection in Mice: A Model for Mucosal Invasion*, Infection and Immunity 51(2):648-52 (1986) (attached and labeled as Exhibit L)). In addition, Madoff et al. reported that adult rodents were used as the animal model for studying Group B streptococci (GBS), and in particular, adult rodents were passively immunized with antiserum to the alpha-C protein (surface-expressed antigenic determinant) and then challenged with an alpha C protein expressing strain of GBS (Madoff et al., *Group B Streptococci Escape Host Immunity by Deletion of Tandem Repeat Elements of the Alpha C Protein*, Proc. Natl. Acad. Sci. U.S.A. 93:4131-36 (April 1996) (attached and labeled as Exhibit M). Moreover, one of ordinary skill in the art would also rely upon the teachings of Goldman et al. which report the use of rodent models of C.neoformans meningitis in the biodistribution and pharmacokinetic studies and indicated as follows, "this study demonstrates the usefulness of the rat as an experimental system for studying issues related to cryptococcosis" (Goldman, D.L. et al., *Pharmacokinetics and Biodistribution of a Monoclonal Antibody of Cryptococcus neoformans Capsular Polysaccharide Antigen in a Rat Model of Cryptococcal Meningitis: Implications for Passive Immunotherapy*, Journal of Medical & Veterinary Mycology 35:271-8 (1997) (attached and labeled as Exhibit N)).

11. Consistent with the experiments conducted in the aforementioned articles, the present application discloses working examples performed on non-human models, that is, rodent models. This practice is consistent with experimental procedures commonly used throughout medicinal research. One of ordinary skill in the art recognizes the probative value that rodent

CB

models provide with respect to applying the experimental procedures to human models.

12. Secondly, one of ordinary skill in the art recognizes the success in experimenting with and administering vectorized peptides to rodent models. I refer to a study conducted by the inventors of the present application. A copy is attached and labeled Exhibit O. The study demonstrates the vectorisation of therapeutic molecules, their delivery to rodent models, and the results demonstrating significant enhancement of activity. In conducting the experiments described therein, the study refers to the following article: Temsamani, Jamal et al., *Improved Brain Uptake and Pharmacological Activity Profile of Morphine-6-Glucuorinide Using a Peptide-Vector-Mediated Strategy*, J. Pharmacol. Exp. Ther., 313:712-719 (2005) (attached and labeled as Exhibit P).

13. The study labeled Exhibit O demonstrates the improved brain uptake and pharmacological activity of compounds similar to morphine-6-glucuronide using the following peptides: SynB1, SynB3 and SynB8, as applied to driving such similar compounds across the BBB in rodent models of the CNS. The study reports the ability to drive compounds not known to cross the BBB, e.g., Dalargin, by using a peptide-vector-mediated strategy as recited in the pending claims to be amended of the present application. As discussed herein, one of ordinary skill in the art recognizes the use of rodent models of the CNS is a widely accepted, routine practice in this art due to their close resemblance to human models of the CNS.

14. Thirdly, one of ordinary skill in the art recognizes the success that has been observed in administering vectorized small molecules to human cells in the state-of-the-prior art at the time the present application was filed. I refer to pages 1 through 3 of the present application. The disclosure provides a brief recitation directed to three main strategies for transporting molecules through the hemato-encephalic barrier, that is, a neurological strategy, a pharmacological strategy for small molecules, and a physiological strategy.

15. It is my opinion that the alleged absence of working examples dealing with human test subjects does not prevent one of ordinary skill in the art from being able to perform the administration step recited in pending amended claim 10 as the aforementioned state-of-the-prior art indicate one of ordinary skill in the art understands how to administer a conjugate of an active substance coupled to vectorized peptides, and administer said conjugate to a patient. One of ordinary skill in the art can readily understand how to couple and succeed in coupling an aforementioned active substance directly or indirectly by a covalent bond to one of the aforementioned peptides, that is, SynB1 or SynB3, and to then administer the conjugate as recited in pending amended claim 10. The state-of-the-prior art and relative skill of those of the art and aptly demonstrated in the aforementioned articles labeled as Exhibits C-N submitted herewith. The description of the specification-as-filed provides a sufficient amount of knowledge to one of ordinary skill in the art to administer the aforementioned conjugate recited in pending amended claim 10.

16. It is my opinion that one of ordinary skill in the art can carry out the administration and treatment steps recited in pending amended claim 10 given the working examples provided in the specification-as-filed taken in conjunction with the state-of-the-prior art and skill level of one of ordinary skill in the art. The description of the specification-as-filed provides sufficient direction, guidance and quantity of experimentation necessary to provide one of ordinary skill in the art the ability to administer the conjugate in the treatment of a CNS disease as recited in pending amended claim 10. I again refer to the state-of-the-prior art discussed herein. One of ordinary skill in the art may need to perform a certain amount of experimentation to administer the aforementioned conjugate in treating a CNS disease according to pending amended claim 10. However, one of ordinary skill in the art will not have to conduct "undue" experimentation in order to administer the conjugate and treat the CNS disease as recited in pending amended claim 10. Given the state-of-the-prior art and knowledge of one of ordinary skill in the art, I also believe one of

ordinary skill in the art can ascertain the effective amount of the conjugate to be administered in carrying out said treatment, determine the end point of the treatment and recognize a successful outcome from administering the conjugate recited in pending amended claim 10.

17. It is my opinion that the alleged absence of working examples involving delivering an active substance across the BBB does not prevent one of ordinary skill in the art from being able to perform the preparation and administration steps recited in pending amended claim 11 as the state-of-the-prior art along with the aforementioned articles labeled Exhibits C-N indicate one of ordinary skill in the art readily understands how to prepare a conjugate using an active substance and a vectorized small molecule. Based upon the state-of-the-prior art and knowledge of one of ordinary skill in the art, it is my opinion that one of ordinary skill in the art can readily understand how to couple and succeed in coupling the aforementioned active substances directly or indirectly by a covalent bond to one of the aforementioned peptides, that is, SynB1 or SynB3, to prepare the conjugate being administered in pending amended claim 11. The description of the specification-as-filed provides a sufficient amount of knowledge to one of ordinary skill in the art to prepare and administer the aforementioned conjugate to drive the substance across the BBB as recited in pending amended claim 11.

18. It is also my opinion that the specification-as-filed taken in conjunction with state-of-the-prior art provides sufficient basis to expect one of ordinary skill in the art will be able to drive an active substance across the BBB to the CNS using the aforementioned conjugate recited in pending amended claim 11 based upon the success of administering vectorized small molecules in human cells. The specification-as-filed provides working examples demonstrating the effectiveness in delivering vectorized peptides across the BBB to the CNS in rodent models, and one of ordinary skill in the art can likewise expect to be able to drive an active substance coupled directly or indirectly to either a SynB1 or SynB3 peptide by a covalent bond across the

CB

BBB to the CNS of a human patient based upon the state-of-the-prior art and knowledge and skill level possessed by one of ordinary skill in the art. These same factors also support my opinion as to the predictable nature in the ability to effectively drive the aforementioned conjugates across the BBB to the CNS. One of ordinary skill in the art may need to perform a certain amount of experimentation to drive a substance across the BBB to the CNS using the aforementioned conjugate preparing according to pending amended claim 11. However, the amount of experimentation necessary will not rise to the level of being "undue" as recognized by one of ordinary skill in the art in order to drive an active substance across the BBB to the CNS as recited in pending amended claim 11.

19. For these reasons, it is my opinion that one of ordinary skill in the art would be able to practice the claimed subject matter of pending amended claims 9-11 without requiring undue experimentation based upon the specification-as-filed, the working examples described therein, the skill level of one of ordinary skill in the art and the state-of-the-prior art.

20. The undersigned declares further that all statements made herein of my own knowledge are true and that all statements made on information and belief are believed to be true; and further that these statements were made with the knowledge that willful false statements and the like so made are punishable by fine or imprisonment, or both, under Section 1001 of Title 18 of the United States Code and that such willful false statements may jeopardize the validity of the application or any patent issuing thereon.

Respectfully submitted,

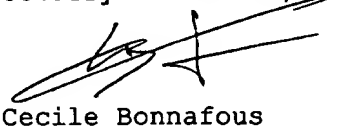

Mrs. Cecile Bonnafous
Dated: 13/08/2007

Exhibit A

Curriculum vitae

Cécile BONNAFOUS
70 rue Callelongue
Bât. 3 Parc Les Colombiers, 13008 Marseille
39 years old,
T: 33 (0) 4 91 22 11 85
E: cecile.bonnafous@innate-pharma.fr

I-UNIVERSITY DIPLOMAS

1992 : Master Degree in Cellular and Digestive Pharmacology , Université Jussieu PARIS VII, France.
1995 Ph.D in Digestive Pharmacology . - Université Jussieu PARIS VII. France
2003 Diplôme d'Expérimentation Animale Niveau I

II PROFESSIONAL EXPERIENCE

2006-present: R&D Manager at **Innate Pharma**, Marseille-France. Responsible of the in vivo Pharmacology. Management of the group responsible of the discovery of drugs targeting the immune system.

2002-2005: Group leader at **Synt:em**. Nîmes, France, Preclinical Research. Managed a group involved in the screening and the development of various drugs for pain and cancer. Set up various models for testing compounds for acute and chronic pain. Managed the timelines, budgets and resources to achieve project objectives. Responsible for the supervision of collaborations with academia and CROs.

1998-2002: Senior Research Scientist at **Rotta Research Laboratorium**, Monza (MI), Italy. Managed a group involved in the discovery of compounds for neuroprotection and for inflammatory bowel diseases (e;g Crohn disease). Managed the timelines, budgets and collaborations.

1995-1997: Post-doct in the Pharmacology Department of **Rotta Research Laboratorium**, Monza (MI), Italy. Set up several in vivo studies of molecules for neuroprotection.

1991-1995: Ph.D in the laboratory of Digestive Pharmacology at **INRA**, Toulouse, France. Role of cholecystokinine and serotonine in digestive side effects associated with benzodiazepines treatment.

III MAIN PUBLICATIONS

Bonnafous c. , martinez j., fargeas m.j., bueno l. Clonazepam-induced intestinal motor disturbances are linked to central nervous system release of cholecystokinin in rats. *Eur. J. Pharmacol: 1993; 237: 237-242.*

Bonnafous c., martinez j., bueno l. Gastrointestinal effects of diazepam- withdrawal are linked to activation of central cholecystokinin-ergic pathways in rats. *J. Pharm. Pharmacol. 1994; 46: 784-788.*

Bonnafous c., bueno l. Different location of benzodiazepine sites involved in gut and behavior effects of benzodiazepine-withdrawal in rats. *Pharmacol. Biochem. Behav. 1994; 49: 253-256.*

Bonnafous c., scatton b., bueno l. Benzodiazepine induced intestinal motor disturbances in rats: mediation by ω_2 (bz_2) sites on capsaicin-sensitive afferent neurones. *Br. J. Pharmacol: 1994; 113: 268-274.*

Louvel d., delvaux m., larrue v., moreau j., bonnafous c., bueno l., frexinos j. Digestive signs during benzodiazepine withdrawal syndrome. *Gastroenterology clin. Biol. 1994; 18: 1038-1039.*

Bonnafous c., lefevre p., bueno l. Benzodiazepine-withdrawal induced gastric emptying disturbances in rats: evidence for 5-ht receptor involvement. *J. Pharm. Exp. Ther. 1995; 273: 995-1000.*

Lanza m., bonnafous c., colombo s., revel l., makovec f. Characterisation of a novel putative cognition enhancer mediating facilitation of glycine effect on strychnine-resistant site coupled to nmda-receptor complex. *Neuropharmacology.1997; 36:1057-1064.*

Colombo s., bonnafous c., revel l., makovec f. Characterization of a novel putative cognition enhancer mediating facilitation of glycine effect on strychnine-resistant sites coupled to nmda receptor complex. Neuropharmacology. 1997 aug; 36(8):1057-64.

Blanc e, bonnafous c, merida p, cisternino s, clair p, scherrman jm, temsamani j. Peptide-vector strategy bypasses p-glycoprotein efflux, and enhances brain transport and solubility of paclitaxel. Anticancer *drugs. 2004 nov;15(10):947-54.*

Temsamani j, bonnafous c, rousselle c, fraisse y, clair p, granier la, rees ar, kaczorek m, scherrmann jm. Improved brain uptake and pharmacological activity profile of morphine-6-glucuronide using a peptide-vector-mediated strategy. *J pharmacol exp ther.* 2005 May;313(2):712-9.

1. (previously presented) The use of a linear peptide coupled to an active substance for diagnosis or therapy of a disorder affecting the CNS for the preparation of a medicine capable of passing through the hemato-encephalic barrier to be used for diagnosis or therapy of a disorder localized in the CNS, the said peptide satisfying one of the following formula (II):

BXXBXXXXBBBXXXXXXB (II),

wherein:

– groups B may be identical or different, and represent an amino acid residue for which the side chain carries a basic group, and

- groups X may be identical or different, and represent a residue of aliphatic or aromatic amino acid, or

the said peptides of formula (II) in retro form, composed of amino acids with a D and/or L configuration, or a moiety of these acids composed of a sequence of at least 5 and preferably at least 7 successive amino acids of peptides of formula (II).

2. (withdrawn) Use according to claim 1, characterized in that in peptides with formula type (I), the hydrophobic amino acids are alanine, valine, leucine, isoleucine, proline, phenylalanine, tryptophan, tyrosine and methionine, and the other amino acids are:

– non–hydrophobic, possibly non–polar amino acids such as glycine, or polar such as serine, threonine, cysteine, asparagine, glutamine, or

– acid (aspartic or glutamic acid), or

– basic (lysine, arginine or histidine), or

– an association of amino acids in these three categories.

3. (withdrawn) Use according to one of claims 1 or 2, characterized in that the formula (I) type peptide includes 6 hydrophobic amino acids and 10 non-hydrophobic amino acids.

4. (previously presented) Use according to claim 1, characterized in that in the peptides in formula type (II):

– B is chosen among arginine, lysine, diaminoacetic acid, diaminobutyric acid, diaminopropionic acid, ornithine and

– X is chosen among glycine, alanine, valine, norleucine, isoleucine, leucine, cysteine, cysteine^{Acm}, penicillamine, methionine, serine, threonine, asparagine, glutamine, phenylalanine, histidine, tryptophan, tyrosine, proline, Abu, carboxylic amino-1–cyclohexane acid, Aib, carboxylic 2–aminotetraline, 4–bromophenylalanine, tert–Leucine, 4 –chlorophenylalanine, beta–cyclohexylalanine, 3, 4–dichlorophenylalanine, 4–fluorophenylalanine, homoleucine, beta–homoleucine, homophenylalanine, 4–methylphenylalanine, 1–naphthylalanine, 2–naphthylalanine, 4–nitrophenylalanine, 3-nitrotyrosine, norvaline, phenylglycine, 3–pyridylalanine and [2-thienyl]alanine.

5. (withdrawn) The use of compounds according to the formula (IV) below:

$A\ (-)_m\ (B)_n$ (IV)

where

– A is a peptide as described above in one of claims 1 to 4,

– B is a substance active in diagnosis or therapy for a disorder of the CNS,

– n is 1 or more, and preferably up to 10, and advantageously up to 5,

– $(-)_m$ represents the linker between A and B, where m is 1 or more, and preferably up to 10 and advantageously up to 5,

for the preparation of a medicine capable of passing through the hemato–encephalic barrier to be used in diagnosis or therapy for a disorder localized in the CNS.

6. (withdrawn) Use according to claim 5, characterized in that in
formula (IV), the $(-)_m$ linker between A and B is a covalent, hydrophobic or ionic linker, cleavable or non–cleavable in physiological media or inside the cells, or a mixture thereof.

7. (withdrawn) Use according to claim 5, for the preparation of a medicine intended for the treatment or prevention of brain cancers, Alzheimer's disease, Parkinson's disease, depression, pain, meningitis.

8. (withdrawn) Use according to claim 6, for the preparation of a medicine intended for the treatment or prevention of brain cancers, Alzheimer disease, Parkinson's disease, depression, pain, meningitis.

9. (original) A method for diagnosis of a Central Nervous System (CNS) disease, comprising administering to a patient a conjugate comprising an active substance for diagnosis of a disease of the CNS coupled directly or indirectly by a covalent bond to one of the following peptides: SynB1 or SynB3.

10. (original) A method for treatment of a Central Nervous System (CNS) disease, comprising administering to a patient a conjugate comprising an active substance for treatment of a disease of the CNS coupled directly or indirectly by a covalent bond to one of the following peptides: SynB1 or SynB3.

11. (original) A method for driving a substance across the Blood Brain Barrier (BBB) to the Central Nervous System (CNS), comprising:

preparing a conjugate comprising an active substance coupled directly or indirectly by a covalent bond to one of the following peptides: SynB1 or SynB3; and

administering said conjugate to a patient.

Exhibit C

J Musculoskel Neuron Interact 2001; 1(4):377-385

Perspective Article

Animal models of rheumatoid arthritis

A.M. Bendele

BolderPATH, Inc., University of Colorado, MCD Biology, Colorado, USA

Abstract

Animal models of arthritis are used to study pathogenesis of disease and to evaluate potential anti-arthritic drugs for clinical use. Therefore morphological similarities to human disease and capacity of the model to predict efficacy in humans are important criteria in model selection. Animal models of rheumatoid arthritis (RA) with a proven track record of predictability for efficacy in humans include: rat adjuvant arthritis, rat type II collagen arthritis, mouse type II collagen arthritis and antigen-induced arthritis in several species. Agents currently in clinical use (or trials) that are active in these models include: corticosteroids, methotrexate, nonsteroidal anti-inflammatory drugs, cyclosporin A, leflunomide interleukin-1 receptor antagonist (IL-1ra) and soluble TNF receptors. For some of these agents, the models also predict that toxicities seen at higher doses for prolonged dosing periods would preclude dosing in humans at levels that might provide disease modifying effects. Data, conduct and features of the various models of these commonly utilized models of RA as well as some transgenic mouse models and less commonly utilized rodent models will be discussed with emphasis on their similarities to human disease.

Keywords: Rheumatoid Arthritis, Adjuvant Arthritis, Type II Collagen Arthritis, Antigen Arthritis, Methotrexate, Dexamethasone, Indomethacin, IL-1ra, TNF-RI

Introduction

Animal models of rheumatoid arthritis are used extensively in research on pathogenesis of inflammatory arthritis and in the pharmaceutical industry in the testing of potential anti-arthritic agents. Important criteria in selection of a model include 1) capacity to predict efficacy of agents in humans, 2) ease of performing the model, reproducibility of data, reasonable duration of test period and 3) similar pathology and/or pathogenesis to that of human disease. In the area of rheumatoid arthritis, there are excellent models that have good track records for predictability. This is in large part due to the fact that numerous agents have been evaluated in clinical trials of this disease and criteria for assessment of efficacy are measurable. Most of the agents (non biologies) currently in use in the treatment of RA have side effects and toxicities that prevent either their long-term use or prevent dosing at levels that might provide superior disease modifying effects. The animal models often predict this phenomenon in that excellent efficacy can be achieved at high doses but prolonged dosing at those levels results in serious toxicity in the animals. Generally, the effective dose 40-50 dose levels are safe for prolonged dosing periods in animals but these doses result in mostly moderate anti-inflammatory effects and modest, if any, beneficial effects on cartilage and bone lesions. In comparison to the osteo-arthritis models, RA models are relatively easy to perform, have good reproducibility of data and are generally of short duration. Most of the RA models have some pathological features that are similar to those occurring in human disease. Important differences include 1) animal models of RA progress much more rapidly than does human disease and thus are characterized by primarily acute inflammatory responses and 2) rodents have a tendency to have marked bone resorption and bone formation (especially periosteal/endosteal) in response to joint inflammation. The use of animal models of RA has contributed greatly to the overall knowledge of processes/mediators important in the generation of inflammation, cartilage destruction and bone resorption, thus leading to important advances in therapeutic intervention in this destructive disease. The focus of this paper will be on the models commonly used for screening/testing of potential pharmaceutical agents with less detailed discussion of the less utilized transgenic animal models. The approach I took when preparing this perspective on RA models was to try to provide the information that is

Corresponding author: Dr. Alison M. Bendele DVM, Ph.D., BolderPATH Inc., University of Colorado, MCD Biology, Campus Box 347, Colorado 80309, USA. E-mail: abendele@sni.net

Accepted 21 January 2001

commonly requested from me when I go to various pharmaceutical companies or academic institutions and am asked questions about research in RA and relevant (to human disease) models. In this paper, I've covered all the models that are commonly used for pharmaceutical testing in RA and placed emphasis on the ones that are considered to be most useful for testing the types of agents that are currently being investigated.

Adjuvant Arthritis

Rat adjuvant arthritis is an experimental model of polyarthritis which has been widely used for preclinical testing of numerous anti-arthritic agents which are either under preclinical or clinical investigation or are currently used as therapeutics in this disease[1-3]. The hallmarks of this model are reliable onset and progression (Figs. 1, 2) of robust, easily measureable, polyarticular inflammation, marked bone resorption and periosteal bone proliferation. Cartilage destruction occurs but is disproportionally mild in comparison to the inflammation and bone destruction that occurs. The pathogenesis/reasons for development of adjuvant disease following injection of arthrogenic preparations are not fully understood despite the fact that numerous studies have contributed to the understanding of various possibilities including reactivity to cartilage proteoglycans, heat shock proteins and interactions with intestinal flora[4-6]. Male Lewis rats (165-200 grams, 7/group) are generally used in studies of adjuvant arthritis. The disease develops in females but is much more variable in onset and severity. Animals should be allowed to acclimate for at least 3 days prior to initiation of experimentation. Induction of adjuvant disease can be done with either Freunds complete (FCA) supplemented with mycobacterium or by injection of the synthetic adjuvant N, N-dioctylddecyl-N', N-bis(2-hydroxy-ethyl) propanediamine (LA)[7]. Adjuvant can be injected at the base of the tail or in one of the foot pads. If injection is into the footpad, it allows study of the acute inflammatory reaction in that local area as well as the immunological reaction that develops approximately 9 days later in the contralateral paw and various organs. Hind paw swelling is monitored from day 9 (onset of disease) to 15 or greater depending on duration desired. In the later stages of disease (day 12+), adjuvant arthritis rats are often relatively immobile due to severity of paw swelling and so require special care to insure that they have access to water and food. To assess disease progression, caliper measurements of ankle joint width or volume using a water displacement device are done prior to the onset of arthritis, and then every other day until the study is terminated on day 15 post injection of the adjuvant. Clinical evidence of arthritis occurs on day 9-10 post injection of adjuvant. Treatments are initiated on day 0 (prophylactic model dosing) or day 8 (therapeutic model). Various stress-related factors including manipulations during the test period (pharmacokinetic sampling), frequency of dosing (QD vs BID) or type of vehicle used can influence the disease progression. However, once a certain methodology is established, controls over various studies will usually progress quite similarly (Fig. 3).

At termination, the tibiotarsal joint is transected at the level of the medial and lateral malleolus for determination of paw weights as another measure of inflammation or its inhibition. Paws are then collected into formalin for histopathological evaluation for beneficial effects on arthritis parameters and also for evaluation of potential deleterious effects of treatment on bone marrow. Obviously a clinically effective inhibitor that results in bone marrow hypocellularity as a mechanism of action would not be a desirable therapeutic agent in RA patients.

Ankle joints (with digits removed) are collected into 10% neutral buffered formalin for at least 24 hours prior to placement in Surgipath decalcifier I (Grayslake, IL.) for

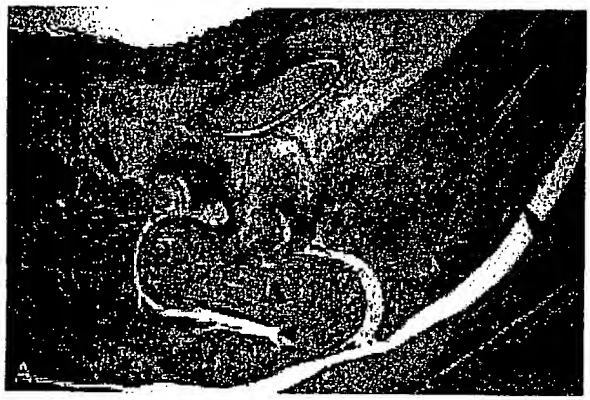

Figure 1a. Photomicrograph of ankle joint from adjuvant arthritic rat 15 days post-adjuvant injection at the base of the tail. Severe periarticular inflammation with marked edema is present with areas of bone resorption (thin arrows) as well as periosteal proliferation (thick arrows) (Hematoxylin and eosin, original magnification= 16X).

Figure 1b. Higher magnification of tibiotarsal area showing bone/growth plate resorption in association with numerous osteoclasts in an area where subchondral bone has largely been resorbed but cartilage (arrow) is largely unaffected. Hematopoietic/adipose marrow has been replaced by marrow composed of mesenchymal cells with embedded inflammatory cells (Hematoxylin and eosin, original magnification= 100X).

approximately 1 week. When decalcification is complete, the ankle joint is transected in the longitudinal plane to give approximately equal halves. Joints are processed for paraffin embedding, sectioned and stained with hematoxylin and eosin for general evaluation and stained with toluidine blue for specific evaluation of cartilage changes if desired. Multiple sections are prepared (if necessary) to ensure that the distal tibia is present with both cortices and abundant distal tibial medullary space available for evaluation. Adjuvant arthritic ankles are given scores of 0-5 for inflammation and bone resorption as previously described[8].

Cartilage damage may or may not be scored in the adjuvant model. We have generally found this to be a minor feature and therefore not reliable for evaluation of potential treatment effects.

Use of the adjuvant model offers an opportunity to study pathological changes in a variety of tissues other than the joints and to develop knowledge of profiles of activity of various types of agents. Particularly useful is the splenomegaly that occurs in this model as certain types of agents (prostaglandin inhibitors) have no beneficial effects on this parameter while reducing paw swelling[3]. Splenomegaly occurs as a result of profound induction of extramedullary hematopoiesis in the red pulp in conjunction with pyogranulomatous inflammation in the red pulp and capsule. These changes are usually in association with mild to marked lymphoid atrophy. Ideally, an agent active in adjuvant disease should restore the spleen weights and morphology to normal as is the case with methotrexate treatment[8].

Hepatomegaly also occurs as a result of hypertrophy of hepatocytes and should be beneficially affected by treatment. Also fairly consistently present in these animals is an anterior uveitis which may be histologically evaluated for treatment effects.

Clinically used agents that are active in adjuvant arthritis include corticosteroids, nonsteroidal anti-inflammatory drugs (NSAIDs) such as indomethacin and low dose methotrexate[8]. The newer biologic agents such as the interleukin-1 receptor antagonist (IL-1ra) and soluble TNF receptors also have activity in this model[9-12]. Demonstration of efficacy with IL-1ra is dependent on maintaining sufficient blood levels for prolonged receptor antagonism either by continuous infusion methodologies or by the use of slow release vehicles[9]. Inhibition of IL-1 in the adjuvant model dramatically inhibits the bone resorption that is a prominent feature of this disease but has little effect on the inflammation. Studies such as these with specific inhibitors used under optimal pharmacokinetic conditions have helped delineate the importance of various cytokines in disease progression in adjuvant disease. Combination therapies, a likely clinical scenario, in this model using IL-1ra and methotrexate have shown the potential for additive effects[10]. Combinations may allow the reduction in dose of more toxic agents such as methotrexate while achieving superior efficacy than could be achieved with either agent alone.

The soluble TNF receptors have also been evaluated for efficacy in this model. A pegylated version of the type I receptor (PEG sTNF-RI) is active against both inflammation and bone resorption[11] and shows additive benefit when used in combination with traditional agents like methotrexate[13] and dexamethasone[12] as well as in combination with IL-1ra[14].

Rat Type II Collagen Arthritis

Rat type II collagen arthritis results when rats are immunized against homologous or heterologous type II collagen. The resulting polyarthritis is characterized by marked cartilage destruction associated with immune complex deposition on articular surfaces, bone resorption and periosteal proliferation, and moderate to marked synovitis

Figure 2. Photomicrograph of ankle joint from adjuvant arthritic rat 6 months post-adjuvant injection at the base of the tail. Severe bone destruction/proliferation with remodeling has resulted in an ankle morphology that is severely distorted. However, despite the extensive bone changes, the articular cartilages (arrows) are relatively unaffected (Toluidine blue, original magnifications 6X).

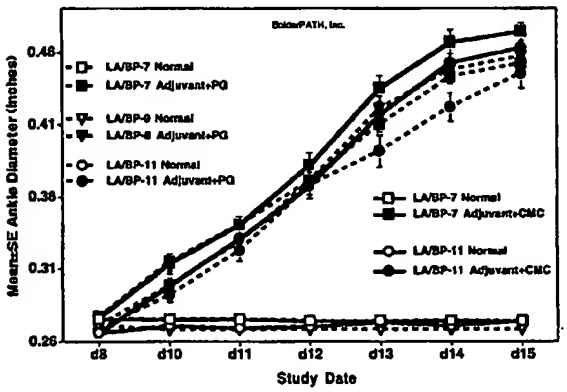

Figure 3. Ankle diameter over time in adjuvant arthritic rats treated with 1% carboxymethylcellulose or propylene glycol from day 0-14. Note consistency of response over various tests using 2 different vehicles. Slight differences warrant the use of an appropriate vehicle control for every test article.

and periarticular inflammation[15,16]. The lesions in type II collagen arthritis are somewhat more analogous to those seen in human RA than are the lesions of adjuvant arthritis (Fig. 4) in that there is more extensive pannus associated cartilage destruction. However, adjuvant arthritis has been used much more extensively for pharmaceutical testing and therefore more data exists for comparison in humans.

Female rats (8/group) are given id/sc injections of bovine type II collagen (2 mg/ml in incomplete Freund's Adjuvant) at the base of the tail and over the back in 3 sites (250µl divided) on day 0 and day 7. Onset of arthritis occurs on days 10-13 and as rats develop the disease they are randomized to study groups and treatment is initiated. Rats are given 6 daily treatments and then killed on day 7 of arthritis for histopathological evaluation[17].

Caliper measurements of ankle joint width are done prior to onset of arthritis, on the day of randomization and on each subsequent study day until termination of the study on arthritis day 7. At termination, the tibiotarsal joint is transected at the level of the medial and lateral malleolus for determination of paw weights as another measure of inflammation. Paws and knees are collected into formalin for histopathological evaluation using a scoring system similar to that described for adjuvant arthritis[8].

Clinically used agents that show activity in established collagen arthritis include corticosteroids, indomethacin and to a lesser extent methotrexate[8]. Because of the short duration of testing in this model (vs adjuvant arthritis) higher, and generally marrow suppressive doses are required to demonstrate efficacy of methotrexate in this model. Biological agents such as IL-1ra and the soluble TNF receptors are active in this test system and combination therapies with IL-1 ra and PEG sTNF-RI show potential for greater than additive effects[14].

Figure 4a. Photomicrograph of ankle joint from type II collagen arthritic rat 7 days post-initial observation of swelling. Moderate periarticular inflammation with edema is present with areas of bone resorption (thin arrows) as well as periosteal proliferation (thick arrows). In contrast to the adjuvant model, cartilage destruction is present in most joints (arrow head) (Toluidine blue, original magnification= 16X).

Other models of rheumatoid arthritis

Mouse Type II Collagen Arthritis

Mice (DBA/1 lacJ) reliably develop polyarthritis when immunized against bovine type II collagen using a variety of methodologies including day 0/day 21 immunizations with and without concurrent boosting with endotoxin or recombinant IL-1. The disease that occurs is usually not symmetrical and any combination of paws/joints may be affected. Since caliper measurement of small mouse ankles is challenging, subjective clinical scoring systems are often used in conjunction with histological scoring methods. Treatments can be prophylactic (generally starting on day 21) or therapeutic (after observation of lesions) and depending on the immunization protocol used and extent of destruction desired, can extend for 10 days to several weeks. Lesions in affected joints resemble those occurring in rat collagen arthritis. This model has been particularly useful in evaluating the effects of biological agents such as IL-1ra and the soluble TNF receptors[18-22]. Enhancement of disease incidence and severity has been demonstrated in mice immunized with type II collagen and concurrently given cytokines such as IL-1[23,24].

Antigen Arthritis

Virtually any animal species can be used in the conduct of antigen arthritis studies. The animal of choice is immunized (subcutaneous or intradermal injections) with the antigen (usually a cationic substance such as methylated bovine serum albumin (m-BSA) which will bind to negatively charged cartilage and be retained in the joint). The antigen is then injected into one or both joints and acute inflammation progressing fairly rapidly to joint destruction ensues. The pathogenesis involves an Arthus reaction on the articular cartilage as antibodies to the positively charged antigen that is

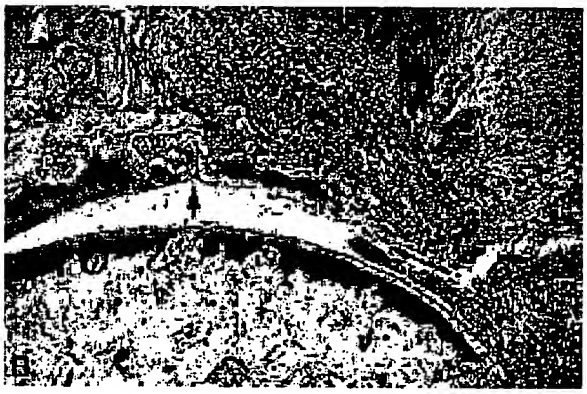

Figure 4b. Higher magnification of tibiotarsal area showing bone resorption in association with numerous osteoclasts in an area where subchondral bone has largely been resorbed and cartilage (arrow) destruction is present in association with inflammatory cell infiltrate (Toluidine blue, original magnification= 100X).

injected form complexes that activate complement locally and result in cartilage destruction. Mouse models of antigen arthritis have been used extensively to study efficacy of biologies and the role of specific cytokines in the various aspects of disease pathogenesis[25-30]. The rabbit model of antigen arthritis is particularly useful when protocols require use of a larger joint[31]. Guinea pigs reliably develop antigen arthritis when immunized twice at 1 week intervals with m-BSA in Freund's complete adjuvant and are then injected intra-articulary with 300 pg of m-BSA, 3 weeks after the first injection. The model can be utilized as a combination prophylactic/therapeutic test using the following method. Three weeks post-initial immunization, inject (day 0) the right knee with m-BSA taking care not to inject the popliteal artery at the posterior aspect of the joint. Guinea pigs routinely develop antibodies which will cause acute death due to anaphylaxis if the antigen is administered systemically. An injection given too deep into the joint space will sometimes connect with this vessel and the result will be instantly apparent. A successful injection into the joint in an optimally immunized guinea pig will result in profound acute swelling within 6 hrs post-injection and this will be sustained at 24 (day 1) and 48 (day 2) hours. This allows identification of optimally sensitized animals and treatment can be initiated on day 1 or 2. On day 3 (animals have now been treated for 2 days), inject the contralateral knee to evaluate the effects of the treatment prophylactically. The lesions of antigen arthritis (Fig. 5a) progress extremely rapidly and in general greater effects of treatments will be observed using the prophylactic scenario. But this scenario is best not used alone unless some sort of preliminary testing is done to identify sensitized animals as up to 10% of a group may not be responders to the immunization. Agents active in human RA (cyclosporin, NSAIDs etc) are active on the prophylactic version of the model. Guinea pigs are insensitive to the action of corticosteroids, so they cannot be used as positive control agents[32]. If the disease is allowed to progress for 2 weeks, histopathological evaluation reveals a highly destructive pannus which has destroyed most of the articular cartilage (Fig. 5).

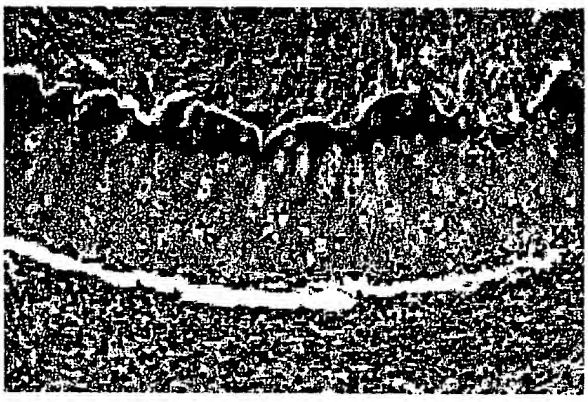

Figure 5a. Photomicrograph of medial knee joint from antigen arthritic guinea pig 7 days post-antigen injection into the knee. Numerous neutrophils are positioned on the surface of partially degraded articular cartilage and resorption of subchondral bone extends to calcified cartilage (Hematoxylin and eosin, original magnification= 100X).

Miscellaneous other rheumatoid arthritis models

Injection of aqueous suspensions of killed group A streptococci or peptidoglycans of their cell walls injected ip into susceptible rats (generally Lewis females are used) results in a biphasic polyarthritis with histological features that are similar to those of adjuvant arthritis[33]. Localized arthritic lesions can also be induced by intra-articular injection of streptococcal cell wall fragments with subsequent (18-25 days later) reactivation of inflammation via systemic administration of cell walls[34]. These models have been used to study the activity of various types of agents such as IL-1ra[35]. In general, the pathology in this model (either method of induction) resembles that of adjuvant arthritis in that there is abundant bone destruction, periosteal new bone formation and depending on the protocol used, varying degrees of cartilage destruction in association with the inflammatory process.

Several mouse strains develop RA-like lesions as a result of genetic manipulations. MRL/lpr mice sporadically develop immune complex polyarthritis, in association with their lymphoproliferative disorder, the incidence and severity of which is enhanced by administration of cytokines such as IL-1[36]. Without the added cytokine enhancement, the disease is too mild and variable in incidence and onset to be useful in pharmaceutical testing or pathogenesis studies.

There are 2 transgenic mouse models that have 100% incidence of inflammatory and destructive lesions resembling those occurring in RA.

Mice in which the TNF-α gene has been eliminated, transfected with a TNF-α gene that lacks the region necessary for cleavage of membrane bound TNF to soluble TNF, over express membrane bound TNF[35]. These animals

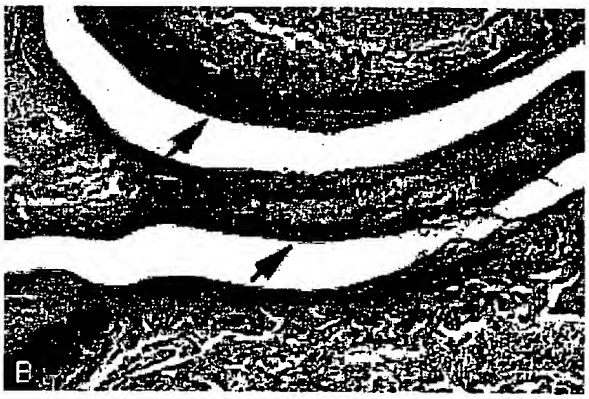

Figure 5b. Photomicrograph of medial knee 21 days post-injection of antigen showing residual attenuated articular cartilage and meniscus with surface fibrovascular pannus (arrows) (Toluidine blue, original magnification=25X).

reliably develop a deforming arthritis in the fore and hind paws beginning at 3 weeks of age. The lesions consist of periarticular inflammation (sometimes in nodular arrangement), bone resorption and retention of calcified cartilage/bone in the metaphysis and medullary cavities (Fig. 6). The soluble TNF receptors (both I and II) are active in inhibiting the disease process and some modulation is seen in animals treated with corticosteroids[37-39].

Other transgenic rodent models such as HLA-B27 transgenic rats[40], and B2-microglobulin-deficient mice lacking expression of HLA-B27[41] or having HLA-B27[42,43] develop spondylarthropathies of varying incidence and severity. These types of models have been used to study the importance of the major histocompatibility complex (MHC) class I proteins in the pathogenesis of inflammatory arthritis.

Mice transgenic for the V_B6 T cell receptor (TCR) (called KRN) crossed with NOD mice reliably develop rheumatoid arthritis-like lesions at about 27 days of age[44] as a result of the chance recognition of a NOD-derived major histocompatibility complex class II molecule by the transgenic TCR. The arthritis is chronic aggressive, bilaterally symmetrical, erosive polyarthritis with joint destruction and clinical deformation. Effects of angiogenesis inhibition on synovial neovascularization demonstrated disease-modifying activities when treatment was started early in the disease progression[45].

Discussion

Ultimate selection of an animal model for studies on pathogenesis or effects of inhibitors of RA requires consideration of the purpose of the study. If the need is for rapid generation of preclinical efficacy/toxicity data to facilitate entry into clinical trials, selection of one of the induced (adjuvant, type II collagen) models is probably most appropriate. Generation of efficacy data in one of these models is procedurally straightforward and therefore should be reproducible. Test animals are readily available should the need for large-scale testing emerge. In addition, these models (adjuvant and collagen arthritis) have excellent track records for predicting activity and toxicity (at high doses of various agents) in humans. So comparative studies between older vs newer anti-arthritics can be done. Also, since these models are highly reproducible, examination of structure activity relationships between various molecules should be easily achievable.

Activity of commonly used small molecule anti-arthritic agents such as dexamethasone, indomethacin (and other NSAIDs including cyclo-oxygenase 2 inhibitors) and methotrexate (adjuvant only) are predicted by the developing rat adjuvant and established rat type II collagen arthritis models.

Dexamethasone and other corticosteroids are used in the clinical treatment of RA but only at low doses[46] because of the toxicities associated with chronic use. Both animal models predict that corticosteroids have the potential to beneficially affect all aspects of RA and that they have the potential to be disease modifying but that toxicities associated with chronic dosing preclude their use at these efficacious doses. So the models predict that only modest clinical responses could be expected with a non-toxic dosing regime.

Indomethacin (and other NSAIDs) are active in both models. Efficacy peaks at 70% inhibition of AUC for paw swelling when daily oral doses of 1-2 mg/kg are given[8]. Inhibition of bone resorption in the adjuvant model also peaks at about 70% at these same doses. Other studies in which rats were dosed for longer periods of time with doses of 4 mg/kg/day have demonstrated the classic NSAID-induced lesions of intestinal and renal papillary necrosis (unpublished data, A. Bendele) thus demonstrating the narrow therapeutic index of this drug. More important however, is the suggestion from the animal bone resorption data that there is no dose that is likely to be profoundly disease modifying. Newer NSAIDs that are selective for cyclooxygenase 2 inhibition will

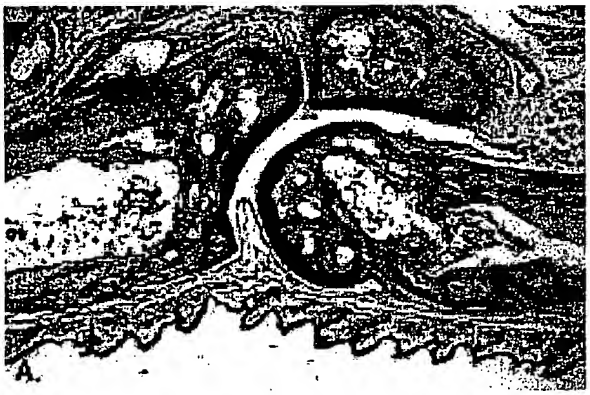

Figure 6a. Photomicrograph of metacarpophalangeal joint from normal mouse (Toluidine blue, original magnification=100X).

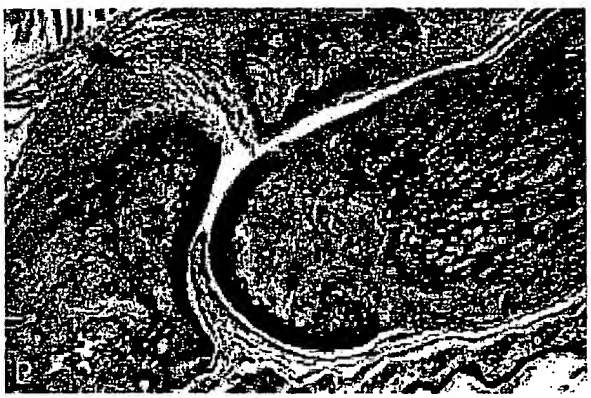

Figure 6b. Photomicrograph of metacarpophalangeal joint from TgA86 mouse over expressing membrane bound TNF. Synovium is thickened as a result of infiltration by inflammatory cells (arrow). Resorption of cortical bone (*) is evident in association with marked retention and filling of the medullary cavity with calcified cartilage and bone (Toluidine blue, original magnification= 25X).

likely eliminate the toxicities of the old cyclooxygenase 1 and 2 inhibitors but it is uncertain what their capacity for disease modification will be. In contrast to results in the adjuvant model, indomethacin showed excellent capacity to inhibit all aspects of rat type II collagen arthritis. Doses of 1-3 mg/kg/day resulted in 50-90% inhibition of clinical as well as histological parameters. So, this model predicts that indomethacin has the capacity to be a disease modifying agent but that prolonged dosing at these levels would result in unacceptable toxicity in the clinical setting. Generally, currently used NSAIDs are regarded as good anti-inflammatory therapy with little potential for disease modification at the doses that are generally safe for prolonged use in humans[47]. Both animal models predicted this and it will be interesting to see if the cyclooxygenase 2 inhibitors have disease modifying activity similar to that seen in rat type II collagen arthritis.

Methotrexate (low dose) has been one of the most successfully used anti-rheumatic agents[48,49]. It is most active in the developing adjuvant model where the opportunity exists to dose it for a longer period (15 days). The ED50 doses are generally 0.06 - 0.075 mg/kg/day. Other studies in which rats were dosed for longer periods of time have demonstrated bone marrow hypocellularity, intestinal lesions and death at doses of 0.1 mg/kg/day (unpublished data, A. Bendele). So, at 1-2 times the moderately effective dose, serious life-threatening toxicity occurs. A dose of 0.1 mg/kg/day can be given for 14 days in this model with the result being complete suppression of disease, thus demonstrating that this agent has the potential to provide disease modifying effects. Therefore, both models predict that methotrexate has the potential to be effective on all aspects of disease but that doses resulting in really dramatic efficacy would not be tolerated long-term. Although many patients have had excellent responses to methotrexate therapy, there is still room for improvement, especially in documentation of disease modification.

The biological agents (cytokine inhibitors), IL-1ra and soluble TNF-R2 (Enbrel) that are currently marketed for treatment of RA, are active in both rat and mouse animal models of arthritis with little or no evidence of toxicity. Likewise, current clinical trials with these agents have demonstrated efficacy and very little toxicity[50-52]. Conclusive clinical data on parameters indicative of disease modification will be needed before definitive statements can be made about the predictability of the animal data for disease modification.

Some of the newer transgenic models have interesting potential for use in delineating factors important in the pathogenesis of RA.

References

1. Pearson CM. Development of arthritis, periarthritis and periostitis in rats given adjuvants. Proc Soc Exp Biol Med 1956; 91:95-100.
2. Carlson RP, Datko LJ, O'Neil-Davis L, Blazek EM, Delustro F, Beideman R, Lewis AJ. Comparison of inflammatory changes in established type II collagen and adjuvant induced arthritis using outbred Wistar rats. Int J Immunopharmacol 1985; 7:811-826.
3. Benslay DN, Bendele, AM. Development of a rapid screen for detecting and differentiating immuno-modulatory vs anti-inflammatory compounds in rats. Agents Actions 1991; 34:254-256.
4. Van Vollenhoven RF, Soriano A, McCarthey PE, Schwartz RL, Garbrecht FC, Thorbecke GJ, Siskind GW. The role of immunity to cartilage proteoglycan in adjuvant arthritis. J Immunol 1988; 141(4):1168-1173.
5. Feige U, Schulmeister A, Mollenhauer J, Brune K, Bang H. A constitutive 65kDa chondrocyte protein as a target antigen in adjuvant arthritis in Lewis rats. Autoimmunity 1994; 17:233-239.
6. van de Langerijt AGM, van Lent PLEM, Hermus ARMM, Sweep CGJ, Cools AR, van den Berg WB. Susceptibility to adjuvant arthritis: relative importance of adrenal activity and bacterial flora. Clin Exp Immunol 1994; 97(1):33-38.
7. Chang Y. Adjuvant polyarthritis. Arthritis Rheum 1980; 23:62-71.
8. Bendele AM, McComb J, Gould T, McAbee T, Sennello G, Chlipala E, Guy M. Animal models of arthritis: relevance to human disease. Toxicologic Pathol 1999; 27:134-142.
9. Bendele AM, McAbee T, Sennello G, Frazier J, Chlipala E, McCabe D. Efficacy of sustained blood levels of interleukin-1 receptor antagonist in animal models of arthritis. Arthritis Rheum 1999; 42:498-506.
10. Bendele A, Sennello G, McAbee T, Frazier J, Chlipala E, Rich B. Effects of interleukin-1 receptor antagonist alone and in combination with methotrexate in adjuvant arthritic rats. J Rheumatol 1999; 26:1225-1229.
11. McComb J, Gould T, Chlipala E, Sennello G, Frazier J, Kieft G, Seely J, Edwards C III, Bendele A. Antiarthritic activity of soluble tumor necrosis factor receptor type I forms in adjuvant arthritis: correlation of plasma levels with efficacy. J Rheumatol 1999; 26:1347-1351.
12. Bendele AM, McComb J, Gould T, Chlipala ES, Seely J, Kieft G, Wolf J, Edwards CK III. Combination benefit of PEGylated soluble tumor necrosis factor receptor type I (PEG sTNF-RI) and dexamethasone or indomethacin in adjuvant arthritic rats. Inflammation Res 1999; 48:453-460.
13. Bendele A, McComb J, Gould T, Guy M, Chlipala L, Sennello R, McAbee T, Edwards C. Combination benefit of treatment with soluble TNF-RI and methotrexate in adjuvant arthritis. Clin Exptl Rheumatol 1999; 553-560.
14. Bendele A, Chlipala L, Sennello R, Frazier J, Edwards C. Combination benefit of treatment with soluble TNF-RI and IL-1ra in rat models of arthritis. Arthritis Rheum 2000; 43:2648-2659.
15. Trentham DE, Townes AS, Kang AH. Autoimmunity to

type II collagen: an experimental model of arthritis. J Exp Med 1977; 146:857-868.
16. Terato K, Hashida R, Miyamoto K, Morimoto T, Kata Y, Kobayashi S, Tajima T, Otake S, Horni H, Nagai Y. Histological, immunological and biochemical studies on type II collagen arthritis in rats. Biomed Res 1982; 3:495-523.
17. Bendele A, McAbee T, Woodward M, Scherrer J, Collins D, Frazier J, Chlipala E, McCabe D. Effects of interleukin-1 receptor antagonist in a slow-release hylan vehicle on rat type II collagen arthritis. Pharm Res 1998; 15:1557-1561.
18. Wooley PH, Whalen JD, Chapman DL, Berger AE, Richard KA, Aspar DG, Staite ND. The effect of an interleukin-1 receptor antagonist protein on type II collagen-induced arthritis and antigen-induced arthritis in mice. Arthritis Rheum 1993; 36:1305-1314.
19. Bakker, AC, Joosten LAB, Arntz OJ, Helsen MA, Bendele AM, van de Loo AJ, van den Berg WB. Gene therapy of murine collagen-induced arthritis: local expression of the human interleukin-1 receptor antagonist protein prevents onset. Arthritis Rheum 1997; 40:893-900.
20. Joosten LAB, Helsen MMA, van de Loo FAJ, van den Berg WB. Amelioration of established type II collagen-induced arthritis (CIA) with anti-IL-1. Agents Actions 1994; 41:C174-C176.
21. Joosten LAB, Helsen MMA, van de Loo FAJ, van den Berg WB. Anticytokine treatment of established type II collagen-induced arthritis in DBA/1 mice. Arthritis Rheum 1996; 39:797-809.
22. Geiger T, Towbin H, Cosenti-vargas A, Zingel O, Arnold J, Rordorf C, Glatt M, Vosbeck K. Neutralization of interleukin-1 B activity in vivo with a monoclonal antibody alleviates collagen-induced arthritis in DBA/1 mice and prevents the associated acute phase response. Clin Exp Rheumatol 1993; 11:515-522.
23. Hom J, Gliszcznski VL, Cole HW, Bendele AM. Interleukin-1 mediated acceleration of type II collagen-induced arthritis: Effects of anti-inflammatory or anti-arthritic drugs. Agents Actions 1991; 33:300-309.
24. Hom J, Bendele AM, Carlsson D. In vivo administration with IL-1 accelerates the development of collagen-induced arthritis in mice. J Immunol 1988; 141:834-841.
25. Brackertz D, Mitchell GF and Mackay IR. Antigen-induced arthritis in mice I. Induction of arthritis in various strains of mice. Arthritis Rheum 1977; 20:841-850.
26. Hunneyball IM, Crossley MJ, Spowage M. Pharmacological studies of antigen-induced arthritis in BALB/c mice I. Characterization of the arthritis and the effects of steroidal and non-steroidal anti-inflammatory agents. Agents Actions 1986; 18:384-393.
27. Van de Loo, AAJ, Arntz OJ, Otterness IG, van den Berg WB. Protection against cartilage proteoglycan synthesis inhibition by anti-interleukin-1 antibodies in experimental arthritis. J Rheumatol 1992; 19:348-356.
28. Van de Loo AAJ, Arntz OJ, Bakker AC, van Lent PLEM, Jacobs MJM, van den Berg WB. Role of interleukin-1 in antigen-induced exacerbations of murine arthritis. Amer J Pathol 1995; 146:239-249.
29. Van de Loo FAJ, Joosten LAB, van Lent PLEM. Role of interleukin-1, tumor necrosis factor α and interleukin-6 in cartilage proteoglycan metabolism and destruction. Effect of in situ blocking in murine antigen and zymosan induced arthritis. Arthritis Rheum 1995; 38:164-172.
30. Van Meurs JBJ, van Lent PLEM, Singer II, Bayne EK, van de Loo FAJ, van den Berg WB. Interleukin-1 receptor antagonist prevents expression of the metallo-proteinase-generated neoepitope VDIPEN in antigen-induced arthritis. Arthritis Rheum 1998; 41:647-656.
31. Henderson B, Thompson RC, Hardingham T, Lewthwaite J. Inhibition of interleukin-1-induced synovitis and articular cartilage proteoglycan loss in the rabbit knee by recombinant human interleukin-1 receptor antagonist. Cytokine 1991; 3:246-249.
32. Zuckerman S, Bendele AM. Regulation of serum tumor necrosis factor in glucocorticoid sensitive and resistant rodent endotoxin shock models. Infect Immun 1989; 57:3009-3013.
33. Cromartie Wj, Craddock JH, Schwab JH, Anderele SK, Yang CH. Arthritis in rats after systemic administration of streptococcal cells or cell wall. J Exp Med 1977; 146:1585-1602.
34. Esser RE, Stimpson SA, Cromartie WJ, Schwab JH. Reactivation of streptococcal cell wall-induced arthritis by homologous and heterologous cell wall polymers. Arthritis Rheum 1985; 28:1402-1411.
35. Schwab JH, Anderle SK, Brown RR, Dalldorf FG, Thompson RC. Pro-and anti-inflammatory roles of interleukin-1 in recurrence of bacterial cell wall-induced arthritis in rats. Infect Immun 1991; 59:4436-4442.
36. Horn J, Cole H, Bendele AM. Interleukin-1 enhances the development of spontaneous arthritis in MRL/lpr mice. Clin Immunol Immunopathol 1990; 55:109-119.
37. Probert L, Akassoglou K, Alexopoulou L, Douni E, Haralambous S, Hill S, Kassiotis G, Kontoyiannis D, Pasparakis M, Plows D, Kolias G. Dissection of the pathologies induced by transmembrane and wild-type tumor necrosis factor in transgenic mice. J Leukocyte Biol 1996; 59:518-525.
38. Edwards CK III, Chlipala EC, Dinarello CA, Reznikov L, Moldawer, LL, Bendele AM. Clinical and histopathologic characterization of arthritis in male and female tumor necrosis factor knockout mice and membrane bound TNF-a transgenic mice injected with M. pulmonis or M. arthritidis. Arthritis Rheum 1999; Abstract 296 Suppl S120.
39. Bendele AM, Dinarello C, Chlipala E, Edwards CK III. Effects of PEG sTNF-RI, IL-1ra or the combination in TNF-α knockout mice expressing a mutant transgenic form of Murine transmembrane TNF. Arthritis Rheum

2000; Abstract 983 Suppl S230.
40. Taurog JD, Maika SD, Satumtira N, Dorris ML, McLean IL, Yanagisawa. Inflammatory disease in HLA-B27 transgenic rats. Immunol Rev 1999; 169:209-223.
41. Kingsbury DJ, Mear JP, Witte DP, Taurog JD, Roopenian DC, Colbert RA. Development of spontaneous arthritis in B2-microglobulin-deficient mice without expression of HLA-B27. Arthritis Rheum 2000; 43:2290-2296.
42. Weinrich S, Hoebe-Hewryk B, van der Horst AR, Boog CJP, Ivanyi P. The role of MCH class I heterodimer expression in mouse ankylosing enthesiopathy. Immunogenetics 1997; 46:35-40.
43. Khare SD, Luthra HS, David CS. Spontaneous inflammatory arthritis in HLA-B27 transgenic mice lacking B2-microglobulin: a model of human spondylarthropathies. J Exp Med 1995; 182:1153-1158.
44. Kouskoff V, Korganov AS, Duchatelle V, Degott C, Benoist C, Mathis D. Organ specific disease provoked by systemic autoimmunity. Cell 1996; 87:811-822.
45. deBrandt M, Grossin M, Weber A, Chopin M, Elbim C, Pla M, Gougerot-Pocidalo M, Gaudry M. Suppression of arthritis and protection from bone destruction by treatment with TNP-470/AGM-1470 in a transgenic mouse model of rheumatoid arthritis. Arthritis Rheum 2000; 43:2056-2063.
46. Butler RC, Davie MWJ, Worsfold M, Sharp, CA. Bone mineral content in patients with rheumatoid arthritis: relationship to low-dose steroid therapy. Br J Rheumatol 1991; 30:86-90.
47. Brooks PM, Day RO. Nonsteroidal anti-inflammatory drugs - differences and similarities. New Engl J Med 1991; 324:1716-1272.
48. Drosos AA, Tsifetaki N, Tsiakou EK, Timpanidou M, Tsampoulas C, Tatsis CK, Kotoulas K, Moutsopoulos HM. Influence of methotrexate on radiographic progression in rheumatoid arthritis: A sixty-month prospective study. Clin Exp Rheumatol 1997; 15:263-267.
49. Seitz M, Loetscher P, Dewald B, Towbin H, Rordorf C, Gallati H, Gerber NJ. Interleukin-1 (IL-1) receptor antagonist, soluble tumor necrosis factor receptors, IL-1 B and IL-8 markers of remission in rheumatoid arthritis during treatment with methotrexate. J Rheumatol 1999; 23:1512-1516.
50. Moreland LW, Margolies G, Heck LW, Saway A, Blosch C, Hanna R, Koopman WJ. Recombinant soluble tumor necrosis factor receptor (p80) fusion protein: toxicity and dose finding trial in refractory rheumatoid arthritis. J Rheumatol 1996; 3:1845-1848.
51. Moreland LW, Baumgartner SW, Schiff MH, Tindall EA, Fleischman RM, Weaver AL, Ettinger RE, Cohen S, Koopman WJ, Mohlen K, Widmer MB, Blosch CM. Treatment of rheumatoid arthritis with a recombinant human tumor necrosis factor receptor (p75)-Fc fusion protein. N Engl J Med 1997; 337:141-147.
52. Campion GV, Lebsack ME, Lookabaugh, Gordon J, Catalano M. Dose range and dose frequency study of recombinant interleukin-1 receptor antagonist in patients with rheumatoid arthritis. Arthritis Rheum 1996; 88:1092-1101.

Exhibit D

Agents and Actions, vol. 34, 1/2 (1991)

0065-4299/91/020254-03 $ 1.50+0.20/0

Development of a rapid screen for detecting and differentiating immunomodulatory vs. anti-inflammatory compounds in rats

D.N. Benslay and A.M. Bendele

Eli Lilly and Company, Indianapolis, IN 46285, USA

Abstract

Polyarthritis can be induced in rats using a synthetic adjuvant, N,N-dioctyldecyl-N', N-bis(2-hydroxyethyl) propanediamine (LA) suspended in oil. The disease is morphologically indistinguishable from the classic adjuvant arthritis induced by Freund's complete adjuvant (FCA). LA injection (7.5 mg/animal) consistently induced paw swelling, splenomegaly and fibrinogen level increases at certain time points. Studies evaluating various protocols and parameters determined that a 15 day assay where agents administered from days 9 through 13, would differentiate immunomodulatory and anti-inflammatory compounds. Parameters utilized were body weight, paw volumes, spleen weights, and fibrinogen levels. Immunomodulatory agents reduce paw swelling, splenomegaly and in some cases fibrinogen levels. NSAIDS reduce paw swelling, *increase* splenomegaly and have no effect on fibrinogen levels. These results indicate that compounds active in the traditional FCA assay can be detected and differentiated with respect to anti-inflammatory vs. immunomodulatory activity in a rapid screen.

Introduction

The Freund's Complete Adjuvant-induced polyarthritis model in rats has been used as a tool for the detection of anti-inflammatory agents for about 30 years since the method was first published by Pearson et al. in 1956 [1]. The test as it is generally run is a long procedure with a lot of variability and not well suited for "screening" large numbers of compounds. Polyarthritis can be induced in rats using a synthetic adjuvant, N,N-dioctadecyl-N',N-bis (2-hydroxyethyl) propanediamine (LA) suspended in oil [2]. The disease is morphologically indistinguishable from the classic adjuvant arthritis induced by Freund's complete adjuvant (FCA). However, in our experience, the synthetic adjuvant produces a more consistent disease in rats. We were interested in developing a rapid screening procedure in rats using LA induction of systemic inflammation which would detect and differentiate immunomodulatory and anti-inflammatory activity of compounds.

Materials and methods

LA injection (7.5 mg/animal) consistently induced paw swelling, splenomegaly and fibrinogen increases at certain time points (Fig. 1). Changes in various other parameters including 1. body weight 2. hematology: CBC, differential leukocyte count and fibrinogen. 3. clinical chemistries: albumen, total iron, glucose, blood urea, nitrogen, creatinine, total bilirubin, alkaline phosphatase and alanine transaminase also were evaluated to determine their utility in a screening situation. In LA injected animals, changes seen were, in general, what would be expected in an inflammatory condi-

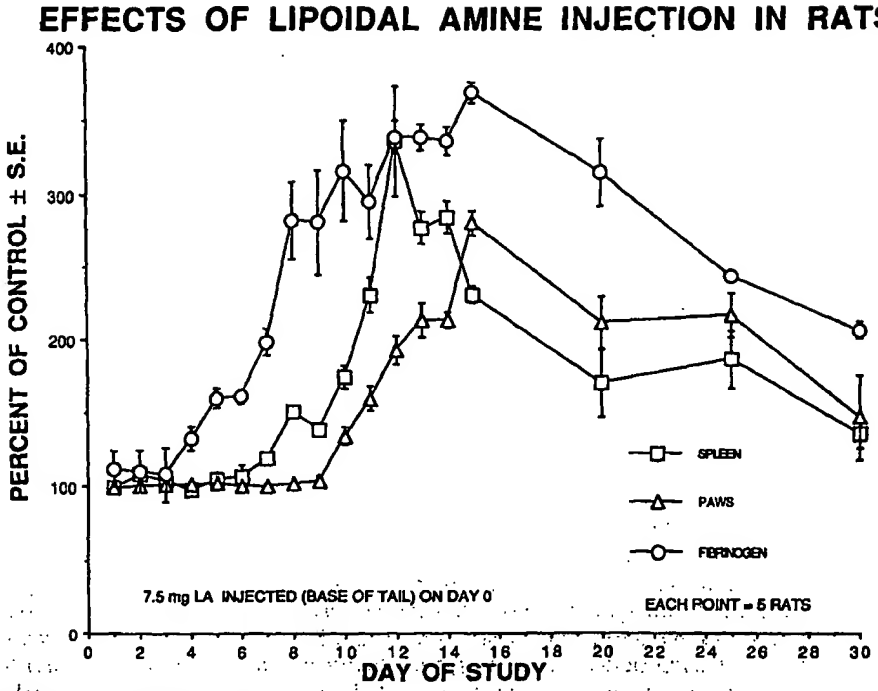

Figure 1
Effects of lipoidal amine injection in rats

tion i.e., decreased body weight, increased paw volume and weight, increased spleen weight, increases in neutrophils and fibrinogen. Changes in clinical chemistry values occurred but were not sufficiently different for inclusion in the evaluation process.

Results of various studies in which dosing of compounds was initiated at different times were evaluated and a protocol using the minimum number of treatment days was chosen. Using this protocol, male Lewis rats (200–225 Gm.) are injected intradermally at the base of the tail on day 0 with LA (7.5 mg). On day 9 the animals are randomly divided into groups of 5 and treatments are started and continued through day 13, a total of 5 daily doses. The animals are not treated on day 14 and taken off test on day 15 at which time they are weighed and the hind paw volumes measured before they are anesthetized and then bled via cardiac puncture. The spleen and both hind feet are removed from the animal and weighed. The weights and volumes are recorded directly into an Excel (data base) computer program that calculates means, standard errors and percent difference from controls. Significance is determined using a two tailed Dunnet t-test on the raw data.

Table 1
Drug profiles in lipoidal amine assay in rats

Agent	Paw swelling	Spleen wt.	Fibrinogen
Cyclosporina A	↓	↓	↓
Methotrexate	↓	↓	↕
Cyclophos.	↓	↓	–
Dexamethasone	↓	↓	–
NSAIDS	↓	↑	–

Results and discussion

Agents representing immuno-suppressants/modulators, corticosteroids and non-steroidal anti-inflammatories were examined in the screen with the following results: (See Table 1) *Cyclosporine A;* at doses of 10–20 mg/kg p.o. normalized body wt. inhibited paw swelling and spleen wt. and de-

creased fibrinogen levels by about 50% from diseased controls. The MED was 5 mg/kg. *Methotrexate:* At doses of 0.5–1 mg/kg p.o. inhibited paw swelling and spleen wt., decreased fibrinogen levels to 50% of diseased control and had no effect on body wt. A dose of 0.25 mg/kg was not effective. *Cyclophosphamide:* At a dose of 7 mg/kg reduced paw swelling, spleen wt. and fibrinogen levels, but had no effect on body wt. A 5 mg/kg dose was ineffective. *Dexamethasone:* At 0.1 mg/kg p.o. inhibited paw swelling and spleen wt. by 100% but had no effect on fibrinogen levels or body wt. *NSAIDS:* (indomethacin, piroxicam, naproxen) Non-toxic but effective doses dramatically reduced paw swelling. Spleen wt. was usually increased above disease controls and there was no effect on fibrinogen levels or body wt.

Lipoidal amine-induced polyarthritis in rats is very similar to the traditional Freund's complete adjuvant-induced polyarthritis that has been used for years to test for anti-inflammatory agents. The LA screen has the advantage of short duration and reduced labor and amount of compound needed to detect activity. By examining the parameter profile the agents can be categorized.

References

[1] C. M. Pearson, *Development of arthritis, periarthritis and periostitis in rats given adjuvant.* Proc. Soc. Exp. Biol. Med. *91*, 95 (1956).

[2] Y. Chang et al., *Adjuvant Polyarthritis.* Arthritis and Rheumatism, *23*, 62–71 (1980).

Exhibit E

AUTOIMMUNITY TO TYPE II COLLAGEN: AN EXPERIMENTAL MODEL OF ARTHRITIS*

By DAVID E. TRENTHAM, ALEXANDER S. TOWNES, and ANDREW H. KANG

(From the Veterans Administration Hospital and Department of Medicine and Biochemistry, University of Tennessee Center for the Health Sciences, Memphis, Tennessee 38104, and the Department of Medicine, Harvard Medical School, Robert B. Brigham Hospital, Boston, Massachusetts 02120)

Immunologic hypersensitivity to collagen, the major structural component of connective tissue, could explain both the systemic nature and chronicity of the inflammation occurring in rheumatoid arthritis. Recent demonstrations of antibodies to collagen in sera from patients with rheumatoid arthritis support this premise (1–8). Also consistent with this hypothesis is the distribution of collagen in structurally distinct types in various tissues. For example, types I and III collagens are found in the skin and parenchyma of several organs, whereas type II exists in cartilage (9). Thus, an immune response to the cartilage type of collagen (type II) could explain the predilection of rheumatoid arthritis to involve diarthrodial joints.

Native collagens consist of three polypeptide chains linked in triple helices. Terminal peptides (telopeptides) do not have a helical structure and are more variable in amino acid content (10). Type I collagen combines two α1-type I chains with one α2-chain and is depicted as $[\alpha 1(I)]_2\alpha 2$. Types II and III collagens are comprised of three α1-type II chains and three α1-type III chains, respectively. Thus, type II is depicted as $[\alpha 1(II)]_3$ and type III as $[\alpha 1(III)]_3$.

Injection of heterologous type I and II collagen in complete Freund's adjuvant has been reported to elicit type-specific antibody responses in rats (11) and mice (12). This paper reports that approximately 40% of rats injected intradermally with native type II collagen, derived from human, chick, or rat cartilage, in either complete or incomplete Freund's adjuvant, develop an inflammatory arthritis. In contrast, type I and III collagen are not arthritogenic. This new animal model suggests that immune responses to type II collagen could play a role in inciting or perpetuating joint inflammation in other arthritides.

Materials and Methods

Rats. Outbred female Wistar, Sprague-Dawley and inbred Wistar-Lewis rats were obtained from Microbiological Associates (Bethesda, Md.), Harlan (Indianapolis, Ind.) or Charles River Breeding Laboratory (Wilmington, Mass.). These rats were housed in metal cages and given water

* Supported by the Medical Research Service of the Veterans Administration and by the U. S. Public Health Service, grants AM 05055, AI 07685, AM 16506, and AM 05076. A preliminary account of part of this work was presented at the National Scientific Meeting of the American Rheumatism Association, 10–11 December 1976, Miami Beach, Fla.

and standard rat chow ad lib. They weighed 150–225 g and were 10–24 wk of age at the time of immunization.

Tissues. The xiphoid cartilage of 3 wk old White Leghorn chicks, rendered lathyritic by administration of β-aminopropionitrile fumarate (BAPN,[1] Sigma Chemical Co., St. Louis, Mo.) (13), was used as the source of chick type II collagen. Similarly, weanling outbred female Wistar rats were given BAPN (0.4%) in water for 3 wk, and their xiphoid and hip cartilage was used after careful dissection to avoid contamination by bone. Human collagens were prepared from neonatal skin and cartilage obtained at autopsy. Skin and cartilage were pulverized in liquid nitrogen with a freezer mill (Spex Industries, Inc., Metuchen, N.J.). All subsequent procedures were performed at 4°C.

Skin Collagens. Type I collagen was extracted from skin powder by overnight suspension with gentle shaking in 5 vol of 0.05 M Tris/1 M NaCl, pH 7.4. After centrifugation (20 min at 20,000 *g*), collagen in the supernate was precipitated by gradual addition of NaCl to a final concentration of 3 M. The precipitate was redissolved in 0.05 M Tris/1 M NaCl and again precipitated in an identical manner. After redissolving in the neutral salt buffer, the collagen was precipitated by the addition of 0.1 vol of 1 M acetic acid. The precipitate was collected and dissolved with 0.5 M acetic acid, reprecipitated with NaCl to a final concentration of 1 M, redissolved with 0.5 M acetic acid, dialyzed exhaustively against 0.1 M acetic acid, and lyophilized.

Additional type I collagen was obtained from the skin pellet after neutral salt extraction by suspending the pellet in 5 vol of 0.5 M acetic acid for 24 h. After an identical subsequent extraction, collagen in both supernates was precipitated by the addition of NaCl to a final concentration of 1 M, redissolved in 0.5 M acetic acid, precipitated again with NaCl, dissolved in acetic acid, dialyzed, and lyophilized. Pepsin-solubilized type I collagen and type III collagen were prepared from the skin residues by methods previously described (14).

Cartilage Collagens. Pepsin-solubilized type II collagen was prepared by washing the cartilage powder with 20 vol of 0.05 M Tris/2 M $MgCl_2$, pH 7.4, at 4°C. The extract was stored at −20°C for subsequent use as a crude proteoglycan complex. The residue was washed twice with distilled water, then suspended in 0.5 M acetic acid, and the pH of the suspension was adjusted to 2.5 by the addition of formic acid. Pepsin (two times crystallized, Worthington Biochemical Corp., Freehold, N.J.) was then added (1/50 g wet weight), and digestion was allowed to proceed for 72 h at 4°C with gentle shaking. The undigested residue was separated by centrifugation (20,000 *g* for 20 min) and extracted two more times with pepsin under identical conditions. The supernates from the three extractions were dialyzed against 0.05 M Tris/0.2 M NaCl, pH 7.6, diluted 10-fold with the buffer and passed through a column of fresh DEAE cellulose (DE 52, Whatman Chemicals, Div. W & R Balston, Maidstone, Kent, England) that had been equilibrated with the same buffer. Collagen was eluted with the buffer and precipitated by the addition of NaCl to make a final concentration of 3 M. The precipitate was dissolved in 0.5 M acetic acid, dialyzed against 0.01 M Na_2HPO_4, and the collagen precipitate was harvested by centrifugation. After resolubilization in acetic acid and precipitation with 1 M NaCl, it was redissolved in acetic acid, dialyzed against 0.1 M acetic acid, and lyophilized.

Soluble type II tropocollagen was obtained from the cartilage of lathyritic chicks or rats. After pulverization, the powder was extracted with a 0.4 ionic strength phosphate buffer, pH 7.6, for 24 h. After an additional extraction, the two supernates were dialyzed against 0.05 M Tris/0.2 M NaCl, pH 7.6, passed through DEAE, and purified in a manner described above for pepsin-extracted collagen.

α-Chains. The constituent α-chains of human or chick type II collagen were prepared by ion exchange chromatography on columns of carboxymethyl-cellulose (CM-cellulose, CM-52, Whatman, Inc., Clifton, N.J.) as previously described (14).

Collagen Analysis. The purity of each collagen preparation was assessed by CM-cellulose chromatography and amino acid analysis by using an automatic analyzer (Beckman Instruments, Inc., Spinco Div., Palo Alto, Calif., model 121) as previously described (14).

Uronic acid assay (15) indicated that proteoglycan contamination of the collagen samples (1 mg/ml 0.1 M acetic acid) was less than the 5 μg/ml minimum detectable by the assay.

Adjuvants. The complete Freund's adjuvant (CFA) used for all collagen immunizations

[1] *Abbreviations used in this paper:* BAPN, β-aminopropionitrile fumarate; CFA, complete Freund's adjuvant; CM-cellulose, carboxymethylcellulose; ICFA, incomplete Freund's adjuvant.

(Difco, code 0638, Difco Laboratories, Detroit, Mich.) contained *Mycobacterium butyricum* at a concentration of 0.5 mg/ml. This preparation failed to induce adjuvant arthritis (16) in 30 Wistar rats when 0.5 ml was emulsified with 0.5 ml 0.1 M acetic acid and injected intradermally on the back.

As a control for the collagen-induced arthritis, adjuvant arthritis was induced by intradermal injection of 0.1 ml complete Freund's adjuvant H37Ra (CFA H37). This preparation contained desiccated, heat-killed *M. tuberculosis* H37 Ra (Difco Laboratories, code 3114) at a concentration of 10 mg/ml in incomplete Freund's adjuvant (ICFA, Difco Laboratories, code 0639).

Sensitization Procedures. Collagen was dissolved in 0.1 M acetic acid at a concentration of 1 mg/ml. Equal volumes of collagen solution and CFA or ICFA were mixed, and a stable emulsion was made with an emulsifier (VirTis 45, VirTis Co., Inc., Gardiner, N.Y.). 1 ml of the cold emulsion was then immediately injected intradermally in four to six sites on the backs of the rats (11). Small ulcers frequently formed at the injection site, but these healed without sequelae in 7–10 days. Control injections consisted of the acetic acid emulsified in CFA or ICFA or human or chick type II collagen dissolved in acetic acid but injected intradermally without adjuvant. As an additional control, 1.0 ml of $MgCl_2$-extractable cartilage proteoglycans containing approximately 100 μg uronate per ml was mixed with 0.5 ml of CFA or ICFA, emulsified, and injected in a manner identical to the collagens. Unless otherwise specified, booster doses consisting of 0.5 mg collagen dissolved in 0.5 ml 0.1 M acetic acid were given intraperitoneally (i.p.) without adjuvant 21 days after primary immunization. 1 ml of the $MgCl_2$ extract was given i.p. after an identical interval to the proteoglycan control animals. Adjuvant arthritis was induced by intradermal injection of 0.1 ml CFA H37 at the base of the tail.

Arthritis Evaluation. Animals were observed daily for the onset of arthritis, and an arthritic index was derived by grading the severity of involvement of each paw from 0 to 4. Scoring was based on the degree of periarticular erythema and edema as well as deformity of the joints, as previously described (16). Swelling of hindpaws was also quantitated by measuring the thickness of the ankle from medial to lateral malleolus with a constant tension caliper (B.C. Ames Co., Waltham, Mass.). Results could be reproducibly expressed to the nearest 0.1 mm.

Histopathology. Animals were sacrificed, and involved paws were amputated on the day of onset of arthritis or at later periods ranging up to 6 mo after onset. After immersion in 10% neutral formalin, the joints were decalcified, imbedded in paraffin, sectioned, and stained with hematoxylin and eosin.

Joint Roentgenography. Sequential joint roentgenograms were made on dental X-ray film (Kodak DF45, Eastman Kodak Co., Rochester, N.Y.)

Bacteriology. Blood was obtained aseptically by cardiac puncture from eight rats within 24 h of the onset of arthritis and inoculated onto sheep blood agar plates. Inflammed synovia obtained from five rats at the onset of arthritis were similarly inoculated onto identical nutrient media and observed for 72 h. Finally, paired sera and synovia from an additional four rats were collected on the day of onset of arthritis and cultured for *Mycoplasma arthritidis* by Microbiological Associates (Bethesda, Md.).

Results

Incidence and Specificity of Collagen-Induced Arthritis. A chronic inflammatory arthritis developed in 144 of 348 rats (41%) injected intradermally on the back with type II collagen derived from human, chick, or rat cartilage and either CFA or ICFA. These data are summarized in Table I. The arthritis could be induced with approximately equal frequency in outbred female Wistar, Sprague-Dawley or inbred Wistar-Lewis strains whether CFA or ICFA was employed. In contrast, type I collagen derived from human, chick, or rat skin or type III collagen derived from human skin were not arthritogenic in a total of 181 rats. In the other control groups, type II collagen without adjuvant, $MgCl_2$-extractable cartilage proteoglycans, denatured α1(II) chains, and the type and dose of CFA or ICFA injected without collagen also did not cause arthritis in a total of 140 rats. Table II summarizes these data in 321 control rats.

TABLE I
Preparations which Induced Arthritis

Preparation injected	Rat strain	Adjuvant		Total
		CFA*	ICFA*	
				%
Human type II‡	Wistar	43/78	14/47	46
Chick type II	Wistar	4/10	15/33	44
Chick type II	Wistar-Lewis		24/60	40
Rat type II‡	Wistar	6/20	17/50	33
Chick type II	Sprague-Dawley		5/10	50
CFA H37	Wistar			40§

* Number of rats developing arthritis/number of rats injected with the preparation in the specified adjuvant. There was no significant difference in the incidence of arthritis induced by heterologous or homologous type II collagens by Chi square analysis.

‡ Pepsin-modified.

§ Incidence (16/40) of adjuvant-induced arthritis, produced by intradermal injection of 0.1 ml adjuvant oil containing *M. tuberculosis* H37Ra (10 mg/ml).

TABLE II
Preparations which Did Not Cause Arthritis

Preparation injected	No. of rats injected		
	Adjuvant		Total
	CFA	ICFA	
Human type I*	45	10	55
Human type I	10	10	20
Chick type I	20	25	45
Rat type I	10	10	20
Human type III*	31	10	41
Human α1(II) chains*	20	10	30
Chick α1(II) chains	10	10	20
Human cartilage proteoglycans	10	10	20
Human type II* without adjuvant			20
Chick type II without adjuvant			10
Acetic acid‡	30	10	40

* Pepsin-modified.

‡ 0.5 ml 0.1 M acetic acid.

Onset and Course of Arthritis. The clinical features of the collagen-induced arthritis were similar whether heterologous or homologous type II collagen was the immunogen or whether CFA or ICFA was used. The onset of arthritis was explosive occurring 14–60 days postimmunization with a peak onset at 20 days and a median onset at 21 days for a group of 61 rats examined daily. Typically, a hindlimb became severely red and edematous within a 16–24-h period such that the arthritic index was 5.0 ± 0.4 (mean ± SEM) for a group of 28 rats evaluated on the day of onset of arthritis. 10 had bilateral hindlimb involvement (Fig. 1), whereas in 18 the disease remained unilateral.

The hindlimb swelling could also be easily quantified by measuring the

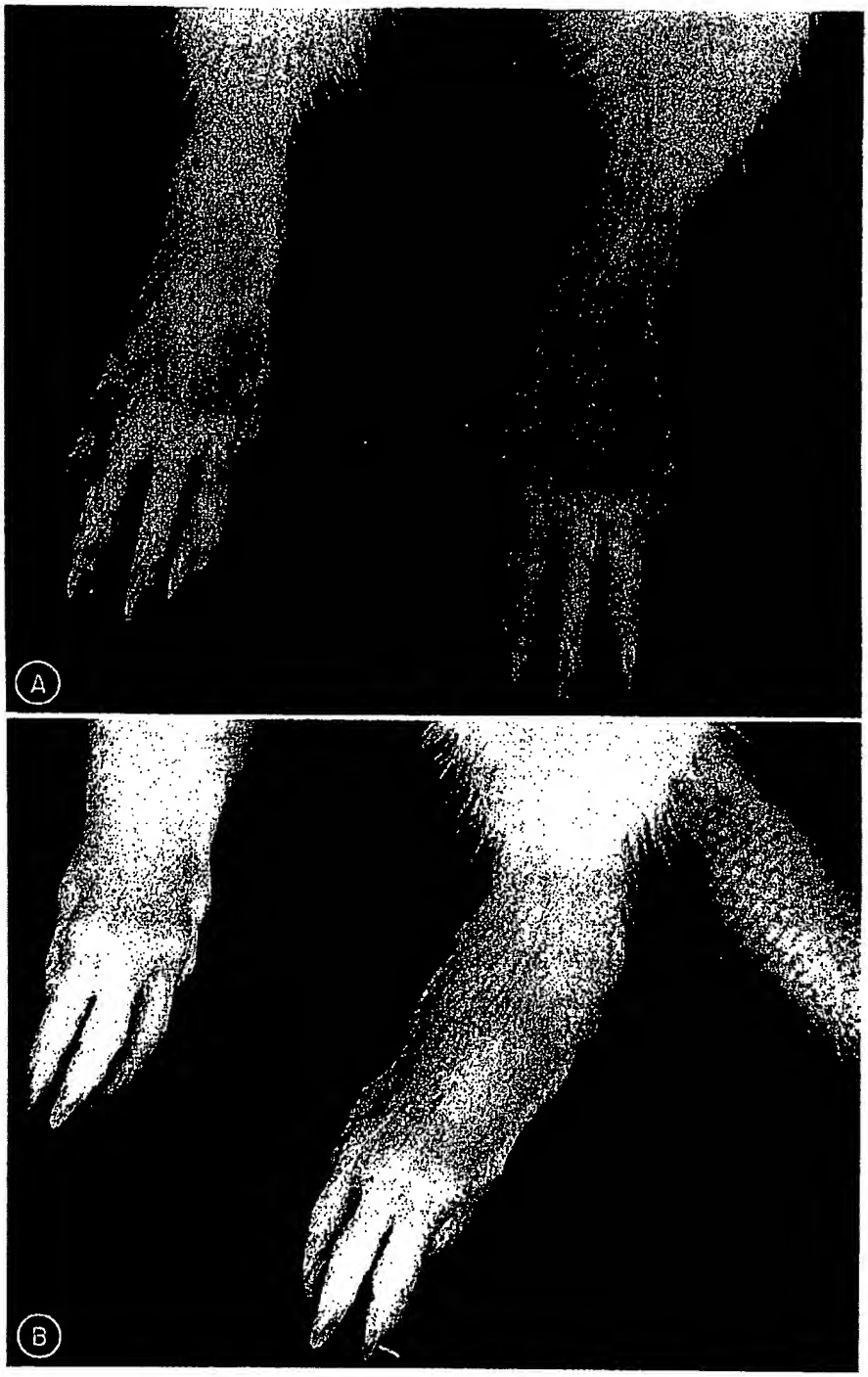

FIG. 1. Comparison of normal rat hindlimbs (A) with those (B) rendered arthritic by intradermal injection of human type II collagen in ICFA. Both arthritic paws were graded as 4 by the arthritic index and had an intermalleolar thickness of greater than 10 mm by constant tension caliper measurement. Ankle thickness of age-matched normal rats was consistently less than 7 mm.

thickness of the ankle between the malleolae with a constant tension caliper. The mean ankle thickness was 10.2 ± 0.3 mm for 10 arthritic joints evaluated on the day of onset of arthritis induced in Wistar-Lewis rats by chick type II collagen in ICFA compared to 6.4 ± 0.1 for 20 ankles from age-matched, uninjected female Wistar-Lewis rats.

No additional limbs became affected after the initial 48 h of disease. Forepaw inflammation occurred in 10% of the entire arthritic population. Involvement was predominately distal with ankle, tarsal, and interphalangeal inflammation. Peak severity occurred within 4 days after the onset with each involved limb usually reaching a maximum score by the arthritic index. Weight bearing on the affected limb was poorly tolerated by the rats, and swelling usually persisted 5–8 wk, gradually culminating in a deformed joint. Nine rats had an identical clinical course but a delayed onset 30–60 days after primary immunization. All had received i.p. booster injections at 21 days.

Spontaneous exacerbations of disease did not occur; however, i.p. booster doses, identical to those given at 21 days, as long as 6 mo after original immunization caused a recrudescence within 3 days in all 11 previously arthritic rats when rechallenged. None of 20 rats which initially remained nonarthritic after injection of type II collagen became arthritic when rechallenged after similar time intervals.

Mild hair and weight loss but no ocular inflammation, hematuria, or mucosal lesions occurred in the arthritic rats. No rat died during active joint inflammation.

Comparison with Adjuvant Arthritis. The clinical features of the type II collagen-induced arthritis were similar to those of adjuvant-induced disease. A single injection of human type II collagen in CFA or ICFA in another group of 62 Wistar rats caused arthritis in 33 (53%), whereas adjuvant arthritis developed in 16 of 40 Wistar rats (40%) injected with CFA H37. Likewise, the onset of clinical disease was similar (mean day of onset 17.0 ± 0.6 for 28 collagen-induced disease rats vs. 15.6 ± 0.4 for 16 adjuvant arthritis rats) as were their mean arthritic indices studied within 48 h of onset (mean 5.0 ± 0.4 for 28 collagen arthritis rats vs. 3.9 ± 0.4 for 16 adjuvant arthritis rats).

Pathology. Groups of six Wistar-Lewis rats were sacrificed before the onset of arthritis on each of days 11–14 after injection of chick type II collagen in ICFA, and their spleen and inguinal and cervical lymph nodes were examined grossly. Marked progressive hypertrophy of these tissues occurred during this period, which immediately preceded the usual time of onset of arthritis. Histopathologic sections of diarthrodial joints showed that injection of type II collagen with ICFA produced a chronic proliferative synovitis which secondarily destroyed articular cartilage and bone. Synovium obtained within 24 h of the onset of arthritis showed marked edema and infiltration by dense aggregates of mononuclear cells and occasional neutrophils. There was no vessel wall necrosis. Serial sections of joints examined at later stages of inflammation showed proliferation of synoviocytes and fibroblasts resulting in synovial hypertrophy and fibrosis. This synovial pannus, in turn, eroded the cartilage and subchondral bone (Fig. 2). Periosteal new bone formation was prominent and uniformly culminated in joint ankylosis. Numerous mononuclear cells persisted in the synovium for longer than 6 mo after the onset of the disease. The axial skeleton was not involved,

FIG. 2. Section of ankle joint taken approximately 2 wk after onset of type II collagen-induced arthritis. Synovial proliferation and intense infiltration by mononuclear cells is producing cartilage and bone erosion. Hematoxylin and eosin × 200.

and sections of the trachea showed no evidence of generalized cartilage inflammation. Likewise, histologic examinations of the skin, lung, and kidney were normal.

Roentgenography. Roentgenographs mirrored the progression from soft tissue swelling, articular bone erosions, and prominent periosteal new bone formation, to bony ankylosis in the carpal, tarsal, metacarpal, metatarsal, and interphalangeal regions (Fig. 3).

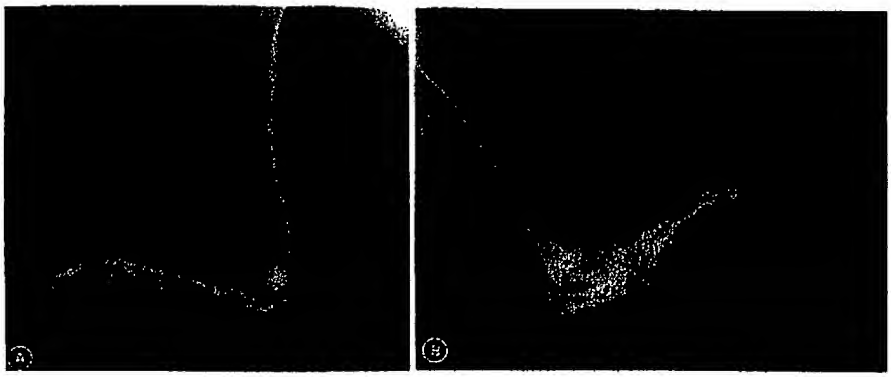

FIG. 3. Comparison of roentgenograph of normal rat hindpaw (A) with that (B) from a rat whose arthritis was induced by chick type II collagen in ICFA. Soft-tissue swelling, bone destruction and periosteal new bone formation are prominent 2 wk after the onset of inflammation.

Additional Attempts to Induce Arthritis. Primary and booster injection regimens employing 2.0 mg per rat of chick type I collagen, human type III collagen, or chick α1(II) chains in CFA failed to induce arthritis in a total of 50 additional rats. Also human type I tropocollagen which had been passed through DEAE in a manner identical to the preparative technique for type II collagen did not cause arthritis in 20 rats. No significant differences in the incidence of arthritis were found with doses of type II collagen ranging from 0.5 to 2.0 mg per rat.

Cultures for Microorganisms. No bacterial or mycoplasmal organisms were detected in blood or synovial cultures taken at the onset of disease.

Discussion

These data demonstrate that heterologous or homologous type II collagen derived from cartilage when injected intradermally on the back with CFA or ICFA induces arthritis in approximately 40% of rats of several strains. The structurally distinct types I and III collagen derived from skin are not arthritogenic. Likewise, the denatured constituent α-chains of type II do not cause disease. Various infections such as *M. arthritidis* (17) or *Salmonella* (18) can cause arthritis in rats. However, an infectious agent or product contaminating our preparations is unlikely to explain our results for several reasons: cultures for microorganisms were negative; the identically prepared collagen failed to induce arthritis when injected in the absence of adjuvant; multiple preparations of type II collagen from human, chick or rat sources induced arthritis; collagens prepared and injected in two geographically separate laboratories caused arthritis at all times of the year; the latent period after injection was longer than that usually observed after inoculation with an infectious agent (17); further, the arthritis had a lengthy course with no spontaneous exacerbations; and finally, the synovial infiltration was mononuclear rather than neutrophilic, even initially.

This type II collagen-induced arthritis is distinct from the previously described adjuvant-induced arthritis of rats (16), since the disease can be produced after injection of type II collagen in oil not containing bacterial preparations. Indeed, the equivalent frequency of arthritis whether CFA or ICFA was employed with the type II collagen is surprising. Possibly, type II collagen per se has an adjuvant capacity, but would still require oil since the protein injected alone was incapable of inducing arthritis. While the precise relationship of the collagen-induced arthritis to adjuvant-induced arthritis is at present uncertain, Steffen and Wick have reported delayed-type skin reactions to rat skin collagen in adjuvant arthritis (19). Moreover, we have found that peripheral blood mononuclear cells from rats with adjuvant arthritis exhibit antigen-induced tritiated thymidine incorporation in vitro to homologous type I and II collagen (20). Hemagglutinating antibodies specific for these native collagens and their α-chains can also be detected in sera from rats with adjuvant arthritis (D. Trentham and J. David, unpublished data). Immunologic hypersensitivity to collagen may thus be a common feature of adjuvant- and collagen-induced arthritis.

The moiety responsible for the arthritogenicity of our cartilage collagen preparations is uncertain, but at present we assume it to be type II collagen. By uronic acid assays and CM-cellulose chromatography, our type II collagen preparations are free from proteoglycan and type I collagen (13) contamination, respectively. A cartilage proteoglycan extract did not cause arthritis. Nonetheless, it is not possible at present to exclude a small amount of proteoglycan linked to collagen being important in the induction of arthritis. The principle responsible for the induction of adjuvant arthritis is of interest in this regard. Initial investigation indicated that arthritogenic activity resided in the wax D fraction which is separated from mycobacteria by ultracentrifugation. Subfractions of wax D containing peptidoglycolipids could also be chromatographically isolated which retained arthritogenic potential (16). Subsequent work suggests that adjuvanticity and arthritogenicity are properties of different glycopeptides contained in these subfractions (21). Finally, it has recently been proposed (22) that the common peptidoglycan backbone of bacterial cell walls explains the ability of extracts from several different bacteria to induce arthritis when emulsified in adjuvant oil. Since these bacterial peptidoglycans may have structural similarities to cartilage proteoglycans, the possible participation of these latter molecules in the induction of our arthritis must be further investigated before it can be firmly concluded that specific determinants on collagen are arthritogenic.

Intact nonhelical telopeptide regions of the type II molecule are not required for arthritogenicity, since pepsin-modified type II collagens were as effective in causing arthritis as the tropocollagen molecules. Although it is difficult to be certain that the helical structure of collagen was maintained during the process of emulsification in oil before injection, the finding that α1(II) chains did not induce arthritis makes this assumption reasonable. As recently demonstrated for myoglobin, the conformational integrity of immunogenic sites on native proteins can be preserved during emulsification in oil (23). Humoral and cellular immune specificities that further distinguish native type II collagen from its

denatured α1(II) chains, presented in a subsequent paper,[2] further support the thesis that sensitization to the helical form of type II collagen was achieved.

Two features of this animal model of arthritis are of particular interest. First, this represents the only experimental model in which disease can be regularly provoked with ICFA injected intradermally with a constituent of homologous tissue, suggesting that an autoimmune process may have been induced with oil not containing bacterial preparations. This is distinct from other models of experimentally-inducible autoimmunity to organ-specific antigens, which usually require injection of CFA with tissue components (24) and demonstrates an unusual property attributable to the type II collagen protein. Second, histopathologic studies show that the primary lesion provoked by type II collagen is a chronic proliferative synovitis. Destruction of articular cartilage and bone appear to be sequelae of synovial inflammation. Mononuclear cells invade and persist in the synovium, suggesting that immune processes may be important in the pathogenesis of disease. These characteristics sufficiently resemble those of rheumatoid arthritis to suggest that this may be an appropriate animal model for the human disease.

In conclusion, type II collagen from either heterologous or homologous sources has been found to be arthritogenic in rats. There is an apparent requirement for type-specific helical determinants in evoking the disease. This conclusion coincides with Hahn et al. (11) concerning the conformationally-dependent antigenic determinants responsible for the humoral specificity of type I and II collagen. By recently achieving passive transfer of this arthritis by spleen and lymph node cells sensitized to type II collagen,[3] we have directly implicated immunologic hypersensitivity to collagen in the causation of this autoimmune disease.

Summary

We have found that intradermal injection of native type II collagen extracted from human, chick or rat cartilage induces an inflammatory arthritis in approximately 40% of rats of several strains whether complete Freund's adjuvant or incomplete Freund's adjuvant is used. Type I or III collagen extracted from skin, cartilage proteoglycans and α1(II) chains were incapable of eliciting arthritis, as was type II collagen injected without adjuvant. The disease is a chronic proliferative synovitis, resembling adjuvant arthritis in rats and rheumatoid arthritis in humans. Native type II collagen modified by limited pepsin digestion still produces arthritis, suggesting that type-specific determinants residing in the helical region of the molecule are responsible for the induction of disease. Since homologous type II collagen emulsified in oil without bacterial preparations regularly causes the disease, this new animal model of arthritis represents a unique example of experimentally-inducible autoimmunity to a tissue component.

---

[2] Trentham, D. E., A. S. Townes, A. H. Kang, and J. R. David. Humoral and cellular sensitivity to collagen in type II collagen-induced arthritis in rats. Manuscript submitted for publication.

[3] Trentham, D. E., R. A. Dynesius, and J. R. David. Passive transfer of type II collagen-induced arthritis by cells. Manuscript in preparation.

We thank Dr. John R. David for his critical evaluation of this work and Ms. Margaret Cirtin, Roselynn Dynesius, and Donna Rowland for their excellent technical assistance and Lynn White for manuscript preparation.

Received for publication 3 May 1977.

References

1. Steffen, C., and R. Timpl. 1963. Antigenicity of collagen and its application in the serological investigation of rheumatoid arthritis sera. *Int. Arch. Allergy Appl. Immunol.* 22:333.
2. Steffen, C., F. Schuster, G. Tausch, R. Timpl, and I. Pecker. 1968. Weitere Untersuchungen über Kollagenantikörper bei Patienten mit primär chronischer Polyarthritis. *Klin. Wochenschr.* 46:976.
3. Steffen, C. 1970. Consideration of the pathogenesis of rheumatoid arthritis as collagen autoimmunity. *Z. Immunitätsforsch.* 139:219.
4. Michaeli, D., and H. H. Fudenberg. 1974. The incidence and antigenic specificity of antibodies against denatured human collagen in rheumatoid arthritis. *Clin. Immunol. Immunopath.* 2:153.
5. Cracchiolo, A., D. Michaeli, L. S. Goldberg, and H. H. Fudenberg. 1975. The occurrence of antibodies to collagen in synovial fluids. *Clin. Immunol. Immunopath.* 3:567.
6. Andriopoulos, N. A., J. C. Bennett, J. Mestecky, and E. J. Miller. 1975. The occurrence of antibodies against native human collagens in synovial fluids of patients with rheumatoid arthritis. *Arthritis Rheum.* 18:384.
7. Andriopoulos, N. A., J. Mestecky, E. J. Miller, and E. L. Bradley. 1976. Antibodies to native and denatured collagens in sera of patients with rheumatoid arthritis. *Arthritis Rheum.* 19:613.
8. Andriopoulos, N. A., J. Mestecky, G. P. Wright, and E. J. Miller. 1976. Characterization of antibodies to the native human collagens and to their component α chains in the sera and the joint fluids of patients with rheumatoid arthritis. *Immunochemistry.* 13:709.
9. Seraffini-Fracassini, A., and J. W. Smith, editors. 1974. Collagen. *In* The Structure and Biochemistry of Cartilage. Churchill Livingston, Edinburgh, Scotland. 29.
10. Traub, W., and K. A. Piez. 1971. The chemistry and structure of collagen. *Adv. Protein Chem.* 25:243.
11. Hahn, E., R. Timpl, and E. J. Miller. 1974. The production of specific antibodies to native collagens with the chain compositions, $[\alpha 1(I)]_3$, $[\alpha 1(II)]_3$ and $[\alpha 1(I)]_2\alpha 2$. *J. Immunol.* 13:421.
12. Nowack, H., E. Hahn, and R. Timpl. 1975. Specificity of the antibody response in inbred mice to bovine type I and type II collagen. *Immunology.* 29:621.
13. Trelstad, R. L., A. H. Kang, S. Igarashi, and J. Gross. 1970. Isolation of two distinct collagens from chick cartilage. *Biochemistry.* 9:4993.
14. Seyer, J. M., E. T. Hutcheson, and A. H. Kang. 1976. Collagen polymorphism in idiopathic chronic pulmonary fibrosis. *J. Clin. Invest.* 57:1498.
15. Bitter, T., and H. M. Muir. 1962. A modified uronic acid carbazole reaction. *Anal. Biochem.* 4:330.
16. Wood, F. D., C. M. Pearson, and A. Tanaka. 1969. Capacity of mycobacterial wax D and its subfractions to induce adjuvant arthritis in rats. *Int. Arch. Allergy Appl. Immunol.* 35:456.
17. Hill, A., and G. J. R. Dagnall. 1975. Experimental polyarthritis in rats produced by *Mycoplasma arthritidis*. *J. Comp. Pathol.* 85:45.

18. Volkman, A., and F. M. Collins. 1973. Polyarthritis associated with *Salmonella* infection in rats. *Infect. Immun.* 8:814.
19. Steffen, C., and G. Wick. 1971. Delayed hypersensitivity reactions to collagen in rats with adjuvant-induced arthritis. *Z. Immunitätsforsch.* 141:169.
20. Trentham, D. E., and J. R. David. 1977. Cellular sensitivity to collagen in adjuvant arthritis. *Clin. Res.* 25:369. Abstr.
21. Stewart-Tull, D. E. S., T. Shimono, S. Kotani, M. Kato, Y. Ogawa, Y. Yamamura, T. Koga, and C. M. Pearson. 1975. The adjuvant activity of a non-toxic, water-soluble glycopeptide present in large quantities in the culture filtrate of *Mycobacteria tuberculosis* strain DT. *Immunology.* 29:1.
22. Hadler, N. M. 1976. A pathogenetic model for erosive synovitis: lessons from animal arthritides. *Arthritis Rheum.* 19:256.
23. Smith, J. A., J. G. R. Hurrell, and S. J. Leach. 1977. Conformational integrity of myoglobin after immunization with Freund's adjuvant. *J. Immunol.* 118:226.
24. Rose, N. R. 1973. Self-recognition and autoimmunity. *In* Principles of Immunology. N. R. Rose, F. Milgrom, and C. J. van Oss, editors. Macmillan, Inc., New York. 217.

British Journal of Anaesthesia 1996; 77: 165–171

Psychophysical and electrophysiological responses to experimental pain may be influenced by sedation: comparison of the effects of a hypnotic (propofol) and an analgesic (alfentanil)

S. PETERSEN-FELIX, L. ARENDT-NIELSEN, P. BAK, M. FISCHER AND A. M. ZBINDEN

Summary

Sedation may influence the responses of some experimental pain models used to test analgesic efficacy. In this study we compared the effects of a sedative (propofol) and analgesic (alfentanil) on: nociceptive reflex to single and repeated electrical stimulations; mechanical pressure pain; and evoked potentials elicited by nociceptive (electrical and laser) and non-nociceptive (acoustical) stimulation. We studied 12 healthy volunteers with two subanaesthetic concentrations of propofol and two analgesic concentrations of alfentanil. Both propofol and alfentanil increased the threshold for nociceptive reflex to single electrical stimulations, but only alfentanil increased the threshold for nociceptive reflex to repeated electrical stimulations. The pressure pain tolerance thresholds were increased significantly by alfentanil, whereas propofol significantly decreased the thresholds (hyperalgesia). Propofol and alfentanil induced similar reductions in the amplitudes of the evoked potentials elicited by nociceptive (electrical and laser) and non-nociceptive (acoustical) stimulation, whereas only alfentanil reduced the perceived pain to nociceptive stimulations. We have shown that sedation can influence both the psychophysical and electrophysiological responses of some experimental pain tests used to measure analgesic efficacy, and that propofol in subhypnotic doses, has no analgesic effect on painful electrical and heat stimulations, but has a hyperalgesic effect on mechanical pressure pain. (*Br. J. Anaesth.* 1996; **77**: 165–171)

Key words

Anaesthetics i.v., propofol. Analgesics opioid, alfentanil. Pain, experimental.

Testing the sensory aspects of pain is hampered by the subjective and multidimensional nature of pain. This has led to a search for quantitative measures. The nociceptive withdrawal reflex to single electrical stimulations of the sural nerve has been proposed as a technique to assess the excitability of the nociceptive system [1, 2]. The size of the evoked potential elicited by painful stimuli has also been found to correlate with the state of the nociceptive system [3, 4]. For conditions when the subject cannot collaborate, nociceptive reflex and evoked potentials would appear to be adequate tests. Spinal polysynaptic nociceptive reflexes have been used in animals for decades. In a recent study [5], we found that subanaesthetic (0.10–0.26 vol % end-tidal) isoflurane concentrations increased significantly the threshold for nociceptive reflex to single electrical stimulations of the sural nerve, but did not change the reaction to pain elicited by heat, cold or pressure, or the threshold for nociceptive reflex to repetitive stimuli. This indicates that the increase in the threshold of the nociceptive reflex to single electrical stimuli might not reflect analgesia but could be caused by sedation. Furthermore, in another study [6] using similar subanaesthetic isoflurane concentrations, we found that the amplitude of evoked vertex potentials elicited by nociceptive laser and intracutaneous electrical stimulations decreased with increasing isoflurane concentration. But isoflurane caused a similar decrease in amplitudes of evoked vertex potentials elicited by non-nociceptive auditory stimuli, indicating that the decrease in amplitude was not caused by an analgesic effect of isoflurane, but could be a result of general depression of neuronal transmission.

Therefore, it seems possible that sedation could influence the responses of some experimental pain models used to assess analgesic efficacy. In this study we compared the effects of sedation (propofol) and analgesia (alfentanil) on the thresholds of the nociceptive reflex to single and repeated electrical stimulations, the amplitude of evoked vertex potentials elicited by nociceptive and non-nociceptive stimuli and detection and tolerance thresholds to mechanically induced pain.

Several studies [7–12] have been designed to see if hypnotics are hyperalgesic in subhypnotic doses, but results are conflicting. As propofol is one of the most widely used hypnotics in anaesthesia, and is also

STEEN PETERSEN-FELIX*, MD, DEEA, MICHAEL FISCHER, MD, ALEX M. ZBINDEN, MD, PHD, Department of Anaesthesiology and Intensive Care, University Hospital of Bern, Switzerland. LARS ERENDT-NIELSEN, PHD, PETER BAK, MSC, Centre for Sensory–Motor Interaction, Laboratory for Experimental Pain Research, University of Aalborg, Denmark. Accepted for publication: February 24, 1996.

* Address for correspondence: Institut für Anästhesie und Intensivbehandlung, Inselspital, CH-3010 Bern, Switzerland.

used for sedation in intensive care, it is important to clarify further its influence on nociception in humans.

Subjects and methods

We studied 12 healthy volunteers (eight male), mean age 26 (range 20–42) yr. They were not receiving any medication, had no allergies or earlier adverse reactions to anaesthesia, and for the female volunteers, were not pregnant. Written informed consent according to the Helsinki Declaration was obtained, and the study was approved by the Ethics Committee of the Faculty of Medicine, University of Bern.

To minimize the risk of acid aspiration, volunteers were tested after a fasting period of at least 6 h. During testing volunteers rested comfortably in the supine position. An i.v. infusion of NaCl-glucose was started and haemoglobin oxygen saturation by pulse oximetry, ECG and non-invasive arterial pressure were monitored continuously during the study.

NOCICEPTIVE REFLEX THRESHOLD TO SINGLE STIMULI

The sural nerve was stimulated behind the lateral malleolus via surface electrodes filled with electrode gel (inter-electrode distance approximately 2 cm). A 25-ms, train-of-five, 1-ms, square-wave impulse (perceived as a single stimulus) was delivered from a computer-controlled constant current stimulator (University of Aalborg, Denmark). Electromyographic reflex responses were recorded from the middle of the biceps femoris and the rectus femoris muscles (surface silver–silver chloride electrodes). The EMG signal was amplified and filtered (1.5–150 Hz) by a Hellige (PPG Hellige GmbH, Germany) single channel EMG–EEG amplifier, recorded and analysed with NFRsys software (University of Aalborg, Denmark). The stimulation current was increased from 1 mA in steps of 1–2 mA until an ipsilateral reflex with an amplitude exceeding 20 μV for at least 10 ms was detected by the computer program. If a reflex was recorded three times at the same current intensity, this intensity was defined as the nociceptive reflex threshold to single stimulation. Maximal stimulation intensity was 80 mA. Eight reflexes, elicited with a stimulation intensity of 1.4 times the threshold intensity, were recorded, averaged and the root mean square (RMS) value in the 80–180-ms interval after the stimulus was calculated with EPsys software (University of Aalborg, Denmark). The volunteer then rated the perceived pain of the eight stimulations on a 10-cm visual analogue scale (VAS).

NOCICEPTIVE REFLEX THRESHOLD TO REPEATED STIMULI

The sural nerve was stimulated as described above, but the single stimulus was repeated five times with a frequency of 2 Hz, as described by Arendt-Nielsen and colleagues [13, 14]. Current intensity was increased from 1 mA in steps of 1–2 mA until a psychophysical or electrophysiological summation was detected by the computer program. The summation thresholds were defined as an increase in pain during the five stimulations (psychophysical summation threshold) or an increase in amplitude of the last one or two reflexes above a fixed limit of 20 μV for at least 10 ms (electrophysiological summation threshold). Maximal stimulation intensity was 80 mA.

MECHANICAL PRESSURE PAIN DETECTION AND PAIN TOLERANCE THRESHOLDS

Pressure pain detection and pain tolerance thresholds were measured on the centre of the pulp of the second (pain detection) and third (pain tolerance) finger of the right hand with an electronic pressure algometer (Somedic AB, Stockholm, Sweden) [15–17]. A probe with a surface area of 0.28 cm^2 was used, and the pressure increase was 30 kPa s^{-1}. Pain detection was defined as the point when pressure turned into pain, and pain tolerance as the point when the volunteer did not want the pressure to be increased further. For determination of both thresholds, the mean of two consecutive measurements was used.

REACTION TIME

A 1000-Hz tone was delivered from a computer with randomized intervals of 3–8 s, and a timer was started simultaneously. The volunteer was told to press a button as fast as possible after each tone. Reaction time was defined as the time from the tone until the volunteer pressed the button. The mean of three consecutive measurements was used.

EVOKED POTENTIALS

Argon laser stimulation

A 200-ms stimulus and a 3-mm laser beam diameter were used. Laser stimuli were applied to the dorsum of the hand (C7 dermatome). Repeated stimulation in the same area was avoided. The pain threshold was defined as a distinct sharp pinprick, and was calculated as the mean of five ascending and five descending series of stimulations. A laser stimulus of 1.4 times the initial pain threshold was used as stimulation for recording of the evoked potentials.

Electrical stimulation

An intracutaneous electrode, as described by Bromm and Meier [4], was used. The finger pulp of the third or fourth finger was stimulated with a blunt 1-mm steel pin electrode, with a digital ring finger electrode placed proximal as reference. A 25-ms, train-of-five, 1-ms, square-wave impulse (perceived as a single stimulus) delivered from a Digitimer DS7 constant current stimulator (Digitimer Ltd, UK) triggered by

a Phillips PM5150 Generator (Phillips GmbH, Germany) was used as stimulus. The horn layer of the epidermis was scraped carefully in a 2 × 2-mm area. Intracutaneous placement was accepted when a stimulation current of less than 0.5 mA was felt as a distinct pinprick. The current was increased from 0 in steps of 0.2 mA until the volunteer scored the stimulus (VAS) as painful as the laser stimulus of 1.4 times the initial laser pain threshold. This intensity was used for recording of the electrical evoked potentials.

Auditory stimulation

Auditory evoked potentials were elicited by click stimulation (Medelec ST 10, Medelec Ltd, UK) with 90 dB applied binaural through acoustically shielded headphones.

Recording

The evoked vertex potentials were recorded from a needle electrode (scalp electrode, 0.3 × 10 mm, Dantec, Denmark), inserted at Cz' *vs* a surface silver–silver chloride electrode on the right mastoid. The signal, in the interval of 0.5 s before the stimulus until 2 s after the stimulus, was amplified and filtered (0.1–30 Hz) with a Hellige (Hellige AG, Germany) single-channel EEG amplifier and recorded, averaged and analysed with EPsys software (University of Aalborg, Denmark). Evoked potentials from 16 stimulations were averaged.

Perceived pain from laser and electrical stimulations

After each series of 16 laser or electrical stimulations, volunteers rated perceived pain on a 10 cm VAS.

MEDICATION

Volunteers were tested on two different days, at least 1 week apart. They received, in randomized order, alfentanil on one day and propofol on the other. The medication was prepared by an anaesthetist who monitored the volunteer and study but did not take part in the measurements. The volunteer and other investigators were blinded as to the medication.

The first concentration of alfentanil (low dose) was attained by a loading dose of 7.5 $\mu g\,kg^{-1}$ i.v. followed by an infusion of 0.1 $\mu g\,kg^{-1}\,min^{-1}$ and the second (high dose) by a loading dose of 15 $\mu g\,kg^{-1}$ i.v. followed by an infusion of 0.3 $\mu g\,kg^{-1}\,min^{-1}$. The first propofol concentration (low dose) was attained by a loading dose of 0.5 $mg\,kg^{-1}$ i.v. followed by an infusion of 10 $\mu g\,kg^{-1}\,min^{-1}$ and the second (high dose) by a loading dose of 1 $mg\,kg^{-1}$ i.v. followed by an infusion of 30 $\mu g\,kg^{-1}\,min^{-1}$.

EXPERIMENTAL DESIGN

The tests were explained to the volunteer and a trial testing was performed in order to familiarize the volunteer with the procedure. Thereafter a baseline test series was performed. Further test series were performed 20 min after each loading dose during the infusion.

STATISTICAL ANALYSIS

The Friedman test for repeated measures analysis of variance on ranks, and the Student–Newman–Keuls test for multiple comparisons were used for statistical analysis. $P < 0.05$ was considered significant.

Results

NOCICEPTIVE REFLEX (TABLE 1)

The threshold for nociceptive reflex to single stimulations was increased significantly by propofol and alfentanil compared with baseline, but there was no difference in the increase caused by propofol or alfentanil. The RMS of the recorded reflex was decreased significantly by propofol and alfentanil compared with baseline, but the high dose of propofol decreased the RMS significantly more than the high dose of alfentanil. The perceived pain to stimulations with a current intensity of 1.4 times the baseline threshold intensity was not decreased by propofol, whereas alfentanil produced a significant decrease in pain intensity compared with baseline. Propofol did not change the psychophysical or electrophysiological threshold for summation of the nociceptive reflex, but both thresholds were increased significantly by alfentanil compared with baseline and the difference between high-dose propofol and high-dose alfentanil was significant.

MECHANICAL PRESSURE (TABLE 1)

The pressure pain detection thresholds tended to be decreased by propofol and increased by alfentanil, but differences from baseline were not significant. However, the difference between high-dose propofol and high-dose alfentanil was significant. The pressure pain tolerance thresholds were decreased significantly by propofol at the high dose, whereas alfentanil increased significantly the threshold at the high dose compared with baseline. The difference between high-dose propofol and high-dose alfentanil was significant.

REACTION TIME (TABLE 1)

Both propofol and alfentanil increased the reaction time compared with baseline, but a significantly larger increase was found with high-dose propofol compared with high-dose alfentanil.

EVOKED VERTEX POTENTIAL LATENCIES (TABLE 2)

A typical evoked vertex potential (laser) is shown in figure 1. Neither propofol nor alfentanil changed the latencies of the vertex evoked potentials, except for N1 latency at the high propofol concentration (increase of 10 % compared with baseline and 16 % compared with high-dose alfentanil).

Table 1 Numerical results from experimental pain tests and reaction time. All values are median (5–95 percentiles), and are expressed as percentage change from baseline (baseline = 100%). *$P < 0.05$ compared with baseline, ns = not significant compared with baseline, P = propofol, A = alfentanil, L = low concentration, H = high concentration

Test	Propofol		Comparison	Alfentanil	
	Low concn	High concn	P–A	Low concn	High concn
Nociceptive reflex threshold	125.0 (85.7–162.5) *B, *H	200.0 (79.3–270.5) *B, *L	ns (PL–AL) ns (PH–AH)	115.4 (93.5–161.2) *B, *H	140.0 (73.9–235.4) *B, *L
Nociceptive reflex RMS	63.2 (34.6–151.9) *B, *H	25.3 (10.7–136.6) *B, *H	ns (PL–AL) *(PH–AH)	81.0 (26.3–105.6) *B	56.1 (15.0–150.8) *B
Nociceptive reflex VAS	100.0 (63.7–117.5) ns	85.4 (60.2–126.6) ns	ns (PL–AL) *(PH–AH)	94.6 (61.5–102.9) *H	78.4 (49.3–101.1) *B, *H
Nociceptive reflex summation psychophysical threshold	104.5 (82.2–131.7) ns	104.5 (87.8–142.6) ns	ns (PL–AL) *(PH–AH)	100.0 (100.0–158.7) *H	127.3 (100.0–215.8) *B, *L
Nociceptive reflex summation electrophysiological threshold	100.0 (84.0–123.9) ns	109.7 (76.4–142.3) ns	ns (PL–AL) *(PH–AH)	109.1 (100.0–128.5) *H	133.3 (100.4–214.2) *B, *L
Pressure pain threshold	90.8 (69.9–115.2) ns	81.8 (73.0–116.6) ns	ns (PL–AL) *(PH–AH)	100.6 (69.8–140.6) ns	115.6 (84.1–163.5) ns
Pressure pain tolerance	97.3 (84.9–110.0) *H	87.2 (70.2–100.8) *B, *L	ns (PL–AL) *(PH–AH)	109.0 (85.0–121.3) *H	117.4 (85.5–136.3) *B, *L
Reaction time	120.1 (77.0–156.2) *H	123.8 (108.5–235.5) *B, *L	ns (PL–AL) *(PH–AH)	109.5 (101.1–134.6) *B	112.7 (98.1–192.1) *B

Table 2 Numerical results from latencies of the evoked potentials (EP). All values (ms) are median (5–95 percentiles). *$P < 0.05$ compared with baseline, ns = not significant compared with baseline, P = propofol, A = alfentanil, B = baseline, L = low concentration, H = high concentration

Test	Propofol			Comparison	Alfentanil		
	Baseline	Low concn	High concn	P–A	Baseline	Low concn	High concn
Laser EP latencies P1	320 (258–382) ns	305 (259–343) ns	324 (222–366) ns	ns (PL–AL) ns (PH–AH)	313 (242–382) ns	320 (228–373) ns	320 (252–352) ns
Laser EP latencies N1	445 (414–492) *H	442 (376–525) *H	488 (387–565) *B, *L	ns (PL–AL) *(PH–AH)	438 (376–514) ns	430 (375–461) ns	422 (360–477) ns
Laser EP latencies P2	641 (492–740) ns	633 (511–763) ns	648 (572–876) ns	ns (PL–AL) ns (PH–AH)	594 (541–664) ns	633 (563–717) ns	641 (532–777) ns
Electrical EP latencies P1	152 (126–179) ns	156 (148–179) ns	148 (103–186) ns	ns (PL–AL) ns (PH–AH)	156 (141–180) ns	156 (133–194) ns	148 (141–202) ns
Electrical EP latencies N1	273 (207–318) ns	254 (228–358) ns	273 (213–397) ns	ns (PL–AL) ns (PH–AH)	281 (227–351) ns	266 (219–379) ns	266 (219–433) ns
Electrical EP latencies P2	434 (338–518) ns	450 (358–569) ns	445 (422–582) ns	ns (PL–AL) ns (PH–AH)	445 (423–634) ns	445 (438–614) ns	477 (319–659) ns
Auditory EP latencies P1	141 (118–155) ns	148 (117–156) ns	148 (126–163) ns	ns (PL–AL) ns (PH–AH)	141 (125–156) ns	148 (133–145) ns	155 (133–164) ns
Auditory EP latencies N1	231 (201–258) ns	227 (204–307) ns	219 (204–335) ns	ns (PL–AL) ns (PH–AH)	234 (203–304) ns	219 (203–326) ns	227 (211–320) ns
Auditory EP latencies P2	403 (368–518) ns	426 (275–459) ns	449 (322–498) ns	ns (PL–AL) ns (PH–AH)	422 (354–497) ns	453 (344–492) ns	453 (300–484) ns

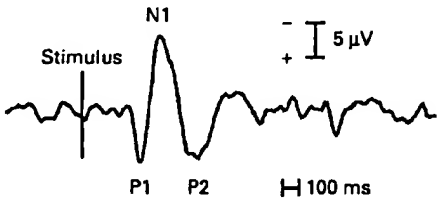

Figure 1 Laser evoked potential, which is the average of 16 evoked potentials elicited by short argon laser stimuli of 200 ms duration.

EVOKED VERTEX POTENTIAL AMPLITUDES (TABLE 3)

Neither propofol nor alfentanil changed the P1/N1 amplitudes of the laser evoked potentials. For the N1/P2 amplitudes of the laser evoked potentials and for the P1/N1 and N1/P2 amplitudes of the electrical and the auditory evoked potentials, both propofol and alfentanil reduced the amplitudes. In several cases (see table 3) propofol produced a significantly larger reduction than alfentanil. High-dose propofol and high-dose alfentanil induced the same amplitude reductions in the evoked potentials elicited by nociceptive stimuli (laser and electrical) as in the evoked potentials elicited by non-nociceptive stimuli (auditory) ($P = 0.12$ for P1/N1 amplitudes and $P = 0.21$ for N1/P2 amplitudes).

PERCEIVED PAIN TO LASER AND ELECTRICAL STIMULATIONS (TABLE 4)

Propofol did not reduce perceived pain (VAS scores) to laser and electrical stimulations, whereas high-dose alfentanil reduced significantly VAS scores

Table 3 Numerical results from amplitudes of the evoked potentials (EP). All values are median (5–95 percentiles), and are expressed as percentage change from baseline (baseline = 100%). *$P < 0.05$ compared with baseline, ns = not significant compared with baseline, P = propofol, A = alfentanil, L = low concentration, H = high concentration

Test	Propofol		Comparison	Alfentanil	
	Low concn	High concn	P–A	Low concn	High concn
Laser EP amplitudes P1/N1	97.8 (59.3–108.8) ns	81.2 (28.6–115.3) ns	ns (PL–AL) ns (PH–AH)	96.0 (44.4–133.0) ns	91.3 (44.6–141.7) ns
Laser EP amplitudes N1/P2	73.2 (27.1–110.7) *B, *H	43.1 (22.3–71.5) *B, *L	NS (PL–AL) *(PH–AH)	78.8 (58.1–125.7) *B	70.8 (41.2–132.1) *B
Electrical EP amplitudes P1/N1	54.7 (43.7–134.9) *B, *H	45.5 (15.9–77.0) *B, *L	*(PL–AL) *(PH–AH)	84.2 (67.4–148.6) *H	71.7 (23.6–132.1) *B, *L
Electrical EP amplitudes N1/P2	58.7 (30.0–76.9) *B	42.1 (32.7–67.8) *B	*(PL–AL) ns (PH–AH)	92.0 (75.3–126.0) *B, *H	78.6 (31.1–133.6) *B, *L
Auditory EP amplitudes P1/N1	70.7 (30.8–198.1) *B	46.1 (19.2–96.5) *B	*(PL–AL) ns (PH–AH)	86.4 (66.6–103.4) *B, *H	77.5 (52.3–85.7) *B, *L
Auditory EP amplitudes N1/P2	73.2 (27.1–110.7) *B, *H	43.1 (22.3–71.5) *B, *L	ns (PL–AL) *(PH–AH)	78.7 (58.1–125.7) *B	70.8 (41.2–132.1) *B

Table 4 Numerical results of perceived pain scores (VAS) from the laser and electrical evoked potentials (EP). All values are median (5–95 percentiles), and are expressed as percentage change from baseline (baseline = 100%). *$P < 0.05$ compared with baseline, ns = not significant compared with baseline, P = propofol, A = alfentanil, L = low concentration, H = high concentration

Test	Propofol		Comparison	Alfentanil	
	Low concn	High concn	P–A	Low concn	High concn
Laser EP VAS	94.9 (50.5–133.3) ns	100.8 (73.8–161.8) ns	ns (PL–AL) ns (PH–AH)	95.2 (62.9–131.1) *H	83.8 (45.2–109.4) *B, *L
Electrical EP VAS	97.2 (56.5–133.1) ns	94.1 (45.2–122.2) ns	ns (PL–AL) *(PH–AH)	95.9 (35.2–120.1) *H	75.5 (23.9–122.9) *B, *L

compared with baseline and low-dose alfentanil. VAS scores were also significantly smaller for high-dose alfentanil compared with high-dose propofol.

Discussion

We have shown that sedation can influence both the psychophysical and electrophysiological responses of some experimental pain tests used to measure analgesic efficacy. Propofol increased the threshold of the nociceptive reflex to single stimulations and decreased the amplitude of the evoked potentials elicited by nociceptive laser and electrical stimulations. This indicates that these may not, under all circumstances, assess the excitability of the nociceptive system. Propofol, in subhypnotic doses, had no analgesic effect on painful electrical and heat stimulations, but had a hyperalgesic effect on pressure pain.

NOCICEPTIVE REFLEX

Willer [18] investigated the relation between nociceptive reflex and perceived pain. The occurrence of the reflex was related closely to the pain threshold, and a linear relation was found between perceived pain and amplitude of the nociceptive reflex. This finding was confirmed later by Chan and Dallaire [19]. The reflex threshold to single stimuli has been found to increase with i.v. morphine [20], extradural morphine [21], i.m. alfentanil [22], but also with the weaker, non-opioid analgesics ketoprofen [23] and acetylsalicylic acid [24]. This indicates that the nociceptive reflex to single electrical stimulations of the sural nerve can be used to demonstrate analgesia produced by pure analgesic drugs. However, sub-anaesthetic (0.10–0.26 vol % end-tidal) isoflurane concentrations significantly increase the threshold for nociceptive reflex to single stimuli, but do not change the reaction to pain elicited by heat, cold or pressure, or the threshold of the nociceptive reflex to repetitive stimuli [5]. Training and attention has been shown to influence the pain threshold and the threshold for the nociceptive reflex [2], and distraction has been shown to decrease the nociceptive reflex [25]. In this study, propofol, in sedative doses, produced the same increase in the nociceptive reflex threshold to single stimulations as alfentanil, but showed hyperalgesic effects for tolerance to mechanical pressure. This indicates that the increase in threshold of the nociceptive reflex could be caused by sedation and not analgesia. The nociceptive reflex to single electrical stimulations may therefore not be a measure of analgesia when the drug tested also has sedative effects. As the nociceptive reflex has a sensory afferent and motor efferent component, the difference between propofol and alfentanil could be explained by stronger depression of the motor component by propofol. However, this would influence reflexes elicited by single and repeated stimulations in the same manner. Propofol did not change the threshold for temporal summation of the nociceptive reflex to repeated stimulations, indicating that the muscle component is not influenced significantly by propofol.

MECHANICAL PRESSURE

Early studies by Clutton-Brock [8, 26] and Dundee [9], using a relatively simple mechanical pressure pain model showed that small doses of thiopentone had a hyperalgesic effect. Our study showed that

propofol, in subhypnotic doses, had a similar hyperalgesic effect on pressure pain. *In vitro* studies in single neurones [27] and isolated spinal cord models [10] showed that propofol and thiopentone depressed spinal nociceptive transmission, but they may have a different effect, through GABA inhibitory neurones, in the intact animal or human [28].

EVOKED VERTEX POTENTIALS

Arendt-Nielsen [3] correlated the amplitude or power of the long latency evoked vertex potential to an argon laser nociceptive thermal stimulation with the intensity of the perceived pain. With this method an analgesic effect of alfentanil [29], ibuprofen [30], paracetamol [31], codeine [32] and extradural morphine [33] has been demonstrated. A recent study failed to show an effect on laser evoked potentials of i.v. morphine [34]. In a recent review on nociceptive laser evoked vertex potentials by Arendt-Nielsen [35], it was suggested that sedation might influence the evoked potential. Evoked potentials to non-nociceptive stimuli should therefore be recorded as a control for sedation. We have shown recently that subanaesthetic isoflurane concentrations (0.10–0.26 vol % end-tidal) also decreased the amplitude of the evoked vertex potentials to painful laser and electrical stimuli [6]. But isoflurane produced a similar reduction in the amplitude of non-pain related auditory evoked vertex potentials recorded with the same paradigm, and did not reduce the perceived pain. In our study, propofol reduced the amplitude of evoked vertex potentials, but showed a hyperalgesic effect in the pain tolerance threshold to mechanical. This indicates that the reduction in amplitude of evoked vertex potentials by propofol and isoflurane is not caused by an analgesic effect. Anker-Møller and co-workers [7] also found a decrease in laser evoked vertex potentials with subhypnotic doses of thiopentone and propofol, but they did not measure the effect on non-pain-related potentials.

DRUG CONCENTRATIONS

The concentrations of propofol and alfentanil used in this study were chosen on empirical grounds, so that the low doses produced slight sedation (propofol) and slight analgesia (alfentanil), and the high doses distinct sedation and analgesia. The reaction time for low-dose propofol was slightly but not statistically increased compared with baseline, but for the high dose a significant increase was found compared with baseline and low-dose propofol. Low-dose alfentanil produced a slight but not significant increase in pain tolerance to mechanical pressure, but for the high dose of alfentanil a significant increase was found compared with baseline and the low dose. Furthermore, the threshold for the nociceptive reflex to single stimulations, and the decrease in the amplitude of the vertex potentials were not different for high-dose propofol and high-dose alfentanil. This indicates that the chosen doses were relevant according to the initial criteria, and that an effect of sedation on the nociceptive reflex and the amplitude of the vertex potentials could be investigated at these concentrations.

SHORT *VS* REPEATED OR LONGER LASTING STIMULATIONS

Arendt-Nielsen and co-workers [36, 37] and Brennum and co-workers [17, 38] have shown that brief localized nociceptive stimuli can be attenuated to a greater extent by extradural lignocaine or morphine than noxious stimulations of longer duration or involving larger areas. That central temporal and spatial summation of nociceptive stimuli are important for determination of anaesthetic efficacy is supported by our study. The responses to experimental pain tests involving short or single stimulations were influenced by the sedative effect of propofol, whereas tests involving longer lasting or repeated stimulations were not. Alfentanil showed the expected analgesia on both the short or single stimulations, and the longer lasting or repeated stimulations used in this study (these results are in accordance with previous studies [22, 29]).

PAIN DETECTION *VS* PAIN TOLERANCE THRESHOLDS

Measuring pain tolerance thresholds and not just pain detection was also important in this study. If we had only measured pain detection thresholds to mechanical pressure, we would not have detected the hyperalgesic effect of propofol on mechanical pain.

This study showed that when experimental pain models were used to measure an analgesic effect, the effects of sedation on both psychophysical and electrophysiological responses must be controlled. It is important to combine threshold measurements and electrophysiological responses with psychophysical pain ratings. Furthermore, models eliciting temporal or spatial summation, or both, of nociceptive stimuli appear to be less influenced by sedation.

Acknowledgement

The study was performed with support from the Desirée and Niels Yde Foundation, and the Danish Basic Research Foundation. The authors thank the anaesthesia research department for excellent technical assistance, especially D. Leibundgut.

References

1. De Broucker T, Willer JC, Bergeret S. The nociceptive flexion reflex in humans: A specific and objective correlate of experimental pain. In: Chapman CR, Loeser JD, eds. *Issues in Pain Measurement*. New York: Raven Press, 1989; 337–352.
2. Willer JC. Nociception flexion reflex as a physiological correlate of pain sensation in humans. In: Bromm B, ed. *Pain Measurements in Man. Neurophysiological Correlates of Pain*. Amsterdam: Elsevier, 1984; 87–110.
3. Arendt-Nielsen L. First pain event related potentials to argon laser stimuli: recording and quantification. *Journal of Neurology, Neurosurgery and Psychiatry* 1990; 53: 398–404.
4. Bromm B, Meier W. The intracutaneous stimulus: a new pain model for algesimetric studies. *Methods and Findings in Experimental and Clinical Pharmacology* 1984; 6: 405–410.
5. Petersen-Felix S, Bak P, Arendt-Nielsen L, Fischer M, Bjerring P, Roth D, Zbinden AM. Analgesic effect in humans of subanaesthetic isoflurane concentrations evaluated by

experimentally induced pain. *British Journal of Anaesthesia* 1995; 75: 55–60.
6. Roth D, Petersen-Felix S, Fischer M, Bak P, Arendt-Nielsen L, Bjerring P, Zbinden AM. Analgesic effect in humans of subanaesthetic isoflurane concentrations evaluated by evoked potentials. *British Journal of Anaesthesia* 1996; 76: 38–42.
7. Anker-Møller E, Spangsbjerg N, Arendt-Nielsen L, Schultz P, Kristensen MS, Bjerring P. Subhypnotic doses of thiopentone and propofol cause analgesia to experimentally induced acute pain. *British Journal of Anaesthesia* 1991; 66: 185–188.
8. Clutton-Brock J. Some pain threshold studies with particular reference to thiopentone. *Anaesthesia* 1960; 15: 71–72.
9. Dundee JW. Alterations in response to somatic pain associated with anaesthesia II: the effect of thiopentone and pentobarbitone. *British Journal of Anaesthesia* 1960; 32: 407–414.
10. Jewett BA, Gibbs LM, Tarasiuk A, Kendig JJ. Propofol and barbiturate depression of spinal nociceptive neurotransmission. *Anesthesiology* 1992; 77: 1148–1154.
11. Wilder-Smith OHG, Kolletzki M, Wilder-Smith CH. Sedation with intravenous infusions of propofol or thiopentone. Effects on pain perception. *Anaesthesia* 1995; 50: 218–222.
12. Stein C, Morgan MM, Leibeskind JC. Barbiturate-induced inhibition of a spinal nociceptive reflex: role of GABA mechanisms and descending modulation. *Brain Research* 1987; 407: 307–311.
13. Arendt-Nielsen L, Brennum J, Sindrup S, Bak P. Electrophysiological and psychophysical quantification of central temporal summation of the human nociceptive system. *European Journal of Applied Physiology* 1994; 68: 266–273.
14. Arendt-Nielsen L, Petersen-Felix S, Fischer M, Bak P, Bjerring P, Zbinden AM. The effect of *N*-methyl-D-aspartate antagonist (ketamine) on single and repeated nociceptive stimuli: a placebo-controlled experimental human study. *Anesthesia and Analgesia* 1995; 81: 63–68.
15. Brennum B, Kjeldsen M, Jensen K, Jensen TS. Measurement of human pressure–pain thresholds on fingers and toes. *Pain* 1989; 38: 211–217.
16. Dahl JB, Rosenberg J, Molke Jensen F, Kehlet H. Pressure pain thresholds in volunteers and herniorrhaphy patients. *Acta Anaesthesiologica Scandinavica* 1990; 34: 673–676.
17. Brennum J, Arendt-Nielsen L, Secher NH, Jensen TS, Bjerring P. Quantitative sensory examination in human epidural anaesthesia and analgesia: effects of lidocaine. *Pain* 1992; 51: 27–34.
18. Willer JC. Comparative study of perceived pain and nociceptive flexion reflex in man. *Pain* 1977; 3: 69–80.
19. Chan CWY, Dallaire M. Subjective pain sensation is linearly correlated with the flexion reflex in man. *Brain Research* 1989; 479: 145–150.
20. Willer JC. Studies on pain. Effects of morphine on a spinal nociceptive flexion reflex and related pain sensation in man. *Brain Research* 1985; 331: 105–114.
21. Willer JC, Bergeret S, Gaudy JH. Epidural morphine strongly depresses nociceptive flexion reflexes in patients with postoperative pain. *Anesthesiology* 1985; 63: 675–680.
22. Petersen-Felix S, Arendt-Nielsen L, Bak P, Bjerring P, Breivik H, Svensson P, Zbinden AM. Ondansetron does not inhibit the analgesic effect of alfentanil. *British Journal of Anaesthesia* 1994; 73: 326–330.
23. Willer JC, De Broucker T, Bussel B, Roby-Brami A, Harrewyn JM. Central analgesic effect of ketoprofen in humans: electrophysiological evidence for a supraspinal mechanism in a double-blind cross-over study. *Pain* 1989: 38: 1–7.
24. Willer JC, Bathien N. Pharmacological modulations on the nociceptive flexion reflex in man. *Pain* 1977; 3: 111–119.
25. Willer JC, Boureau F, Albe-Fessard D. Supraspinal influences on nociceptive flexion reflex and pain sensation in man. *Brain Research* 1979; 179: 61–68.
26. Clutton-Brock J. Pain and the barbiturates. *Anaesthesia* 1961; 16: 80–88.
27. Kitahata LM, Ghazi-Saidi K, Yamashita M, Kosaka Y, Bonikos C, Taub A. The depressant effect of halothane and sodium thiopental on the spontaneous and evoked activity of dorsal horn cells: lamina specificity, time course and dose dependence. *Journal of Pharmacology and Experimental Therapeutics* 1975; 195: 515–521.
28. Kitahata LM, Saberski L. Are barbiturates hyperalgesic? *Anesthesiology* 1992; 77: 1059–1061.
29. Arendt-Nielsen L, Øberg B, Bjerring P. Analgesic efficacy of i.m. alfentanil. *British Journal of Anaesthesia* 1990; 65: 164–168.
30. Nielsen JC, Bjerring P, Arendt-Nielsen L, Petterson KJ. A double-blind placebo controlled, cross-over comparison of the analgesic effect of ibuprofen 400 mg and 800 mg on laser-induced pain. *British Journal of Clinical Pharmacology* 1990; 30: 711–715.
31. Nielsen JC, Bjerring P, Arendt-Nielsen L, Petterson KJ. Analgesic efficacy of immediate and sustained release paracetamol and plasma concentrations of paracetamol. Double blind, placebo-controlled evaluation using painful laser stimulation. *European Journal of Clinical Pharmacology* 1992; 42: 261–264.
32. Sindrup SH, Brøsen K, Bjerring P, Arendt-Nielsen L, Larsen U, Angelo HR, Gram LF. Codeine increases pain thresholds to copper vapor laser stimuli in extensive but not poor metabolizers of spartine. *Clinical Pharmacology and Therapeutics* 1990; 48: 686–693.
33. Arendt-Nielsen L, Øberg B, Bjerring P. Hypoalgesia following epidural morphine: a controlled quantitative experimental study. *Acta Anaesthesiologica Scandinavica* 1991; 35: 430–435.
34. van der Burght M, Elkjær Rasmussen S, Arendt-Nielsen L, Bjerring P. Morphine does not affect laser induced warmth and pin prick pain thresholds. *Acta Anaesthesiologica Scandinavica* 1994; 38: 161–164.
35. Arendt-Nielsen L. Characteristics, detection, and modulation of laser-evoked vertex potentials. *Acta Anaesthesiologica Scandinavica* 1994; 38 (Suppl. 98).
36. Arendt-Nielsen L, Øberg B, Bjerring P. Quantitative assessment of extradural bupivacaine analgesia. *British Journal of Anaesthesia* 1990; 65: 633–638.
37. Arendt-Nielsen L, Anker-Møller E, Bjerring P, Spangsberg N. Onset phase of spinal bupivacaine analgesia assessed quantitatively by laser stimulation. *British Journal of Anaesthesia* 1990; 65: 639–642.
38. Brennum J, Arendt-Nielsen L, Horn A, Secher NH, Jensen TS. Quantitative sensory examination during epidural anaesthesia and analgesia in man: effects of morphine. *Pain* 1993; 52: 75–83.

[CANCER RESEARCH 51, 3274-3280, June 15, 1991]

Irradiated Nude Rat Model for Orthotopic Human Lung Cancers[1]

Randy B. Howard, Henry Chu, Bernard E. Zeligman, Tere Marcell, Paul A. Bunn, Theodore L. McLemore, David W. Mulvin, Michael E. Cowen, and Michael R. Johnston[2]

Departments of Surgery [R. B. H., T. M., D. W. M., M. E. C., M. R. J.], Pathology [H. C.], and Radiology [B. E. Z.], and the University of Colorado Cancer Center [P. A. B., M. R. J., R. B. H.] of the University of Colorado School of Medicine, Denver, Colorado 80262; and the Developmental Therapeutics Program, Division of Cancer Treatment, National Cancer Institute, Frederick Cancer Research Facility, Frederick, Maryland 21701 [T. L. M.]

ABSTRACT

The development of improved animal models for biological and preclinical studies of human lung cancer is important because lung cancer is the leading cause of cancer death in the United States. To determine whether the Rowett nude rat could serve as an orthotopic (organ-specific) model of this disease, nude rats (CR: NIH-RNU), with and without 500 rads of prior γ-irradiation, were implanted intrabronchially with 10^7 cultured cells from 3 human lung cancer lines. Without irradiation, the NCI-H460 large-cell undifferentiated carcinoma had a 54% take-rate, whereas the NCI-H125 adenosquamous carcinoma and A549 adenocarcinoma had take-rates of 7 and 33%, respectively; irradiation increased the respective take-rates to 100, 83, and 90%. In irradiated rats, tumor age *versus* weight measurements showed progressive growth for all three tumors, with growth rates in the order: NCI-H460 > A549 > NCI-H125, requiring approximately 3, 5, and 9 weeks, respectively, for average tumor sizes to exceed 500 mg. The small-cell carcinoma cell line NCI-H345 was implanted only into irradiated rats and resulted in more slowly growing tumors. Histopathological study showed all model tumor types to have histological characteristics consistent with the clinical tumors from which the cell lines were derived. Each tumor type had a different growth pattern, with some of the the A549- and NCI-H125-derived tumors metastasizing to contralateral lung and/or regional lymph nodes. There was no evidence for immunological rejection in irradiated, tumor-bearing rats. Nonirradiated, implanted rats without gross tumor exhibited peribronchiolar mononuclear cell infiltration with or without fibrosis, suggesting prior immunological rejection. The successful orthotopic growth of these 4 human lung cancer cell lines in irradiated nude rats suggests that this model could be useful for biological and preclinical studies of human lung cancer, both in intact rats and via *ex vivo* perfusion of their tumor-bearing lungs.

INTRODUCTION

A rising incidence combined with a lack of effective methods for either early detection or treatment has made lung cancer the leading cause of cancer death in the United States (1–4). It is therefore imperative to develop improved animal models of this disease for *in vivo* biological and preclinical studies. Both s.c. (5–7) and subrenal capsule (8–10) rodent models have previously been used for such studies, but it is now appreciated that nude rodents with human tumor material implanted in orthotopic (organ-specific) sites offer better tumorigenicity and metastatic potential than these ectopic (abnormally positioned) models (5, 11–19). In addition to the improved modeling of human cancer biology, orthotopic studies might also better model the pharmacokinetic compartments and pharmacodynamics relevant to treatment of human cancers (11).

Orthotopic nude mouse models have recently been developed for a number of human cancers, including those of the lung, colon, pancreas, kidney, brain, and skin (11–19). The orthotopic mouse model for lung cancer developed by McLemore *et al.* (11, 12) has thus far been used primarily for comparative modeling studies. Using this model, it has been shown that (*a*) a variety of cultured human cancer cell lines, as well as some enzymatically disaggregated clinical specimens, can be successfully propagated by i.b.[3] implantation; (*b*) human lung cancer cell lines implanted i.b. frequently exhibit mediastinal invasion; (*c*) i.b. cell implantation requires fewer cells and results in much higher tumor-related mortality than does s.c. implantation; and (*d*) the histological characteristics of i.b. implanted cell lines resemble those of the parent tumor from which the cell lines were derived. The efficient propagation, mediastinal invasion, and lethality seen in this orthotopic mouse model suggest that it should provide clear advantages over previously used models for *in vivo* biological and preclinical study of human lung cancer.

On the other hand, the nude mouse model is not ideal for some applications because of its small size; the nude rat (20) is often more convenient. For *in vivo* experimentation, nude rats (*a*) more readily allow surgical procedures and/or repeated blood sampling and (*b*) can carry a much greater tumor burden (particularly with orthotopic tumors), thereby increasing both the time available to study the tumor and the amount of tumor tissue obtainable. In addition, the considerably larger lung size of nude rats facilitates *ex vivo* perfusion of their tumor-bearing lungs, a technique for performing well-controlled biological and preclinical studies of *in situ* orthotopic human lung cancers.[4]

A disadvantage of Rowett nude rats is their relative immunocompetence compared to nude mice. Previous studies of nude rats given ectopic injections (s.c.) of human tumor material have shown reduced take rates compared to nude mice and a tendency for the tumors to spontaneously regress (20–26). It is unknown, however, whether nude rats can be used for orthotopic (i.b.) human lung cancer growth and whether additional immunosuppression would be beneficial in this rat model. We have modified the i.b. implantation method described by McLemore *et al.* (11, 12) to answer these questions.

MATERIALS AND METHODS

Human Tumor Cell Lines. Human lung cancer cell lines NCI-H125, NCI-H460, NCI-H345, and A549 (27) were obtained from Drs. J. Minna, A. Gazdar, and J. Mayo (National Cancer Institute, Frederick Cancer Research Facility). All cell lines were recovered from cryopreserved seed stock and cultivated in standard tissue culture flasks (Costar, Cambridge, MA) in RPMI 1640 (GIBCO, Grand Island, NY) containing 10% heat-inactivated fetal bovine serum (Irvine Scientific, Santa Ana, CA) without antibiotics. Cells were maintained at 37°C in a humidified incubator gassed with 5% CO_2 in air. When cells growing in monolayers were 60–80% confluent, they were subcultured or harvested for implantation using trypsin-EDTA (Sigma, St. Louis, MO).

Received 5/21/90; accepted 4/8/91.

The costs of publication of this article were defrayed in part by the payment of page charges. This article must therefore be hereby marked *advertisement* in accordance with 18 U.S.C. Section 1734 solely to indicate this fact.

[1] Supported by NIH National Cooperative Drug Discovery Group Program Grant CA46088 and University of Colorado Cancer Center Core Grant CA46934.

[2] To whom requests for reprints should be addressed, at the Division of Cardiothoracic Surgery, Campus Box C310, University of Colorado Health Sciences Center, 4200 E. 9th Avenue, Denver, CO 80262.

[3] The abbreviation used is: i.b., intrabronchial.

[4] D. W. Mulvin, R. B. Howard, D. H. Mitchell, P. Noker, C. A. Kruse, T. Marcell, M. Tagawa, P. A. Bunn, and M. R. Johnston. An orthotopic nude rat lung perfusion model for preclinical testing of therapies for human lung cancer, submitted for publication.

Cells to be implanted were washed twice in RPMI 1640, counted with a hemocytometer, and adjusted to the correct concentration of trypan blue-viable cells in 100 μl of the same medium. All cell lines were previously shown to be human by karyotype analysis and were regularly screened for *Mycoplasma* infection.

Animals. Male or female nude (CR: NIH-RNU) rats (obtained from the National Cancer Institute, Frederick Cancer Research Facility) were received in the nude rodent reverse isolation facility at the University of Colorado Health Sciences Center at 4 weeks of age and acclimated for 1 week before entering study protocols. Rats were kept in previously sterilized filter-topped cages and fed autoclaved food and water *ad libitum*. Manipulations were done under sterile conditions in a laminar flow hood. All studies had previously been approved by the institutional Animal Care and Use Committee.

Tumor Cell Implantation. On the morning of the day of implantation, 5-week-old rats to be irradiated were given 500 rads of whole-body γ-radiation from a ^{60}Co source (Atomic Energy of Canada Limited γ-Beam 150 Irradiator; Ontario, Canada) at 150 rads/min while confined upright in a gas-sterilized plastic holding apparatus (Harvard Bioscience, South Natick, MA). That afternoon, all rats were anesthetized i.m. with ketamine/xylazine (Parke-Davis, Morris Plains, NJ; Mobay, Shawnee, KS; 80 and 12 mg/kg, respectively) and intrabronchially implanted (11, 12) with 10^7 tumor cells using a 20-gauge, 2-inch-long Teflon catheter (Deseret Medical, Inc., Sandy, UT) passed into the right caudal lobe via a small tracheostomy incision. After closing the wounds with sterile clips and recovery in cages warmed on heating pads, the rats were returned to their shelves and treated prophylactically with Augmentin (Beecham Labs, Bristol, TN) at 0.35 mg/ml drinking water for 2 weeks.

Determination of Take-rates. Take-rates were measured in irradiated and nonirradiated rats by determining what fraction of rats implanted with each cell line had evidence of gross tumor after a period previously shown to allow the development of sizable (>0.5 g) tumors in irradiated rats. The times required for tumor development were: NCI-H460, 3 weeks; A549, 5 weeks; NCI-H125, 10 weeks.

The protocol was as follows. On at least three separate occasions, groups of rats (3–8 each) were implanted with each cell line, with and without prior irradiation. The animals were visually monitored 3 times/week for evidence of tumor development. Rats exhibiting early morbidity (5–10%) were euthanized by an overdose of ketamine/xylazine and autopsied; those dying unexpectedly before their scheduled sacrifice (5–10%) were also autopsied. Autopsied rats in these categories with obvious tumors were included in the study. Such animals without obvious tumors were excluded since it was impossible to determine whether a tumor might have developed if the rat had survived until the originally intended time of sacrifice. About 5% of the rats died from tumors growing in the pleural space; they were considered failed implantations and excluded from the study. To determine whether there was tumor development subsequently followed by regression, each animal was radiographed (see below) every 2–3 weeks until sacrifice.

At the predetermined intervals, all animals were euthanized as above and their heart-lung blocks were removed. Each lung lobe was palpated for evidence of a tumor. In cases where tumors were clearly present they were either removed and weighed or fixed in the intact heart-lung block for histopathological characterization (see below). When tumors were not clearly determined to be present by palpation, most heart-lung blocks were separated into individual lung lobes which were then individually cut into 1–2-mm-wide strips for more careful examination. However, at least 2 nonirradiated rats, implanted with each cell line and without palpable tumors, were fixed for histopathological characterization of any inflammatory or immunological reaction at the implantation sites. Since nonirradiated NCI-H125-implanted rats require about 10 weeks for sizable tumor growth, it was uncertain whether any inflammatory or immunological response occurring immediately in these animals would still be visible at 10 weeks. Therefore, 2 of these animals were also euthanized early, at 2 weeks postimplantation, for histological characterization.

Determination of Growth Rates. Groups of irradiated rats (3–8 each) were implanted with each cell line on at least 3 different occasions. Animals were visually monitored 3 times/week; those exhibiting early morbidity (about 5%) were euthanized and excluded from the study; those dying suddenly (also about 5%) were likewise excluded. All other rats were randomly sacrificed and autopsied, and their tumors were weighed at different time intervals as follows: NCI-H460, 10–19 or 20–29 days; A549, 20–29, 30–39, or 40–49 days; NCI-H125, 40–49, 50–59, or 60–69 days. A graph of average tumor weight *versus* time interval was constructed.

Chest Roentgenographic Studies. Ketamine/xylazine-anesthetized rats were radiographed in anteroposterior and right lateral recumbent positions using a conventional radiographic unit (GX 1050; Picker International, Inc., Highland Heights, OH) with a 1.2-mm nominal focal spot and a retractable mirror. The receptor was a double emulsion mammographic type (T-Mat M film and Min-R fast screens; Eastman Kodak Co., Rochester, NY) used without a grid. Typical exposure factors were 29 kVp, 300 mA, and 17 msec, with the mirror retracted. The limit of detection was a tumor diameter of approximately 3 mm.

Histopathological Study. To characterize the growth patterns of each type of tumor, heart-lung blocks were removed from a number of euthanized animals with gross evidence of tumor; the lungs were fixed by tracheal perfusion with 20 ml of 10% buffered formalin and placed in a container of the same solution for at least 48 h. All lung lobes and mediastinum were embedded in paraffin, stained with H & E, and examined in a blinded fashion by a board-certified pathologist (H. C.). In addition, the lungs of at least 2 nonirradiated rats implanted with each cell line and found to be without tumors at such times as tumors were normally expected in irradiated rats were similarly fixed and stained, and the right caudal lobe was then examined for evidence of inflammatory or immunological reaction or microscopic tumor at the implantation site.

RESULTS

Take-rate estimations were based on the results of both radiography and gross autopsy follow-up of each animal. Each rat was radiographed[5] (Fig. 1) periodically and then sacrificed and autopsied after an interval previously shown sufficient for that particular cell line to grow to a tumor size of approximately 500 mg. Every rat radiographically positive for tumor was later found to have gross tumor at autopsy; therefore the possibility that tumors grew and then regressed before sacrifice was excluded.

Table 1 summarizes the tumor take-rates for the three different human lung cancer cell lines implanted intrabronchially with and without prior irradiation. The NCI-H125 adenosquamous cell line had a take-rate of 7% in untreated rats and 83% with prior irradiation. Large-cell carcinomas arising from the NCI-H460 large-cell line were present in 54% of the rats without and 100% of the rats with prior irradiation. The third cell line, the A549 adenocarcinoma, had a 33% take-rate without pretreatment and improved to 90% with prior irradiation. Since completing this study, rats have routinely been irradiated prior to implantation with each of these cell lines; take-rates have consistently been comparable to those shown here.

Over 1000 rats have received injections thus far, with a surgical mortality rate of 5–10%. Approximately 90% of confirmed tumors were found in the right caudal lobe; most tumors arising outside the right caudal lobe were found in the pleural space. These "extrapulmonary" tumors were presumed to arise from an injection made after accidentally passing the cannula through the visceral pleura; such tumors with the NCI-H460 cell line tended to be particularly aggressive and rapidly killed the rats by lung compression. A very small percentage of tumors

[5] B. E. Zeligman, R. B. Howard, T. Marcell, H. Chu, R. P. Rossi, D. W. Mulvin, and M. R. Johnston. Chest roentgenographic technique for demonstrating human lung tumor xenografts in nude rats, submitted for publication.

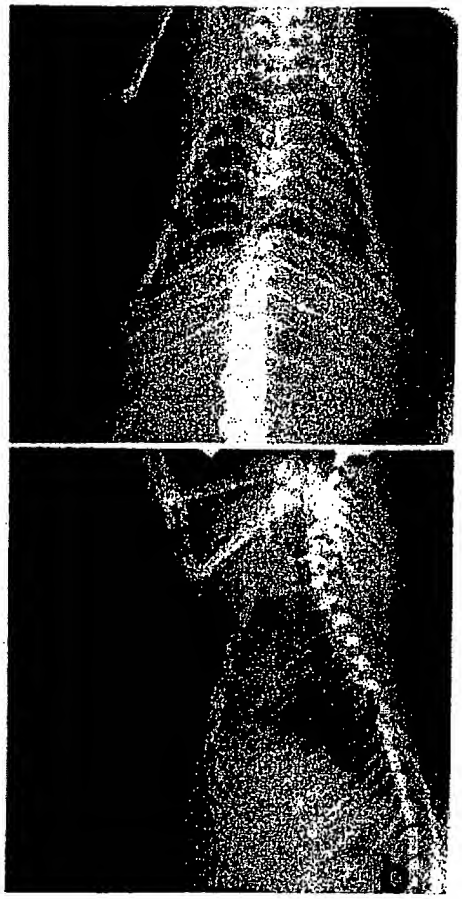

Fig. 1. Roentgenogram of a nude rat right caudal lobe lung tumor 6 mm in diameter arising from NCI-H460 cells. The tumor is clearly visible (*arrows*) in both anteroposterior (*a*) and right lateral (*b*) views.

Table 1 *Intrabronchial tumor take-rates for nude rats with or without prior γ-irradiation*[a]

Cell line	Treatment	Take-rate (%)
NCI-H125	None	1/15 (7)
	500r[b]	19/23[c] (83)
NCI-H460	None	7/13 (54)
	500r[b]	21/21[c] (100)
A549	None	6/18 (33)
	500r[b]	19/21[c] (90)

[a] Determined by gross inspection of 1–2 mm thick lung slices at the following times postimplantation: NCI-H460, 3 weeks; A549, 5 weeks; NCI-H125, 10 weeks.

[b] Rads of cobalt γ-radiation.

[c] Significantly different from untreated at $P \leq 0.05$ (Fisher's exact test).

(<3%) were found within other lung lobes, usually on the right side. Occasionally, small tumors were also found in the s.c. tissue surrounding the tracheostomy site.

Each of the three tumor types shown in Table 1 had different growth rates and distinctive cytological and histological characteristics. Tumors from the NCI-H125 adenosquamous cells grew the slowest (Fig. 2), requiring 9 or 10 weeks to produce a tumor weighing approximately 500 mg. Histologically (Fig. 3), within the right caudal lobe these tumors grew in both parenchyma and bronchi and formed nests with the appearance of poorly differentiated adenocarcinomas ($n = 6$); there was no evidence of squamous differentiation in any of the tumors examined. Three of four heart-lung blocks examined showed metastasis to the left lung, and 2 of 4 had mediastinal lymph node metastases. This was the only cell line of the four lung cancer cell lines examined where left lung metastases were observed. None of the tumors showed evidence of immunological rejection, and necrosis was minimal.

Tumors arising from the NCI-H460 large-cell line grew very rapidly (Fig. 2), requiring 2 to 3 weeks to reach the 500-mg size range. If not euthanized, most of these rats died from their tumors within 4 weeks. Right caudal lobe tumors from this cell

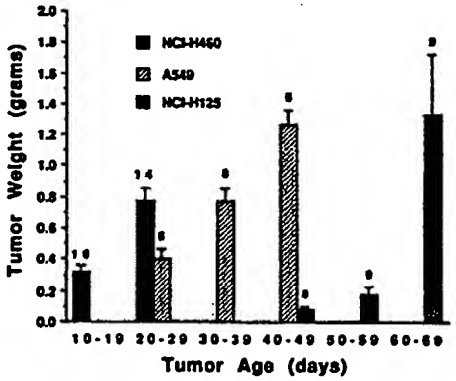

Fig. 2. Tumor weight *versus* age data for tumors arising from i.b. implantation of 10^7 cells from three different cultured human lung cancer cell lines into irradiated rats: NCI-H460 large-cell carcinoma, A549 adenocarcinoma, and NCI-H125 adenosquamous carcinoma. The numbers above each column are the number of animals per group. *Columns*, mean; *bars*, SE.

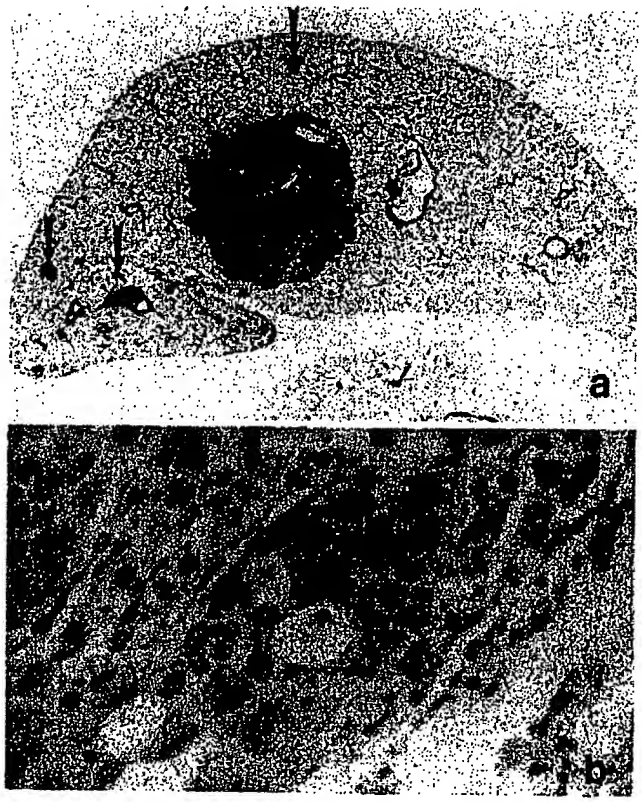

Fig. 3. Light micrographs of a 9-week-old, H & E-stained, right caudal lobe tumor arising from i.b. implantation of NCI-H125 cells. *a*, tumor invading the parenchyma from a large airway. Cancer cell deposits represent either metastases or aerogenous spread (*arrows*). × 9. Similar deposits were also found in the left lung of rats with this tumor type. *b*, nest of cancer cells growing among other less organized cancer cells, typical of a poorly differentiated adenocarcinoma. × 350.

line manifested as large-cell undifferentiated carcinomas growing in both airway and parenchyma (n = 6), but especially within the airway (Fig. 4). Necrosis was common and was estimated to range from 10 to 40%. No evidence of lung or lymph node metastasis or immunological rejection was seen in any of the rats.

The A549 adenocarcinoma cells gave rise to tumors growing at an intermediate rate (Fig. 2), producing a 500-mg tumor in 4 to 5 weeks. Right caudal lobe tumors from this cell line also appeared as poorly differentiated adenocarcinomas (n = 5) growing in both the parenchyma and the airway (Fig. 5). Cellular heterogeneity was seen in tumors from this cell line; a light-colored foamy cell predominated, but clusters of darkly staining cells were also seen. Tumors ranged from less than 10% to over 40% necrotic but showed no evidence of immunological rejection. Lung metastases were not seen, but 2 of 5 animals had mediastinal lymph node metastases.

Cells from a human small-cell carcinoma, NCI-H345, were implanted only into irradiated rats. A total of 8 rats received implantations. No tumor was found at autopsy in single rats euthanized at 3 and 6 weeks postimplantation. In four rats euthanized at 8 weeks, one had a small (4-mm-diameter) tumor. Two remaining rats, which were radiographically negative at 7 weeks, became positive at 10 weeks. Autopsy of these rats at 11 weeks confirmed the presence of medium-sized (~300 mg) tumors in the right caudal lobes. Histological study (Fig. 6) showed growth in both parenchyma and bronchi. Both had typical small-cell cytology, little necrosis, no apparent tendency to metastasize, and no evidence of immunological rejection.

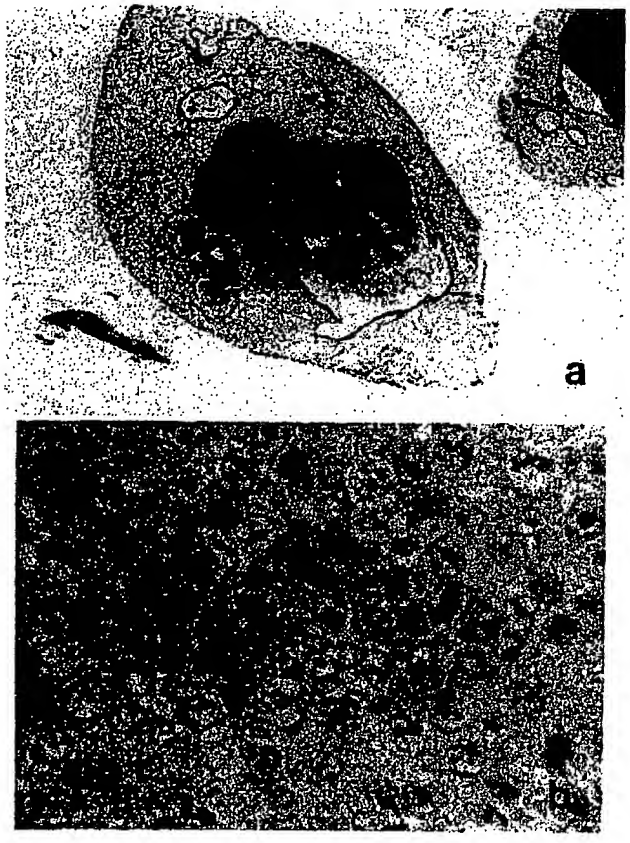

Fig. 4. Light micrographs of a 2-week-old, H & E-stained, right caudal lobe tumor arising from i.b. implantation of NCI-H460 cells. *a*, partially necrotic tumor located predominantly in an airway. × 9. *b*, abundant cytoplasm, vesicular nuclei, and prominent nucleoli typical of a large-cell, undifferentiated carcinoma. × 350.

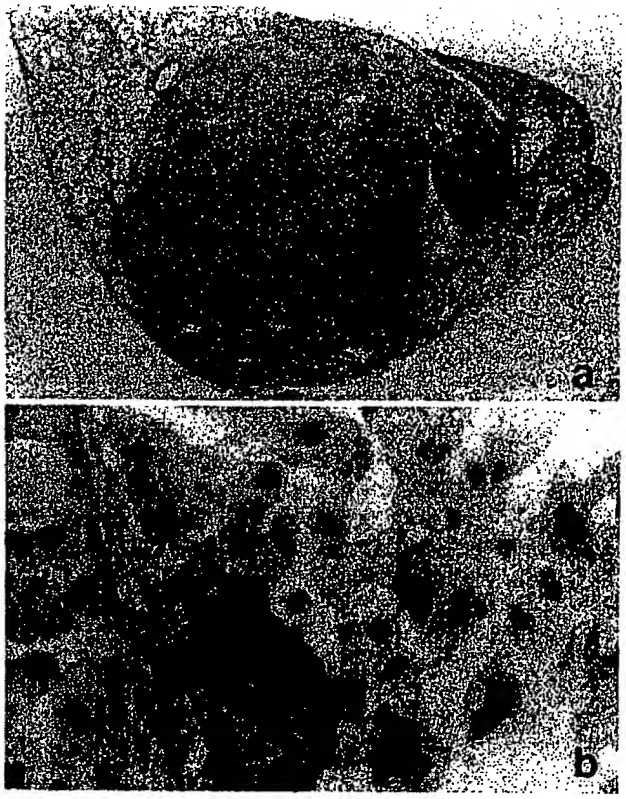

Fig. 5. Light micrographs of a 5-week-old, H & E-stained, right caudal lobe tumor arising from i.b. implantation of A549 cells. *a*, tumor containing predominantly light-staining cancer cells with islands of dark-staining cells. × 9. *b*, island of dark cells surrounded by the lighter-colored foamy cells typical of a poorly differentiated adenocarcinoma. × 350.

Microscopic examination of the right caudal lobes of 6 nonirradiated rats implanted with NCI-H125 cells, A549 cells, or NCI-H460 cells (2 rats with each) and without gross evidence of tumor at 10, 5, and 3 weeks postimplantation, respectively, revealed local inflammatory responses consistent with immunological rejection in all rats. Fig. 7*a* shows peribronchiolar mononuclear cell infiltration in a rat implanted 10 weeks earlier with NCI-H125 cells. Peribronchiolar fibrosis accompanied by mononuclear cell infiltration 5 weeks after implantation of A549 cells is seen in Fig. 7*b*.

Two weeks after implantation of NCI-H125 cells, 2 rats were sacrificed to look for early evidence of immunological rejection, in case the evidence was no longer present at 10 weeks in this more slowly growing tumor. Both rats showed peribronchiolar mononuclear cell invasion; one of them had a small *in situ* tumor, bordered by an area containing mononuclear cells and fibrosis (Fig. 7*c*).

DISCUSSION

In this study we have implanted cultured human cancer cell lines intrabronchially into Rowett nude rats to explore the utility of these rats for growing orthotopic human lung cancer xenografts. The effect of additional immunosuppression was examined for three cell lines: a large-cell carcinoma (NCI-H460) and two adenocarcinomas (NCI-H125 and A549). Prior treatment with 500 rads of γ-radiation resulted in take-rates

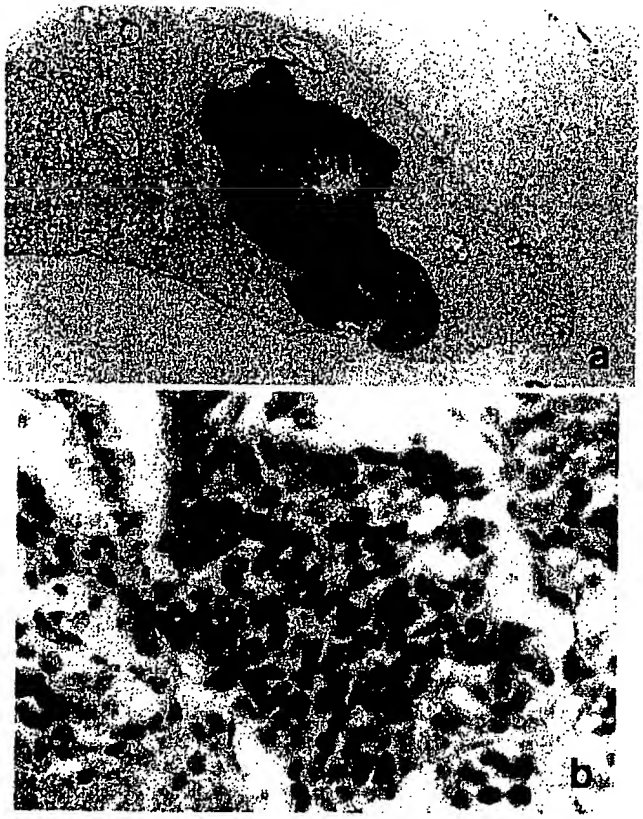

Fig. 6. Light micrographs of an 11-week-old, H & E-stained, right caudal lobe tumor arising from i.b. implantation of NCI-H345 cells. *a*, local parenchymal growth of a tumor with very little necrosis. × 9. *b*, small cancer cells with small nuclei and salt-and-pepper chromatin typical of a small-cell carcinoma. × 350.

above 82% for all three cell lines. Without irradiation, take-rates were below 34% for the two adenocarcinomas. All tumors examined had a cytology and histology consistent with those of the parent tumors from which the cell lines were derived. Each type of tumor showed distinct growth patterns and rates; none showed any evidence of immunological rejection. Some NCI-H125- and A549-derived tumors metastasized within the thorax. In nonirradiated rats in which gross evidence of tumor was lacking, peribronchial fibrosis and/or mononuclear cell infiltration were seen in the right caudal lobe.

The relative order of take-rates in nonirradiated rats (NCI-H460 > A549 > NCI-H125; Table 1) was the same as the relative order of growth rates in irradiated rats (Fig. 2). This suggests that the growth rate may be the major factor determining take-rates in nonirradiated Rowett nude rats, but cell line-specific factors such as antigenicity could also be important. Take-rates for s.c. injections of human tumor material are also dependent on the cell or tissue type implanted (20–24).

Evidence presented here that whole-body irradiation significantly increased i.b. lung tumor take-rates (Table 1) is also consistent with previous reports showing increased take-rates for s.c. tumor xenografts after irradiation in either nude rats or mice (26, 28). The mechanism by which irradiation facilitates ectopic and orthotopic tumor establishment in nude rodents is not precisely known. Since natural killer cells, macrophages, and plasma cells are relatively resistant to such treatment, it seems more likely that damage to some B- or "T-like" cell population might be relevant (for a discussion, see Ref. 29). Regardless of the mechanism involved, our high take-rates suggest that Rowett nude rats, irradiated 2 to 6 hours before cell implantation, are a practical animal model for the i.b. growth of a variety of human lung cancer cell lines.

Microscopic analysis of these orthotopic lung tumors showed both histological and cytological characteristics consistent with the tumor from which the cell line was originally derived (Figs. 3–6). Others have shown that tumors or cell lines implanted s.c. into nude rats also maintain an appearance similar to that of the parent tumor (20, 23, 25, 30–31), although stromal differences, especially tumor encapsulation, are frequently seen in s.c. but not orthotopic tumor xenografts (14–16).

Fig. 7. Light micrographs of H & E-stained, right caudal lung lobes of nonirradiated rats showing evidence of mononuclear cell infiltration and/or fibrosis without gross tumor. *a*, peribronchiolar mononuclear cell infiltration (*arrows*) 10 weeks after NCI-H125 cell implantation. × 40. *b*, area adjacent to an airway 5 weeks after A549 cell implantation. × 40. Immediately below the airway epithelium is an area of fibrosis (*F*); nearby airway smooth muscle (*arrows*) with associated mononuclear cells. *c*, lung tissue taken 2 weeks after implantation of NCI-H125 cells reveals a small *in situ* tumor (*arrows*) next to normal airway epithelium; below the tumor and epithelium is an area of fibrosis and mononuclear cell infiltration. × 250.

Unlike ectopic tumors previously described in the s.c. nude rat model (21, 25, 26, 30), two of our orthotopic tumor types (NCI-H125 and A549) exhibited metastasis. Both cell lines gave rise to regional lymph node metastases in about half of the rats examined; in addition, left lung metastases were also found in rats with NCI-H125 cell-derived tumors. The notable lack of metastasis in s.c. tumor-bearing nude rats suggests that the orthotopic nature of our tumors is the important variable. Enhancement of metastasis in orthotopic as compared to s.c. tumor models has previously been reported in nude mice (13–17).

In contrast, the two NCI-H345 small-cell carcinoma tumors studied showed no evidence of metastatic spread. These tumors also grew more slowly than the other lung cancer cell lines. Since in humans small-cell carcinomas grow rapidly and metastasize quickly (32), our limited evidence suggests that this cell line implanted i.b. in nude rats is not an optimal model for its human correlate.

Tumor growth rates in this study varied over a wide range (Fig. 2) in the order NCI-H460 > A549 > NCI-H125 > NCI-H345. This rank order seems to conflict with mortality data from i.b.-implanted nude mice (11), which showed H125-derived tumors to be at least as rapidly lethal as the H460 and A549 cell lines. Whether this was due to interspecies variation, interlaboratory cell line differences, or both, is unknown.

Within this study, the growth rates and the degree of necrosis seen in each type of tumor (as estimated histologically) appeared to be directly related. The rapidly growing NCI-H460 and A549 exhibited much more necrosis than the more slowly growing NCI-H125 and NCI-H345 tumors. This difference may simply be due to tumor cell growth outstripping neovascularization in the rapidly growing tumors, but it could also be influenced by cell line-related differences in the release of angiogenic factors. It should be noted that the tumor characteristics observed in this study resulted from growth from 10^7 implanted cells. It is possible that injection of fewer cells might result in less necrotic and better vascularized tumors with or without a different growth pattern. The relatively large number of cells used was selected primarily to maximize take rates, since McLemore *et al.* (11, 12) have shown i.b. mortality (presumably reflecting take-rates) to be cell dose-related in nude mice.

Histological examination of the lungs of nonirradiated rats without gross evidence of tumors, at a time when large tumors could be expected in irradiated rats, revealed findings consistent with immunological rejection, *i.e.*, local fibrosis and/or mononuclear cell infiltration (Fig. 7, *a* and *b*). Since none of the tumor-bearing rats we examined histologically exhibited these characteristics, our findings suggest both that immunological rejection is the primary reason for lack of tumor take in nonirradiated rats and that irradiation eliminated this immune response. Further evidence for such a response is the presence of mononuclear cells and fibrosis directly associated with the small *in situ* NCI-H125 tumor 2 weeks after implantation in a nonirradiated rat (Fig. 7*c*).

The reason for take rates of less than 100% in irradiated rats implanted with NCI-H125 and A549 cells is unknown but could be due to immune recovery in some of the rats, more stringent growth requirements of these cell lines, incomplete expulsion of the tumor cells in the implantation syringe, or accidental mechanical dislodging of the implanted cells from their caudal lobe implantation site.

Previous studies of human tumor tissue s.c. xenografts in nude rats have shown that most tumor grafts tend to regress after reaching a certain size or age (20–26), presumably due to immunological rejection (24). Such a tendency was not evident in this study. In fact, rats bearing the rapidly growing NCI-H460 and A549 tumors invariably died of their tumors if they were not euthanized. Moreover, although we have not attempted to follow survival of rats bearing the more slowly growing NCI-H125 and NCI-H345 tumors past 10–12 weeks of tumor age, the age *versus* weight profile of the NCI-H125 tumor-bearing rats suggests progressive growth up to this time in rats with established tumors. It is unclear why none of the tumor types in this study regressed; both an orthotopic location and prior irradiation of the rats may be important factors. In one study (26), s.c. liver tumors in nude rats given 600 rads of X-rays 10 days before cell implantation still showed a tendency to regress after 30–50 days. This suggests either that progressive tumor growth in nude rats requires both orthotopic implantation and irradiation or that irradiation 10 days before implanting cancer cells may be a less effective method of immunosuppression than our protocol.

In summary, we have shown that 4 different human lung cancer cell lines, representing 3 different histological types of cancer, will grow when orthotopically implanted into irradiated Rowett nude rats. The histological and cytological characteristics of the different histological types were distinct and consistent with their tissues of origin; two of them exhibited metastatic behavior within the thorax. Progressive growth was maintained in all three of the cell lines in which growth rates were studied and up to 10 weeks of tumor age in the most slowly growing of the three tumor types. Our data suggest that the irradiated Rowett nude rat should be useful for biological and preclinical studies of orthotopic model human lung cancers. The larger size of nude rats *versus* nude mice should make the rat model particularly useful for *in vivo* applications in which complicated surgery, repeated blood sampling, or large volumes of tumor are required. Larger lungs also make the rat model particularly advantageous for *ex vivo* lung perfusion studies.

ACKNOWLEDGMENTS

We thank Drs. J. Minna, A. Gazdar, and J. Mayo for supplying most of the cell lines used in this study. We also thank Carol Williams for help with typing the manuscript.

REFERENCES

1. Silverberg, E. Cancer statistics, 1985. CA Cancer J. Clin., *35:* 19–35, 1985.
2. Horm, J. W., Asire, A. J., Young, J. L., and Pollack, E. S. SEER Program: Cancer Incidence and Mortality in the United States, 1973–1981. NIH Publication 85-1837. Bethesda, MD: Department of Health and Human Services, 1984
3. Loeb, L. A., Ernster, V. L., Warner, K. E., Abbotts, J., and Laszlo, J. Smoking and lung cancer: an overview. Cancer Res., *44:* 5940–5958, 1984.
4. American Cancer Society. 1986 Facts and Figures, pp. 1–32. New York: American Cancer Society, 1986.
5. Fidler, I. J. Rationale and methods for the use of nude mice to study the biology and therapy of human cancer metastasis. Cancer Metastasis Rev., *5:* 29–49, 1986.
6. Rygaard, J., and Poulsen, C. O. Heterotransplantation of a human malignant tumor to "nude" mice. Acta Pathol. Microbiol. Scand., *77:* 758–760, 1969.
7. Sharkey, F. E., and Fogh, J. Considerations in the use of nude mice for cancer research. Cancer Metastasis Rev., *3:* 341–360, 1984.
8. Aamdal, S., Fodstad, O., and Pihl, A. Human tumor xenografts transplanted under the renal capsule of conventional mice. Growth rates and host immune response. Int. J. Cancer, *34:* 725–730, 1984.
9. Aamdal, S., Fodstad, O., and Pihl, A. Methodological aspects of the 6-day subrenal capsule assay for measuring response of human tumors to anticancer agents. Anticancer Res., *5:* 329–338, 1985.
10. Bogden, A. E., Haskell, P. M., LePage, D. J., Kelton, D. E., Cobb, W. R., and Esber, H. J. Growth of human tumor xenografts implanted under the

renal capsule of normal immunocompetent mice. Exp. Cell Biol., *47:* 281–293, 1979.
11. McLemore, T. L., Liu, M. C., Blacker, P. C., Gregg, M., Alley, M. C., Abbot, B. J., Shoemaker, R. H., Bohlman, M. E., Litterst, C. C., Hubbard, W. C., Brennan, R. H., McMahon, J. B., Fine, D. L., Eggleston, J. C., Mayo, J. G., and Boyd, M. R. Novel intrapulmonary model for orthotopic propagation of human lung cancers in athymic nude mice. Cancer Res., *47:* 5132–5140, 1987.
12. McLemore, T. L., Eggleston, J. C., Shoemaker, R. H., Abbott, B. J., Bohlman, M. E., Liu, M. C., Fine, D. L., Mayo, J. G., and Boyd, M. R. Comparison of intrapulmonary, percutaneous intrathoracic, and subcutaneous models for the propagation of human pulmonary and nonpulmonary cancer cell lines in athymic nude mice. Cancer Res., *48:* 2880–2886, 1988.
13. Shapiro, W. R., Basler, G. A., Chernik, N. L., and Posner, J. B. Human brain tumor transplantation into nude mice. J. Natl. Cancer Inst., *62:* 447–453, 1979.
14. Cornil, I., Man, S., Fernandez, B., and Kerbel, R. S. Enhanced tumorigenicity, melanogenesis, and metastases of a human malignant melanoma after subdermal implantation in nude mice. J. Natl. Cancer Inst., *81:* 938–944, 1989.
15. Morikawa, K., Walker, S. M., Nakajima, M., Pathak, S., Jessup, J. M., and Fidler, I. J. Influence of organ environment on the growth, selection and metastasis of human colon carcinoma cells in nude mice. Cancer Res., *48:* 6863–6871, 1988.
16. Naito, S., von Eschenbach, A. C., and Fidler, I. J. Different growth pattern and biologic behavior of human renal cell carcinoma implanted into different organs of nude mice. J. Natl. Cancer Inst., *78:* 377–385, 1987.
17. Tan, M. H., and Chu, T. M. Characterization of the tumorigenic and metastatic properties of a human pancreatic tumor cell line (ASPC-1) implanted orthotopically into nude mice. Tumor Biol., *6:* 89–98, 1985.
18. Vezeridis, M. P., Doremus, C. M., Tibbetts, L. M., Tzanakakis, G., and Jackson, B. T. Invasion and metastasis following orthotopic transplantation of human pancreatic cancer in the nude mouse. J. Surg. Oncol., *40:* 261–265, 1989.
19. Naito, S., von Eschenbach, A. C., Giavazzi, R., and Fidler, I. J. Growth and metastasis of tumor cells isolated from a human renal cell carcinoma implanted into different organs of nude mice. Cancer Res., *46:* 4109–4115, 1986.
20. Festing, M. F. W., May, D., Connors, T. A., Lovell, D., and Sparrow, S. An athymic nude mutation in the rat. Nature (Lond.), *274:* 365–366, 1978.
21. Colston, M. J., Fieldsteel, A. H., and Dawson, P. J. Growth and regression of human tumor cell lines in congenitally athymic (*rnu/rnu*) rats. J. Natl. Cancer Inst., *66:* 843–848, 1981.
22. Drewinko, B., Moskwa, P., Lotzova, E., and Trujillo, J. M. Successful heterotransplantation of human colon cancer cells to athymic animals is related to tumor cell differentiation and growth kinetics and to host natural killer cell activity. Invasion Metastasis, *6:* 69–82, 1986.
23. Linden, C. J., and Johansson, L. Progressive growth of a human pleural mesothelioma xenografted to athymic rats and mice. Br. J. Cancer, *58:* 614–618, 1988.
24. Maruo, K., Ueyama, Y., Kuwahara, Y., Hioki, K., Saito, M., Nomura, T., and Tamaoki, N. Human tumour xenografts in athymic rats and their age dependence. Br. J. Cancer, *45:* 786–789, 1982.
25. Stragand, J. J., Drewinko, B., Henderson, S. D., Grossie, B., Stephens, L. C., Barlogie, B., and Trujillo, J. M. Growth characteristics of human colonic adenocarcinomas propagated in the Rowett athymic rat. Cancer Res., *42:* 3111–3115, 1982.
26. Shouval, D., Schuger, L., Levij, I. S., Reid, L. M., Neeman, Z., and Shafritz, D. A. Comparative morphology and tumourigenicity of human hepatocellular carcinoma cell lines in athymic rats and mice. Virchows Archiv. A Pathol. Anat. Histopathol., *412:* 595–606, 1988.
27. Giard, D. J., Aaronson, S. A., Todaro, G. J., Arnstein, P., Kersey, J. H., Dosik, H., and Parks, W. P. *In vitro* cultivation of human tumors: establishment of cell lines derived from a series of solid tumors. J. Natl. Cancer Inst., *51:* 1417–1423, 1973.
28. Prehn, O. M., and Outzen, H. C. Primary tumor immunity in nude mice. Int. J. Cancer, *19:* 688–691, 1977.
29. Farnsworth, A., Wotherspoon, J. S., and Dorsch, S. E. Postirradiation recovery of lymphoid cells in the rat. Transplantation (Baltimore), *46:* 418–425, 1988.
30. Davies, G., Duke, D., Grant, A. G., Kelly, S. A., and Hermon-Taylor, J. Growth of human digestive tumour xenografts in athymic nude rats. Br. J. Cancer, *43:* 53–58, 1981.
31. Matthews, P. N., Grant, A. G., and Hermon-Taylor, J. The growth of human bladder and kidney cancers as xenografts in nude mice and rats. Urol. Res., *10:* 293–299, 1982.
32. Feld, R., Ginsberg, R. J., and Payne, D. G. Treatment of small cell lung cancer. *In:* J. A. Roth, J. C. Ruckdeschel, and T. H. Weisenburger (eds.), Thoracic Oncology, pp. 229–263. Philadelphia: W. B. Saunders Company, 1989.

Vol. 4, 887–894, April 1998

An Orthotopic Model of Human Pancreatic Cancer in Severe Combined Immunodeficient Mice: Potential Application for Preclinical Studies[1]

Ramzi M. Mohammad, Ayad Al-Katib, George R. Pettit, Vainutis K. Vaitkevicius, Urwashi Joshi, Volkan Adsay, Adhip P. N. Majumdar, and Fazlul H. Sarkar[2]

Division of Hematology and Oncology [R. M. M., A. A-K., V. K. V.], Division of Gastroenterology, Department of Internal Medicine [A. P. N. M.] and Department of Pathology [U. J., V. A., F. H. S.], Wayne State University School of Medicine, Karmanos Cancer Institute, Detroit, Michigan 48201, and Cancer Research Institute and Department of Chemistry, Arizona State University, Tempe, Arizona 85287 [G. R. P.]

ABSTRACT

Pancreatic adenocarcinoma is one of the most incurable and least understood of all human cancers. It is the fourth leading cause of cancer-related mortality in males (after lung, prostate, and colon) and in females (after lung, breast, and colon) in the United States with <2–3% of patients surviving >5 years. In an attempt to search for more effective therapies for this disease, we report here, for the first time, an effective treatment, the combination of gemcitabine and auristatin-phenethylamine (PE), against an orthotopic implantation of a human pancreatic adenocarcinoma cell line (HPAC) in severe combined immunodeficient (SCID) mice. Tumor implantation was performed by injecting 100 μl of the HPAC cell suspension (1×10^6 cells) directly into the pancreas of 5-week-old SCID mice. After implantation, tumor formation was checked twice a week. All palpable tumors were detected within 21 days (100% take rate), and tumors were confirmed histologically to be pancreatic adenocarcinoma. For the subsequent efficacy trial, tumor-bearing SCID mice were randomized into four groups with five mice in each group. One served as a control, the second received gemcitabine alone (2.5 mg/kg/injection i.p.), the third received auristatin-PE alone (2.0 mg/kg/injection i.v.), and the fourth group received the combination of gemcitabine (i.p.) and auristatin-PE (1.5 mg/kg/injection i.v.). All animals were euthanized 7 days after the completion of their treatments, and the pancreases were resected. Histological examination revealed the tumors to be adenocarcinoma. The tumors were composed of diffuse sheets of cells interrupted by glandular spaces containing secretory material. Cytologically, the tumor cells were large, pleomorphic, and hyperchromatic. Many cells contained intracellular lumina containing mucin. Immunohistochemical studies showed strong $p21^{WAF1}$ (p21) expression but no immunoreactivity with p53 and Her-2/neu antibodies. The mean pancreatic weight in the gemcitabine/auristatin-PE combination group was significantly ($P = 0.014$) lower (0.84 ± 0.639 g) when compared with those of the control (2.91 ± 1.19 g) and gemcitabine alone (1.84 ± 0.796 g; $P = 0.064$) groups. In addition, the mean weight in the combination group approached statistical significance when compared with the auristatin-PE group alone (1.16 ± 0.635 g; $P = 0.028$). We conclude that the combination of gemcitabine and auristatin-PE is an effective treatment against HPAC tumors in this xenograft model and more effective than treatment with either gemcitabine or auristatin-PE alone and could be considered for future animal studies with pancreas cancer and/or for human clinical trials.

INTRODUCTION

Adenocarcinoma of the pancreas is presently estimated to be the fourth leading cause of cancer death for males (after lung, prostate, and colon) and females (after lung, breast, and colon) in the United States (1–3), with an average survival of approximately 6 months (4). Its etiology is unknown, and no generally effective treatment is presently available. Overall, the incidence is decreasing in whites and increasing in blacks, especially in black females, with probability of death reaching 95%. Present treatment of localized adenocarcinoma of the pancreas is limited to surgical and chemo-radiotherapeutic options; however, these options have not made a significant impact on the course of this disease. Less than 2–5% of patients are alive at 5 years. Systemic chemotherapy usually consists of 5-fluorouracil or 5-fluorouracil-containing regimens (5, 6). However, none of these therapies are effective (curative). Newer chemotherapeutic agents such as gemcitabine hydrochloride (2′,2′-difluorodeoxycytidine) have shown antitumor activity against a variety of solid tumors (7, 8), including pancreatic tumors, but the prognosis and overall survival remain poor. For example, a recently completed Phase II trial of gemcitabine in 5-fluorouracil-refractory cancer showed a response rate of only 27%, with median

Received 8/5/97; revised 11/24/97; accepted 1/16/98.

The costs of publication of this article were defrayed in part by the payment of page charges. This article must therefore be hereby marked *advertisement* in accordance with 18 U.S.C. Section 1734 solely to indicate this fact.

[1] This work was substantially supported by the Marlin Pemberton Memorial Fund for Pancreatic Cancer Research established at the Karmanos Cancer Institute, a generous grant from Eli Lilly Co., and the Outstanding Investigator Award CA-443440-1A1-09 (to G. P.) awarded by the division of Cancer Treatment, Diagnosis and Centers, National Cancer Institute, Department of Health and Human Services, and the Arizona Control Research Commission.

[2] To whom requests for reprints should be addressed, at Department of Pathology, Wayne State University School of Medicine, 9374 Scott Hall, 540 East Canfield Avenue, Detroit, Michigan 48201. Phone: (313) 745-1418; Fax: (313) 745-9299; E-mail: fsarkar@med.wayne.edu.

Table 1 Efficacy of gemcitabine and its combination with auristatin-PE in orthotopic xenografts of the HPAC cell line

Agent	Dose (mg/kg/injection)	Route	No. of animals	No. of injections	Weight ± SD (g)	Range (g)
Diluent	0.0	i.p.	5	10	2.91 ± 1.19	1.4–4.3
Gemcitabine	2.5	i.p.	5	10	1.84 ± 0.796 ($P = 0.15$)	0.9–2.8
Auristatin-PE	2.0	i.v.	5	3	1.16 ± 0.635 ($P = 0.028$)	0.6–2.2
Gemcitabine + Auristatin-PE	2.5 + 1.5	i.p. + i.v.	5	10 + 3	0.84 ± 0.639 ($P = 0.014$)	0.3–1.9

duration of 14 weeks and median survival of 3.85 months (9). Therefore, the search for new therapies continues.

As part of the National Cancer Institute natural products program, a number of novel agents with anti-solid tumor activity derived from marine products have been identified. The dolastatins represent one such group of novel agents. Dolastatin 10 was isolated from the shell-less marine mollusk *Dolabela auricularia* (sea hare) in 1984 and reported in 1987 (10). It is a linear tetrapeptide (with three unique amino acids) linked to a complex primary amine (11) that interacts with tubulin to inhibit microtubule polymerization (12). Auristatin-PE is a structural analogue of dolastatin 10 with the dolaphenine unit substituted with PE[3] (13).

s.c. implantation of human pancreatic cancer cell line in SCID or nude mice has proven useful in the study of the preclinical efficacy of novel therapeutic agents *in vivo*. Although most human malignant tumors grow well as xenografts in nude or SCID mice in the s.c. site, they seldom metastasize, despite their malignant characteristics (14, 15). To mimic the pattern of local growth of pancreatic cancer in the pancreas organ, the implantation of human pancreatic tumor cell line in the pancreas of nude mice (orthotopic implantation) was found to reproduce local and distal dissemination (16–18) with a 100% take rate and retention of tumor metastatic behavior in 50–100% of nude mice (19, 20). However, an orthotopic model of human pancreatic cancer in the SCID mouse has not been documented.

In this study, we investigated the antitumor effect of gemcitabine and its combination with auristatin-PE in a SCID mouse orthotopic xenograft model using the HPAC cell line.

MATERIALS AND METHODS

Cell Line and Culture. The HPAC (21) cell line used in this study was obtained from American Type Culture Collection (Bethesda, MD). The cell line was cultured in DMEM:F12 (1:2) medium supplemented with 5% fetal bovine serum, 15 mM HEPES, 2 μg/ml insulin, 5 μg/ml transferrin, 40 ng/ml hydrocortisone, and 10 ng/ml epidermal growth factor. The HPAC cells were incubated in a humidified 5% CO_2 incubator at 37°C. The medium was replaced with fresh medium as needed, and cells were maintained by serial passaging after trypsinization.

Tested Agents. Auristatin-PE is a new structural modification of dolastatin 10, which was isolated from the sea hare *Dolabela auricularia* (10). Auristatin-PE was dissolved in DMSO at 3–10 mg/ml, and it was used at either 2.0 mg/kg/injection i.v. or 1.5 mg/kg/injection i.v. Gemcitabine (Eli Lilly & Co., Indianapolis, IN) was used at 2.5 mg/kg/injection i.p.

Laboratory Animals. Five-week-old female ICR-SCID mice weighing 20–22 g were obtained from Taconic Laboratory (Germantown, NY) and used to develop an orthotopic model bearing the HPAC cells. The mice were acclimatized and housed in a sterile environment where cages, bedding, food, and water were autoclaved.

Orthotopic Model. HPAC cells were suspended in serum-free RPMI 1640 at a concentration of 10^7 cells/ml. The viability of the cells was >90%. Five SCID mice were used to determine the take rate. General anesthesia was performed using ketamine (70 mg/kg i.p.) + xylazine (6 mg/kg i.p.). A left lateral laparotomy was performed, and the spleen and distal pancreas were mobilized. Approximately 100 μl of the HPAC cell suspension (~10^6 cells) were injected into the pancreas. The abdominal incision was closed using a surgical staple, and analgesia was administered for immediate pain relief. After implantation, the SCID mice were inspected daily for 1 week for any bleeding or wound complications and were checked for tumor formation twice a week by palpation. Palpable tumors were detected after 21 days in all of the mice (100% take rate) and were confirmed histologically to be pancreatic adenocarcinoma.

Histological Characterization of HPAC Cells. Tumors grown in the pancreas of untreated SCID mice were excised, fixed in formalin, and embedded in paraffin. Five-μm tissue sections were obtained and stained with H&E for routine microscopic examination. Mucicarmine histochemical stain was used to determine the presence of mucin production by the tumor cells.

Immunohistochemistry was performed using antibodies to Her-2/neu (Zymed, San Francisco, CA; 1:10 dilution), $p21^{WAF1}$ (Oncogene Research Products, Cambridge, MA; 1:10 dilution), and p53 (D07; Vector Laboratories, Burlingame, CA; 1:100 dilution) to investigate the expression of these growth factor receptor and cell cycle regulators. For immunohistochemical staining, 5-μm sections from formalin-fixed, paraffin-embedded tissues were mounted on sialinized slides and incubated in a 60°C oven for 60 min. The sections were deparaffinized in xylene, rehydrated in 100% and 95% ethanol, respectively, dipped in 3% hydrogen peroxide to block endogenous peroxidases, and microwaved in a 1-liter citrate buffer for antigen retrieval. The slides were then rinsed in water and in buffered horse serum solution for 10 min to block nonspecific protein binding and subsequently incubated with appropriate antibodies

[3] The abbreviations used are: PE, phenethylamine; SCID, severe combined immunodeficient; HPAC, human pancreatic adenocarcinoma.

at room temperature for 30 min, rinsed three times with modified PBS, and reincubated with biotinylated secondary antibody, rinsed again, and incubated with avidin-peroxidase solution for 20 min at room temperature. Finally, the slides were rinsed in water, stained in AEC substrate solution for 20 min, counterstained with hematoxylin for 3–5 min, and blued in ammonia water (0.2% ammonium hydroxide) for 10 s.

Efficacy Trial Design. For the subsequent drug efficacy trials, the mice were randomly removed and assigned to four treatment groups after 7 days from implantation (before implanted cells developed into palpable tumors) as shown in Table 1. Five mice served as the control, and five mice were treated with gemcitabine (2.5 mg/kg/injection) given i.p. daily 5 days/week for 2 weeks. The third group was treated with auristatin-PE alone (2.0 mg/kg/injection) given i.v. (via the tail vein) every other day for a total of three injections, and the fourth group was treated with the combination of gemcitabine (i.p.) plus auristatin-PE at 1.5 mg/kg/injection (Table 1). Doses were determined based on previous studies with these agents (22). It is important to note that the drug doses of auristatin-PE were reduced from 2.0 mg/kg/injection to 1.5 mg/kg/injection for combination treatment to avoid toxicity. All animals were euthanized 1 week after the completion of the treatment. The whole pancreas containing tumors were surgically removed from all animals, and their weights were recorded. Tumors were divided into two halves; one-half was frozen, and the other half was fixed in neutral buffered formalin for pathological examination.

RESULTS

Establishment and Characterization of the HPAC Orthotopic Xenografts. All SCID mice, injected (implanted) with HPAC cells, developed palpable tumors (100% take rate) within 21 days after implantation (Fig. 1), which were found to be adenocarcinoma. The tumors excised from the mice were examined initially under routine light microscopy. Histologically, the tumor cells formed viable nodular masses with variable sizes. They were relatively well circumscribed with pushing borders, compressing the adjacent pancreas (Fig. 2*A*). Uninvolved spleen and pancreas were unremarkable, with no evidence of local or distant metastases. The tumors were composed of diffuse sheets of cells, frequently interrupted by glandular spaces that contained secretory material (Fig. 2*B*), a common finding in adenocarcinomas. Cytologically, the cells were large, pleomorphic, and hyperchromatic, and the chromatin was clumped and irregular, all features of malignant cells. Many cells contained intracellular lumina containing mucin as shown by the Mucicarmine stain (Fig. 3*A*). This stain also highlighted the abundance of the glands within the tumor. In contrast, the tumors grown s.c. showed better differentiation, as reported in our previous study (22). They showed multilobular, cystic growth pattern with occasional villous, papillary projections. Cytologically, the cells were blend, elongated (cigar shaped), and well polarized. Chromatin was relatively fine, and the nucleoli were less prominent. They also had abundant cytoplasm. The overall appearance of these cells lining the cysts was more akin to that of intestinal-type adenocarcinoma (data not shown). The $p21^{WAF1}$ immunostaining of orthotopic tumors

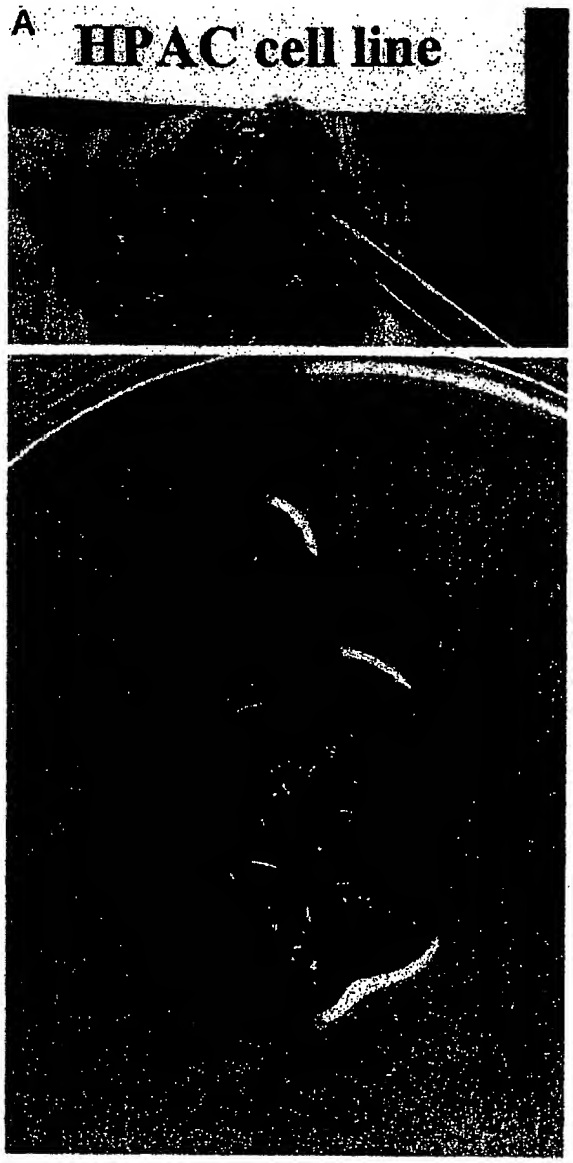

Fig. 1 *A*, the pancreas with tumor shown *in situ* during dissection from the animal. *B*, nodularity of the pancreas due to tumor.

showed strong and diffuse positivity of the tumor cell nuclei (Fig. 3*B*), whereas no immunoreactivity was observed for p53 and Her-2/neu.

Microscopic examination of the cell line grown in culture also showed sheets of epithelial cells with focal clumping, reminiscent of gland formation. In these foci of clumping, tumor cells also showed distinctive vacuolization of the cytoplasm (Fig. 4*A*), some of which contained mucin (Fig. 4*B*), as assessed by Mucicarmine stain, indicating glandular differentiation as indicated above.

Orthotopic Xenografts and *in Vivo* Drug Efficacy. Drug efficacy trials were conducted on orthotopic xenografts implanted with HPAC cells 7 days after surgery. Table 1 shows

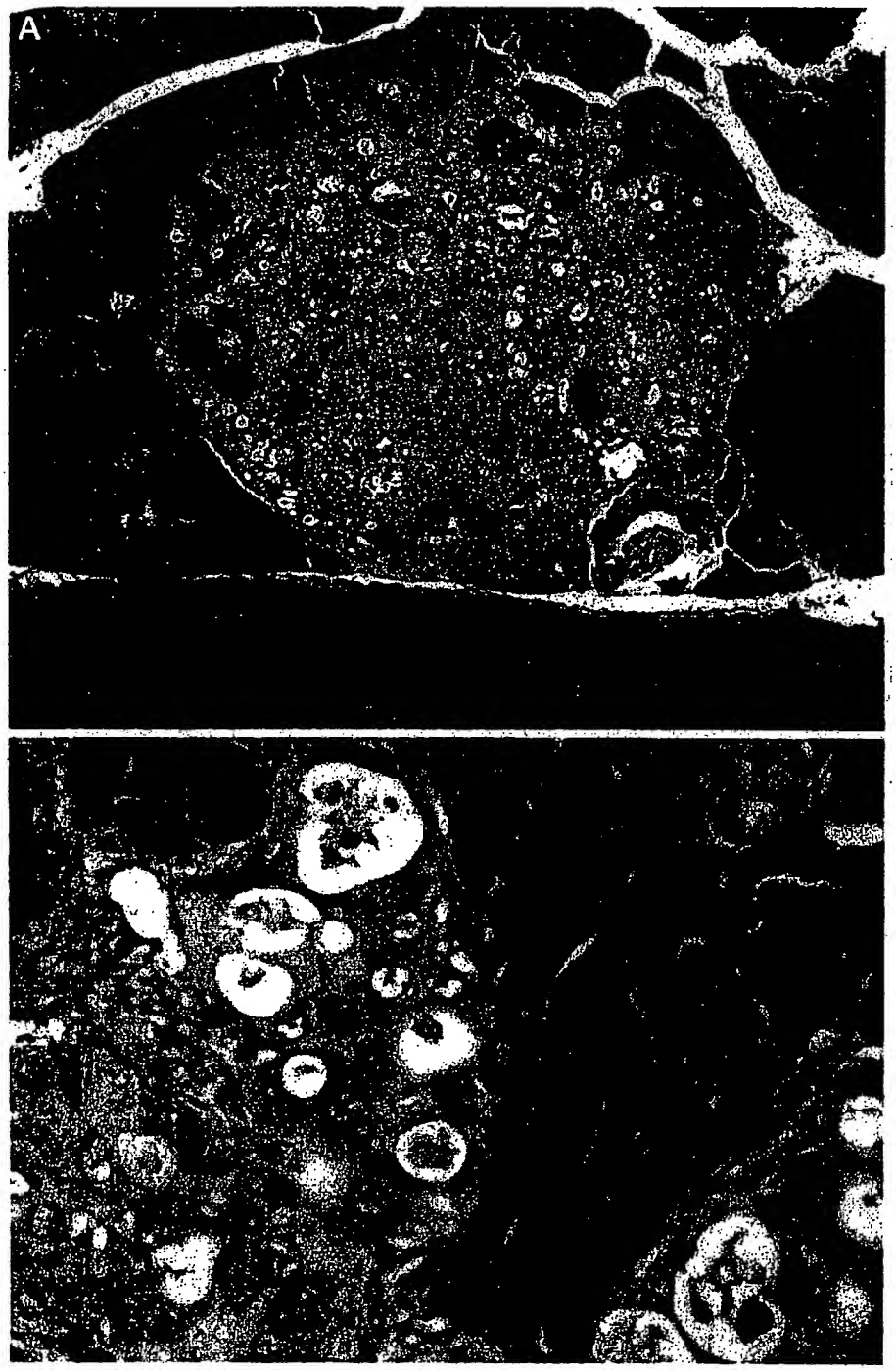

Fig. 2 *A*, a relatively circumscribed tumor mass situated in the pancreas and abutting the spleen. The tumor is formed of diffuse sheets of cells, with foci of glandular differentiation, represented by microcystic spaces that contain secretory material (*B*). The cells are large, hyperchromatic, and pleomorphic. Chromatin is vesicular and clumped, and prominent nucleoli are present. Some cells contain intracellular lumina.

the antitumor activity of gemcitabine, auristatin-PE, and their combinations, compared with that of the control mice (receiving only diluent), *in vivo*. Results indicate that gemcitabine inhibited the growth of the HPAC tumor significantly with mean tumor weight and SD of 1.84 ± 0.796 g ($P = 0.15$), compared with the control group 2.91 ± 1.19 g ($P = 0.028$). Similarly, the mean tumor weight in the auristatin-PE-treated group was lower (1.16 ± 0.635 g, $P = 0.028$) compared with untreated control. Moreover, when gemcitabine (i.p.) was administered with auristatin-PE (i.v.) in combination, the tumor weight significantly

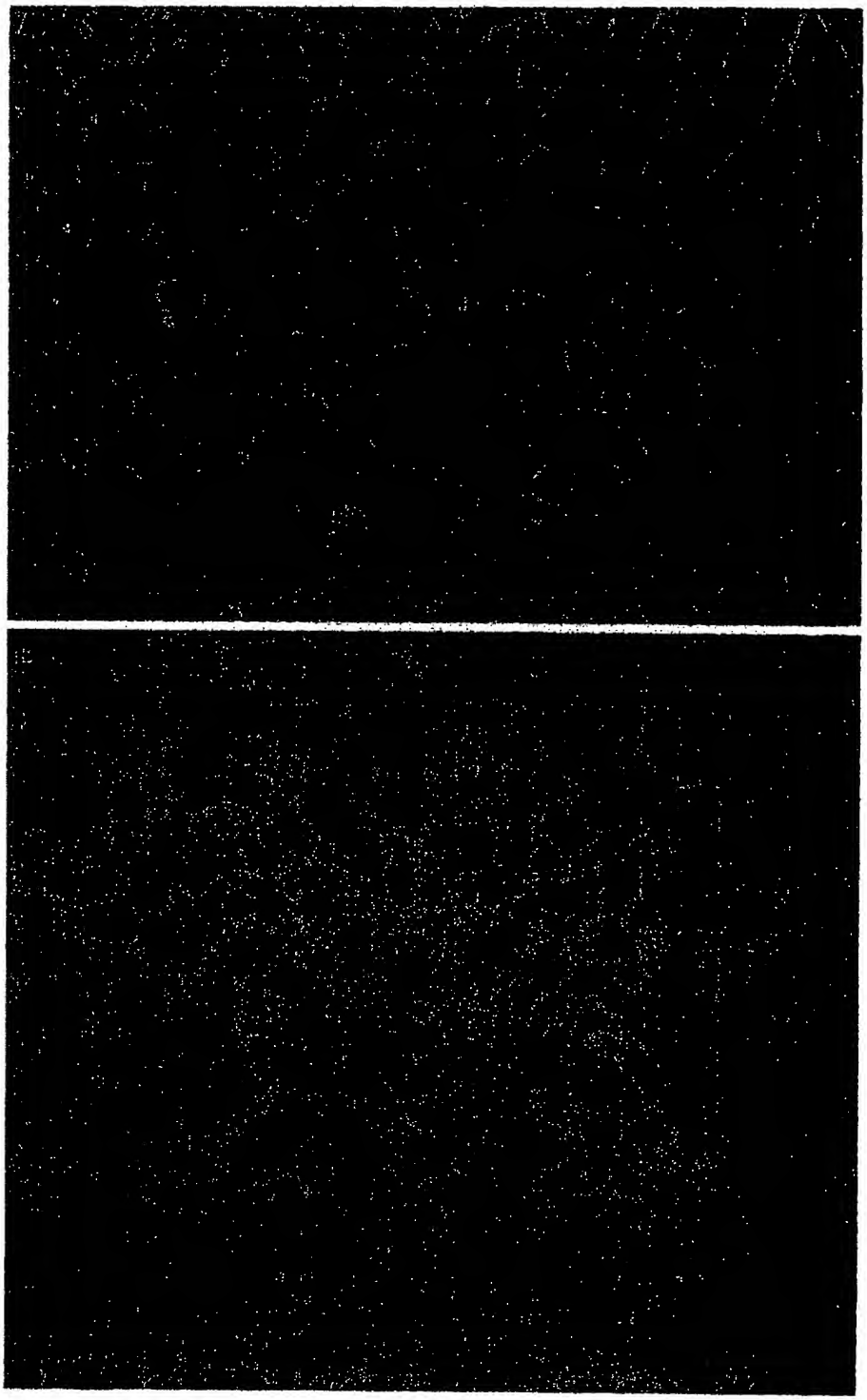

Fig. 3 *A*, Mucicarmine histochemical stain shows the glandular spaces, and intracellular lumina contain abundant mucin (*red*), a pathognomonic finding of adenocarcinomas. Adjacent acinar pancreatic tissue is devoid of mucin, as expected. *B*, immunohistochemical stain with p21 antibody shows strong and diffuse positivity (*brown*) of the tumor cell nuclei. Mitotic figures were prominent (*arrows*).

decreased to 0.84 ± 0.639 g ($P = 0.014$) when compared with the control, but it was statistically insignificant when compared with either gemcitabine alone ($P = 0.44$) or auristatin-PE alone ($P = 0.064$). It is important to note that the concentration of auristatin-PE was higher in the single-treatment group compared with the treatment combination group. Although there was a different range of tumor weights in controls (1.4–4.3 g), gemcitabine (0.9–2.8 g), auristatin-PE (10.6–2.2 g), and gemcitab-

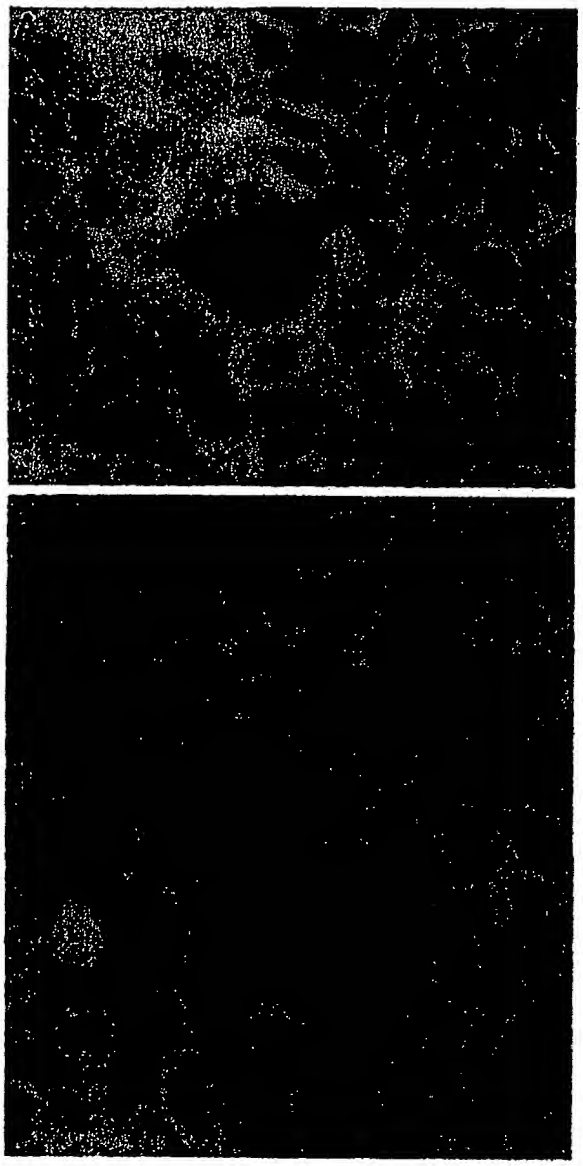

Fig. 4 This photomicrograph of the cell line shows a diffuse sheet of epithelial cells with focal clumping. At the center of the slide (*A*) is a large malignant cell with distinctive vacuolization of the cytoplasm, evidence of abortive glandular differentiation. Some cells in the clumped foci contain intracellular mucin (*B, arrow*), further evidence of glandular differentiation (adenocarcinoma; mucinous stain).

ine + auristatin-PE (0.3–1.9 g), the mean tumor volume was significantly reduced in the treatment combination group. It is important to note that the weight of a normal pancreas ranges from 0.25 to 0.35 g. These results provide preliminary evidence to support further studies in this animal model with metastatic pancreas cancer cells (our future studies are under way to establish an orthotopic model with either PANC-1, PAN-12, PANC-4, or our KCI-MOH1 cells) and opens the door for future clinical trials using the combination of gemcitabine with auristatin-PE.

DISCUSSION

In an attempt to search for more effective therapies for the cancer of the pancreas, we report the results of a preliminary study using a combination of gemcitabine and auristatin-PE against an orthotopic implantation of a HPAC cell line in a SCID mouse model. Gemcitabine given concurrently with auristatin-PE resulted in significantly higher antitumor activity compared with control or gemcitabine alone.

In this study, histological examination of all tumors from control and treated pancreas showed carcinoma (Fig. 2) with focal gland formation (Fig. 2B) and intracellular as well as luminal mucin production (Fig. 3*A*), characteristic features of adenocarcinomas, including pancreatic ductal adenocarcinoma. Microscopic examination of the cultured cell line also showed features of adenocarcinoma with focal vacuolization of the tumor cells (Fig. 4*A*) reminiscent of intracellular lumina (gland) formation and mucin-positive globules (Fig. 4*B*). The present study was designed to develop an orthotopic model in SCID mice with human pancreas cancer cells that grow in culture and show local growth when implanted in the orthotopic site without metastasis as a cleaner system prior to addressing the issue of metastasis. Therefore, these tumors did not show any local or distant metastases, which is due to the nature of the HPAC cell line rather than the orthotopic site. Similar observations have been reported recently by Reyes *et al.* (20). Although p53 and Her-2/neu were negative, $p21^{WAF1}$ showed diffuse and strong positivity (Fig. 3*B*) of the tumor cell nuclei, which correlates with the high-grade appearance of tumor cell nuclei (23). The tumors grown in the s.c. site, however, showed a different growth pattern and differentiation. Cyst and gland formations were much more prominent, and the cytology of the cells was of well-differentiated adenocarcinoma, as demonstrated earlier (22). In contrast, tumors grown orthotopically (Fig. 2) appeared poorly differentiated, strongly suggesting the effects of tropic factors in tumor growth.

The primary purpose of our study was to develop more effective treatment modalities by evaluating novel therapeutic agents against human pancreatic cancer using an orthotopic model. This model is believed to be more clinically relevant for drug evaluation compared with other models with the s.c. implantation of pancreatic cells. Although most malignant cells grow s.c. as xenografts in animals, they seldom metastasize, despite the malignant nature of the original human tumors (14, 15). Most of the orthotopic transplantation of human pancreatic cancer used either primary pancreatic carcinomas taken from patients or established cell lines to study local and distant metastases (14–20) in nude mice; however, no such studies are reported in SCID mice. Malignant human tumors implanted s.c. into SCID mice rarely metastasize; thus, it may not be a suitable model for drug efficacy trials prior to human therapy, although Marincola *et al.* (17) showed that adoptive immunotherapy with human lymphokine-activated killer cells and human recombinant interleukin 2 is an effective therapy against human pancreatic cancer growing s.c. in nude mice. Thus, the development of an orthotopic model of human pancreatic tumor is desirable, and

our preliminary results are very encouraging. Because most if not all human pancreas cancer show evidence of local or distant metastases at the time of diagnosis, orthotopic tumors of HPAC cells may not be the ideal model of human pancreas cancer. Similar results were also discussed in a recent report (20), where 50% of the primary tumors implanted orthotopically showed local and distal metastases, although all tumors used in this study caused disseminated disease in patients. Because the present study was designed to have a system without complications of metastases, our future studies will focus on the development of an orthotopic SCID mouse tumor model with human tumors that will show local and distant dissemination for clinical therapy prior to human clinical trials with novel chemotherapeutic agents.

Among the rapidly increasing number of marine invertebrate-derived antineoplastic agents against solid tumors, dolastatin 10 has been selected for future clinical development. Auristatin-PE is an improved analogue that is closely related structurally and in which the dolaphenine unit is replaced by a PE group (13). Dolastatin 10 is very effective in inhibiting tubulin polymerization at a lower concentration compared with vincristine (24) and has additional mechanisms of action on tubulin that are quite different from those caused by *Vinca* alkaloids (12, 25). Because of the promising preclinical data of gemcitabine and that of auristatin-PE (data not shown) against the KCI-MOH1 pancreatic xenograft model (22), we attempted to study the antitumor activity of gemcitabine alone, auristatin-PE alone, and their combinations in a SCID orthotopic model bearing HPAC tumors. Our data clearly reveal that auristatin-PE and gemcitabine alone inhibit the growth of the HPAC tumor significantly with a mean weight of the pancreas by about 60% (tumor weight of 1.16 ± 0.635 g and 1.84 ± 0.796 g in treated groups, respectively, *versus* 2.91 ± 1.19 g in the untreated control group). Moreover, when gemcitabine was administered (i.p.) concurrently with auristatin-PE (i.v.), the weight significantly decreased by 72% (0.84 ± 0.639 g in the treated group *versus* 2.91 ± 1.19 g in the control group), indicating a greater efficacy of the combination therapy.

An inherent question in any preclinical model is its relevance to the treatment of the actual human disease and whether animals with s.c. implantation respond to treatment differently than in the orthotopic implantation. Previously, our group (22) reported that gemcitabine treatment (2.5 mg/kg/injection) was active against a human pancreatic cell line (KCI-MOH1) implanted s.c. However, all animals bearing KCI-MOH1 tumors died after the 10th injection of auristatin-PE. In this study, we reduced the dose and changed the injection schedule of the auristatin-PE for both single and combination treatment groups. In addition, we chose to give gemcitabine i.p. rather than i.v., based on our many trial experiments where administration of gemcitabine and auristatin-PE i.v. with multiple injections caused severe technical difficulties (tail vein obstruction), and thus the experiments were terminated. It is well accepted that gemcitabine is an effective agent when administered i.p., which showed promising results in our present study. However, studies are under way in our laboratory to address this issue, and we should be able to design future studies to administer gemcitabine and auristatin-PE through i.v. injections to validate our preliminary results in this orthotopic model.

In conclusion, our preliminary data suggest that the combination of gemcitabine and auristatin-PE is an effective treatment against HPAC cells grown as xenografts in this SCID mouse model and that the combination treatment is more effective than treatment with gemcitabine or auristatin-PE alone. Undoubtedly, further animal studies are needed where orthotopic tumor size can be measured effectively (by magnetic resonance imaging or other imaging techniques) prior to therapy to establish the full efficacy of treatment in the survival of animals. In addition, orthotopic implantation of tumors from patients showing local and distal dissemination should be an ideal orthotopic model for evaluating novel therapeutic strategy for the successful treatment of human pancreatic tumors. Based on our preliminary results, we suggest that auristatin-PE could be considered for clinical trials in pancreatic cancer and might optimally be given in combination with gemcitabine. However, further chemotherapeutic studies are needed in this animal model using human tumor cell lines showing local and distant metastases prior to human therapy.

REFERENCES

1. Parker, S. L., Tong, T., Bolen, S., and Wingo, P. A. Cancer statistics. CA Cancer J. Clin., *47:* 5–27, 1997.

2. Gudjonnson, B. Carcinoma of the pancreas: 50 years of surgery. Cancer (Phila.), *60:* 2284–2303, 1987.

3. Warshaw, A. W., and Fernandez-del Castillo, C. Pancreatic carcinoma. N. Engl. J. Med., *326:* 455–465, 1992.

4. Lillemore, K. D. Current management of pancreatic carcinoma. Ann. Surg., *221:* 133–148, 1995.

5. Casper, E. S., and Kelson, D. P. Adenocarcinoma of the pancreas: overview of workup and management. Adv. Oncol., *11:* 17–22, 1995.

6. Kelly, D. M., and Benjamin, I. S. Pancreatic carcinoma. Ann Oncol., *6:* 19–28, 1995.

7. Hertel, L. W., Boder, G. B., Kroin, J. S., Rinzel, S. M., Poore, G. A., and Todd, G. C. Evaluation of the anti-tumor activity of gemcitabine (2′,2′-difluoro-2′-deoxycytidine). Cancer Res., *50:* 4417–4422, 1990.

8. Grindey, G. B., Hertel, L. W., and Plunkett, W. Cytotoxicity and anti-tumor activity of 2′,2′-difluoro-2′-deoxycytidine (gemcitabine). Cancer Invest., *8:* 313–318, 1990.

9. Rothenberg, M. L., Moore, M. J., Cripps, M. C., *et al.* A Phase II trial of gemcitabine in patients with 5-FU-refractory pancreas cancer. Ann. Oncol., *7:* 347–353, 1996.

10. Pettit, G. R., Kamano, Y., Herald, C. L., Tuinman, A. A., Boettner, F. E., Kizu, H., Schmidt, J. M., Baczynskyj, L., Tomer, K. B., and Bontems, R. J. The isolation and structure of a remarkable marine animal antineoplastic constituent: dolastatin 10. J. Am. Chem. Soc., *109:* 6883–6894, 1987.

11. Pettit, G. R. The dolastatins. *In:* W. Herz, G. W. Kirby, R. E. Moore, W. Steglich, and C. Tamm (eds.), Progress in the Chemistry of Organic Natural Products, pp. 2–63. New York: Springer, 1997.

12. Bai, R., Roach, M. C., Jayaram, S. K., Barkoczy, J., Pettit, G. R., Luduena, R. F., and Hamel, E. Differential effects of active isomers, segments, and analogs of dolastatin 10 on ligand interactions with tubulin. Correlation with cytotoxicity. Biochem. Pharmacol., *45:* 1503–1515, 1993.

13. Pettit, G. R., Srirangam, J. K., Barkoczy, J., Williams, M. D., Durkin, K. P., Boyd, M. R., Bai, R., Hamel, E., Schmidt, J. M., and Chapuis, J. C. Antineoplastic agents 337. Synthesis of dolastatin 10 structural modifications. Anti-Cancer Drug Design, *10:* 529–544, 1995.

14. Fogh, J., Orfeo, T., Tiso, J., Sharkey, F. E., Fogh, J. M., and Daniels, W. P. Twenty-three new human tumor lines established in nude mice. Exp. Cell Biol., *48:* 229–239, 1980.

15. Sordat, B. C., Ueyama, Y., and Fogh, J. Metastasis of tumor xenografts in the nude mouse. *In:* J. Fogh and B. C. Giovanella (eds.),

The Nude Mouse in Experimental and Clinical Research, Vol. 2, pp. 95–143. New York: Academic Press, 1982.

16. Vezeridis, M. P., Doremus, C. M., Tibbetts, L. M., Tznnakakis, G., and Jackson, B. T. Invasion and metastasis following orthotopic transplantation of human pancreatic cancer in the nude mouse. J. Surg. Oncol., *40:* 261–265, 1989.

17. Marincola, F. M., Drucker, B. J., Siao, B. Y., Hough, K. L., and Holder, W. D. The nude mouse as a model for the study of human pancreatic cancer. J. Surg. Res., *47:* 520–529, 1989.

18. Tan, M. H., and Chu, T. M. Characterization of the tumorigenic and metastatic properties of a human pancreatic tumor cell line (AsPc-1) implanted orthotopically into nude mice. Tumor Biol., *6:* 89–98, 1985.

19. Fu, X., Guadagni, F., and Hoffman, R. M. A metastatic nude-mouse model of human pancreatic cancer constructed orthotopically with histologically intact patient specimens. Proc. Natl. Acad. Sci. USA, *89:* 5645–5649, 1992.

20. Reyes, G., Villanueva, A., Garcia, C., Sancho, S. J., Piulats, J., Liuis, F., and Capella, G. Orthotopic xenografts of human pancreatic carcinomas acquire genetic aberrations during dissemination in nude mice. Cancer Res., *56:* 5713–5719, 1996.

21. Joshi, U. S., Dergham, S. T., Chen, Y. Q., Dugan, M. C., Crissman, J. D., Vaitkevicius, V. K., and Sarkar, F. H. Inhibition of pancreatic tumor cell growth in culture by $p21^{waf1}$ recombinant adenovirus. Pancreas, in press, 1998.

22. Mohammad, R. M., Dugan, M. C., Mohamed, A. N., Almatchy, V. P., Flake, T. M., Dergham, S. T., Shields, A. F., Al-Katib, A. M., Vaitkevicius, V. K., and Sarkar, F. H. Establishment of human pancreatic tumor xenograft model: potential application for preclinical evaluation of novel therapeutic agents. Pancreas, *16:* 19–25, 1998.

23. Dergham, S. T., Dugan, M. C., Joshi, U. S., Chen, Y. Q., Kucway, R., Du, W., Smith, D., Arlauskas, P., Crissman, J. D., Vaitkevicius, V. K., and Sarkar, F. H. The clinical significance of $p21^{WAF-1}$ and p53 expression in pancreatic adenocarcinoma. Cancer, *80:* 372–381, 1997.

24. Bai, R., Pettit, G. R., and Hamel, E. Dolastatin 10, a powerful cytostatic peptide derived from a marine animal. Inhibition of tubulin polymerization mediated through the *Vinca* alkaloid binding domain. Biochem. Pharmacol., *39:* 1941–1949, 1990.

25. Luduena, R. F., Roach, M. C., Prasad, V., and Pettit, G. R. Interaction of dolastatin 10 with bovine brain tubulin. Biochem. Pharmacol., *43:* 539–543, 1992.

Exhibit J

INFECTION AND IMMUNITY, Feb. 1978, p. 741-744
0019-9567/78/0019-0741$02.00/0

Vol. 19, No. 2
Printed in U.S.A.

Adult Mice as a Model for Early Onset Group B Streptococcal Disease

D. E. WENNERSTROM* AND R. W. SCHUTT

Department of Microbiology and Immunology, The University of Arkansas for Medical Sciences, Little Rock, Arkansas 72201

Received for publication 12 August 1977

The intravenous inoculation of adult mice with virulent group B streptococci serotype Ia resulted in fulminating sepsis with extensive colonization of the lungs and kidneys. The time course of the infection lasting 24 to 40 h, extensive pulmonary colonization, and resistance of the type Ia organism to phagocytosis in the absence of specific antibody suggest that mice are an appropriate model for the study of early onset streptococcal infection of human neonates.

Group B streptococci are recognized as major etiological agents causing infection of the newborn. One clinical syndrome produced by these organisms has been described as early onset infection, which is characterized by a rapidly fulminant sepsis with symptoms of respiratory distress and shock during the first 24 h after birth (3). It has a mortality rate that approaches 100% and is accompanied by significant pathological changes of the lungs, which include interstitial hemorrhage, pneumonia, pulmonary congestion, and intraalveolar gram-positive cocci (1, 3, 5).

Serotype Ia is the predominant organism causing the early onset syndrome (3). Klesius et al. have found that type Ia is seldom attacked by polymorphonuclear leukocytes from humans, baboons, or chimpanzees (6). Further, Mathews et al. have described a specific opsonizing antibody, which is required for the opsonization of type Ia, whereas the other types of group B streptococci were opsonized nonspecifically by human plasma (8). These investigations have suggested that fatal sepsis results when an exposed infant lacks phagocytic activity, opsonizing antibody, or type-specific agglutinins.

An animal model is needed for the systematic investigation of those factors of both the host and group B streptococci, which are determinants of the ability of these organisms to cause disease. The animal models that have been proposed have required exposure to large numbers of group B streptococci administered as aerosols to infant rats (T. Y. Sabet, P. L. Kelly, and E. N. Fox, Abstr. Annu. Meet. Am. Soc. Microbiol. 1977, B66, p. 26), rabbits (M. Sherman, E. Goldstein, W. Lippert, and R. Wennberg, Abstr. Annu. Meet. Am. Soc. Microbiol. 1977, B67, p. 26), or intravenously to adult mice (4). However, the organisms either failed to initiate a progressive infection or they initially decreased in the tissues. Therefore, it seemed reasonable to investigate the infection of mice by type Ia because Lancefield et al. have demonstrated that the type Ia organism can be made highly virulent for these animals (7).

Group B streptococci types Ia and III were a generous gift from R. C. Lancefield. Each organism was grown in Todd-Hewitt broth and then passaged 10 times in male BALB/c mice weighing 20 to 25 g, as described by Lancefield et al. (7). The subsequent intraperitoneal 50% lethal doses of the Ia and III types in 0.5 ml of saline were 17.0×10^0 colony-forming units (CFU) and 1.9×10^8 CFU, respectively.

Figure 1 shows the growth curve of the virulent type Ia in the blood of five mice after intravenous inoculation with 0.2 ml of saline containing 670 CFU from an exponential-phase culture. The infection was monitored by sampling 100 or 20 μl of blood from the tail vein and plating according to standard methods. The sepsis was rapidly fulminant, reaching a maximum amount of 9.6×10^4 CFU/0.1 ml of blood at 16 h and remaining near 1×10^5 CFU/0.1 ml thereafter. Symptoms of the infection characterized by lethargy and labored breathing appeared at 16 h and progressed until 28 h when the animals were moribund. A larger dose of 2.8×10^3 CFU killed four of five mice within 24 h after intraperitoneal challenge.

To determine the effect of the sepsis on the colonization of the mouse tissue, groups of five mice each were killed at selected hours after intravenous challenge with 670 to 690 CFU. Spleens, livers, kidneys, and lungs were aseptically removed, weighed, and homogenized with a mortar and pestle, and the number of CFU was determined by plating (Table 1). The number of streptococci per 0.1 g of tissue (wet weight)

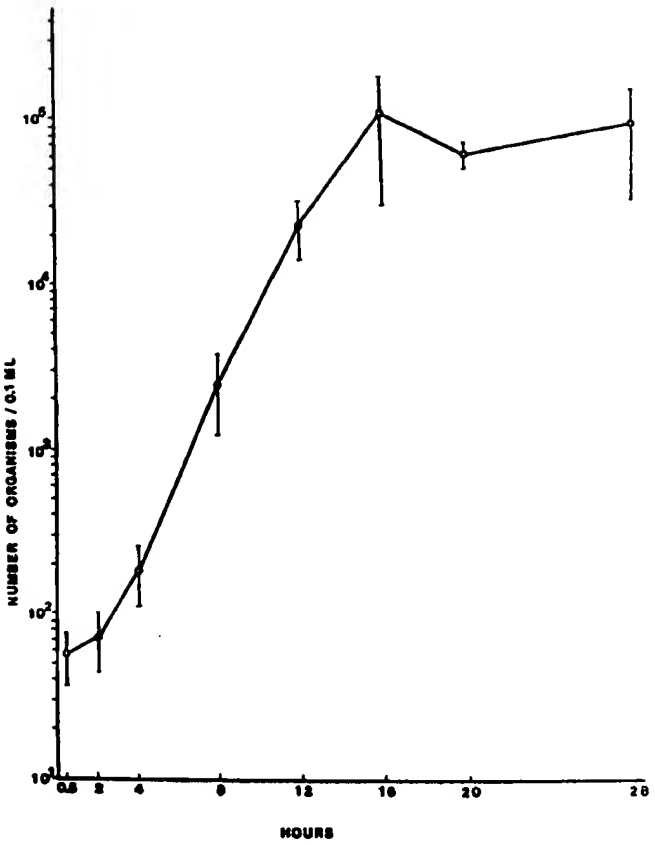

FIG. 1. *Time course of proliferation of type Ia in the blood of BALB/c mice sampled at various times after intravenous inoculation with 670 CFU/0.2 ml. Each point is the mean number of CFU from five mice ± the standard deviation.*

TABLE 1. *Growth in vivo of group B streptococci in five mouse tissues*

Time[a] (h)	No. of streptococci[b]				
	Blood	Liver	Spleen	Lung	Kidney
0.5	$6.9 \times 10^1 \pm 1.6$	$6.3 \times 10^1 \pm 0.5$	$2.2 \times 10^2 \pm 0.7$	$1.1 \times 10^2 \pm 0.5$	$2.5 \times 10^1 \pm 0.9$
4	$3.6 \times 10^1 \pm 1.3$	$3.6 \times 10^1 \pm 1.7$	$2.5 \times 10^2 \pm 0.7$	$4.6 \times 10^1 \pm 3.5$	$2.6 \times 10^1 \pm 1.3$
8	$1.8 \times 10^2 \pm 0.4$	$1.0 \times 10^2 \pm 0.3$	$8.5 \times 10^2 \pm 2.2$	$2.9 \times 10^2 \pm 1.0$	$7.6 \times 10^1 \pm 1.6$
28[c]	$8.0 \times 10^4 \pm 5.2$	$2.7 \times 10^4 \pm 0.1$	$7.3 \times 10^4 \pm 6.1$	$6.7 \times 10^5 \pm 0.7$	$3.8 \times 10^5 \pm 0.2$
37	$1.1 \times 10^5 \pm 0.5$	$8.9 \times 10^4 \pm 2.71$	$1.3 \times 10^5 \pm 1.45$	$5.2 \times 10^6 \pm 1.14$	$3.2 \times 10^6 \pm 3.3$

[a] A 0.2-ml portion of saline containing 6.9×10^2 organisms was injected into a lateral tail vein at zero time.
[b] Each value is the mean number of streptococci per 0.1 ml of blood or 0.1 g of organ from five mice ± the standard deviation.
[c] Animals for this time were inoculated in a separate experiment (Fig. 1) and received 6.7×10^2/0.2 ml.

increased with time in all tissues sampled. The spleen and lungs were prominently colonized 30 min after challenge, whereas the lungs and kidneys contained a log greater number of organisms than the other tissues late in the infection.

The involvement of each tissue in the infection is more easily seen in Table 2, which presents for each time after challenge (Table 1) the number of bacteria in a tissue as a percentage of that obtained from the five tissues tested at that time. It is apparent that the relative colonization

TABLE 2. *Distribution[a] in vivo of virulent group B streptococci in five mouse tissues*

Time (h)	Group B streptococci (%)				
	Blood	Liver	Spleen	Lung	Kidney
0.5	14.0	12.7	45.0	23.2	5.1
4	9.2	9.1	63.4	11.6	6.6
8	11.8	6.9	56.9	19.2	5.1
28	6.5	2.2	6.0	54.2	31.1
37	1.2	1.0	1.5	60.0	36.2

[a] Computed from the data in Table 1.

TABLE 3. *Phagocytosis of virulent and avirulent strains of group B streptococci by mouse peritoneal macrophages*

Streptococcus type	Antiserum to Ia	Phagocytosis[a] (cpm)	% cpm phagocytized	No. of organisms[b] phagocytized
Ia[c]	−	124.8 ± 17.2	0.6	4.1×10^4
Ia	+	429.1 ± 141.0	1.9	1.4×10^5
III[d]	−	2569.8 ± 216.8	7.7	8.1×10^5

[a] The mean number of counts per minute of triplicate samples ± the standard deviation after a 60-min incubation.

[b] The product of the specific activity of the organisms (CFU/counts per minute) and the number of counts per minute retained in the vials after subtraction of background counts per minute (49 ± 5.6).

[c] 7.3×10^6 CFU containing 2.2×10^4 cpm.

[d] 1.0×10^7 CFU containing 3.4×10^4 cpm.

of blood, liver, and spleen decreased, whereas that of the lungs and kidneys increased with progressing infection. These results suggest that the lungs and kidneys are primary sites of involvement in the fulminating sepsis by the virulent type Ia organism.

The growth of the bacteria in the blood and organs after challenge with 40 50% lethal doses (690 CFU) suggested that the type Ia organism evaded the cellular defense mechanisms of the mice. The ability of mouse cells to phagocytize the organism was tested quantitatively by incubating radioactively labeled streptococci with macrophages that had been isolated from the peritoneal cavity (Table 3). The organisms were labeled by incubation of 6×10^7 CFU for 3 h with 10 μCi of [1-^{14}C]sodium oleate (Amersham/Searle, specific activity 51 mCi/mmol) complexed to 2 mg/ml of fatty acid-free bovine serum albumin (Miles Laboratories) (9). Normal macrophages (3 ml from 6 mice) were obtained by adding to the peritoneal cavity Earle balanced salt solution (Pacific Biologicals) containing added $CaCl_2$ (1.8 mM), $MgSO_4$ (0.8 mM), glutamine (2 mM), minimal essential medium amino acids (Grand Island Biological Co.), and 10% newborn calf serum (GIBCO) that had been heat-inactivated at 56°C for 30 min. A 1-ml portion of a 1:8 dilution in medium was added to scintillation vials, and the cells were allowed to attach for 60 min at 37°C. The medium was then decanted, and 1 ml of fresh medium was added followed by 0.2 ml of labeled streptococci in saline containing 2.2×10^4 cpm (type Ia) or 3.4×10^4 cpm (type III). The vials were incubated for 60 min at 37°C. Macrophages attached to coverslips and stained with Giemsa were observed to contain intracellular streptococci after incubation in Leighton tubes under similar conditions. Radioactivity was determined in the washed phagocytes by counting in Bray solution (2). Background counts (mean 49 ± 5.6 standard deviation) were those retained in a set of uninoculated vials. Table 3 shows that the virulent type Ia was minimally attacked, whereas the avirulent type III was phagocytized to a much greater extent. The addition of 0.2 ml of antiserum to the incubation medium containing type Ia increased phagocytosis by threefold. The antiserum was raised in BALB/c mice by an intraperitoneal injection each week for 3 weeks with 0.5 ml of saline containing 5×10^8 CFU that had been killed by heating to 80°C for 1 h. Antiserum was collected 10 days after the last injection and agglutinated type Ia, but not type III, organisms when diluted 1:10. Passive immunization of mice with 0.2 ml of undiluted antiserum intravenously 30 min before intravenous challenge with 670 CFU was completely protective. The same volume of injected antiserum diluted 1:10 protected four of five mice. These results show the importance of antibody for phagocytic activity by mouse cells and subsequent protection of the animal from infection by the Ia organism.

In this study, the infection of adult mice by virulent group B streptococci type Ia has been found to be markedly similar to group B early onset neonatal disease in the time course of infection, principal organ involvement, and requirement for specific antibody for the opsonization and phagocytosis of the organism. These results suggest that the mouse is a good model for the study of the infectious process of this organism.

This investigation was supported by the Public Health Service General Research Support grant SO7RR05350 from the Division of Research Resources to the University of Arkansas for Medical Sciences.

LITERATURE CITED

1. Ablow, R. C., S. G. Driscoll, E. L. Effmann, I. Gross, C. J. Jolles, R. Uauy, and J. B. Warshaw. 1976. A comparison of early-onset group B streptococcal neonatal infection and the respiratory-distress syndrome of the newborn. N. Engl. J. Med. 294:65–70.
2. Bray, G. A. 1960. A simple efficient liquid scintillator for counting aqueous solutions in a liquid scintillation counter. Anal. Biochem. 1:279–285.
3. Franciosi, R. A., J. D. Knostman, and R. A. Zimmerman. 1973. Group B streptococcal neonatal and infant infections. J. Pediatr. 82:707–718.
4. Furtado, D. 1976. Experimental group B streptococcal

infections in mice: hematogenous virulence and mucosal colonization. Infect. Immun. 13:1315–1320.
5. Katzenstein, A.-L., C. Davis, and A. Braude. 1976. Pulmonary changes in neonatal sepsis due to group B β hemolytic streptococcus: relation to hyaline membrane disease. J. Infect. Dis. 133:430–435.
6. Klesius, P. H., R. A. Zimmerman, J. A. Mathews, and D. H. Krushak. 1973. Cellular and humoral immune response to group B streptococci. J. Pediatr. 83:926–932.
7. Lancefield, R. C., M. McCarty, and W. N. Everly. 1975. Multiple mouse-protective antibodies directed against group B streptococci: special reference to antibodies effective against protein antigens. J. Exp. Med. 142:165–179.
8. Mathews, J. H., P. H. Klesius, and R. A. Zimmerman. 1974. Opsonin system of the group B streptococcus. Infect. Immun. 10:1315–1320.
9. Wennerstrom, D. E., and H. M. Jenkin. 1976. The effect of two isomeric octadecenoic acids on the lipid metabolism and growth of Novikoff hepatoma cells. Biochim. Biophys. Acta 431:469–480.

INFECTION AND IMMUNITY, Feb. 1986, p. 648-652
0019-9567/86/020648-05$02.00/0

Vol. 51, No. 2

Experimental Meningococcal Infection in Mice: A Model for Mucosal Invasion

IRVING E. SALIT[1,2]* AND LEWIS TOMALTY[2]

Division of Infectious Diseases, Toronto General Hospital,[1] and Institute of Medical Sciences, University of Toronto,[2] Toronto, Ontario M5G 2C4, Canada

Received 21 August 1985/Accepted 26 October 1985

A more complete understanding of meningococcal disease has been hampered by the lack of an appropriate animal model. Previous models have utilized injections of meningococci, which precludes the study of nasopharyngeal colonization and invasion. We have developed a model for meningococcal disease in which litters of 5-day-old mice are challenged intranasally with 10^7 viable meningococci. Bacteremia is monitored by jugular venous blood cultures, and cerebrospinal fluid is sampled by cisternal punctures. Human disease-associated and carrier strains were compared; nasopharyngeal colonization was similar for these bacteria, but the case-associated strains were much more frequently invasive and caused bacteremia. Twenty-one percent of bacteremic animals had meningitis. There was an age-related susceptibility to infection which correlated inversely with the levels of serum complement. Preinjection of iron dextran increased the number of animals which were bacteremic, the concentration of bacteria in blood, and nasopharyngeal colonization. Noncapsular variants of virulent meningococci did not colonize nasopharyngeal tissue in vivo, and they were not invasive. This neonatal mouse model mimics meningococcal disease as seen in humans and may be useful in studying the initial events in the pathogenesis of meningococcal disease.

Neisseria meningitidis, the meningococcus, remains a major cause of endemic and epidemic bacterial meningitis despite the availability of effective polysaccharide vaccines (13). To study the pathogenesis of meningococcal disease and to test the effectiveness of vaccines, numerous animal models have been developed over the years; these have included experimental meningococcal infection in monkeys (9), mice (16, 18), rabbits (2), chicken embryos (3), and guinea pigs (1, 11). All of these models have required the injection of bacteria either directly into the cerebrospinal fluid, into the bloodstream, or into subcutaneous chambers. It is suspected that some of the illness in the experimental models has been due to the direct injection of toxic bacterial products. Mouse models have become very popular for the study of meningococcal infection; Miller (18) first described the intraperitoneal injection of meningococci in hog gastric mucin, which enhances the virulence of the bacteria. Iron was later found to be an acceptable substitute for mucin (5). These models have been used to test the ability of potential vaccines to prevent either murine death or bacteremia after intraperitoneal injection of meningococci (21). None of these animal models, however, adequately mimics the pathogenesis of meningococcal disease in humans, especially since they bypass the mucosal colonization and invasion steps. In addition to protecting against clinical illness, appropriate vaccines should also have the ability to prevent meningococcal carriage in the nasopharynx and hence eliminate the major reservoir of infection. We have previously studied experimental meningococcal infection in rats, guinea pigs, and mice (25, 26). The most appropriate experimental model involved using neonatal mice who developed nasopharyngeal carriage followed by bacteremia, meningitis, and death.

We describe below meningococcal virulence factors and murine host factors which are important in this model.

* Corresponding author.

MATERIALS AND METHODS

Bacterial strains. Strains of *N. meningitidis* isolated from blood or spinal fluid were designated "case strains," whereas those derived from the pharynxes of asymptomatic persons were designated "carrier strains." The strains which were used in this study and previous studies (25, 26) were characterized as to capsular serogroup and serotype (serogroup/serotype). Disease-associated strains were B16B6 (B/2a), M986 (B/2a,7), 3006 (B/2b), BB80 (B/2), M1011 (B/2,10), BB106 (C/2), BB138 (C/2), BB155 (C/2), and VM63 (nongroupable). Carrier strains were M990 (B/6), DRES 03 (B/15), DRES 18 (B/nontypable), M992 (B/5), VM112 (X), VM49 (B), and VM82 (Z). The noncapsular variants were derived from the group B encapsulated parent strains by selecting naturally occurring mutants on antiserum-agar plates (6, 7). The absence of encapsulation was confirmed before intranasal challenge by the antiserum-agar method (7).

All strains were stored frozen at −80°C in sterile 5% (wt/vol) monosodium glutamate and 5% (wt/vol) bovine serum albumin. Before use in inoculation studies, the bacteria were partially thawed, liberally inoculated onto clear gonococcal typing agar (27), and grown overnight at 37°C in an atmosphere of 5% CO_2. Bacteria were then removed from the agar plate by using sterile cotton-tipped swabs and were transferred to 15- by 100-mm test tubes containing 5 ml of brain heart infusion broth. The bacterial suspensions were rotated end over end for 3 h at 37°C until an optical density of 0.35 was achieved at a wavelength of 540 nm with a Coleman junior 2A linear spectrophotometer. This corresponds to 1×10^9 to 3×10^9 CFU/ml. The exact number of CFU was determined by making 10-fold serial dilutions in brain heart infusion broth. Stock bacterial strains were always renewed with bacteria of the same strain which had been recently reisolated from infected animals. This was done to ensure that virulence determinants were not lost by repeated in vitro passaging.

Mouse model. Natural litters of Swiss CD1 mice (13 to 17 pups per litter) were obtained from Charles River Breeding

TABLE 1. Comparative colonization and bacteremia after intranasal inoculation of case- and carrier-associated meningococci[a]

Source of strain	Iron dextran	Bacteremia	Colonization	Mortality
Case[b]	−	110/397 (28)	86/270 (32)	3/397 (0.7)
	+	184/354 (52)	144/191 (75)	59/354 (17)
Carriers[c]	−	11/94 (12)	31/82 (38)	0/94 (0)
	+	6/83 (7)	42/93 (45)	2/83 (2)

[a] Data are given as the number of animals with bacteremia (or colonization or mortality)/total, with the percentage in parentheses. The statistical significance values of the comparisons were as follows. (i) For iron-pretreated animals (case strains versus controls not pretreated), bacteremia, colonization, and mortality, $P < 0.001$. (ii) For iron-pretreated animals (carriers versus case strains), bacteremia and colonization, $P < 0.001$, and mortality, $P < 0.01$. (iii) For iron-pretreated animals (carrier strains versus controls not pretreated), bacteremia, colonization, and mortality, not significant. (iv) For animals with no iron pretreatment (carrier versus case strains), bacteremia, $P < 0.05$, and colonization and mortality, not significant.

[b] Nine strains: serogroup B type 2 (five strains), serogroup C type 2 (three strains), and nongroupable (one strain).

[c] Seven strains: serogroup B (five strains), serogroup X (one strain), serogroup 29e,Z (1 strain). None was serotype 2.

Laboratories, Inc., Wilmington, Mass., and were atraumatically inoculated intranasally with 10^7 meningococci as previously described (26). Briefly, bacterial suspensions containing 10^9 CFU/ml were aspirated into 0.5-ml glass syringes to which were attached 5-mm-long, blunted, 30-gauge needles. Without any anesthesia, 0.01 ml was atraumatically inoculated into one nostril. Blood cultures were taken at 3, 24, and 48 h by puncturing the internal jugular vein with a 25-gauge needle. Samples (0.01 ml) of blood were withdrawn and placed on agar plates. Nasal cultures were obtained by washing the nasal passages with 0.05 ml of brain heart infusion broth, which was then immediately placed on agar plates.

At 3 to 6 h before intranasal inoculation, some animals also received intraperitoneal injections of iron dextran (Imferon, Pfizons Corp. Ltd., Scarborough, Ontario) at a dosage of 250 mg of iron per kg. Control animals received saline.

Cerebrospinal fluid was sampled by inserting a 25-gauge needle into the nape of the neck and then into the cisterna magna (19). This procedure could be done repeatedly on an animal without mortality.

After inoculations all animals were observed and weighed daily. Deaths were tabulated, and selected animals underwent pathological examination.

Complement studies. Cobra venom factor from *Naja naja*, obtained from Cordis Laboratories, Miami, Fla., was reconstituted in phosphate-buffered saline, and portions were frozen at −80°C. At 24 h before intranasal instillation of meningococci, mice received 200 U of the venom factor per kg. At 24 h after injection there was no C3 present, as measured by a sensitive alternate complement pathway assay employing ^{51}Cr-labeled erythrocytes (17). In addition, A/J mice which were deficient in the fifth component of complement (Jackson Laboratories, Bar Harbor, Maine) were challenged with meningococci as described above.

Statistical methods. Fourfold tables were constructed, and the chi-square values (χ^2) were determined by using Yates' correction for continuity.

RESULTS

Comparative colonization and bacteremia. Five-day-old litters of mice were inoculated intranasally with strains derived from human patients with meningitis or carriers (Table 1). In the animals which had not been pretreated with iron dextran, the rates of bacteremia were significantly higher in pups in which the disease-associated isolates were instilled intranasally. Despite the higher rates of bacteremia, nasopharyngeal colonization rates and mortality were not significantly different in the groups which were challenged with either carrier- or case-derived isolates. Intraperitoneal injection of iron dextran significantly enhanced rates of bacteremia, colonization, and mortality in those mice which were challenged with the disease-associated isolates. Iron dextran did not alter these parameters in the mice challenged with carrier strains. Of the mice which were bacteremic from case-derived strains, 21% (4 of 19) had infected cerebrospinal fluid as determined by cisternal puncture (26).

To ensure that bacteria were not being directly injected into mucosal tissue or even into the bloodstream, an alternate form of instillation was used. Using a Pasteur pipette, 100 μl of meningococci was dropped onto the external nares. The mice quickly aspirated the fluid into the internal nares. Animals which were challenged in this manner had identical results to those which had intranasal instillation with a blunt needle (data not shown).

We then determined the rates of bacteremia in relationship to the numbers of bacteria instilled intranasally. In the absence of iron, an inoculum of at least 10^5 disease-associated bacteria was required to produce any detectable bacteremia (Fig. 1). This increased to 20% when 7×10^8 bacteria were used. Injections of iron dextran significantly enhanced rates of bacteremia and reduced the minimum infective dose so that even after challenge with 700 bacteria, 10% of animals were bacteremic.

Quantitative blood cultures were also done to determine the level of bacteremia under different circumstances. With the virulent strain B16B6, almost 90% of the animals which were bacteremic had less than 10^3 organisms per ml of blood (Fig. 2). Injection of iron dextran not only increased rates of bacteremia (Table 1) but also increased the concentration of bacteria in those with positive blood cultures (Fig. 2). The mortality was highest in those animals with more than 10^4 bacteria per ml of blood.

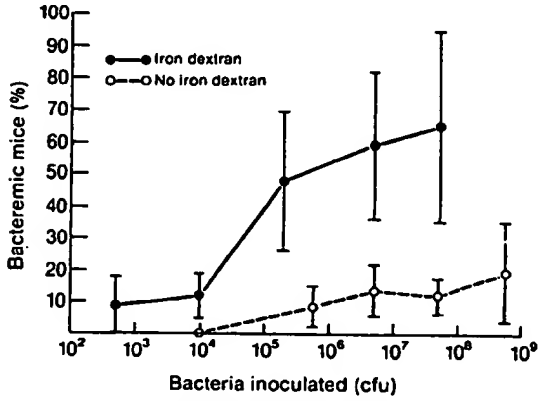

FIG. 1. Comparison of rates of bacteremia in neonatal mice 24 h after intranasal instillation of *N. meningitidis* B16B6 (○). Iron dextran was given intraperitoneally to another group of animals at the time of intranasal challenge (●). Each point represents the mean and standard deviation of the results from a minimum of four litters (at least 45 pups).

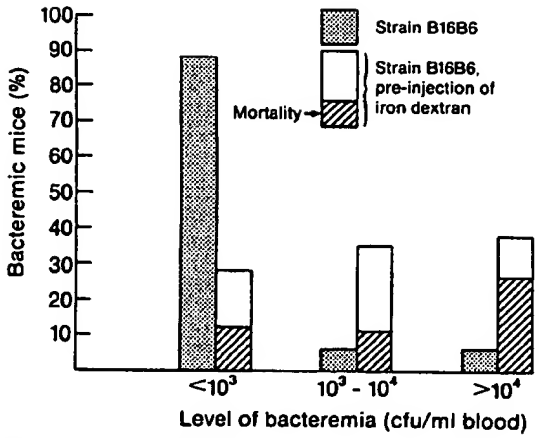

FIG. 2. Intranasal inoculation of 5-day-old pups with *N. meningitidis* B16B6. Mice which were not bacteremic were eliminated from this analysis. Quantitation of the degree of bacteremia was done on animals which had received meningococci alone or together with iron dextran. There was a 24% (24 of 99) rate of bacteremia without iron dextran and a 73% (81 of 111) rate of bacteremia in pups treated with iron.

The duration of bacteremia and colonization was assessed by doing repeated blood and nasal cultures at 3 h and then daily for 4 days. No further colonization or bacteremia was detectable by day 4 (age 9 days) (Table 2).

Role of the capsule. Encapsulated and noncapsular variants of strains M986 and 3006 were tested for their ability to colonize the nasopharynx and invade into the bloodstream (Table 3). Rates of bacteremia were markedly reduced in the noncapsular variants compared with the parent strains. A small number of mice became bacteremic after receiving the unencapsulated variant of strain 3006; however, approximately 5% of colonies reverted to the parent encapsulated form as detected on antiserum agar plates. No group B polysaccharide was detectable on strain M986. The noncapsular variants of both strains also colonized the nasopharynx to a significantly lesser extent than the parental strains.

Role of serum complement. We previously found that, in this model, there was an inverse relationship between the age of the mice and susceptibility to meningococcal bacteremia (26). Since humans may be susceptible to meningococcal disease because of complement deficiency (22), we wanted to determine whether the increased susceptibility of mice was also due to low complement levels. Serum complementary activity was measured at different ages and was found to be undetectable during the first week of life, rising to one-fifth of the adult levels by the second week of life. With equivalent numbers of male and female mice, the 50% hemolytic complement levels were 150, 30, and <5 U/ml at 6 weeks, 10 days, and <10 days of age, respectively. Rates of bacteremia are known to diminish in this model by 10 days, and bacteremia does not occur at 6 weeks of age.

To confirm the absence of serum complement at 5 days of age, cobra venom factor was injected intraperitoneally, and mice were challenged intranasally with the virulent strain B16B6 (Table 4). Cobra venom factor eliminated total hemolytic complement from adult animals by 24 h. After preinjection of neonatal mice with cobra venom factor, there was no enhancement of rates of bacteremia, levels of bacteremia, nasal colonization, or mortality. Similarly, there was no significant change in mortality when strain B16B6 was instilled into mice which have a congenital deficiency of C5. However, there was an increase in rates of bacteremia (25% versus 69%) as well as colonization (35% versus 100%).

TABLE 2. Duration of bacteremia and colonization in neonatal mice[a]

Time after i.n.[b] instillation (h)	Bacteremia		Colonization	
	No iron	With iron	No iron	With iron
3	6/40 (15)	ND[c]	ND	ND
24	16/100 (16)	104/174 (60)	ND	ND
48	21/103 (20)	61/120 (51)	19/53 (36)	70/109 (64)
72	2/78 (3)	2/32 (6)	3/46 (7)	2/32 (6)
96	0/78 (0)	0/40 (0)	0/46 (0)	0/40 (0)

[a] Data are given as the number of animals with bacteremia (or colonization)/total, with the percentage in parentheses. *N. meningitidis* B16B6 was used.
[b] i.n., Intranasal.
[c] ND, Not done.

TABLE 3. Comparison of colonization and invasiveness of encapsulated and nonencapsulated meningococcal variants[a]

Strain	Description	Bacteremia	Nasal colonization
M986 (B/2a,7)[b]	Encapsulated	14/40 (35)[c]	18/36 (50)[c]
	Noncapsular variant	0/54 (0)[c]	3/54 (6)[c]
3006 (B/2b)[b]	Encapsulated	17/37 (46)	37/37 (100)
	Noncapsular variant	7/76 (9)	17/76 (22)

[a] Data are given as the number of animals with bacteremia (or colonization)/total, with the percentage in parentheses.
[b] (Serogroup/serotype).
[c] $P < 0.001$, compared with noncapsular variant.

DISCUSSION

There have been many descriptions of animal models for meningococcal disease ever since *N. meningitidis* was clearly associated with epidemic cerebrospinal meningitis (28). The most popular model has been the mouse bacteremia model, which requires intraperitoneal injections of meningococci alone (16), in hog gastric mucin (18), or in iron dextran (5).

None of the previously described experimental models for meningococcal disease fully satisfies the criteria of an ideal model. Some suggested criteria for an experimental animal model (14) are as follows: (i) the portal of entry and route of dissemination must be similar to those in human disease, (ii) bacteria which are virulent for humans should also be virulent for the experimental animals, (iii) the course of disease should be predictable, (iv) it should be reproducible, (v) experimental lesions should be similar to those in human

TABLE 4. Effects of cobra venom factor on neonatal mice[a]

Treatment	Bacteremia		Nasal colonization	Mortality
	No./total (%)	Bacterial concn (CFU/ml, 10^3)		
Controls	24/99 (24)	1.4 ± 2.6	29/97 (30)	2/99 (2)
Cobra venom factor	55/223 (25)	1.8 ± 2.5	19/68 (28)	8/223 (4)

[a] Strain B16B6 was injected intranasally. Except for bacterial concentration, data are given as the number of animals with bacteremia (or colonization or mortality)/total, with the percentage in parentheses.

disease, (vi) the techniques should be relatively simple, and (vii) the pathophysiologic events must be similar to those occurring in humans (8). It is doubtful that any one animal model for meningococcal disease can meet all of these requirements.

Unfortunately none of the previously described models includes a mucosal colonization phase followed by bacterial invasion; this has precluded a study of the initial events in meningococcal disease. Similar problems had existed with models for *Haemophilus influenzae* until the development of the neonatal rat model, which utilizes intranasal instillation of bacteria (19).

We have described a neonatal mouse model for meningococcal disease in which the intranasal inoculation of bacteria is followed by a phase of nasopharyngeal colonization (25, 26). Virulent and avirulent strains attach to and colonize the murine nasopharynx to the same degree, but it is mainly those strains which are virulent for humans which invade through the nasal mucosa and cause bacteremia. About 20% of bacteremic animals do develop culture-positive purulent meningitis. Histopathologic studies indicate that smaller numbers of animals develop leptomeningitis and ventriculitis (26). There is an age-related susceptibility to meningococcal disease in this model, with resistance increasing after the first week of life; this resistance was correlated with increasing levels of serum complement. Protection against meningococcal disease in humans is also correlated with the presence of serum bactericidal activity. Complement-deficient humans are at increased risk for systemic meningococcal disease (22); similarly, we found that congenital C5-deficient mice had enhanced rates of bacteremia.

Injection of iron dextran increased rates of bacteremia, level of bacteremia, and nasopharyngeal colonization, but only for those strains which are intrinsically virulent. It is well known that iron enhances the virulence of many bacteria (4). Host iron is not readily available to bacteria because it is strongly bound to iron-binding proteins, and there is only an extremely small amount of free iron available in serum unless extrinsic iron is provided. Pathogenic neisseriae such as the meningococcus can utilize iron which is bound to transferrin; however, infection is associated with hypoferremia, which reduces the amount of iron available in the transferrin iron pool. Virulence is enhanced when iron saturation of transferrin is maintained at high levels by exogenous iron (15).

In this neonatal mouse model, the most virulent strains were encapsulated and had the serotype 2 antigen. Carrier-associated strains, however, did not invade despite the fact that all were encapsulated. None had the serotype 2 antigen. In humans, the serotype 2 antigen is also a major virulence determinant in invasive strains; carrier strains may be encapsulated or unencapsulated but rarely have the serotype 2 antigen (10). Factors responsible for meningococcal adherence are poorly defined, although pili appear to mediate adherence to human pharyngeal cells in vitro (24) and the A or C polysaccharide inhibits attachment to and agglutination of human erythrocytes in vitro (23). In the present study, organisms with the group B polysaccharide on their surface were more efficient in colonizing the nasopharynx in vivo than were the noncapsular variants. Studies in humans with the A and C polysaccharide vaccines do suggest that anticapsular polysaccharide antibodies can similarly reduce pharyngeal colonization (12, 20). This implies that the group B polysaccharide may mediate meningococcal attachment in vivo. Other explanations are possible. (i) An important adhesin might be lost during the preparation of the noncapsular variant. (ii) Invasion may allow enhanced nasopharyngeal colonization by a "reverse invasion" procedure whereby bacteria from the bloodstream recolonize the nasopharynx; this is unlikely since the colonization rates are similar for the invasive and noninvasive strains. (iii) "Serum factors" may kill some meningococci in the nasopharynx. The in vivo colonization is enhanced by iron dextran. The mechanism is uncertain, but may involve some of the above factors, an interaction with the adhesin, increased growth rate, or a change in bacterial production of an adhesive molecule.

It is now possible to study in more detail the early phase of meningococcal disease including nasopharyngeal colonization, the poorly understood invasion through the mucosa, and ultimately bacteremia and meningitis. In addition, one can also study the ability of vaccines and passively transfused antibodies to inhibit mucosal colonization.

ACKNOWLEDGMENTS

This work was supported by grant MA 7371 from the Medical Research Council of Canada.

We thank Patti Jackson for excellent secretarial assistance.

LITERATURE CITED

1. **Branham, S. E., and R. D. Lillie.** 1932. Notes on experimental meningitis in rabbits. Public Health Rep. 47:2137–2150.
2. **Branham, S. E., R. D. Lillie, and A. M. Pabst.** 1937. Experimental meningitis in guinea pigs. Public Health Rep. 52: 1135–1142.
3. **Buddingh, G. J., and A. D. Polk.** 1939. The pathogenesis of meningococcus meningitis in the chick embryo. J. Exp. Med. 70:499–512.
4. **Bullen, J. J.** 1981. The significance of iron in infection. Rev. Infect. Dis. 3:1127–1138.
5. **Calver, G. A., C. P. Kenny, and G. Labergne.** 1976. Iron as a replacement for mucin in the establishment of meningococcal infection in mice. Can. J. Microbiol. 22:832–838.
6. **Craven, D. E., and C. E. Frasch.** 1978. Pili-mediated and nonmediated adherence of Neisseria meningitidis and its relationship to invasive disease, p. 250–252. *In* G. F. Brooks, E. C. Gotschlich, K. K. Holmes, W. D. Sawyer, and F. E. Young (ed.), Immunobiology of *Neisseria gonorrhoeae*. American Society for Microbiology, Washington, D.C.
7. **Craven, D. E., and C. E. Frasch.** 1979. Serogroup identification of meningococci by a modified antiserum agar method. J. Clin. Microbiol. 9:547–548.
8. **DeVoe, I. W.** 1982. The meningococcus and mechanisms of pathogenicity. Microbiol. Rev. 46:162–190.
9. **Flexner, S.** 1907. Experimental cerebrospinal meningitis in monkeys. J. Exp. Med. 9:142–166.
10. **Frasch, C. E., and S. S. Chapman.** 1973. Classification of Neisseria meningitidis Group B into distinct serotypes. III. Application of a new bactericidal inhibition technique to distribution of serotypes among cases and carriers. J. Infect. Dis. 127:149–154.
11. **Frasch, C. E., and J. D. Robbins.** 1978. Protection against group B meningococcal disease. II. Infection and resulting immunity in a guinea pig model. J. Exp. Med. 147:619–628.
12. **Gotschlich, E. C., I. Goldschneider, and S. Artenstein.** 1969. Human immunity to the meningococcus. J. Exp. Med. 129:1385–1395.
13. **Hankins, W. A., J. M. Gwaltney, Jr., J. O. Hendley, J. D. Farquhar, and J. S. Samuelson.** 1982. Clinical and serological evaluation of a meningococcal polysaccharide vaccine groups. A. C. Y. and W135 (41306). Proc Soc. Exp. Biol. Med. 169:54–57.
14. **Harter, D. H., and R. G. Petersdorf.** 1960. A consideration of the pathogenesis of bacterial meningitis: review of experimental and clinical studies. Yale J. Biol. Med. 32:280–309.
15. **Holbein, B. E.** 1980. Iron-controlled infection with *Neisseria*

meningitidis in mice. Infect. Immun. 29:886–891.
16. Huet, M. M., and A. Suire. 1976. Mise en evidence de la bacteriemie chez la souris. C. R. Acad. Sci. 283:421–422.
17. Joiner, K. A., R. Shahon, and J. A. Gelfand. 1979. A sensitive microassay for the murine alternative complement pathway. J. Immunol. Methods 31:283–290.
18. Miller, C. P. 1933. Experimental meningococcal infection of mice. Science 78:340–341.
19. Moxon, E. R., A. L. Smith, D. R. Averill, and D. H. Smith. 1974. Haemophilus influenzae meningitis in infant rats after intranasal inoculations. J. Infect. Dis. 129:154–162.
20. Peltola, H., P. H. Makela, H. Kayhty, H. Jousimies, E. Herva, K. Hällström, A. Sivonen, O.-V. Renkonen, O. Pettay, V. Karanko, P. Ahronen, and S. Sarna. 1977. Clinical efficacy of meningococcus group A capsular polysaccharide vaccine in children three months to five years of age. N. Engl. J. Med. 297:686–691.
21. Peppler, M. S., and C. E. Frasch. 1982. Protection against group B *Neisseria meningitidis* disease: effect of serogroup B polysaccharide and polymyxin B on immunogenicity of serotype protein preparations. Infect. Immun. 37:264–270.
22. Ross, S. C., and P. Densen. 1984. Complement deficiency states and infection: epidemiology, pathogenesis and consequences of Neisserial and other infections in an immune deficiency. Medicine 63:243–273.
23. Salit, I. E. 1981. Hemagglutination by Neisseria meningitidis. Can. J. Microbiol. 27:586–593.
24. Salit, I. E., and G. Morton. 1981. Adherence of *Neisseria meningitidis* to human epithelial cells. Infect. Immun. 31:430–435.
25. Salit, I. E., and L. Tomalty. 1984. Experimental meningococcal infection in neonatal mice: differences in virulence between strains isolated from human cases and carriers. Can. J. Microbiol. 30:1042–1045.
26. Salit, I. E., E. Van Melle, and L. Tomalty. 1984. Experimental meningococcal infection in neonatal animals: models for invasiveness. Can. J. Microbiol. 30:1022–1029.
27. Swanson, J. 1978. Studies on gonococcus infection. XII. Colony color and opacity variants of gonococci. Infect. Immun. 19:320–331.
28. Welchselbaum, A. 1887. Ueber die Aetiologie der akuten meningitis cerebrospinalis. Fortschr. Med. 5:575–583.

Exhibit K

INFECTION AND IMMUNITY, Mar. 1980, p. 1023-1032
0019-9567/80/03-1023/10$02.00/0

Vol. 27, No. 3

Production of Bacteremia and Meningitis in Infant Rats with Group B Streptococcal Serotypes

PATRICIA FERRIERI,[1]* BARBARA BURKE,[1, 2] AND JoANN NELSON

Departments of Pediatrics[1] and Laboratory Medicine and Pathology,[2] University of Minnesota, Minneapolis, Minnesota 55455

Group B streptococcal strains, representing the five major serotypes, were inoculated into infant rats by intranasal, oral, and intraperitoneal routes. Bacteremia regularly followed injection by the intraperitoneal route. Four strains (three of type III) isolated from human cerebrospinal fluid appeared more virulent for 5-day-old rats. Injection of fewer than 10 colony-forming units of one strain, a type III, led to bacteremia and death in 27% of animals. The cumulative bacteremia and mortality rate with this strain was 66% in animals given inocula of <10 to 10^3 colony-forming units. Bacteremia developed by 24 to 48 h with concentrations of $>10^5$ colony-forming units per ml of blood, and death occurred soon afterward. Among bacteremic animals, positive cerebrospinal fluid cultures were found in 97%, and cerebrospinal fluid bacterial concentrations were equal to or exceeded bacterial counts in blood. The susceptibility of infant rats to infection with type Ia, Ic, or III strains was age dependent. Histopathological studies of the brain and meninges in 34 bacteremic animals with culture-positive cerebrospinal fluid revealed that 5- to 10-day-old animals had numerous bacteria distributed in a perivascular pattern but, with one exception, no leukocytic infiltration. In contrast, three of the 11- to 12-day-old and two 15-day-old animals had very thickened meninges infiltrated with polymorphonuclear leukocytes, macrophages, and bacteria.

The group B *Streptococcus* has become the focus of intensive research activity in recent years because of its association with life-threatening infections in the neonatal period (4). It has been estimated that over 12,000 newborn infants each year in the United States (4) develop, sepsis/meningitis due to group B streptococci (GBS) and that 50 to 60% of these infants die (4). Moreover, this organism is one of the two major etiological agents of purulent meningitis in children between 1 week and 2 months of age (1, 4, 6) and in some centers is currently the leading agent of meningitis (1, 4, 6).

Epidemiological studies have documented how commonly GBS are transmitted to newborn infants from mothers who are genital or rectal carriers of the organism (2, 3, 5, 12, 20). In infants with meningitis of either "early" or "late" onset, reported in the United States, there is a striking predominance of serotype III GBS (1, 4, 5, 28). This predominance of type III organisms raises the question of whether these organisms possess unique biological features that favor dissemination or invasion of the meninges. There are still many unanswered questions about the pathogenicity of GBS and the immunological susceptibility of immature hosts to disease due to these bacteria.

The clinical syndromes of acute GBS disease in newborn infants have stimulated studies in various animal models. For example, adult mice have been used as models for disease due to type Ia (27), and now methods have been developed recently to demonstrate mouse susceptibility to type III (8). Eleven- and twelve-day-old chicken embryos have been a suitable model for studying septicemia due to GBS type III and protection from infection with type-specific antibody (25).

The infant rat model was chosen for the present studies because of its demonstrated suitability for studying sepsis/meningitis due to *Haemophilus influenzae* b (18, 24) and *Escherichia coli* (9, 13). The goals were to examine the capacity for all of the five major group B types to produce bacteremia and meningitis in suckling rats, to compare different routes for establishing infection, and to examine variables which influence host susceptibility, dissemination of infection, and host response to infection, such as inflammation.

MATERIALS AND METHODS

Animals. Pregnant albino Sprague-Dawley rats in late gestation were obtained from Bio-Lab Corp. (White Bear Lake, Minn.) and gave birth in our animal quarters 3 to 5 days after arrival. Each adult rat and

her litter (average size of 12 pups) were housed in separate, solid, opaque cages with filter hoods made of spun-bonded polyester (Lab Products Co., Garfield, N.J.) under standard conditions (25°C; relative humidity 40%) with a 7 a.m. to 7 p.m. light schedule. Purina rat chow plus water was available ad libitum. There was minimal handling of the rat pups during the first 4 days of life. Infant rats were not inoculated at less than 4.5 days of age.

Bacteria. The GBS strains were all beta-hemolytic and were isolated from the blood, cerebrospinal fluid (CSF) of newborn infants, human genital tract, and normal skin sites (11). Strain 76-043, type III, isolated from the CSF of an infant was studied most intensively. Identification of the serological group was by the hot acid extraction and capillary precipitin method of Lancefield (14), and typing was done by immunodiffusion in agar (22) with antisera prepared in our laboratory (grouping) and antisera provided by the Center for Disease Control, Atlanta, Ga. (typing). Cultures of the original isolates were lyophilized and had not been passaged in the laboratory.

The streptococcal strains were grown at 37°C to late-log phase and quickly frozen (in an alcohol-Dry Ice bath) in 1- to 2-ml portions and stored at −20°C. For each inoculation log-phase organisms were subcultured overnight, transferred to fresh Todd-Hewitt broth and grown for 2 h at 37°C. Bacteria were suspended in Todd-Hewitt broth and diluted to the desired number of colony-forming units (CFU) for inoculation. Quantitation of the inoculum size was done by utilizing optical density at 620 nm in a Coleman Jr. II spectrophotometer (Coleman Instruments Div., Oak Brook, Ill.) along with spread plating in duplicate on tryptose blood agar base plates (Difco Laboratories, Detroit, Mich.) containing 6% defibrinated sheep blood. Bacterial CFU per milliliter were enumerated from the platings. Purity checks were done on all cultures prepared for animal inoculation.

Inoculation of animals. For intraperitoneal (i.p.) injection of infant rats, the desired number of CFU of bacteria was delivered in a volume of 0.1 ml with a no. 25 gauge needle attached to a tuberculin syringe. Adult rats received a volume of 1 ml. Intranasal inoculation was performed by introducing a sterilized plastic pipette tip attached to an automatic pipetter (Pipetman, Rainin Instrument Co., Brighton, Mass.) into the anterior nares of an unanesthetized rat and delivering 0.01 ml of bacteria. No difficulty was found in delivering the entire amount. Care was taken to avoid trauma to the nares. Oral feedings of group B streptococci were given by a technique similar to that used for intranasal inoculation; animals sucked on the pipette tips, and volumes of 0.01 ml were easily dispensed into the mouth of 5-day-old rats. Larger volumes were given to older animals.

Inoculations were performed between 1,300 and 1,500 h, and clinical observations were made at frequent intervals each day. Animals were weighed daily.

Sampling of body fluids. Blood cultures of infant rats were obtained daily for the first 3 days postinjection and then at spaced intervals. The tail was cleansed with 70% alcohol and amputated, and blood was collected in 10- to 50-μl amounts (with Micropipet Disposable Pipettes, Clay Adams Division of Becton, Dickinson and Co., Parsippany, N.J.) that were inoculated onto blood agar plates for counting CFU of bacteria. Bacteria were identified on the basis of typical colonial morphology and hemolysis on blood agar, and selected cultures were grouped serologically. Blood was obtained from adult rats by cannulating a tail vein with a no. 20 gauge needle.

CSF was obtained by puncture of the cisterna magna by a method similar to one previously described (17). Five to ten microliters of CSF was drawn into a 10-μl microcapillary pipette and inoculated onto blood agar plates for counting CFU of bacteria. CSF cell counts were not done, but visual inspection of the fluid was done to note any blood-tinged color.

Postmortem examination and histological methods. Critically ill animals, close to death, were sacrificed electively by a lethal dose of ether. CSF samples, tail vein blood, and blood from cardiac puncture were obtained immediately. After exsanguination, samples of lung, liver, and spleen were obtained; the kidney was bisected, and all tissues were placed in 10% Formalin after sampling for bacterial cultures. The animals were decapitated, and the entire head was immersed in 10% Formalin and held for at least 1 week before being cut into coronal sections. The tissues were embedded in paraffin, cut 6 μm thick, and stained with hematoxylin and eosin, and a tissue Gram stain was used to demonstrate bacteria. Animals discovered shortly after death were processed also as above except that CSF flow was impeded at times. If death had occurred hours before discovery, organ cultures were taken, but tissues were not processed if autolysis was evident. At the conclusion of experiments, all surviving animals were sacrificed and examined as for critically ill animals. The tissues were examined microscopically by one of us (B.B.) without knowledge of the type and size of the bacterial inoculum, the culture results, or circumstances of death. Meningitis was defined as the presence of bacteria and inflammatory cells within the meninges.

Statistical methods. The chi-square test was used to determine the significance of differences. The Yates correction was used when numbers were small in any of the subgroups.

RESULTS

Route of inoculation and effect on bacteremia and mortality. Initially, three different routes for administering GBS to infant rats were examined (Table 1). By using strain 76-043, a serotype III isolated from human CSF, 5-day-old animals, inoculated intranasally with an inoculum size as high as 10^8 CFU of bacteria, were resistant to infection. Only one animal developed a transient bacteremia with a concentration of 2×10^2 CFU/ml of blood and survived to the time of sacrifice when CSF was found to be sterile. The other intranasally inoculated animals had no clinical illness and also had culture-negative CSF. Five- to seven-day-old animals given 10^6 to 10^8 CFU of bacteria by mouth had no detectable bacteremia. In contrast, animals injected i.p. with this strain, with lower bacterial inocula,

TABLE 1. *Relationship of the route of inoculation of GBS in infant rats and differences in bacteremia and death*[a]

Age of animals (days)	Route of inoculation	Inoculum size	Outcome	
			Bacteremia (%)	Mortality (%)
5	Intranasal	10^1–10^5	1/38[b] (3)	0/38[c] (0)
5–7	Oral	10^6–10^8	0/49 (0)	0/49 (0)
5	i.p.	$<10^1$–10^4	74/111 (67)	74/111 (67)

[a] All animals received GBS strain 76-043, serotype III.

[b] Number of animals with positive blood cultures/number of animals inoculated. This animal had transient bacteremia and at sacrifice had culture-negative CSF.

[c] Number of animals that died within 72 h with organ cultures positive for GBS/number of animals inoculated. Survivors were followed for longer than 1 week and were sacrificed electively to confirm absence of infection. The intranasally inoculated animals also had CSF samples taken for culture, and they were negative.

had a high mortality with most deaths in the 24- to 48-h period after injection. The differences in outcome between animals injected i.p. compared with animals inoculated intranasally or orally were significant ($P < 0.001$). At autopsy, the bacteremic animals had cultures yielding large quantities of GBS from multiple organs. Because of the initial success in inducing bacteremia in infant rats with the i.p. route, it was used for subsequent studies.

Virulence of GBS strains of all serotypes for 5-day-old rats. The capacity of several strains of GBS to produce lethal infection in 5-day-old animals was examined. The outcome, expressed as death with positive cultures for GBS, after injection of 10^2 to 10^4 CFU of bacteria was variable (Table 2). The highest mortality rates (73 to 94%) were seen after injection with four strains, one a type Ib and three of type III, all isolated from human CSF. Injection of the Ia and Ic strains produced a lower mortality in animals, but the type II strain did not produce infection or death even when 6×10^5 CFU of bacteria were injected. With injection of 10^6 CFU of this strain, lethal infection was seen in three of three animals.

It was apparent from daily examinations which animals were ill, because early signs of minimal weight gain, then weight loss, were followed rapidly by inactivity, rapid and panting respirations, and poor color. These animals always had bacteremia and positive cultures for GBS at autopsy.

Inoculum size of strain 76-043 and mortality. In earlier experiments it was demonstrated that strain 76-043, type III, was capable of inducing bacteremia and death in young animals after injection of small numbers of bacteria. A total of 109 5-day-old animals were injected with inocula of <10 to 10^3 CFU, and the animals were followed for death associated with infection (Fig. 1). Mortality increased progressively from 27% with the lowest inoculum of <10 CFU to 100% with the highest inoculum. The cumulative mortality was 66%.

Influence of bacteremia on CSF infection. With strain 76-043, the likelihood of having GBS isolated from CSF after bacteremia was examined (Table 3). Among 38 animals injected with varying bacterial inocula, there were 29 animals who had bacteremia detected by tail blood sam-

TABLE 2. *Mortality in 5-day-old infant rats injected with group B streptococcal strains*

Strain	Serotype	Source	No. of animals injected with 10^2 to 10^4 CFU	No. (%) that died with positive cultures[a]
74-562	Ia	Umbilicus	21	4 (19)
76-039	Ib	CSF	21	16 (76)[b]
74-430	Ic	Blood	29	9 (31)
74-138	II	Blood	12	0 (0)
74-681	III	CSF	11	8 (73)[b]
76-041	III	CSF	19	15 (79)[b]
76-043	III	CSF	35	33 (94)[b]

[a] Animals died within 72 h of injection and had blood and multiple organs culture-positive for GBS. Survivors were followed for longer than 1 week and were sacrificed electively to confirm absence of infection.

[b] The differences in mortality following i.p. injection with serotypes Ib and III compared with Ia, Ic, and II were significant, $P < 0.001$.

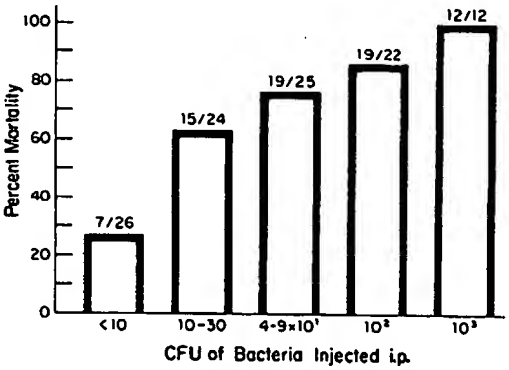

FIG. 1. *Five-day-old infant rats were injected i.p. with varying inocula of GBS strain 76-043, serotype III. Figures above bars indicate number of animals that died within 72 h with blood and multiple organs culture-positive for GBS/number of animals inoculated.*

TABLE 3. *Influence of bacteremia on CSF cultures in infant rats injected with GBS strain 76-043, serotype III*

Premortem blood culture with GBS	CSF culture for GBS	
	Positive	Negative
Positive ($n = 29$)[a]	28	1[b]
Negative ($n = 9$)	0	9[c]

[a] A total of 38 animals were examined: 20 were 5 days old, 6 were 9 to 10 days old, and 12 were 11 to 12 days old at time of injection.

[b] This culture was from a 5-day-old animal.

[c] The difference in CSF cultures between bacteremic and nonbacteremic animals was significant, $P < 0.001$.

pling, and 97% of them had positive CSF cultures. One 5-day-old animal had cleared its bacteremia of 10^3 CFU/ml of blood by the time of sacrifice and had a negative CSF culture. Animals with negative blood cultures obtained daily had negative CSF at the time of sacrifice ($P < 0.001$). Animals who developed bacteremia with concentrations of bacteria of 10^5 to 10^6 per ml of blood never recovered and died within 24 h; CSF cultures in such animals (when done in parallel) were always positive in concentrations equal to or greater than the concentration of bacteria in the blood. Low-grade bacteremia (10^2 to 10^3 CFU/ml of blood) was seen in other experiments in <5% of animals and at times lingered for a few days before clearing spontaneously. These animals, usually older than 10 days, were at a lower risk of having positive CSF cultures than animals with a higher degree of bacteremia.

CSF leukocyte and erythrocyte counts were not done because only small amounts of CSF were available. Although small amounts of blood may contaminate the CSF obtained by the technique of micropuncture of the cisterna magna, in approximately 90 to 95% of occasions the samples were clear to the eye. Since in the present studies bacterial concentrations in the CSF were equal to or frequently greater than that of blood, the recovery of GBS from CSF was interpreted as an indication of true infection of this fluid. However, it was not considered evidence of meningitis.

Age-related susceptibility to infection and death. The susceptibility of rats of various ages to lethal infection with three different GBS strains was studied. After injection with 76-043, type III, 54% of 5-day-old animals succumbed to infection with $<10^2$ CFU of bacteria and 94% of animals given 10^2 to 10^4 CFU died (Fig. 2). The differences in mortality between 5- and 9- to 10-day-old animals injected with 10^2 to 10^4 CFU of bacteria were significant ($P < 0.001$). Nine- to ten-day-old and 11- to 12-day-old animals were more resistant to higher inocula of GBS. Adult rats were also studied and demonstrated only 29% mortality after injection with 10^7 to 10^8 CFU compared with 80% mortality in 11- to 12-day-old animals ($P < 0.05$). However, adult rats that received 10^9 to 10^{10} CFU of GBS developed a fulminant clinical course with a high mortality (88%), and death occurred ordinarily by 48 h after injection.

This increasing resistance to infection with age was also seen in animals injected with types Ia and Ic (Table 4). These two strains had comparable capacity to produce lethal infections in 5-day-old animals after 10^2 to 10^4 CFU were injected. Animals were less susceptible to higher inocula of 10^5 to 10^6 CFU at 9 to 10 days of age, with differences in mortality of 35 to 50% (types Ic and Ia, respectively), compared with 5-day-old animals given the same inocula.

Histopathological findings of meningitis. Although it was common to find GBS in the CSF of terminally ill infant rats, it was not valid

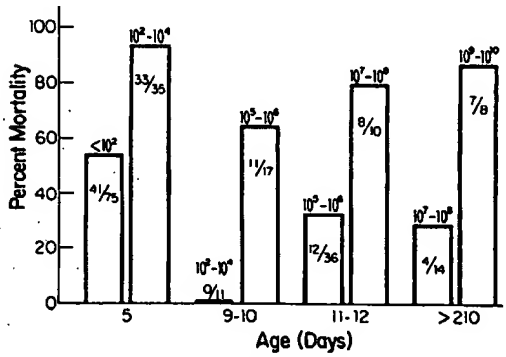

FIG. 2. *Age-related susceptibility to lethal infection with strain 76-043, serotype III. The concentration of the bacterial inoculum is indicated above the bars. Number of animals that died within 72 h with positive cultures/number of animals inoculated is indicated within the bars.*

TABLE 4. *Age-related susceptibility of infant rats to infection with varying inocula of GBS serotypes Ia and Ic*[a]

Inoculum size (CFU of bacteria)	Mortality (%) in animals injected at:			
	5 days with:		9–10 days with:	
	Ia	Ic	Ia	Ic
10^2–10^4	4/21[b] (19)	9/29 (31)		0/3 (0)
10^5–10^6[c]	5/10 (50)	3/7 (43)	0/3 (0)	1/12 (8)
10^7–10^8	4/4 (100)		3/5 (60)	7/9 (78)

[a] Animals received i.p. injection of strain 74-562, type Ia or 74-430, type Ic.

[b] Number of animals that died within 72 h with organ cultures positive for GBS/number of animals inoculated.

[c] Analysis of combined mortality after injection with 10^5 to 10^6 CFU of serotypes Ia and Ic in 5-day compared with 9- to 10-day-old animals revealed a significant difference ($P < 0.05$).

to diagnose meningitis in these animals without histological examination of the brain and, particularly, the meninges. There were 34 animals with documented bacteremia who had culture-positive CSF samples obtained when death occurred (by 48 h after injection). Autopsies were performed shortly afterwards and tissues were processed for hematoxylin and eosin stain and Gram stain. These animals were of four different ages at the time of injection of GBS by the i.p. route. It is noteworthy that similar concentrations of bacteria were recovered from their blood and CSF (Table 5). However, only 2 of 11 5-day-old animals had bacteria found in Gram stains of the brain and meninges, and none had inflammatory cells. Six of twelve 9- to 10-day-old animals had collections of meningeal bacteria, but only one animal had a minimal inflammatory response. Six of nine 11- to 12-day-old animals had bacteria seen in meningeal tissue, and three of the six had an inflammatory reaction. Eight of the 9- to 10-day-old animals and eight of the 11- to 12-day-old animals received 10^6 CFU of bacteria i.p., and they had an equivalent intensity of bacteremia (mean CFU per milliliter of blood and standard deviation were comparable) and similar bacterial concentrations in CSF. Statistical analysis of these small numbers of animals revealed no significance in the trend of the older animals to mount an inflammatory response. The most impressive tissue evidence of meningitis was seen in the two 15-day-old animals. There was no difference in the time of death between animals with versus without a meningeal inflammatory response.

The animals showing inflammation typically had markedly thickened leptomeninges due to hyperemia, edema, the presence of numerous gram-positive cocci, and marked infiltration by polymorphonuclear leukocytes and macrophages. The infiltrate and bacteria were found principally surrounding meningeal vessels. Similar infiltrates and bacteria were noted in the perivascular spaces within the cerebral cortex. Leukocytes could be found within the lumen of vessels and emigrating through them, although necrotizing vasculitis was not a feature.

The animals showing no acute inflammatory response typically had only minimally thickened leptomeninges with virtual absence of edema and leukocyte infiltration. Hyperemia of meningeal vessels was found together with numerous gram-positive cocci. In general, the bacteria occupied a perivascular position, but in some animals, bacteria could be found within the vessel lumen and transmurally through its wall as well.

Examples of the tissue response to infection in a 9- to 10-day-old animal and a 15-day-old animal are shown in Fig. 3 and 4. These animals were given similar inocula of strain 76-043, and both had bacterial concentrations in the blood and CSF at the time of death of 10^5 and 10^6 CFU/ml, respectively.

Histopathology of other tissues. Although bacteria were seen in the lungs, liver, and kidney in many animals of various age groups, the presence of an inflammatory response was rare in these organs.

TABLE 5. *Correlation of age, bacterial inoculum, magnitude of bacteremia, and CSF bacterial counts with histopathology of meninges in animals that died*[a]

Age at injection (days)	No. of animals injected with designated CFU of bacteria	Bacteremia (mean CFU/ml of blood)	Mean CFU/ml of CSF	No. of animals with meningeal	
				Bacteria	Inflammatory cells
5	5 ($1–3 \times 10^1$)	7.0×10^5	8.2×10^5	1	0
	3 (10^2-10^3)	1.6×10^5	4.0×10^5	1	0
	3 (10^6)	1.8×10^6	2.6×10^6	0	0
9–10	2 (10^5)	1.8×10^5	6.0×10^5	1	0
	8 (10^6)	1.0×10^6	7.9×10^5	4	0
	2 (10^7)	8.4×10^5	5.3×10^5	1	1[b]
11–12	8 (10^6)	1.4×10^6	3.3×10^5	5	2
	1 (10^7)	2.0×10^5[c]	2.0×10^5[c]	1	1
15	2 (10^6)	4.4×10^5	1.7×10^6[c]	2	2

[a] All of the animals received 76-043, serotype III, with the exception that three of the 5-day animals received 74-562, serotype Ia, and that two of the 9- to 10-day animals received 74-430, serotype Ic, and one received 74-562, serotype Ia. Death occurred within 48 h of injection.

[b] A few inflammatory cells were present.

[c] This is the value for one animal.

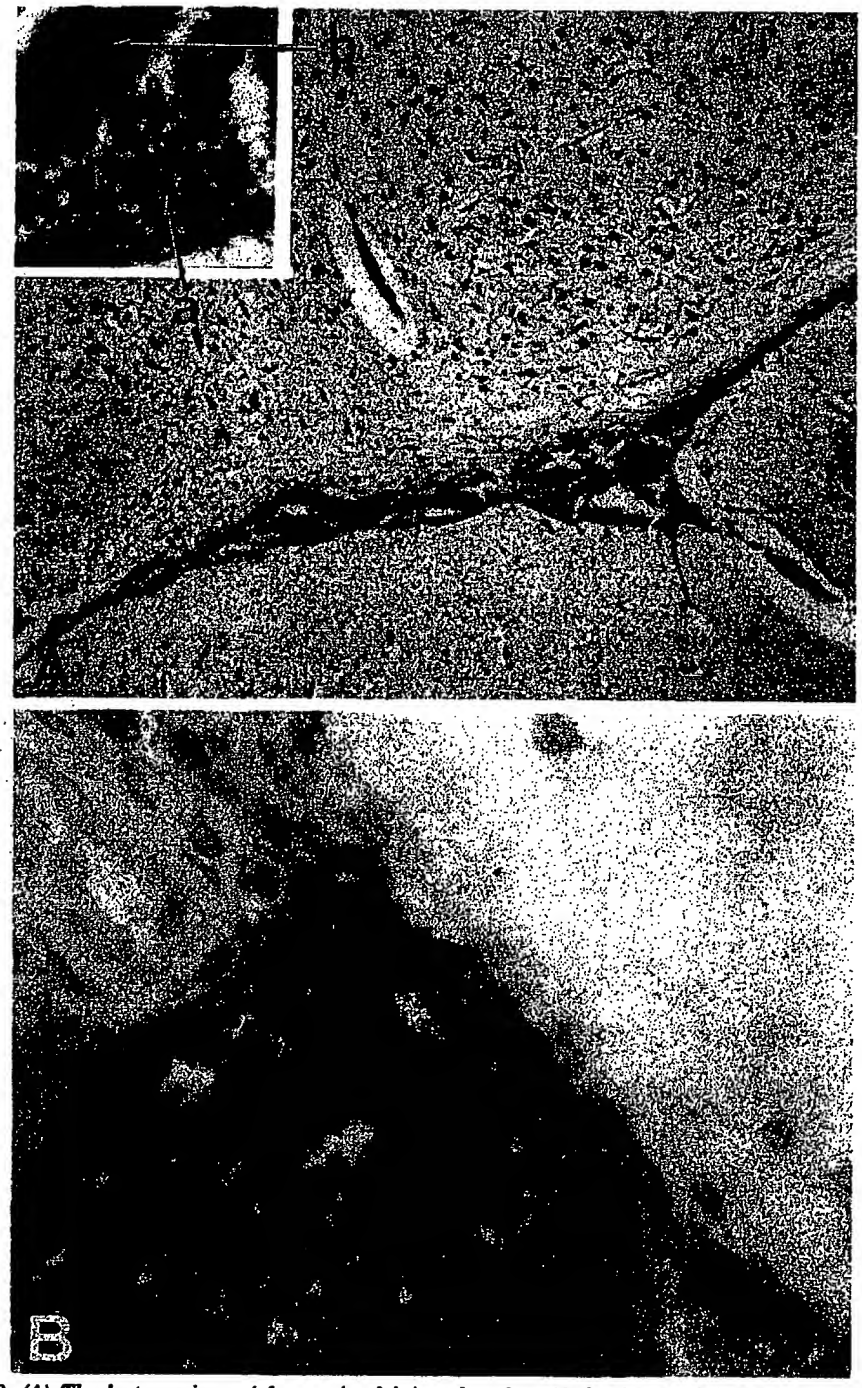

FIG. 3. *(A) The leptomeninges (of an animal injected at 9 to 10 days) are minimally thickened by the numerous bacteria present. There is virtual absence of edema and inflammatory cell infiltrate. Meningeal vessels are dilated and filled with erythrocytes (×116). Inset: Arrow a points to large numbers of bacteria. Arrow b indicates erythrocytes in the lumen of a meningeal vein. Note absence of inflammatory cells in the leptomeninges (×600). (B) Gram stain of the leptomeninges demonstrates massive numbers of gram-positive cocci. Portions of a small meningeal artery (left upper photograph) and a dilated meningeal vein (left lower photograph) are seen, and their walls are virtually devoid of bacteria (×1,160).*

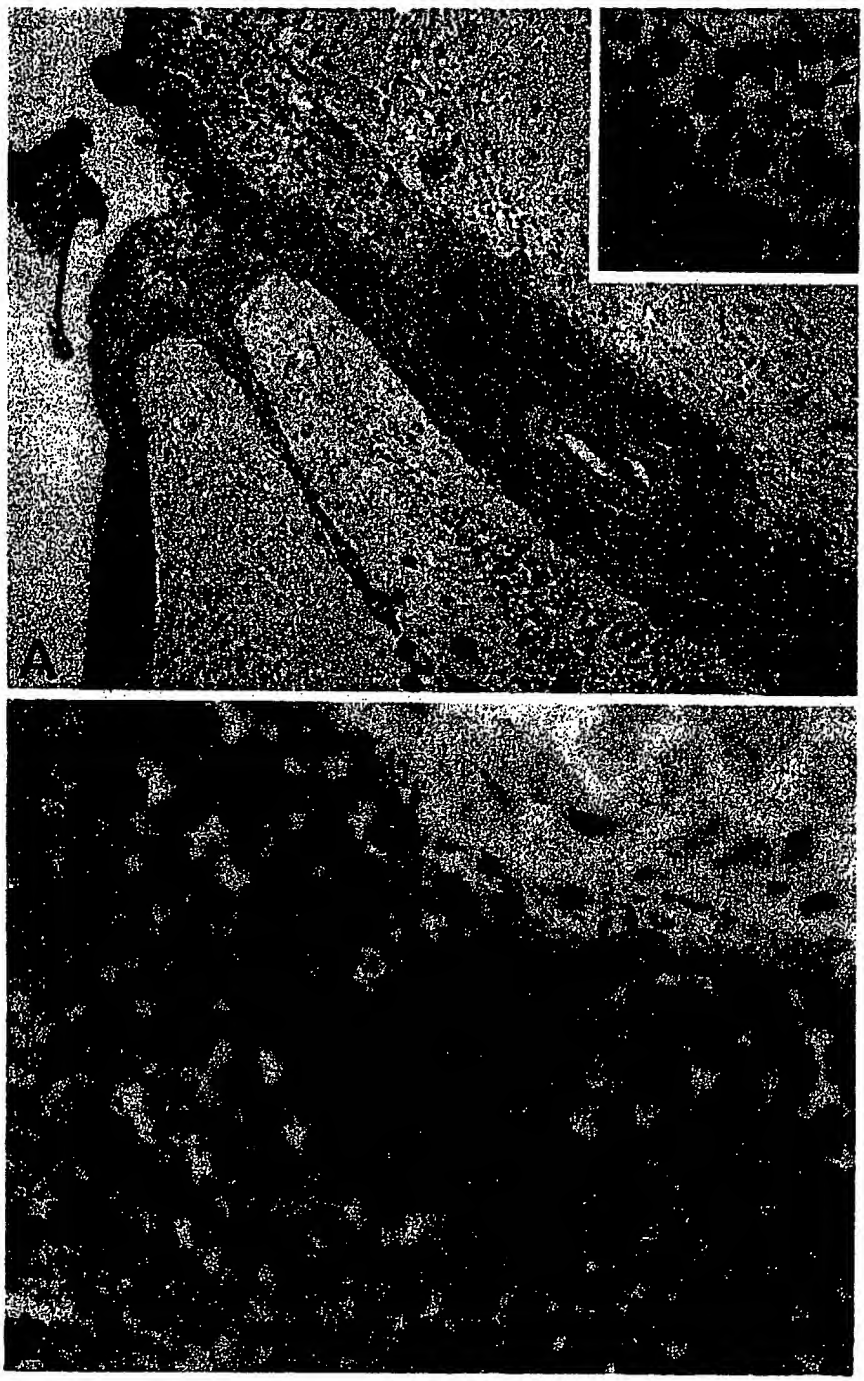

FIG. 4. *(A) The leptomeninges (of an animal injected at 15 days) are markedly thickened due to the presence of numerous bacteria, edema, acute inflammatory infiltrate, and hyperemia. Bacteria surround a branch of a meningeal artery and inflammatory cells can be seen in the lumen of the vessel (×116). Inset: Arrows point to two polymorphonuclear leukocytes in the leptomeningeal infiltrate (×600). (B) Gram stain of the leptomeninges demonstrates innumerable gram-positive cocci. A small portion of the wall of the meningeal artery shown in Fig. 4A is visible in the right upper part of the photograph. Bacteria are principally perivascular in distribution (×1,160).*

DISCUSSION

Rapidly fatal infections in newborn human infants due to GBS continue to pose a major challenge in perinatal medicine (1, 4). Although septicemia in the early newborn period has been associated with all the types of GBS, type III remains the most prevalent one associated with early onset meningitis and also with meningitis beyond the first week to 10 days of life (1, 4, 28). Whether type III GBS possess specific biological properties which confer any advantages for neuroinvasion is unclear. It is of interest, however, that type III strains recovered from human cases of septicemia and meningitis produce, in general, larger amounts of the extracellular enzyme neuraminidase compared with other types, and type III strains from individuals with disease produce more enzyme then type III strains recovered from asymptomatically colonized individuals (16).

Many aspects of the pathogenesis of septicemia and meningitis in humans are obscure and deserve further study. It is advantageous to have an animal model of infection with GBS which has some human parallels.

An infant animal model permits an opportunity to study age-dependent factors which may contribute to susceptibility to infection with various infectious agents and to assess the development of host mechanisms that are involved in modifying infection and disease. The 11- to 12-day-old chicken embryo for example, was an effective model for studying GBS type III bacteremia and antibody modification of disease (25). Although the infant rat has been used for extensive studies of *H. influenzae* b sepsis and meningitis (18, 24) as well as for more recent studies of *E. coli* bacteremia (9, 13), less information has been available on its usefulness in the study of GBS infections. Employing large inocula of 5×10^6 GBS type Ia and III in 2- to 2.5-day-old rats, Crumrine et al. found that subcutaneous injection of bacteria led to infection and death, more fulminant for animals given type Ia. It also appeared that type III organisms did not exhibit the invasive capacity shown by type Ia (M. H. Crumrine, M. W. Balk, and G. W. Fischer, Abstr. Annu. Meet. Am. Soc. Microbiol. 1976, B47, p. 18).

In the present study inoculation of bacteria by the i.p. route was chosen when bacteremia did not occur after oral feedings of bacteria and was seen only rarely after intranasal inoculation. This was a curious finding since the intranasal route has been excellent for initiating bacteremia and meningitis in similarly aged animals with *H. influenzae* b (18). *E. coli* strains possessing various polysaccharide antigens have been given orally, as well as by the i.p. route, with initiation of bacteremia and then meningitis (9, 13). Intranasal inoculation of *E. coli* strains has been less successful in initiating infection (13).

Using the i.p. route for injection, GBS strains representative of each serotype demonstrated a capacity for initiating bacteremia that led to lethal infection within 72 h. The four strains isolated from human CSF (three of type III) produced infection and death in 84% of animals given 10^2 to 10^4 CFU of bacteria compared with a mortality rate of 21% in animals injected with strains of type Ic and II isolated from blood and type Ia, a skin strain. Although these strains had not been passaged in the laboratory, differences among these strains may exist that influence pathogenicity. In fact, differences in opsonic requirements of GBS strains of the same serotype have been shown in vitro (23), suggesting that non-type-specific antigens also may play a role in immunity to these organisms.

If bacteremia developed in the 5-day-old sucklings injected with these strains, it was by 24 to 48 h and the concentration of bacteria in the blood invariably exceeded 10^5 CFU/ml. Widespread bacterial dissemination occurred then with a fatal outcome. The clinical findings in these animals were similar to those of human infants, including lethargy, tachypnea, and cyanosis with a relentlessly rapid course progressing to death (26).

It is of note that the four human CSF strains, included in these studies, have been tested for streptococcal pyrogenic exotoxin production. Rabbits were injected with ethanol-precipitated cell-free supernatant fluids of GBS growth and observed for typical streptococcal pyrogenic exotoxin fever curves. They were not seen, and none of these rabbits had enhanced susceptibility to the injection of *S. typhimurium* endotoxin (P. M. Schlievert and D. W. Watson, unpublished data).

The type III organism, 76-043, used for many of these studies was of particular interest because so few organisms were capable of initiating bacteremia and death. With an inoculum as low as <10 CFU, a mortality of 27% was seen. The incidence of bacteremia and death in a group of 109 animals injected with inocula of <10 to 10^3 CFU of this strain was 66%, and the number of deaths was directly related to the size of the inoculum. Since this strain had not been passaged in animals to increase its virulence, it is curious that animals were so susceptible to it.

If 5- to 12-day-old animals became bacteremic after i.p. injection with strain 76-043, the likelihood of having positive CSF cultures was nearly 100% and the concentrations of bacteria in the CSF were, ordinarily, 10^5 to 10^6 CFU/ml

of fluid. These CSF bacterial counts were comparable to counts reported by Feldman for a group of five patients with GBS meningitis whose CSF bacterial counts ranged from 4.5×10^3 to 10^5 CFU/ml (10). Occasional animals cleared low-grade bacteremia, and they were less likely to disseminate bacteria to the CSF.

The resistance to infection seen in progressively older animals injected with either a type Ia, Ic, or III strain resembled the human situation where it is less common to have fulminant septicemia develop after the first week to 10 days of life (1, 4, 26). Effective killing of GBS requires functioning phagocytes and type-specific antibody (7). Since the older infant rats would not have developed type-specific antibodies (without a previous exposure to GBS), it is possible that progressive maturation of the reticuloendothelial system offered animals protection from lethal infection following i.p. inoculation.

The absence of inflammation observed in sections of brain and meninges of younger animals who died with preceding bacteremia and positive CSF cultures was intriguing. In vivo, this may have reflected an intrinsic immaturity of neutrophils or delay of neutrophil outpouring in response to an infectious stimulus as a function of age. Alternatively, the bacteria or its elaborated products may have inhibited neutrophil chemotaxis or inhibited differentiation of phagocytic cells at marrow sites of production. It is of interest that newborn human infants have demonstrated poor neutrophil chemotaxis (15). In the absence of antibody, however, a deficiency of effective phagocytes at the site of bacterial entry (or in the blood or tissues) may contribute to the extremely high mortality seen with infection due to GBS. Recently, Schuit and Debiasio have reported that peritoneal leukocytes and macrophages of newborn rats responded poorly to i.p. GBS infection in contrast to adult rats (Program Abstr. Intersci. Conf. Antimicrob. Agents Chemother. 19th, Boston, Abstr. no. 317, 1979). Parallels in infected human infants include frequently observed neutropenia that has correlated with higher mortality (19) and the histological finding of numerous bacteria but a paucity of inflammatory cells in the lungs and meninges of a few premature infants who succumbed to systemic infection with GBS (21). Further studies are necessary to gain a better understanding of these observations.

ACKNOWLEDGMENTS

This work was supported by Public Health Service grant AI-13926 from the National Institutes of Health.

We thank Mary Ryan and Jean Ubl for their expert secretarial assistance. We appreciate the encouragement provided by Lewis W. Wannamaker and also his critical review of the manuscript.

LITERATURE CITED

1. Anthony, B. F., and D. M. Okada. 1977. The emergence of group B streptococci in infections of the newborn infant. Annu. Rev. Med. 28:355–369.
2. Anthony, B. F., D. M. Okada, and C. J. Hobel. 1978. Epidemiology of group B *Streptococcus*: longitudinal observations during pregnancy. J. Infect. Dis. 137:524–530.
3. Badri, M. S., S. Zawaneh, A. C. Cruz, G. Mantilla, H. Baer, W. N. Spellacy, and E. M. Ayoub. 1977. Rectal colonization with group B *Streptococcus*: relation to vaginal colonization of pregnant women. J. Infect. Dis. 135:308–312.
4. Baker, C. J. 1977. Summary of the workshop on perinatal infections due to group B *Streptococcus*. J. Infect. Dis. 136:137–152.
5. Baker, C. J., and F. F. Barrett. 1973. Transmission of group B streptococci among parturient women and their neonates. J. Pediatr. 83:919–925.
6. Baker, C. J., F. F. Barrett, R. C. Gordon, and M. D. Yow. 1973. Suppurative meningitis due to streptococci of Lancefield group B: a study of 33 infants. J. Pediatr. 83:724–729.
7. Baltimore, R. S., D. L. Kasper, C. J. Baker, and D. K. Goroff. 1977. Antigenic specificity of opsonophagocytic antibodies in rabbit anti-sera to group B streptococci. J. Immunol. 118:673–678.
8. Baltimore, R. S., D. L. Kasper, and J. Vecchitto. 1979. Mouse protection test for group B *Streptococcus* type III. J. Infect. Dis. 140:81–88.
9. Bortolussi, R., P. Ferrieri, and L. W. Wannamaker. 1978. Dynamics of *Escherichia coli* infection and meningitis in infant rats. Infect. Immun. 22:480–485.
10. Feldman, W. E. 1976. Concentrations of bacteria in cerebrospinal fluid of patients with bacterial meningitis. J. Pediatr. 88:549–552.
11. Ferrieri, P. 1979. Group B streptococcal sepsis/meningitis in infant rats, p. 164–165. *In* M. T. Parker (ed.), Pathogenic streptococci. Proceedings of the VII International Symposium on Streptococci and Streptococcal Diseases. Reedbooks, Ltd., Chertsey.
12. Ferrieri, P., P. P. Cleary, and A. E. Seeds. 1977. Epidemiology of group-B streptococcal carriage in pregnant women and newborn infants. J. Med. Microbiol. 10:103–114.
13. Glode, M., A. Sutton, E. R. Moxon, and J. B. Robbins. 1977. Pathogenesis of neonatal *Escherichia coli* meningitis: induction of bacteremia and meningitis in infant rats fed *E. coli* K1. Infect. Immun. 16:75–80.
14. Lancefield R. 1938. A micro precipitin-technic for classifying hemolytic streptococci and improved methods for producing antisera. Proc. Soc. Exp. Biol. Med. 38: 473–478.
15. Miller, M. E. 1971. Chemotactic function in the human neonate: humoral and cellular aspects. Pediatr. Res. 5: 487–492.
16. Milligan, T. W., C. J. Baker, D. C. Straus, and S. J. Mattingly. 1978. Association of elevated levels of extracellular neuraminidase with clinical isolates of type III group B streptococci. Infect. Immun. 21:738–746.
17. Moxon, E. R., and P. T. Ostrow. 1977. *Haemophilus influenzae* meningitis in infant rats: role of bacteremia in pathogenesis of age-dependent inflammatory response in cerebrospinal fluid. J. Infect. Dis. 135:303–307.
18. Moxon, E. R., A. L. Smith, D. R. Averill, and D. H. Smith. 1974. *Haemophilus influenzae* meningitis in infant rats after intranasal inoculation. J. Infect. Dis. 129:154–162.
19. Nieburg, P. I. 1976. Prognostic/diagnostic factors in group B beta hemolytic streptococcal (GBBS) and other neonatal sepsis. Pediatr. Res. 10:402.
20. Pass, M. A., B. M. Gray, S. Khare, and H. C. Dillon,

Jr. 1979. Prospective studies of group B streptococcal infections in infants. J. Pediatr. 95:437–443.
21. Quirante, J., R. Ceballos, and G. Cassady. 1974. Group B beta hemolytic streptococcal infection in the newborn. I. Early onset infection. Am. J. Dis. Child. 128: 659–665.
22. Rotta, J., R. M. Krause, R. C. Lancefield, W. Everly, and H. Lackland. 1971. New approaches for the laboratory recognition of M types of group A streptococci. J. Exp. Med. 134:1298–1315.
23. Shigeoka, A. O., R. T. Hall, and H. R. Hill. 1979. Strain specificity of opsonins for group B streptococci types II and III. Infect. Immun. 23:438–445.
24. Smith, A. L., D. H. Smith, D. R. Averill, J. Marino, and E. R. Moxon. 1973. Production of *Haemophilus influenzae* b meningitis in infant rats by intraperitoneal inoculation. Infect. Immun. 8:278–290.
25. Tieffenberg, J., L. Vogel, R. R. Kretschmer, D. Padnos, and S. P. Gotoff. 1978. Chicken embryo model for type III group B beta-hemolytic streptococcal septicemia. Infect. Immun. 19:481–485.
26. Wannamaker, L. W., and P. Ferrieri. 1975. Streptococcal infections-updated, p. 26–32. *In* H. F. Dowling (ed.), Disease-a-Month. Year Book Medical Publishers, Inc., Chicago.
27. Wennerstrom, D. E., and R. W. Schutt. 1978. Adult mice as a model for early onset group B streptococcal disease. Infect. Immun. 19:741–744.
28. Wilkinson, H. W. 1978. Group B streptococcal infection in humans. Annu. Rev. Microbiol. 32:41–57.

Exhibit L

INFECTION AND IMMUNITY, Feb. 1986, p. 648–652
0019-9567/86/020648-05$02.00/0

Vol. 51, No. 2

Experimental Meningococcal Infection in Mice: A Model for Mucosal Invasion

IRVING E. SALIT[1,2]* AND LEWIS TOMALTY[2]

Division of Infectious Diseases, Toronto General Hospital,[1] and Institute of Medical Sciences, University of Toronto,[2] Toronto, Ontario M5G 2C4, Canada

Received 21 August 1985/Accepted 26 October 1985

A more complete understanding of meningococcal disease has been hampered by the lack of an appropriate animal model. Previous models have utilized injections of meningococci, which precludes the study of nasopharyngeal colonization and invasion. We have developed a model for meningococcal disease in which litters of 5-day-old mice are challenged intranasally with 10^7 viable meningococci. Bacteremia is monitored by jugular venous blood cultures, and cerebrospinal fluid is sampled by cisternal punctures. Human disease-associated and carrier strains were compared; nasopharyngeal colonization was similar for these bacteria, but the case-associated strains were much more frequently invasive and caused bacteremia. Twenty-one percent of bacteremic animals had meningitis. There was an age-related susceptibility to infection which correlated inversely with the levels of serum complement. Preinjection of iron dextran increased the number of animals which were bacteremic, the concentration of bacteria in blood, and nasopharyngeal colonization. Noncapsular variants of virulent meningococci did not colonize nasopharyngeal tissue in vivo, and they were not invasive. This neonatal mouse model mimics meningococcal disease as seen in humans and may be useful in studying the initial events in the pathogenesis of meningococcal disease.

Neisseria meningitidis, the meningococcus, remains a major cause of endemic and epidemic bacterial meningitis despite the availability of effective polysaccharide vaccines (13). To study the pathogenesis of meningococcal disease and to test the effectiveness of vaccines, numerous animal models have been developed over the years; these have included experimental meningococcal infection in monkeys (9), mice (16, 18), rabbits (2), chicken embryos (3), and guinea pigs (1, 11). All of these models have required the injection of bacteria either directly into the cerebrospinal fluid, into the bloodstream, or into subcutaneous chambers. It is suspected that some of the illness in the experimental models has been due to the direct injection of toxic bacterial products. Mouse models have become very popular for the study of meningococcal infection; Miller (18) first described the intraperitoneal injection of meningococci in hog gastric mucin, which enhances the virulence of the bacteria. Iron was later found to be an acceptable substitute for mucin (5). These models have been used to test the ability of potential vaccines to prevent either murine death or bacteremia after intraperitoneal injection of meningococci (21). None of these animal models, however, adequately mimics the pathogenesis of meningococcal disease in humans, especially since they bypass the mucosal colonization and invasion steps. In addition to protecting against clinical illness, appropriate vaccines should also have the ability to prevent meningococcal carriage in the nasopharynx and hence eliminate the major reservoir of infection. We have previously studied experimental meningococcal infection in rats, guinea pigs, and mice (25, 26). The most appropriate experimental model involved using neonatal mice who developed nasopharyngeal carriage followed by bacteremia, meningitis, and death.

We describe below meningococcal virulence factors and murine host factors which are important in this model.

* Corresponding author.

MATERIALS AND METHODS

Bacterial strains. Strains of *N. meningitidis* isolated from blood or spinal fluid were designated "case strains," whereas those derived from the pharynxes of asymptomatic persons were designated "carrier strains." The strains which were used in this study and previous studies (25, 26) were characterized as to capsular serogroup and serotype (serogroup/serotype). Disease-associated strains were B16B6 (B/2a), M986 (B/2a,7), 3006 (B/2b), BB80 (B/2), M1011 (B/2,10), BB106 (C/2), BB138 (C/2), BB155 (C/2), and VM63 (nongroupable). Carrier strains were M990 (B/6), DRES 03 (B/15), DRES 18 (B/nontypable), M992 (B/5), VM112 (X), VM49 (B), and VM82 (Z). The noncapsular variants were derived from the group B encapsulated parent strains by selecting naturally occurring mutants on antiserum-agar plates (6, 7). The absence of encapsulation was confirmed before intranasal challenge by the antiserum-agar method (7).

All strains were stored frozen at −80°C in sterile 5% (wt/vol) monosodium glutamate and 5% (wt/vol) bovine serum albumin. Before use in inoculation studies, the bacteria were partially thawed, liberally inoculated onto clear gonococcal typing agar (27), and grown overnight at 37°C in an atmosphere of 5% CO_2. Bacteria were then removed from the agar plate by using sterile cotton-tipped swabs and were transferred to 15- by 100-mm test tubes containing 5 ml of brain heart infusion broth. The bacterial suspensions were rotated end over end for 3 h at 37°C until an optical density of 0.35 was achieved at a wavelength of 540 nm with a Coleman junior 2A linear spectrophotometer. This corresponds to 1×10^9 to 3×10^9 CFU/ml. The exact number of CFU was determined by making 10-fold serial dilutions in brain heart infusion broth. Stock bacterial strains were always renewed with bacteria of the same strain which had been recently reisolated from infected animals. This was done to ensure that virulence determinants were not lost by repeated in vitro passaging.

Mouse model. Natural litters of Swiss CD1 mice (13 to 17 pups per litter) were obtained from Charles River Breeding

TABLE 1. Comparative colonization and bacteremia after intranasal inoculation of case- and carrier-associated meningococci[a]

Source of strain	Iron dextran	Bacteremia	Colonization	Mortality
Case[b]	−	110/397 (28)	86/270 (32)	3/397 (0.7)
	+	184/354 (52)	144/191 (75)	59/354 (17)
Carriers[c]	−	11/94 (12)	31/82 (38)	0/94 (0)
	+	6/83 (7)	42/93 (45)	2/83 (2)

[a] Data are given as the number of animals with bacteremia (or colonization or mortality)/total, with the percentage in parentheses. The statistical significance values of the comparisons were as follows. (i) For iron-pretreated animals (case strains versus controls not pretreated), bacteremia, colonization, and mortality, $P < 0.001$. (ii) For iron-pretreated animals (carriers versus case strains), bacteremia and colonization, $P < 0.001$, and mortality, $P < 0.01$. (iii) For iron-pretreated animals (carrier strains versus controls not pretreated), bacteremia, colonization, and mortality, not significant. (iv) For animals with no iron pretreatment (carrier versus case strains), bacteremia, $P < 0.05$, and colonization and mortality, not significant.

[b] Nine strains: serogroup B type 2 (five strains), serogroup C type 2 (three strains), and nongroupable (one strain).

[c] Seven strains: serogroup B (five strains), serogroup X (one strain), serogroup 29e,Z (1 strain). None was serotype 2.

Laboratories, Inc., Wilmington, Mass., and were atraumatically inoculated intranasally with 10^7 meningococci as previously described (26). Briefly, bacterial suspensions containing 10^9 CFU/ml were aspirated into 0.5-ml glass syringes to which were attached 5-mm-long, blunted, 30-gauge needles. Without any anesthesia, 0.01 ml was atraumatically inoculated into one nostril. Blood cultures were taken at 3, 24, and 48 h by puncturing the internal jugular vein with a 25-gauge needle. Samples (0.01 ml) of blood were withdrawn and placed on agar plates. Nasal cultures were obtained by washing the nasal passages with 0.05 ml of brain heart infusion broth, which was then immediately placed on agar plates.

At 3 to 6 h before intranasal inoculation, some animals also received intraperitoneal injections of iron dextran (Imferon, Pfizons Corp. Ltd., Scarborough, Ontario) at a dosage of 250 mg of iron per kg. Control animals received saline.

Cerebrospinal fluid was sampled by inserting a 25-gauge needle into the nape of the neck and then into the cisterna magna (19). This procedure could be done repeatedly on an animal without mortality.

After inoculations all animals were observed and weighed daily. Deaths were tabulated, and selected animals underwent pathological examination.

Complement studies. Cobra venom factor from *Naja naja*, obtained from Cordis Laboratories, Miami, Fla., was reconstituted in phosphate-buffered saline, and portions were frozen at −80°C. At 24 h before intranasal instillation of meningococci, mice received 200 U of the venom factor per kg. At 24 h after injection there was no C3 present, as measured by a sensitive alternate complement pathway assay employing ^{51}Cr-labeled erythrocytes (17). In addition, A/J mice which were deficient in the fifth component of complement (Jackson Laboratories, Bar Harbor, Maine) were challenged with meningococci as described above.

Statistical methods. Fourfold tables were constructed, and the chi-square values (χ^2) were determined by using Yates' correction for continuity.

RESULTS

Comparative colonization and bacteremia. Five-day-old litters of mice were inoculated intranasally with strains derived from human patients with meningitis or carriers (Table 1). In the animals which had not been pretreated with iron dextran, the rates of bacteremia were significantly higher in pups in which the disease-associated isolates were instilled intranasally. Despite the higher rates of bacteremia, nasopharyngeal colonization rates and mortality were not significantly different in the groups which were challenged with either carrier- or case-derived isolates. Intraperitoneal injection of iron dextran significantly enhanced rates of bacteremia, colonization, and mortality in those mice which were challenged with the disease-associated isolates. Iron dextran did not alter these parameters in the mice challenged with carrier strains. Of the mice which were bacteremic from case-derived strains, 21% (4 of 19) had infected cerebrospinal fluid as determined by cisternal puncture (26).

To ensure that bacteria were not being directly injected into mucosal tissue or even into the bloodstream, an alternate form of instillation was used. Using a Pasteur pipette, 100 μl of meningococci was dropped onto the external nares. The mice quickly aspirated the fluid into the internal nares. Animals which were challenged in this manner had identical results to those which had intranasal instillation with a blunt needle (data not shown).

We then determined the rates of bacteremia in relationship to the numbers of bacteria instilled intranasally. In the absence of iron, an inoculum of at least 10^5 disease-associated bacteria was required to produce any detectable bacteremia (Fig. 1). This increased to 20% when 7×10^8 bacteria were used. Injections of iron dextran significantly enhanced rates of bacteremia and reduced the minimum infective dose so that even after challenge with 700 bacteria, 10% of animals were bacteremic.

Quantitative blood cultures were also done to determine the level of bacteremia under different circumstances. With the virulent strain B16B6, almost 90% of the animals which were bacteremic had less than 10^3 organisms per ml of blood (Fig. 2). Injection of iron dextran not only increased rates of bacteremia (Table 1) but also increased the concentration of bacteria in those with positive blood cultures (Fig. 2). The mortality was highest in those animals with more than 10^4 bacteria per ml of blood.

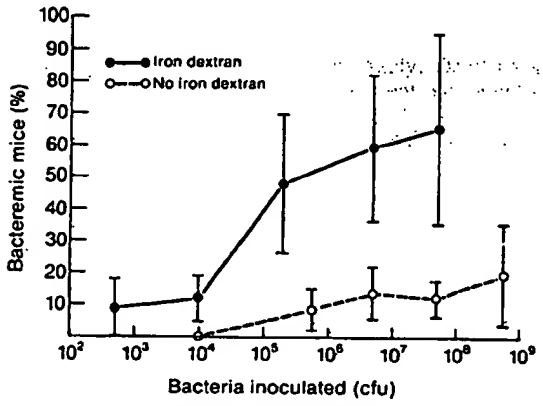

FIG. 1. Comparison of rates of bacteremia in neonatal mice 24 h after intranasal instillation of *N. meningitidis* B16B6 (○). Iron dextran was given intraperitoneally to another group of animals at the time of intranasal challenge (●). Each point represents the mean and standard deviation of the results from a minimum of four litters (at least 45 pups).

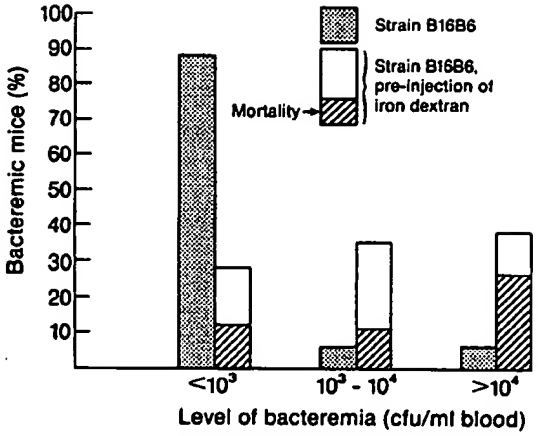

FIG. 2. Intranasal inoculation of 5-day-old pups with *N. meningitidis* B16B6. Mice which were not bacteremic were eliminated from this analysis. Quantitation of the degree of bacteremia was done on animals which had received meningococci alone or together with iron dextran. There was a 24% (24 of 99) rate of bacteremia without iron dextran and a 73% (81 of 111) rate of bacteremia in pups treated with iron.

The duration of bacteremia and colonization was assessed by doing repeated blood and nasal cultures at 3 h and then daily for 4 days. No further colonization or bacteremia was detectable by day 4 (age 9 days) (Table 2).

Role of the capsule. Encapsulated and noncapsular variants of strains M986 and 3006 were tested for their ability to colonize the nasopharynx and invade into the bloodstream (Table 3). Rates of bacteremia were markedly reduced in the noncapsular variants compared with the parent strains. A small number of mice became bacteremic after receiving the unencapsulated variant of strain 3006; however, approximately 5% of colonies reverted to the parent encapsulated form as detected on antiserum agar plates. No group B polysaccharide was detectable on strain M986. The noncapsular variants of both strains also colonized the nasopharynx to a significantly lesser extent than the parental strains.

Role of serum complement. We previously found that, in this model, there was an inverse relationship between the age of the mice and susceptibility to meningococcal bacteremia (26). Since humans may be susceptible to meningococcal disease because of complement deficiency (22), we wanted to determine whether the increased susceptibility of mice was also due to low complement levels. Serum complementary activity was measured at different ages and was found to be undetectable during the first week of life, rising to one-fifth of the adult levels by the second week of life. With equivalent numbers of male and female mice, the 50% hemolytic complement levels were 150, 30, and <5 U/ml at 6 weeks, 10 days, and <10 days of age, respectively. Rates of bacteremia are known to diminish in this model by 10 days, and bacteremia does not occur at 6 weeks of age.

To confirm the absence of serum complement at 5 days of age, cobra venom factor was injected intraperitoneally, and mice were challenged intranasally with the virulent strain B16B6 (Table 4). Cobra venom factor eliminated total hemolytic complement from adult animals by 24 h. After preinjection of neonatal mice with cobra venom factor, there was no enhancement of rates of bacteremia, levels of bacteremia, nasal colonization, or mortality. Similarly, there was no significant change in mortality when strain B16B6 was instilled into mice which have a congenital deficiency of C5. However, there was an increase in rates of bacteremia (25% versus 69%) as well as colonization (35% versus 100%).

TABLE 2. Duration of bacteremia and colonization in neonatal mice[a]

Time after i.n.[b] instillation (h)	Bacteremia		Colonization	
	No iron	With iron	No iron	With iron
3	6/40 (15)	ND[c]	ND	ND
24	16/100 (16)	104/174 (60)	ND	ND
48	21/103 (20)	61/120 (51)	19/53 (36)	70/109 (64)
72	2/78 (3)	2/32 (6)	3/46 (7)	2/32 (6)
96	0/78 (0)	0/40 (0)	0/46 (0)	0/40 (0)

[a] Data are given as the number of animals with bacteremia (or colonization)/total, with the percentage in parentheses. *N. meningitidis* B16B6 was used.
[b] i.n., Intranasal.
[c] ND, Not done.

TABLE 3. Comparison of colonization and invasiveness of encapsulated and nonencapsulated meningococcal variants[a]

Strain	Description	Bacteremia	Nasal colonization
M986 (B/2a,7)[b]	Encapsulated	14/40 (35)[c]	18/36 (50)[c]
	Noncapsular variant	0/54 (0)[c]	3/54 (6)[c]
3006 (B/2b)[b]	Encapsulated	17/37 (46)	37/37 (100)
	Noncapsular variant	7/76 (9)	17/76 (22)

[a] Data are given as the number of animals with bacteremia (or colonization)/total, with the percentage in parentheses.
[b] (Serogroup/serotype).
[c] $P < 0.001$, compared with noncapsular variant.

DISCUSSION

There have been many descriptions of animal models for meningococcal disease ever since *N. meningitidis* was clearly associated with epidemic cerebrospinal meningitis (28). The most popular model has been the mouse bacteremia model, which requires intraperitoneal injections of meningococci alone (16), in hog gastric mucin (18), or in iron dextran (5).

None of the previously described experimental models for meningococcal disease fully satisfies the criteria of an ideal model. Some suggested criteria for an experimental animal model (14) are as follows: (i) the portal of entry and route of dissemination must be similar to those in human disease, (ii) bacteria which are virulent for humans should also be virulent for the experimental animals, (iii) the course of disease should be predictable, (iv) it should be reproducible, (v) experimental lesions should be similar to those in human

TABLE 4. Effects of cobra venom factor on neonatal mice[a]

Treatment	Bacteremia		Nasal colonization	Mortality
	No./total (%)	Bacterial concn (CFU/ml, 10^3)		
Controls	24/99 (24)	1.4 ± 2.6	29/97 (30)	2/99 (2)
Cobra venom factor	55/223 (25)	1.8 ± 2.5	19/68 (28)	8/223 (4)

[a] Strain B16B6 was injected intranasally. Except for bacterial concentration, data are given as the number of animals with bacteremia (or colonization or mortality)/total, with the percentage in parentheses.

disease, (vi) the techniques should be relatively simple, and (vii) the pathophysiologic events must be similar to those occurring in humans (8). It is doubtful that any one animal model for meningococcal disease can meet all of these requirements.

Unfortunately none of the previously described models includes a mucosal colonization phase followed by bacterial invasion; this has precluded a study of the initial events in meningococcal disease. Similar problems had existed with models for *Haemophilus influenzae* until the development of the neonatal rat model, which utilizes intranasal instillation of bacteria (19).

We have described a neonatal mouse model for meningococcal disease in which the intranasal inoculation of bacteria is followed by a phase of nasopharyngeal colonization (25, 26). Virulent and avirulent strains attach to and colonize the murine nasopharynx to the same degree, but it is mainly those strains which are virulent for humans which invade through the nasal mucosa and cause bacteremia. About 20% of bacteremic animals do develop culture-positive purulent meningitis. Histopathologic studies indicate that smaller numbers of animals develop leptomeningitis and ventriculitis (26). There is an age-related susceptibility to meningococcal disease in this model, with resistance increasing after the first week of life; this resistance was correlated with increasing levels of serum complement. Protection against meningococcal disease in humans is also correlated with the presence of serum bactericidal activity. Complement-deficient humans are at increased risk for systemic meningococcal disease (22); similarly, we found that congenital C5-deficient mice had enhanced rates of bacteremia.

Injection of iron dextran increased rates of bacteremia, level of bacteremia, and nasopharyngeal colonization, but only for those strains which are intrinsically virulent. It is well known that iron enhances the virulence of many bacteria (4). Host iron is not readily available to bacteria because it is strongly bound to iron-binding proteins, and there is only an extremely small amount of free iron available in serum unless extrinsic iron is provided. Pathogenic neisseriae such as the meningococcus can utilize iron which is bound to transferrin; however, infection is associated with hypoferremia, which reduces the amount of iron available in the transferrin iron pool. Virulence is enhanced when iron saturation of transferrin is maintained at high levels by exogenous iron (15).

In this neonatal mouse model, the most virulent strains were encapsulated and had the serotype 2 antigen. Carrier-associated strains, however, did not invade despite the fact that all were encapsulated. None had the serotype 2 antigen. In humans, the serotype 2 antigen is also a major virulence determinant in invasive strains; carrier strains may be encapsulated or unencapsulated but rarely have the serotype 2 antigen (10). Factors responsible for meningococcal adherence are poorly defined, although pili appear to mediate adherence to human pharyngeal cells in vitro (24) and the A or C polysaccharide inhibits attachment to and agglutination of human erythrocytes in vitro (23). In the present study, organisms with the group B polysaccharide on their surface were more efficient in colonizing the nasopharynx in vivo than were the noncapsular variants. Studies in humans with the A and C polysaccharide vaccines do suggest that anti-capsular polysaccharide antibodies can similarly reduce pharyngeal colonization (12, 20). This implies that the group B polysaccharide may mediate meningococcal attachment in vivo. Other explanations are possible. (i) An important adhesin might be lost during the preparation of the noncapsular variant. (ii) Invasion may allow enhanced nasopharyngeal colonization by a "reverse invasion" procedure whereby bacteria from the bloodstream recolonize the nasopharynx; this is unlikely since the colonization rates are similar for the invasive and noninvasive strains. (iii) "Serum factors" may kill some meningococci in the nasopharynx. The in vivo colonization is enhanced by iron dextran. The mechanism is uncertain, but may involve some of the above factors, an interaction with the adhesin, increased growth rate, or a change in bacterial production of an adhesive molecule.

It is now possible to study in more detail the early phase of meningococcal disease including nasopharyngeal colonization, the poorly understood invasion through the mucosa, and ultimately bacteremia and meningitis. In addition, one can also study the ability of vaccines and passively transfused antibodies to inhibit mucosal colonization.

ACKNOWLEDGMENTS

This work was supported by grant MA 7371 from the Medical Research Council of Canada.

We thank Patti Jackson for excellent secretarial assistance.

LITERATURE CITED

1. **Branham, S. E., and R. D. Lillie.** 1932. Notes on experimental meningitis in rabbits. Public Health Rep. 47:2137–2150.
2. **Branham, S. E., R. D. Lillie, and A. M. Pabst.** 1937. Experimental meningitis in guinea pigs. Public Health Rep. 52: 1135–1142.
3. **Buddingh, G. J., and A. D. Polk.** 1939. The pathogenesis of meningococcus meningitis in the chick embryo. J. Exp. Med. 70:499–512.
4. **Bullen, J. J.** 1981. The significance of iron in infection. Rev. Infect. Dis. 3:1127–1138.
5. **Calver, G. A., C. P. Kenny, and G. Labergne.** 1976. Iron as a replacement for mucin in the establishment of meningococcal infection in mice. Can. J. Microbiol. 22:832–838.
6. **Craven, D. E., and C. E. Frasch.** 1978. Pili-mediated and nonmediated adherence of Neisseria meningitidis and its relationship to invasive disease, p. 250–252. *In* G. F. Brooks, E. C. Gotschlich, K. K. Holmes, W. D. Sawyer, and F. E. Young (ed.), Immunobiology of *Neisseria gonorrhoeae*. American Society for Microbiology, Washington, D.C.
7. **Craven, D. E., and C. E. Frasch.** 1979. Serogroup identification of meningococci by a modified antiserum agar method. J. Clin. Microbiol. 9:547–548.
8. **DeVoe, I. W.** 1982. The meningococcus and mechanisms of pathogenicity. Microbiol. Rev. 46:162–190.
9. **Flexner, S.** 1907. Experimental cerebrospinal meningitis in monkeys. J. Exp. Med. 9:142–166.
10. **Frasch, C. E., and S. S. Chapman.** 1973. Classification of Neisseria meningitidis Group B into distinct serotypes. III. Application of a new bactericidal inhibition technique to distribution of serotypes among cases and carriers. J. Infect. Dis. 127:149–154.
11. **Frasch, C. E., and J. D. Robbins.** 1978. Protection against group B meningococcal disease. II. Infection and resulting immunity in a guinea pig model. J. Exp. Med. 147:619–628.
12. **Gotschlich, E. C., I. Goldschneider, and S. Artenstein.** 1969. Human immunity to the meningococcus. J. Exp. Med. 129:1385–1395.
13. **Hankins, W. A., J. M. Gwaltney, Jr., J. O. Hendley, J. D. Farquhar, and J. S. Samuelson.** 1982. Clinical and serological evaluation of a meningococcal polysaccharide vaccine groups. A. C. Y. and W135 (41306). Proc Soc. Exp. Biol. Med. 169:54–57.
14. **Harter, D. H., and R. G. Petersdorf.** 1960. A consideration of the pathogenesis of bacterial meningitis: review of experimental and clinical studies. Yale J. Biol. Med. 32:280–309.
15. **Holbein, B. E.** 1980. Iron-controlled infection with *Neisseria*

meningitidis in mice. Infect. Immun. 29:886–891.
16. Huet, M. M., and A. Suire. 1976. Mise en evidence de la bacteriemie chez la souris. C. R. Acad. Sci. 283:421–422.
17. Joiner, K. A., R. Shahon, and J. A. Gelfand. 1979. A sensitive microassay for the murine alternative complement pathway. J. Immunol. Methods 31:283–290.
18. Miller, C. P. 1933. Experimental meningococcal infection of mice. Science 78:340–341.
19. Moxon, E. R., A. L. Smith, D. R. Averill, and D. H. Smith. 1974. Haemophilus influenzae meningitis in infant rats after intranasal inoculations. J. Infect. Dis. 129:154–162.
20. Peltola, H., P. H. Makela, H. Kayhty, H. Jousimies, E. Herva, K. Hällström, A. Sivonen, O.-V. Renkonen, O. Pettay, V. Karanko, P. Ahronen, and S. Sarna. 1977. Clinical efficacy of meningococcus group A capsular polysaccharide vaccine in children three months to five years of age. N. Engl. J. Med. 297:686–691.
21. Peppler, M. S., and C. E. Frasch. 1982. Protection against group B *Neisseria meningitidis* disease: effect of serogroup B polysaccharide and polymyxin B on immunogenicity of serotype protein preparations. Infect. Immun. 37:264–270.
22. Ross, S. C., and P. Densen. 1984. Complement deficiency states and infection: epidemiology, pathogenesis and consequences of Neisserial and other infections in an immune deficiency. Medicine 63:243–273.
23. Salit, I. E. 1981. Hemagglutination by Neisseria meningitidis. Can. J. Microbiol. 27:586–593.
24. Salit, I. E., and G. Morton. 1981. Adherence of *Neisseria meningitidis* to human epithelial cells. Infect. Immun. 31:430–435.
25. Salit, I. E., and L. Tomalty. 1984. Experimental meningococcal infection in neonatal mice: differences in virulence between strains isolated from human cases and carriers. Can. J. Microbiol. 30:1042–1045.
26. Salit, I. E., E. Van Melle, and L. Tomalty. 1984. Experimental meningococcal infection in neonatal animals: models for invasiveness. Can. J. Microbiol. 30:1022–1029.
27. Swanson, J. 1978. Studies on gonococcus infection. XII. Colony color and opacity variants of gonococci. Infect. Immun. 19:320–331.
28. Weichselbaum, A. 1887. Ueber die Aetiologie der akuten meningitis cerebrospinalis. Fortschr. Med. 5:575–583.

Proc. Natl. Acad. Sci. USA
Vol. 93, pp. 4131–4136, April 1996
Microbiology

Group B streptococci escape host immunity by deletion of tandem repeat elements of the alpha C protein

(*Streptococcus agalactiae*/antigenic variation/bacterial antigens/repetitive sequences)

LAWRENCE C. MADOFF*†‡, JAMES L. MICHEL*, ELIZABETH W. GONG*, DAVID E. KLING*, AND DENNIS L. KASPER*

*Channing Laboratory, Department of Medicine, Brigham and Women's Hospital, and †Division of Infectious Diseases, Beth Israel Hospital, Harvard Medical School, Boston, MA 02115

Communicated by Frederick M. Ausubel, Massachusetts General Hospital, Boston, MA, December 28, 1995 (received for review November 15, 1995)

ABSTRACT **Group B streptococci (GBS) are the most common cause of neonatal sepsis, pneumonia, and meningitis. The alpha C protein is a surface-associated antigen; the gene (*bca*) for this protein contains a series of tandem repeats (each encoding 82 aa) that are identical at the nucleotide level and express a protective epitope. We previously reported that GBS isolates from two of 14 human maternal and neonatal pairs differed in the number of repeats contained in their alpha C protein; in both pairs, the alpha C protein of the neonatal isolate was smaller in molecular size. We now demonstrate by PCR that the neonatal isolates contain fewer tandem repeats. Maternal isolates were susceptible to opsonophagocytic killing in the presence of alpha C protein-specific antiserum, whereas the discrepant neonatal isolates proliferated. An animal model was developed to further study this phenomenon. Adult mice passively immunized with antiserum to the alpha C protein were challenged with an alpha C protein-expressing strain of GBS. Splenic isolates of GBS from these mice showed a high frequency of mutation in *bca*—most commonly a decrease in repeat number. Isolates from nonimmune mice were not altered. Spontaneous deletions in the repeat region were observed at a much lower frequency (6×10^{-4}); thus, deletions in that region are selected for under specific antibody pressure and appear to lower the organism's susceptibility to killing by antibody specific to the alpha C protein. This mechanism of antigenic variation may provide a means whereby GBS evade host immunity.**

Group B streptococci (GBS) are the leading cause of pneumonia, sepsis, and meningitis in neonates in the United States and are increasingly recognized as a cause of invasive infection in immunocompromised and debilitated adults (1–3). GBS are part of the normal vaginal microflora of many women and colonize neonates during birth. Neonatal resistance to invasive GBS infection is related, in part, to maternal antibodies to the type-specific polysaccharides acquired transplacentally (4). On the basis of these findings, maternal immunization has been suggested as a strategy for the prevention of GBS infection in neonates (5).

The alpha C protein of GBS is a surface-expressed antigenic determinant present on many clinical isolates that is capable of eliciting protective antibody-mediated immunity in experimental animals (6–8). The alpha C protein, like the capsular polysaccharide of GBS and the M proteins of group A streptococci, may confer resistance to opsonophagocytic killing in the absence of type-specific antibody (9). The gene, *bca*, encoding the prototype alpha C protein from strain A909 has been sequenced, and several domains have been defined, including a signal sequence and a C-terminal membrane anchor domain that are typical of those found in other surface proteins of Gram-positive cocci (10). An N-terminal region encoding 185 aa is followed by a series of nine identical tandem repeats of 246 nt. The antigen appears as a series of evenly spaced bands on SDS/PAGE. Clinical isolates of GBS that express the alpha C protein display antigens of molecular size that varies with the number of tandem repeats contained within the gene; we have reported strains of GBS that express alpha C proteins ranging in size from 62.5 to 167 kDa (9).

We have previously shown that isolates of GBS vary in their susceptibility to opsonophagocytic killing in the presence of monoclonal antibody to the alpha C protein and that the extent of killing is proportional to the size of the alpha C protein expressed and to the number of tandem repeats within the gene (9). We also previously described a series of paired strains of GBS obtained from mothers and neonates in Majorca, Spain. Among 14 pairs that expressed the alpha C protein, two isolates from neonates showed a diminution in molecular size of the alpha C protein when compared with the corresponding maternal isolate (11).

Because nucleotide sequence repeats are hot spots for genetic recombination, we hypothesized that size variability in the alpha C protein results from recombination of intragenic repeats. We thus considered the possibility that this size change represented a form of antigenic variation, perhaps selected for by the presence of maternal antibody. Diminution in repeat number and in the corresponding size of the alpha C protein might reduce the ability of alpha-specific serum to opsonize a given strain for phagocytic killing.

We demonstrate that the neonatal isolates with altered alpha C proteins arose from the maternal isolate by intragenic deletion in *bca*. We further show that such deletions occur frequently in a mouse model of GBS infection in the presence of immune serum raised to the alpha C protein. Thus, deletions within the repeat-containing alpha C protein of GBS appear to play a role in evasion of type-specific host immunity in GBS infection by causing antigenic variation.

MATERIALS AND METHODS

Bacterial Strains. Strain A909 is the prototype Ia/C GBS strain originally obtained from the collection of Rebecca Lancefield (Rockefeller University, New York) (12). Clinical isolates of GBS were obtained from vaginal culture of parturient women prospectively studied at a single maternity hospital in Majorca, Spain, and from surface sites on their neonates as described (11). The isolates that were found by immunoblot with monoclonal antibody to express the alpha C protein were chosen for further study.

The publication costs of this article were defrayed in part by page charge payment. This article must therefore be hereby marked "*advertisement*" in accordance with 18 U.S.C. §1734 solely to indicate this fact.

Abbreviations: GBS, group B streptococci; cfu, colony-forming unit(s).

‡To whom reprint requests should be addressed at: Channing Laboratory, Brigham and Women's Hospital, 180 Longwood Avenue, Boston, MA 02115.

Antisera. To generate antiserum to the alpha C protein, that protein was expressed in a phage T7 polymerase system. The *bca* gene encoding the prototype alpha C protein from strain A909 of GBS was subcloned into plasmid pT7-7 (13). PCR mutagenesis was used to create a new *Nde* I site at the ATG start site of the *bca* gene and thus ligate the start site of the gene with the optimal spacing from the T7 promoter and ribosome-binding site on the plasmid (14). Purification of recombinant alpha C protein to homogeneity was achieved with ion exchange followed by gel filtration chromatography. The final product (r-alpha) was >99% pure as assessed by silver-stained polyacrylamide gel and compared with Western blot by monoclonal antibody (data not shown). Two New Zealand White rabbits (6–8 kg) were immunized s.c. with 50 μg of r-alpha emulsified in complete Freund's adjuvant and then immunized 3 and 6 weeks later with the same dose in incomplete Freund's adjuvant. Immune serum was obtained 2 weeks after the final boost. Western blot analysis used 4G8, a protective monoclonal antibody directed toward the repeat region of the alpha C protein as described (15).

Isolation of Spontaneous Mutants. To determine the frequency of spontaneous alpha C protein deletions, a single colony of GBS strain A909 was inoculated into Todd–Hewitt broth (THB) and grown overnight at 37°C. A 10^{-4} dilution of overnight cultures (10 μl) was spread on blood agar plates and incubated overnight at 37°C. Individual colonies were transferred onto Todd–Hewitt broth plate grids and incubated overnight at 37°C; the colonies were screened for alpha antigen expression by colony blot hybridization.

Colony Immunoblots. Disks of nitrocellulose were placed on the plates containing colonies of GBS and lifted to remove surface proteins (16). The disks were placed in a blocking buffer {[phosphate-buffered saline (PBS)]/0.5% Tween 20/5% skim milk} and gently rocked for 30 min at room temperature. The blocking solution was removed, and ascites containing the alpha antigen monoclonal antibody 4G8 was added at a 1:1000 dilution in PBS/0.5% Tween 20. After a 1-h incubation, blots were washed three times with PBS/0.5% Tween 20 and incubated with alkaline phosphatase-conjugated anti-mouse antibodies at a 1:1000 dilution in PBS/0.5% Tween 20 for 1 h at room temperature. Blots were then washed twice in PBS/0.5% Tween 20 and once in $MgCl_2/Na_2CO_3$. Alkaline phosphatase development reagent (Sigma) was added to detect the conjugate.

Opsonophagocytic Assay. The functional capacity of antibodies to the alpha C protein of GBS was assessed by an opsonophagocytic assay measuring *in vitro* killing of GBS (17). In brief, a 300-μl vol of human polymorphonuclear leukocytes (≈3 × 10^6 cells) was mixed with the test GBS strain [≈1.5 × 10^6 colony-forming units (cfu)], 50 μl of human serum (as a complement source), and 100 μl of antibody diluted 1:100. Viable GBS cells were enumerated as 10-fold dilutions on blood agar plates immediately and after 60-min incubation at 37°C; the difference was calculated as killing. The result is reported as the "log kill," which is the difference between log cfu before and after incubation for at least two measurements per strain. Human serum was prepared for use as a complement source by absorption on ice for 30 min with GBS of homologous serotype. The bacteria were removed by centrifugation and filter sterilization, and the absorbed serum was stored in aliquots at −80°C.

Isolation of DNA from GBS. Chromosomal DNA was prepared from GBS strains by a modification of published methods (16). Briefly, late stationary cultures of GBS in Todd–Hewitt broth (100 ml) were washed with 0.2 M sodium acetate, suspended in 10 ml of Tris/EDTA and glucose [0.1 M Tris (pH 7.0), 0.01 M EDTA, and 25% glucose], and incubated with 200 μg of *N*-acetylmuramidase (Mutanolysin; Sigma) for 1 h at 37°C. The suspension was pelleted and then resuspended in 9 ml of Tris/EDTA with 0.5% Sarkosyl; 10 μg of RNase and 5 mg of Pronase were added sequentially, each for 10 min at 37°C. The mixture was extracted with phenol/chloroform/isoamyl alcohol, ethanol precipitated, and spooled onto a glass rod. The DNA was air-dried, rinsed with 70% ethanol, and dissolved in 1 ml of H_2O.

Restriction Enzyme Analysis of Chromosomal DNA. Chromosomal DNA was analyzed for restriction fragment length polymorphisms by the method of Fasola *et al.* (18). Briefly, 10-μg samples of chromosomal DNA were incubated with *Hae* III, 60–100 units at 37°C for 18 h. Agarose gel electrophoresis was performed, and the bands were visualized with ethidium bromide.

Mouse Passage. A mouse model of infection was developed to demonstrate selection for GBS strains with deletions or truncations of the alpha C protein gene. CD-1 female outbred mice (6–8 weeks of age; Charles River Breeding Laboratories) were rendered immune to lethal challenge with GBS by passive immunization with alpha-specific antiserum (or preimmune control antiserum), 0.25 ml i.p. Mice were challenged 24 h later with lethal doses of the A909 (prototype Ia/C) strain of GBS [10^5 for preimmune or 10^6–10^7 for postimmune grown to mid-logarithmic phase (A_{650} = 0.3) diluted in Todd–Hewitt broth] delivered i.p. After 24 h, mice were killed, and the spleens were homogenized and plated. GBS isolates were then examined for expression of alpha C protein by Western blot analysis with alpha-specific monoclonal antibody.

Southern Blot Hybridization. Digests of chromosomal DNA were separated on agarose gel, denatured, and transferred onto GeneScreen hybridization transfer membranes (NEN) by UV cross-linking (Stratalinker 1800, Stratagene). Hybridizations were performed with a commercial kit (enhanced chemiluminescence; Amersham) according to the manufacturer's instructions. Briefly, the support is prehybridized to reduce nonspecific binding and then probed with peroxidase-labeled single-stranded DNA fragments, which are then oxidized to emit light. Fragments were probed with the entire *bca* gene in the expression plasmid pT7-7 (10, 13).

PCR. PCR was used to analyze the gene size and better define the region of the gene where deletions occurred. The forward primer was chosen within the region encoding the N terminus of the gene: 5′-TGCAGAGTACAGGAAGGGCT-3′, and the reverse primer began 30 bases 3′ to the gene: 5′-TGTTCACACCAATAAATGGTGA-3′ (Fig. 1). Chromosomal DNA from each mutant or clinical isolate (200 ng) was used as template, 50 pM of each primer was added, and PCR was performed with *Thermus aquaticus* (*Taq*) DNA polymerase (5 units), its accompanying buffer, dNTP (0.05 mM), and $MgCl_2$ (1 mM) (Boehringer Mannheim) in a total volume of 100 μl. The reaction was cycled through 94°C for 1 min, 63°C for 1 min, 72°C for 2 min 25 times, with a terminal extension at 72°C for 7 min in a DNA thermal cycler model 480

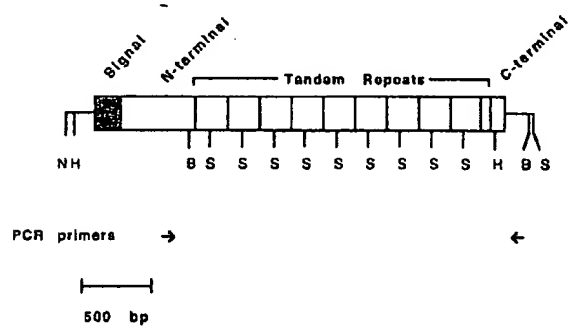

FIG. 1. Map of *bca* gene showing partial restriction endonuclease map, regions of the protein from the deduced amino acid sequence, and locations of primers used for PCR-amplification of the repeat region. N, *Nde* I; H, *Hin*dIII; S, *Sty* I; B, *Bsa*BI (*Mam* I).

(Perkin–Elmer/Cetus) (14). PCR products were examined by electrophoresis on 1.5% agarose gel.

RESULTS

Opsonophagocytic Killing of Maternal and Infant Isolates in the Presence of Alpha-Specific Antiserum. As previously noted (11), 2 of the 14 GBS isolates from infants expressed alpha C proteins of smaller molecular size than the protein expressed in isolates recovered from their mothers (Fig. 2). To determine whether the observed change in the phenotype of the alpha C protein would confer a biologic change to the organism, the discordant maternal and neonatal isolates were incubated with antibody specific for the alpha C protein in the presence of human serum complement and human peripheral blood leukocytes for 1 h. In each case, the maternal isolates were susceptible to opsonic killing by antiserum to the alpha C protein, but the neonatal isolates resisted such killing and proliferated (Table 1). Thus, the neonatal isolates, with deletions in alpha, were resistant to killing in the presence of alpha-specific antibody. In the absence of alpha-specific antibody, all strains were able to proliferate (data not shown).

Restriction Enzyme Analysis of Chromosomal DNA and Southern Blot Hybridization. All 14 pairs were subjected to restriction analysis of chromosomal DNA by digestion with *Hae* III and electrophoresis on agarose gel. Corresponding maternal–infant isolates appeared identical, except for those with discrepant alpha C protein size (representative strains shown in Fig. 3*A*). In each of these two pairs of isolates, a single band differed between maternal and infant isolates (arrows). Each pair of isolates could be distinguished from the others by the restriction fragment pattern.

Southern hybridization performed with the *bca* gene delineated a single band in each strain (Fig. 3*B*). In the two discrepant strain pairs, this band comigrated with the altered band seen on the ethidium bromide-stained gel. This result indicated that the band accounting for the discrepancy on restriction enzyme analysis of chromosomal DNA contained the gene for the alpha C protein and was consistent with an alteration in the size of the gene causing the discrepancy in restriction fragment pattern. Among the concordant strains, the migration of the hybridizing band was the same within each pair.

Frequency of Alpha Antigen Spontaneous Deletions in GBS. Colonies of GBS were screened for the lack of alpha antigen expression to determine the frequency of alpha antigen spontaneous deletion mutants. Derivatives of a single colony of A909 expressing the nine-repeat alpha C protein were screened for alpha expression by colony immunoblot; 3.06×10^3 cfu were screened with the alpha antigen monoclonal antibody 4G8 as a probe (7). Two colonies were not detected with this antibody. These independent isolates were confirmed to contain deletions of five tandem repeats by Western and Southern blot analyses (data not shown), thereby indicating that the frequency of alpha spontaneous deletions is $\approx 6.5 \times 10^{-4}$.

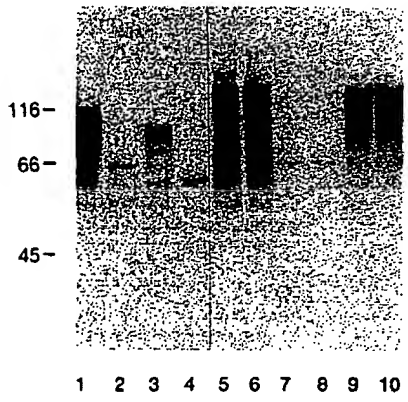

FIG. 2. Western blots with alpha-specific monoclonal antibody of mother–infant paired isolates from Majorca, Spain. Strain 73 (lane 1) is the maternal isolate and strain 72 (lane 2) is the corresponding neonatal isolate. Strain 144 (lane 3) is the maternal isolate and strain 140 (lane 4) is the corresponding neonatal isolate. Lanes 5–10 show representative maternal–neonatal pairs in which the sizes of the alpha C protein were the same. The size discrepancies in lanes 1–4 were previously noted (11) but are illustrated here for clarity.

Mouse Passage Experiments. To determine whether selective pressure could account for the high observed frequency of deletions among neonatal GBS, GBS were passaged through mice rendered immune to the alpha C protein. Mice were passively immunized with either immune rabbit antiserum raised to the recombinant alpha C protein or preimmune rabbit serum. They were then challenged with the prototype alpha C protein-positive GBS strain. Isolates recovered from the spleens of four immune and four nonimmune mice were randomly chosen (28 per mouse) for Western blot analysis with alpha-specific antiserum. Of the isolates from immune mice, 49 (44%) showed no alpha C protein, 34 (30%) showed immunoreactive alpha C protein of smaller molecular mass (range 46–100 kDa), and 29 (26%) showed full-sized alpha C protein (representative Western blots shown in Fig. 4). All 112 isolates from the control animals immunized with nonimmune serum showed full-sized alpha C protein. To determine the consequences of the observed mutations for antibody-mediated opsonophagocytic killing of the strains, representative mouse-passaged isolates were incubated in the presence of human peripheral blood leukocytes, serum as a complement source, and rabbit antibody specific for the alpha C protein for 1 h (as for the human isolates). Each of the truncated and deleted mutants showed decreased killing relative to the parent strain (Table 1). One isolate (number 25) with intact, full-sized alpha was also tested and remained susceptible to opsonophagocytic killing.

Analysis of GBS Strains by PCR of the *bca* Repeat Region. To further define the location of the mutations occurring in the passaged GBS strains and in the human maternal–neonatal strain pairs, the tandem repeat region of the *bca* gene was amplified using PCR. Five of the strains isolated after mouse passage, which represented the diversity of strains recovered (including one strain that did not express immunoreactive alpha, one apparently unaltered strain, and three expressing differing sizes of alpha C protein), were further examined by PCR of the repeat region of *bca*. The discrepant maternal–neonatal paired clinical isolates were also examined by PCR of the alpha repeat region. The sizes of the repeat region of the alpha C protein genes from the Majorca isolates and the mouse-passaged isolates were determined by PCR with primers flanking this region. The size of the PCR products correlated with the molecular mass of the largest protein band as seen on Western blot analysis with 4G8 antibody (Table 1). The smallest PCR fragment generated (mutants 1 and 5) corresponded to one full repeat and the additional 33 nt of a partial repeat.

DISCUSSION

The alpha C protein of GBS is a known target of protective immunity (6–9, 12, 19). Although the biological function is unknown, its most striking structural feature is a series of nine tandem repeats that are identical at the nucleotide level (10). Repeat sequences in surface proteins from Gram-positive bacteria have been suggested to play a role in bacterial binding to host structures (20, 21). However, the identical nature of the repeat sequences at the DNA level, rather than allowing for conservative substitutions, suggests that the repeats play an important role at the nucleotide level. We hypothesized that this degree of conservation between repeats must have adaptive importance to have been preserved through evolution.

Table 1. Characteristics of GBS strains and opsonophagocytic killing in the presence of alpha antigen-specific rabbit antiserum

Strain number	Alpha C protein molecular mass (kd)	Source of isolate	PCR fragment size (kb)	Calculated number of full repeats	Killing (log cfu ± SD)*
A909†	116	Prototype	2.30	9	1.3 ± 0.03
A909 M1	None	Mouse passaged	0.18	1	−0.13 ± 0.6
A909 M5	38	Mouse passaged	0.17	1	0.39 ± 0.3
A909 M21	46	Mouse passaged	0.45	2	0.76 ± 0.4
A909 M10	70	Mouse passaged	1.03	4	0.02 ± 0.6
A909 M25	116	Mouse passaged	2.37	9	1.40 ± 0.09
73 (Mother A)‡	116	Human maternal	2.31	9	0.76 ± 0.07
72 (Neonate A)	74	Human neonatal	1.34	5	−0.096 ± 0.06
144 (Mother B)	100	Human maternal	1.76	7	0.34 ± 0.12
140 (Neonate B)	62	Human neonatal	1.02	4	−0.23 ± 0.1

*Amount of test strain killed after 1-h incubation with antiserum, serum complement, and human PMNs.
†Prototype Ia/C strain and parent for mouse-passaged mutants.
‡The size discrepancies between the alpha C proteins in these human maternal and neonatal isolates have been previously noted (11) and are listed here for clarity.

Repeating sequences of DNA are common among many proteins of Gram-positive bacteria and indeed among antigens of many other species of prokaryotes and eukaryotes (22–28).

We have shown that strains of GBS passed from mother to neonate, an important step in the pathogenesis of neonatal GBS infection, undergo mutations in the repeat region of the *bca* gene and that these mutations coincide with a loss of susceptibility to antibody-mediated killing by polymorphonuclear leukocytes. The resulting repeat number variants are presumably less well-recognized by antibody and thus less susceptible to opsonophagocytic killing. We further demonstrate that these mutations can occur both *in vitro* and *in vivo* and are readily selected for in an animal model of invasive GBS infection. All of the mutants studied contain fewer repeats than the parent strain and are less susceptible to alpha-specific antibody-mediated opsonophagocytic killing than the wild-type strain. However, there does not appear to be exact direct correlation between the size of the deletion and the magnitude of antibody-mediated opsonophagocytic killing. This variability in killing may be due to the inherent imprecision of the assay (which comprises several biologic components), to unobserved phenotypic changes occurring in the mutants, or to other immunologic factors such as conformational presentation of the antigen. Many of the mutants obtained *in vivo* appear to contain one full repeat and one partial repeat, a finding that supports (but does not prove) the hypothesis that homologous recombination of intragenic repeats is the mechanism of mutation. It is interesting that one of the mutants (strain 1) generates a PCR product of the repeat region that would correspond to one full and one partial repeat. Yet the strain fails to express a protein that reacts with antiserum to intact alpha C protein, which suggests that, after deletion, another mutation completely blocks expression of the alpha C protein.

The M proteins of group A streptococci are the best characterized of Gram-positive surface proteins and have similarities with the alpha C protein (29). Like the alpha C protein, they are targets of protective immunity, protect the organism from phagocytic killing, and share sequence homology in signal and C-terminal membrane anchor regions. The M6 protein of group A streptococci is a surface antigen important in virulence of and immunity to this bacterium that contains intragenic repeating sequences not identical at the nucleotide level (23, 30). These organisms undergo spontaneous mutations in the *emm6* gene by homologous recombination at intragenic repeats that result in variation in size and in antigenic and opsonic epitopes. These variants appear to occur at a lower frequency than do variants of the alpha C protein ($\sim 10^{-6}$ isolates per cfu), perhaps owing to the nonidentical nature of the tandem repeats in the *emm6* gene (31). Other M proteins also contain nonidentical repeats and probably exhibit this behavior (30). However, the biologic consequences of these mutations in natural infections are not known.

Moxon has proposed the concept of "contingency" loci; these are sites that allow more frequent mutations to occur so as to promote phenotypic diversity in a population and enhance adaptation to environmental changes (32). Many such

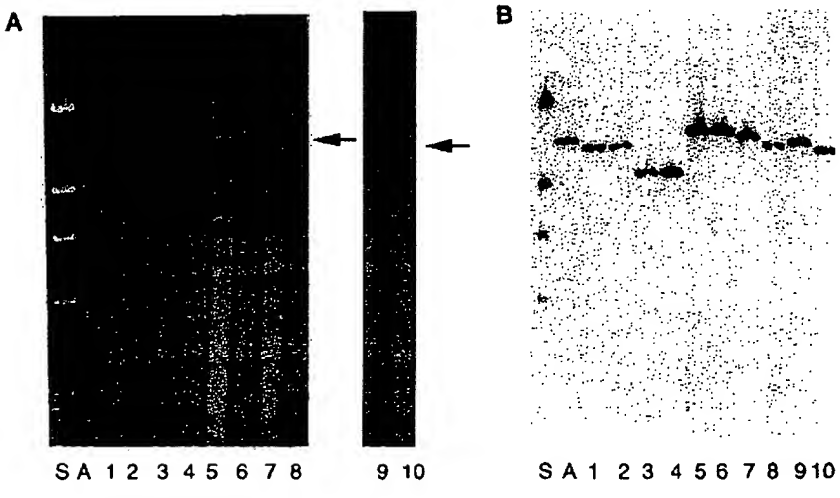

FIG. 3. (*A*) Digests of chromosomal DNA with *Hae* III from maternal–child paired GBS isolates. Three representative pairs of the 12 concordant pairs (lanes 1–6) and the 2 discordant pairs (lanes 7–10) are shown. Beginning with lane 1, adjacent pairs of odd- and even-numbered lanes contain maternal and neonatal isolates, respectively. Lane A contains the control strain A909. The arrows show aberrant bands present in lanes 7 and 9 (maternal strains 144 and 73) not visible in lanes 8 and 10 (corresponding neonatal strains 140 and 72). Concordant strains were identical. (*B*) Southern blot of the same gel hybridized with a probe for the alpha C protein gene *bca*. The aberrant bands are caused by a change in the size of the restriction fragment containing the *bca* gene.

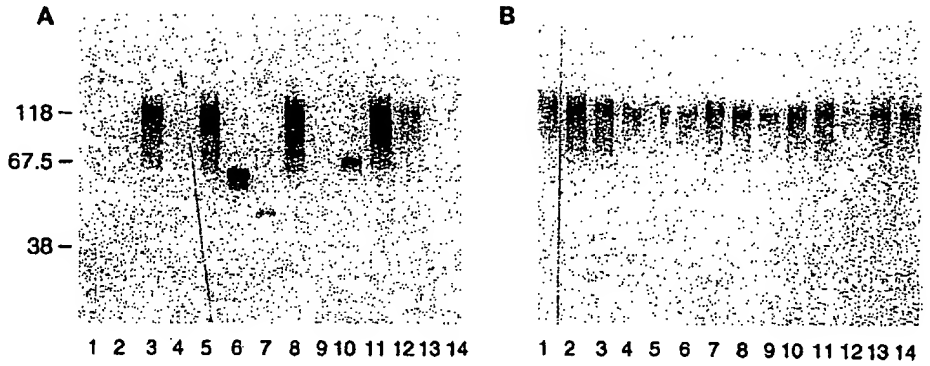

FIG. 4. Sequential strains of GBS isolated from the spleens of a mouse that received (*A*) alpha-specific immune serum or (*B*) received preimmune serum followed by challenge with alpha-positive GBS. Extracts of the strains are immunoblotted with alpha C protein-specific monoclonal antibody. All of the strains recovered from the nonimmune animals expressed the wild-type alpha phenotype. A high proportion of those from the immune animals expressed an altered phenotype.

highly mutable loci in pathogenic bacteria incorporate repeated DNA elements that may affect the expression of a phenotypic element. For example, strains of *Haemophilus influenzae* may either express or lack fimbriae. The switching mechanism was found to lie in a dinucleotide repeat (33). The number of repeats upstream of the gene controls the spacing between the −10 and −35 consensus sequence elements and thereby controls the efficiency of RNA polymerase binding and thus the level of fimbrial protein expression. Antigenic variation is a widely described phenomenon among pathogenic microorganisms, and a variety of genetic mechanisms underlie these phenotypic changes. Other methods of antigenic variation in bacterial proteins have been described that involve the introduction of DNA from outside the gene. For example, gonococcal pilin genes undergo homologous recombination with partial pilin genes outside of the region of expression, thus producing an antigenically altered pilin protein (34, 35). *Borrelia* species produce variable major protein variation by replacement of an active gene with an inactive gene (36). Antigenic variation appears to be an important and common mechanism of adaptation for pathogens that, to our knowledge, has not previously been described in GBS.

The striking identity of the repeats in the alpha C protein and the existence of a known protective epitope within the repeat lead us to hypothesize that the alpha C protein gene undergoes mutation, most likely by homologous recombination of identical intragenic repeats, which induces an alteration in the size (and repeat content) of the antigen. This change must affect the protective epitope in its interaction with antibody and thus allows the organism to elude antibody-mediated host immunity. This antigenic change could result from a decrease in the number of antibody-binding sites, alteration in the conformation of antibody-binding sites, and/or by decreased exposure of the antigen on the surface of the organism.

The observation of decreases in tandem repeat number of the alpha C protein under selective antibody pressure raises the question of what conditions might select for a larger number of tandem repeats. Such conditions must exist; otherwise one would expect all strains to display a small number of repeats, whereas, in fact, wild-type clinical isolates typically display 9 or 10 tandem repeats (9). Because other repeat-containing proteins are involved in binding to host factors (21), perhaps the repeat region of the alpha C protein is involved in colonization by GBS, and replication under colonizing conditions would favor a larger number of repeats.

A more thorough study of the phenomenon of antigenic variation by repeat number alteration has practical significance in the rational design of protein-based bacterial vaccines. A better understanding of the immunologic characteristics that allow protective epitopes to be altered should improve our ability to develop vaccines protective against the numerous pathogens expressing repeat-containing antigens.

We gratefully acknowledge the participation of Juan Hervas and Vincent Benedi in providing the maternal and neonatal clinical isolates. We thank Michael Wessels for valuable advice and discussion and Joanna Goldberg for thoughtful review of the manuscript. This research was supported in part by U.S. Public Health Service Contract N01-AI-25152 and National Institutes of Health grants AI00981, AI28500, AI08222, and AI23339.

1. Baker, C. & Edwards, M. (1990) in *Infectious Diseases of the Fetus and Newborn Infant*, eds. Remington, J. S. & Klein, J. O. (Saunders, Philadelphia), pp. 742–811.
2. Farley, M. M., Harvey, R. C., Stull, T., Smith, J. D., Schuchat, A., Wenger, J. D. & Stephens, D. S. (1993) *N. Engl. J. Med.* **328**, 1807–1811.
3. Madoff, L. C. & Kasper, D. L. (1993) in *Obstetric and Perinatal Infections*, ed. Charles, D. (Mosby, St. Louis), pp. 210–224.
4. Baker, C. J. & Kasper, D. L. (1976) *N. Engl. J. Med.* **294**, 753–756.
5. Baker, C. J. & Kasper, D. L. (1985) *Rev. Infect. Dis.* **7**, 458–467.
6. Bevanger, L. & Naess, A. I. (1985) *Acta Pathol. Microbiol. Immunol. Scand. B* **93**, 121–124.
7. Madoff, L. C., Michel, J. L. & Kasper, D. L. (1991) *Infect. Immun.* **59**, 204–210.
8. Michel, J. L., Madoff, L. C., Kling, D. E., Kasper, D. L. & Ausubel, F. M. (1991) *Infect. Immun.* **59**, 2023–2028.
9. Madoff, L. C., Hori, S., Michel, J. L., Baker, C. J. & Kasper, D. L. (1991) *Infect. Immun.* **59**, 2638–2644.
10. Michel, J. L., Madoff, L. C., Olson, K., Kling, D. E., Kasper, D. L. & Ausubel, F. M. (1992) *Proc. Natl. Acad. Sci. USA* **89**, 10060–10064.
11. Hervas, J. A., Gonzalez, L., Gil, J., Paoletti, L. C., Madoff, L. C. & Benedi, V. J. (1993) *Clin. Infect. Dis.* **16**, 714–718.
12. Lancefield, R. C., McCarty, M. & Everly, W. N. (1975) *J. Exp. Med.* **142**, 165–179.
13. Tabor, S. & Richardson, C. C. (1985) *Proc. Natl. Acad. Sci. USA* **82**, 1074–1078.
14. Ausubel, F. M., Brent, R., Kingston, R. E., Moore, D. D., Seidman, J. G., Smith, J. A. & Struhl, K. (1993) *Current Protocols in Molecular Biology* (Wiley, New York).
15. Madoff, L. C., Michel, J. L. & Kasper, D. L. (1991) *Infect. Immun.* **59**, 204–210.
16. Wanger, A. R. & Dunny, G. M. (1987) *Infect. Immun.* **55**, 1170–1175.
17. Baltimore, R. S., Kasper, D. L., Baker, C. J. & Goroff, D. K. (1977) *J. Immunol.* **118**, 673–678.
18. Fasola, E., Livdahl, C. & Ferrieri, P. (1993) *J. Clin. Microbiol.* **31**, 2616–2620.
19. Stalhammar, C. M., Stenberg, L. & Lindahl, G. (1993) *J. Exp. Med.* **177**, 1593–1603.

20. Gaillard, J. L., Berche, P., Frehel, C., Gouin, E. & Cossart, P. (1991) *Cell* **65**, 1127–1141.
21. Dramsi, S., Dehoux, P. & Cossart, P. (1993) *Molec. Microbiol.* **9**, 1119–1122.
22. Kemp, D. J., Coppel, R. L. & Andeu, R. F. (1987) *Annu. Rev. Microbiol.* **41**, 181–208.
23. Hollingshead, S. K., Fischetti, V. A. & Scott, J. R. (1987) *Mol. Gen. Genet.* **207**, 196–203.
24. Wallis, A. E. & McMaster, W. R. (1987) *J. Exp. Med.* **166**, 1814–1824.
25. Ibanez, C. F., Affranchino, J. L., Macina, R. A., Reyes, M. B., Leguizamon, S., Camargo, M. E., Aslund, L., Pettersson, U. & Frasch, A. C. (1988) *Mol. Biochem. Parasitol.* **30**, 27–33.
26. Anderson, B. E., McDonald, G. A., Jones, D. C. & Regnery, R. L. (1990) *Infect. Immun.* **58**, 2760–2769.
27. Yother, J. & Briles, D. E. (1992) *J. Bacteriol.* **174**, 601–609.
28. Zheng, X., Teng, L. J., Watson, H. L., Glass, J. I., Blanchard, A. & Cassell, G. H. (1995) *Infect. Immun.* **63**, 891–898.
29. Fischetti, V. A. (1991) *Sci. Am.* **264**, 58–65.
30. Jones, K. F., Hollingshead, S. K., Scott, J. R. & Fischetti, V. A. (1988) *Proc. Natl. Acad. Sci. USA* **85**, 8271–8275.
31. Hollingshead, S. K., Jones, K. F. & Fischetti, V. A. (1991) in *Genetics and Molecular Biology of Streptococci, Lactococci, and Enterococci*, eds. Dunny, G., Cleary, P. & McKay, L. (Am. Soc. Microbiol., Washington, DC), pp. 174–178.
32. Moxon, E. R., Rainey, P. B., Nowak, M. A. & Lenski, R. E. (1994) *Curr. Biol.* **4**, 24–33.
33. Moxon, E. R. (1992) *J. Infect. Dis.* **165**, Suppl. 1, S77–S81.
34. Connell, T. D., Black, W. J., Kawula, T. H., Barritt, D. S., Dempsey, J. A., Kverneland, K. J., Stephenson, A., Schepart, B. S., Murphy, G. L. & Cannon, J. G. (1988) *Mol. Microbiol.* **2**, 227–236.
35. Seifert, H. S., Wright, C. J., Jerse, A. E., Cohen, M. S. & Cannon, J. G. (1994) *J. Clin. Invest.* **93**, 2744–2749.
36. Barbour, A. G., Carter, C. J., Burman, N., Freitag, C. S., Garon, C. F. & Bergstrom, S. (1991) *Infect. Immun.* **59**, 390–397.

Journal of Medical & Veterinary Mycology 1997, 35, 271–278 Accepted 11 March 1997

Pharmacokinetics and biodistribution of a monoclonal antibody to *Cryptococcus neoformans* capsular polysaccharide antigen in a rat model of cryptococcal meningitis: implications for passive immunotherapy

D. L. GOLDMAN, ARTURO CASADEVALL* & L. S. ZUCKIER†

*Division of Infectious Diseases, Department of Pediatrics, Albert Einstein College of Medicine, 1300 Morris Park Ave, Bronx, NY 10461, USA; Division of Infectious Diseases, *Department of Medicine, Albert Einstein College of Medicine, 1300 Morris Park Ave, Bronx, NY 10461, USA; Division of Infectious Diseases, †Department of Nuclear Medicine, Albert Einstein College of Medicine, 1300 Morris Park Ave, Bronx, NY 10461, USA*

Several investigators have developed monoclonal antibodies against the capsular polysaccharide of *Cryptococcus neoformans* which have potential therapeutic applications. Using a rat model of *C. neoformans* meningitis, we studied the biodistribution and pharmacokinetics of a murine anticryptococcal capsular monoclonal antibody (mAb 2H1) after intravenous and intracisternal administration. After intravenous administration of ^{125}I-labelled 2H1 to infected rats, there was no detectable localization of ^{125}I in the brain or cerebrospinal fluid by either gamma-camera imaging of the whole animal or organ scintillation counting. In contrast, direct intracisternal instillation of 2H1 to infected rats resulted in persistent intracranial activity. In addition, the whole body half-life of intravenously administered radio labelled mAb 2H1 was significantly reduced in infected rats compared with uninfected rats. Our observations suggest that if high central nervous system (CNS) levels of mAb are needed to achieve a therapeutic effect in human *C. neoformans* meningoencephalitis, direct administration of mAb into the cerebrospinal fluid or modification of the mAb to increase penetration into the CNS may be required. Furthermore, higher or more frequent dosing of mAb may be required to maintain therapeutic levels in the presence of infection. This study demonstrates the usefulness of the rat as an experimental system for studying issues related to cryptococcosis.

Keywords *Cryptococcus neoformans*, distribution, kinetics, monoclonal antibody

Introduction

Cryptococcus neoformans is a ubiquitous encapsulated fungus that frequently produces lethal infections in immunosuppressed patients. Six to eight per cent of patients with AIDS present with cryptococcal meningoencephalitis and mortality is high despite antifungal therapy [1]. Individuals who survive the initial presentation are routinely managed with lifetime suppressive therapy to prevent recurrence of infections [2]. In response to the limitations of current treatment, several investigators have explored the efficacy of passive antibody therapy in the form of monoclonal antibodies (mAbs) directed against the capsular polysaccharide of *C. neoformans* [3–8]. Anticapsular mAbs prolong survival and decrease organ fungal burdens in animal models of *C. neoformans* infection [4–7,9] and enhance the therapeutic efficacy of amphotericin B, fluconazole and 5-flurocytosine [8,10,11]. The mechanisms of antibody-mediated protection are believed to include enhancement of macrophage and natural killer cell mediated phagocytosis [12,13]. For antibody to enhance phagocytosis, it must reach the site

Correspondence: Dr L. S. Zuckier, Department of Nuclear Medicine, Albert Einstein College of Medicine, Ullmann 121, 1300 Morris Park Ave, Bronx, NY 10461, USA. Tel: (718) 430-2605; Fax: (718) 792-6236.

of infection. Cryptococcal meningoencephalitis presents several unique problems for antibody therapy. First, the yeast releases large amounts of capsular polysaccharide (CNPS) into serum and tissues which may bind to, and thereby sequester, therapeutic antibodies. Second, the blood-brain barrier presents an obstacle to the diffusion of antibody into the central nervous system (CNS). The effects of these factors on mAb are not well understood and are difficult to study in murine models due to the small size of mice which makes obtaining cerebrospinal fluid (CSF) and CNS imaging studies problematic.

In this study, we report on the pharmacokinetics and biodistribution of intravenously and intracisternally administered ^{125}I-labelled anticryptococcal capsular mAb (2H1) in a rat model of cryptococcal meningitis. Intracisternal injection of *C. neoformans* in rats results in meningitis with disseminated infection and high levels of serum CNPS antigen. This model provides a system for studying potential problems and solutions related to passive anticryptococcal immunotherapy in humans.

Materials and methods

Animals

Male adult Fischer rats weighing between 250 and 280 g were obtained from Taconic Farms (Germantown, NY). For 1 week prior to the study, three drops of potassium iodide in the form of Lugol's solution (USP, Regional Service Center, Inc., Woburn, MA) were added to each bottle of drinking water to block non-specific thyroid uptake of radioiodine.

Organisms

C. neoformans strain 24067 (serotype D) was obtained from the American Type Culture Collection (Rockville, MD) and grown in Sabouraud glucose broth (Difco Laboratories, Detroit, MI) for 3 days at 30 °C. Organisms were washed three times with 0·2 M phosphate buffered saline (PBS), pH 7·2.

Intracisternal infection

Rats were anaesthetized by intraperitoneal injection of 75 mg kg^{-1} of sodium pentobarbital (Anpro Pharmaceutical, Arcadia, CA). Their heads were shaved, and cleansed with 70% ethanol. A 23 gauge needle was inserted into the basal cistern as indicated by free return flow of CSF and a volume of 0·2 ml PBS containing either $4{\cdot}4 \times 10^4$ *C. neoformans* (infected group) or no organisms (sham infection group) was injected.

Antibodies

mAb 2H1 is a murine IgG1 mAb which binds *C. neoformans* capsular polysaccharide (CNPS) [14]. mAb 2H1 was purified from ascites by Protein G affinity chromatography (Pierce, Rockford, IL) and quantitated by ELISA [15] relative to MOPC21 (Cappel, West Chester, PA), an IgG1 standard which was also used as an irrelevant control IgG1. mAbs 2H1 and MOPC21 were iodinated with either ^{125}I or ^{131}I, to a specific activity of approximately 1 μCi μg^{-1} using the Iodogen method (Pierce, Rockford, IL). Free iodine was separated from iodinated mAb by exclusion chromatography over a Sephadex G-25 column (Pharmacia, Piscataway, NJ).

Organ fungal burden and CNPS antigen levels

Organ fungal burdens and CNPS antigen levels in infected rats were determined in four rats which did not receive mAb. Nine days after intracisternal infection, the liver, lungs, kidneys and brain from each rat was removed, weighed and homogenized in PBS. CSF was obtained from three of four rats via basal cistern puncture. Homogenates and CSF samples were diluted and plated on Sabaroud glucose agar and colonies were counted after 48 h of incubation at 30 °C. CNPS levels in the serum and CSF of rats were measured by ELISA as described [8].

Organ radioactive counting

Organ radioactive counting was performed by measuring gamma counts of extirpated organs in a gamma-counter (Compugamma 1282, LKB Wallac, Turku, Finland) after injection of ^{125}I-labelled mAb. To correct tissue activity for the non-specific persistence of mAb in the vascular bed, a second ^{131}I-labelled irrelevant mAb was administered by tail-vein injection 1 h prior to death. One hour following injection of irrelevant mAb, CSF was obtained by intracisternal puncture and the rats were killed by lethal injection of sodium pentobarbital. The peritoneum was opened and approximately 2–3 ml of blood was withdrawn from the inferior vena cava using a 22 gauge needle. Spleen, brain, kidneys, lungs and liver were removed and blotted to eliminate excess blood. All specimens were weighed and their radioactive counts measured in both ^{125}I and ^{131}I windows, with standard correction of crosstalk between windows.

Antibody-derived ^{125}I counts were expressed on a per organ and per gram basis, and the latter was also normalized by the specific activity of each rat's blood to generate a tissue-to-blood localization ratio. ^{131}I-MOPC21 activity in each sample was used as a vascular marker to correct for non-specific counts in the vascular bed, based on the assumption that there is no specific tissue localization of

the irrelevant mAb over the 1 h time period. The ratio of ^{125}I to ^{131}I counts in the venous blood sample was multiplied by the ^{131}I counts of each tissue sample to estimate and correct for the ^{125}I-mAb counts deriving from blood. The corrected ^{125}I counts were also expressed on a per organ and per gram basis, and the latter was further normalized by ^{125}I-mAb activity in the blood to yield a corrected tissue-to-blood localization ratio.

Scintillation imaging

Scintillation imaging of ^{125}I-mAb distribution in anaesthetized rats was performed using a gamma-camera (Pho/Gamma III, Nuclear Chicago Inc., Des Plaines, IL) and nuclear medicine image analysis computer system (Gamma-11, Digital Co., Maynard, MA). Radiography grids (Liebel Flarsheim Co, Cincinnati, Ohio) were used for collimation of the low-energy photons from ^{125}I. Images were acquired for 10 min or until pixel saturation.

Intravenous mAb administration

Five μCi of either ^{125}I-2H1 or ^{125}I-MOPC21 were administered by tail vein injection 8 days after intracisternal inoculation of *C. neoformans* or PBS alone. Of the five infected rats, three received ^{125}I-2H1 (experimental group) and two received ^{125}I-MOPC21 (irrelevant mAb group). Two rats injected with PBS intracisternally received ^{125}I-2H1 (sham infection group). Gamma-camera imaging was performed on all rats at 2, 24 and 48 h after mAb administration. Five of the seven rats were then killed and their organs were assayed in a gamma scintillation counter using the described dual-isotope technique. The remaining sham and experimental rats were each re-imaged at 72 h, after which time they were killed. These rats were dissected and their organs and carcasses were imaged to verify location of the visualized activity.

Intracisternal mAb administration

A second group of six rats was infected intracisternally with *C. neoformans* and 7 days later injected with ^{125}I-2H1 ($n = 3$) or ^{125}I-MOPC21 ($n = 3$) intracisternally. Rats were imaged at 0·5, 2·5, 24, 48 and 96 h after mAb injection and were then killed and their organs removed and gamma counts determined.

Antibody half-life

In two experiments, whole-body antibody clearance was measured in infected and uninfected rats after tail vein injection of 1 μg of ^{125}I-labelled 2H1, 8 days following intracisternal injection of *C. neoformans* or PBS. Rats were anaesthetized as above and whole body scintillation counts were measured immediately after tail vein injection and at frequent intervals over a several week period. In the first experiment, two non-infected and a single infected rat were studied using an animal whole body scintillation counter (ARMAC Detector, Packard, Downers Grove, IL) interfaced to a multichannel analyser (Series 35, Canberra, Meriden, CT). In the second experiment, three infected and three non-infected rats were assayed, with scintillation counting performed using a cylindrical scintillation crystal (Canberra, Meriden, CT) interfaced to the multichannel analyser.

After correction for background and isotopic decay, radioactive counts were expressed as a percentage of the initial count rate for each rat. Half-time of whole body clearance of the mAb was calculated from clearance curves by non-linear regression using a pharmacokinetics software package (PCNONLIN, SCI Software, Inc., Lexington, KY). Data prior to 48 h was omitted to minimize potential contribution from an initial phase of rapid mAb clearance.

Statistics were calculated with a Student's *t*-test using Primer of Biostatistics software (McGraw-Hill, New York, NY).

Results

Organ fungal burden and CNPS antigen levels

Brain, lung, spleen, liver and kidney fungal burdens 9 days after intracisternal infection, expressed as log CFU per mg of tissue ± 1 SD, were 7·06 ± 0·11, 7·17 ± 0·42, 4·93 ± 0·26, 4·54 ± 0·36 and 4·06 ± 0·52, respectively. Because the pia and portions of the arachnoid are adherent to the removed brain, CFUs observed in the brain sample include meningeal fungal burden. Elevated levels of CNPS were noted in the serum and CSF on day 9 (mean ± 1 SD): 431 ± 323 and 320 ± 216 μg ml^{-1}, respectively. CNPS was not detectable in uninfected rats. There was no mortality in infected or uninfected rats.

Intravenous administration

All rats which received intravenous ^{125}I-labelled mAb had intense ^{125}I-mAb activity over the mediastinum and liver on gamma-camera imaging throughout the period of observation, consistent with relatively slow clearance of mAb from the blood pool. Of the three groups of rats, only the experimental group demonstrated localization of radioactivity to the head and splenic regions, seen by 24 h and peaking at 48 h (Fig. 1). Lateral images of these rats localized the radioactivity to the ventral portion of the neck, in the region of the thyroid gland, without noticeable concentration of activity in the more dorsal

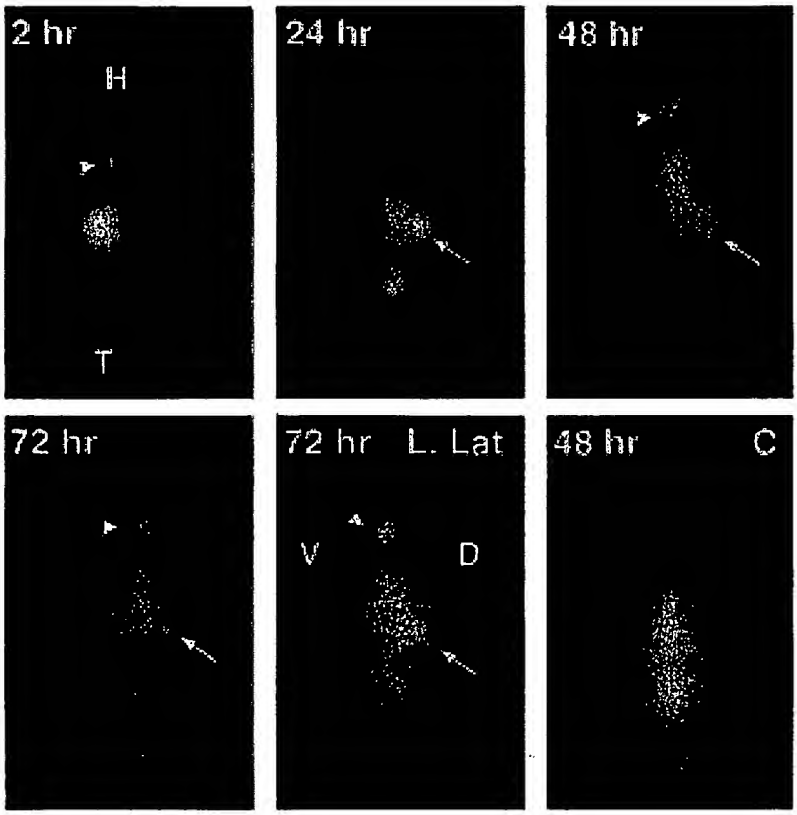

Fig. 1 Gamma-camera images following intravenous administration of mAbs. Representative images of infected rats administered 2H1 and imaged at 2, 24, 48 and 72 h demonstrate early accumulation of activity over the anterior neck, in the thyroid region (arrow head), with increasing activity noted over the spleen (arrows). All images are acquired in the ventral projection, unless indicated. H and T denote the head and tail regions, respectively. D and V denote the dorsal and ventral surfaces. A sham-infected control (C), imaged at 48 h after 2H1 administration, demonstrates relative distribution of counts in the heart and abdominal blood pool, without pronounced neck or splenic activity. Images of the infected rat administered control MOPC21 were similar to the sham-infected control (not shown).

intracranial region. In the rat from the experimental group killed at 72 h, post-mortem imaging of the brain, skull and carcass failed to demonstrate labelled mAb in association with the brain.

Scintillation counting of the removed samples (Fig. 2) demonstrated negligible ^{125}I activity in the brain and CSF in any of the three groups. When counts from the brain sample were corrected for residual blood activity, the level was further reduced towards background level. The spleen of the infected 2H1 rats was the only organ with a localization ratio above 1, indicating a concentration of activity exceeding that of the blood.

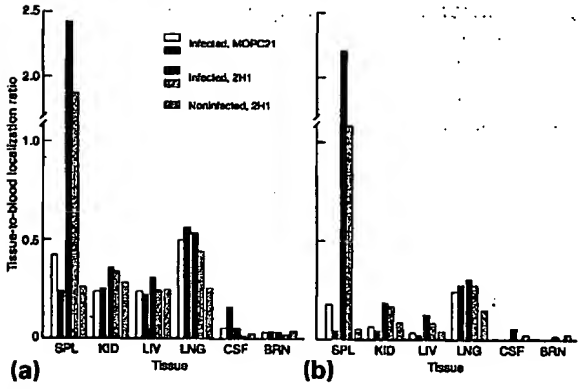

Fig. 2 Uncorrected (a) and corrected (b) tissue-to-blood localization ratios after IV administration of ^{125}I-mAbs (see text). The low values of CSF, brain and organ counts are rendered even smaller after correction is made for persistent vascular activity. The only organ with activity exceeding that of blood is the spleen in infected rats given ^{125}I-2H1. Each bar represents gamma counts from a single rat.

Intracisternal administration

Imaging of infected rats given intracisternal mAb revealed that mAb was initially localized to the skull and spinal cord regions, in the area of the subarachnoid space (Fig. 3). Rats given CNPS-specific mAb demonstrated a systemic blush with localization of activity to the splenic region, which was apparent 2-5 h after mAb injection. In rats receiving irrelevant mAb, systemic blush was not apparent until 1 day after mAb injection, and there was no detectable splenic enhancement. In contrast to the control mAb, rats which received CNPS-specific mAb demonstrated persistence of intracranial activity through 4 days postintracisternal administration with lateral

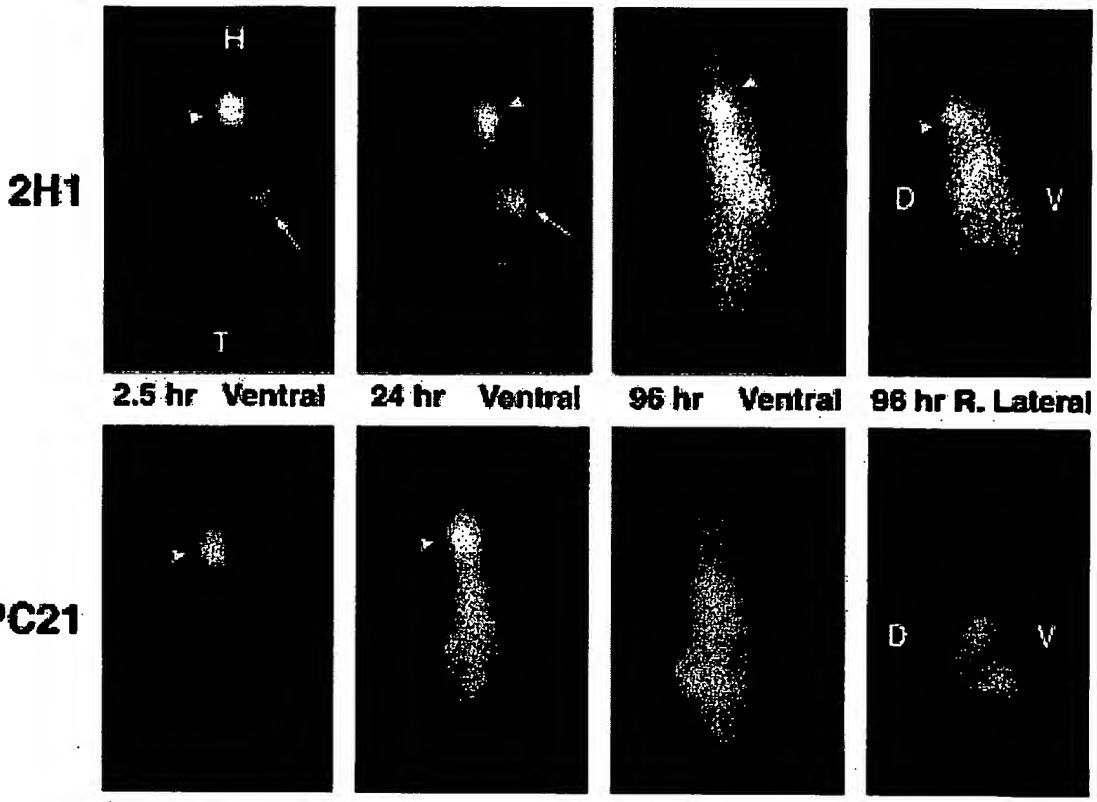

Fig. 3 Gamma-camera images following intrathecal administration of specific 2H1 mAb (top row) and control MOPC21 (bottom row) in infected rats. Images obtained at 2·5, 24 and 96 h in ventral and right lateral projections are shown. H and T denote the head and tail regions, respectively. D and V denote the dorsal and ventral surfaces. With specific mAb, splenic activity (arrows) is pronounced even by 24 h. Furthermore, there is much greater retention of intracranial activity (arrow head) at the 96 h delayed time point in the specific mAb group, compared with the controls.

imaging clearly localizing the radioactivity to the dorsal aspect of the head, in the intracranial region (Fig. 3).

Scintillation counting of organs and body fluid removed from infected rats which received intracisternal mAb (Fig. 4) demonstrated low ^{125}I counts in the brain and CSF. Although ^{125}I counts were low, rats which were given 2H1 had significantly higher ^{125}I counts in the brain compared with rats which were given MOPC21 ($P = 0{\cdot}017$). Rats given intracisternal 2H1 also demonstrated elevated splenic activity; however, the difference compared with rats which had received intracisternal MOPC21 was not significant at the $P = 0{\cdot}05$ level ($P = 0{\cdot}063$).

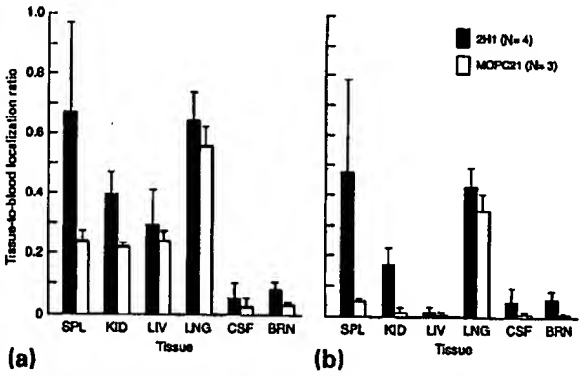

Fig. 4 Uncorrected (a) and corrected (b) tissue-to-blood localization ratios after intracisternal administration of mAbs (see text). Error bars indicate 1 standard deviation.

Antibody half-life

Whole body clearance of intravenously administered ^{125}I-2H1 (Fig. 5) in both the uninfected and infected rats was consistent with a model of first order kinetics. Half-life ranged between 7·4 and 11·7 days in non-infected rats and was shortened to between 2·8 and 6·5 days in *C. neoformans* infected rats. In both sets of measurements, half-life of disappearance in the infected rats was significantly

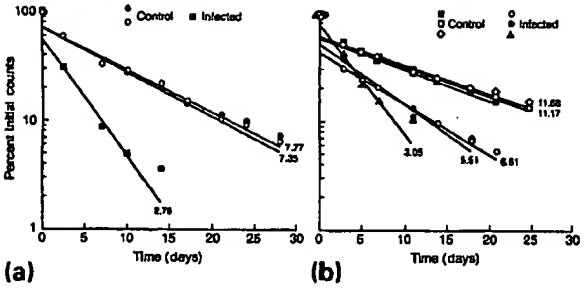

Fig. 5 Whole body clearance of ^{125}I-2H1 in non-infected and infected rats in two separate experiments (a and b). Non-linear regression lines for the second (beta) phase of clearance have been plotted for each rat based on data from 2 days and onwards. Whole body clearance of infected rats is accelerated relative to non-infected controls. Numbers refer to half-lives in days.

shorter than in the uninfected controls (Fig. 5), although variation was noted, especially between experiments.

Discussion

The rat model of cryptococcal meningitis has several advantages over other animal models for studying the biodistribution and penetration of mAb into the CNS. Rats, unlike rabbits, are susceptible to cryptococcal infection and do not require treatment with steroids to establish infection [16]. Treatment with steroids may affect the penetration of intravenously administered mAb into the CNS by decreasing inflammation and reducing blood–brain barrier permeability. In contrast to mice, the larger size of rats provides easier access to the CSF, thereby allowing quantitative measurements of mAb penetration.

Intracisternal inoculation of *C. neoformans* ATCC 24067 in Fischer rats results in a lymphocytic meningitis with extensive extra-CNS disease but with minimal brain parenchymal involvement. The pathology of infection, as described [17], is similar to that of some human cases. Infection in the rat was accompanied by high levels of CNPS in the serum and CSF as well as high fungal burdens in the lung, spleen, liver, and kidneys. AIDS patients with cryptococcal meningoencephalitis often demonstrate elevated serum CNPS levels as well as extraneural cryptococcal infection. In one study, 31% of AIDS patients with cryptococcal meningoencephalitis had serum CNPS antigen levels greater than 1:1024 [18]. Approximately 35% AIDS patients with cryptococcal meningoencephalitis have been reported to have extrameningeal cryptococcosis [19]. Elevated levels of systemic CNPS may impede the localization of systemically administered anticryptococcal antibody to the CNS by binding antibody in the periphery. The rat system we describe provides a tool for studying these interactions and for developing strategies to increase anticapsular mAb localization to the CNS in the context of systemic disease.

In previous studies, a protective effect of systemically administered 2H1 in a murine model of CNS infection has been demonstrated [7]. Systemic administration of CNPS-binding mAb has been shown to prolong survival, decrease serum CNPS levels and decrease organ fungal burden (including brain fungal burden) in infected mice. Despite these published findings, our present imaging and organ counting studies in infected rats which had received CNPS-specific mAb intravenously failed to demonstrate ^{125}I counts in the CSF or brain parenchyma. It is conceivable that the protective effects of 2H1 in murine studies may be due to biologically significant levels of mAb within the CNS, but in amounts that are below the threshold of detection of our methods. Detection of minute amounts of mAb in the CSF and parenchyma is difficult as a result of the large persistent blood pool of radiolabelled mAb, although the dual-isotope technique of subtracting irrelevant mAb, as performed in our study, did reduce background significantly. Furthermore, gamma-camera imaging and organ scintillation-counting give only a static indication of mAb distribution and may not account for fluxes of mAb which may rapidly traffic through the CNS. Alternatively, it is possible that the protective effect of 2H1 in CNS disease are due solely to effects of mAb outside of the CNS, affecting the systemic dissemination of infection and perhaps reducing the serum and tissue levels of CNPS antigen, which is known to have immunosuppressive properties [20–22]. Finally, it may be that when using 'tracer' amounts of mAb, as in our study, high serum and tissue CNPS levels bind the relatively small amount of CNPS-specific mAb making it unavailable for CNS localization. In murine studies in which protective effects of anticapsular mAb have been demonstrated, milligram doses of mAb were used. A potential solution to the problem of using small quantities of radiolabelled mAb is to administer radiolabelled mAb in the context of unlabelled mAb or to administer sequential doses of unlabelled and labelled mAb.

As an alternative to the limited penetration of mAb into the CNS after intravenous administration, we administered mAb directly into the subarachnoid space of infected rats. Of note, direct instillation of antibody into the subarachnoid space was used in the preantibiotic era as a treatment of meningococcal meningitis [23], and represents an effective means of bypassing the blood–brain barrier. Our studies demonstrated that CNPS specific mAb entered the peripheral circulation earlier (within 2·5 h of mAb administration) than irrelevant mAb. In rabbits, intracisternally administered *C. neoformans* polysaccharide is known to rapidly diffuse into the intravascular space [24]. It is possible that this transport

mechanism may have resulted in the co-clearance of bound mAb out of the CNS. Despite the earlier egress of CNPS specific mAb, imaging studies also demonstrated that CNPS specific mAb remained visible intracranially for a greater duration than irrelevant mAb, conceivably representing antigen-specific binding. This finding was confirmed by organ scintillation counting studies which demonstrated that there was significantly greater ^{125}I counts in the brain of rats which had received specific mAb.

The whole body half-life of intravenously administered ^{125}I-2H1 in uninfected rats was between 7·4 and 11·7 days which is similar to the half-life of the IgG1 isotype in mice [25]. We have previously showed a close identity between whole body and intravascular half-life of mAb in mice [8]. In infected rats, whole body mAb half-life was noticeably reduced, possibly due to accelerated catabolism of mAb after binding to antigen lodged in the tissues, or because of accelerated clearance of circulating mAb–antigen complexes leading to their catabolism. Either mechanism could explain the pronounced localization of ^{125}I-2H1 to the spleen of infected rats. Intravenously administered CNPS has been previously shown to localize in the spleen and this phenomenon is likely to occur as well as *in vivo* infection [26].

In summary, in our model of intracisternal *C. neoformans* infection, several findings relating to passive mAb therapy were noted. The half-life of clearance of anti-CNPS antibodies in infected rats was reduced compared with uninfected rats. Second, anti-CNPS mAbs accumulated outside of the CNS compartment, in the spleen, but not within the CNS to any great degree. Finally, intracisternally administered mAbs persists within the CNS. Implications for clinical trials of passive immunotherapy are that the shorter half-life of mAb 2H1 in infected rats suggests a need for more frequent or larger doses of mAb to achieve adequate therapeutic levels in patients with cryptococcal infection. If high CNS levels of mAb are needed for a therapeutic effect, direct instillation into the subarachnoid space may be advantageous. Alternatively, antibodies engineered to cross the blood–brain barrier, such as transferrin derivatives with enhanced brain penetration [27], may be of benefit. The present model promises to be useful in the testing and development of antibodies engineered for strategies designed to increase antibody availability in the CNS.

Acknowledgements

A.C. is supported by NIH grants RO1-AI33774 and RO1-AI13342 and D.G. is supported by NIH grant AIO-1300. L.Z. was supported by NIH Physician Scientist Award CA1503. We thank Sam Chun for his assistance in mAb biodistribution studies.

References

1 Zuger A, Louie E, Holzman RS, *et al.* Cryptococcal disease in patients with the acquired immunodeficiency syndrome: diagnostic features and outcome of treatment. *Ann Intern Med* 1986; **104**: 234–40.

2 Zuger A, Shuster M, Simberkoff MS, *et al.* Maintenance amphotericin B for cryptococcal meningitis in the acquired immunodeficiency syndrome (AIDS). *Ann Intern Med* 1988; **109**: 592–3.

3 Dromer F, Charreire J. Improved amphotericin B activity by a monoclonal anti-*Cryptococcus neoformans* antibody: study during murine cryptococcosis and mechanisms of action. *J Infect Dis* 1991; **163**: 1114–20.

4 Dromer F, Charreire J, Contrepois A, *et al.* Protection of mice against experimental cryptococcosis by anti-*Cryptococcus neoformans* monoclonal antibody. *Infect Immun* 1987; **55**: 749–52.

5 Sanford JE, Lupan DM, Schlageter AM, Kozel TR. Passive immunization against *Cryptococcus neoformans* with an isotype-switch family of monoclonal antibodies reactive with cryptococcal polysaccharide. *Infect Immun* 1990; **58**: 1919–23.

6 Mukherjee J, Scharff MD, Casadevall A. Protective murine monoclonal antibodies to *Cryptococcus neoformans*. *Infect Immun* 1992; **60**: 4534–41.

7 Mukherjee J, Pirofski LA, Scharff MD, Casadevall A. Antibody-mediated protection in mice with lethal intracerebral *Cryptococcus neoformans* infection. *Proc Natl Acad Sci USA* 1993; **90**: 3636–40.

8 Mukherjee J, Zuckier LS, Scharff MD, Casadevall A. Therapeutic efficacy of monoclonal antibodies to *Cryptococcus neoformans* glucuronoxylomannan alone and in combination with amphotericin B. *Antimicrob Agents Chemother* 1994; **38**: 580–7.

9 Mukherjee S, Lee S, Mukherjee J, *et al.* Monoclonal antibodies to *Cryptococcus neoformans* capsular polysaccharide modify the course of intravenous infection in mice. *Infect Immun* 1994; **62**: 1079–88.

10 Mukherjee J, Feldmesser M, Scharff MD, Casadevall A. Monoclonal antibodies to *Cryptococcus neoformans* glucuronoxylomannan enhance fluconazole efficacy. *Antimicrob Agents Chemother* 1995; **39**: 1398–405.

11 Feldmesser M, Mukherjee J, Casadevall A. Combination of 5-flucytosine and capsule binding monoclonal antibody in the treatment of murine *Cryptococcus neoformans* infections and *in vitro*. *J Antimicrob Chemother* 1996; **37**: 617–22.

12 Griffin FM. Roles of macrophage Fc and C3b receptors in phagocytosis of immunologically coated *Cryptococcus neoformans*. *Proc Natl Acad Sci USA* 1981; **78**: 3853–7.

13 Nabavi N, Murphy JW. Antibody-dependent natural killer cell-mediated growth inhibition of *Cryptococcus neoformans*. *Infect Immun* 1986; **51**: 556–62.

14 Casadevall A, Mukherjee J, Devi SJN, *et al.* Antibodies elicited by a *Cryptococcus neoformans* glucuronoxylomannan-tetanus toxoid conjugate vaccine have the same specificity as those elicited in infection. *J Infect Dis* 1992; **65**: 1086–93.

15 Tijssen P. The immobilization of immunoreactants on solid phases. In: Burdon RH, van Knippernberg PH, eds. *Practice and Theory of Enzyme Immunoassays*. Amsterdam: Elsevier, 1985: 297–328.

16 Perfect JR, Lang SDR, Durack DT. Chronic cryptococcal meningitis: a new experimental model in rabbits. *Am J Pathol* 1980; **101**: 177–94.

17 Goldman DL, Casadevall A, Cho Y, Lee SC. *Cryptococcus neoformans* meningitis in the rat. *Lab Invest* 1996; **75**: 759–70.

18 Saag MS, Powderly WG, Cloud GA, *et al.* Comparison of amphotericin B with fluconazole in the treatment of acute AIDS-associated cryptococcal meningitis. *N Engl J Med* 1992; **326**: 83–9.

19 Powderly WG, Saag MS, Cloud GA, *et al.* A controlled trial of fluconazole or amphotericin B to prevent relapse of cryptococcal meningitis in patients with the acquired immunodeficiency syndrome. *N Engl J Med* 1992; **326**: 793–8.

20 Dong ZM, Murphy JW. Intravascular cryptococcal culture filtrate (CneF) and its major component, glucuronoxylomannan, are potent inhibitors of leukocyte accumulation. *Infect Immun* 1995; **63**: 770–8.

21 Kozel TR, Gotschlich EC. The capsule of *Cryptococcus neoformans* passively inhibits phagocytosis of the yeast by macrophages. *J Immunol* 1982; **129**: 1675–80.

22 Kozel TR, Gulley WF, Cazin J. Immune response to *Cryptococcus neoformans* soluble polysaccharide: immunological unresponsiveness. *Infect Immun* 1977; **18**: 701–70.

23 Flexner S. The results of the serum treatment in thirteen hundred cases of epidemic meningitis. *J Exp Med* 1913; **17**: 553–76.

24 Bennett JE, Hasenclever HF. *Cryptococcus neoformans* polysaccharide: studies of serologic properties and role in infection. *J Immunol* 1965; **94**: 916–20.

25 Pollock RR, French DL, Metlay JP, *et al.* Intravascular metabolism of normal and mutant mouse immunoglobulin molecules. *Eur J Immunol* 1990; **20**: 2021–7.

26 Goldman DL, Lee SC, Casadevall A. Tissue localization of *Cryptococcus neoformans* glucuronoxylomannan in the presence and absence of specific antibody. *Infect Immun* 1995; **63**: 3448–53.

27 Friden PM, Walus LR, Musso GF, *et al.* Anti-transferrin receptor antibody and antibody-drug conjugates cross the blood-brain barrier. *Proc Natl Acad Sci USA* 1991; **88**: 4771–5.

PATENT: PEPTIDIC VECTORS FOR TRANSPORTING SUBSTANCES THROUGH THE BLOOD-BRAIN BARRIER FOR USE IN DIAGNOSIS OR THERAPY OF A CNS DISORDER

This invention relates to the use of peptides as vectors for the transfer of active molecules through the blood-brain barrier (BBB) for applications in therapy and in diagnosis. The examiner argued that the brain uptake observed with the peptide vectors (SynB vectors) is not an indication of an enhancement of efficacy. Here we show, for various drugs, that vectorisation of therapeutic molecules can result in a significant enhancement of activity.

1) Morphine-6-Glucuronide

Morphine-6-glucuronide (M6G), an active metabolite of morphine, has been shown to have significantly attenuated brain penetration relative to that of morphine. We have conjugated morphine-6-glucuronide to a peptide vector SynB3 in order to enhance its brain uptake and its analgesic potency after systemic administration.

Materials And Methods

All the materials and Methods are described in J. Temsamani et al, Improved brain uptake and pharmacological activity profile of morphine-6-glucuronide using a peptide-vector-mediated strategy. (2005). *J Pharmacol Exp Ther*. 313:712-719.

Results

We measured the brain uptake of free M6G and Syn1001 using the *in situ* brain perfusion technique in mice as described in Temsamani et al (2005). The brain uptake of free M6G was very low after 60 sec of perfusion (Kin = 0.024 +/- 0.02 µl/g/sec) (Figure 1). In contrast, conjugation of M6G to the SynB3 vector significantly enhanced its brain uptake, giving a Kin of 1.27 +/- 0.5 µl /g/sec.

We measured the effect of M6G and Syn1001, administered subcutaneously, in mice using the tail flick assay at different doses in order to determine the ED50 (does that will induce 50% of the analgesic effect). The ED50 for Syn1001 was 1.25 mg/kg.eq while for M6G it was 5 mg/kg. This indicates that Syn1001 is 4 times more potent than free M6G. Interestingly,

time-course studies with Syn1001 revealed a longer duration of action compared to M6G. The effect of Syn1001, at a dose 4-fold less than M6G, lasted about 300 min while the effect of M6G was about 120 min (Figure 2).

2) Dalargin

Dalargin is a hexapeptide analog of leu-enkephalin containing D-Ala in the second position and an additional C-terminal arginine. These modifications modulate the stability of dalargin in the blood stream and brain while at the same time modifying to some extent its receptor selectivity. While the intracerebroventricular injection of this peptide has been shown to induce analgesic action, its systemic administration shows no activity in central analgesic mechanisms. The reason for this is because dalargin is known not to cross the BBB. We have shown that SynB vectors improve the delivery of dalargin into the brain and that this enhancement in uptake is accompanied by a significant increase in its pharmacological potency in an animal model of nociception (see Rousselle et al, 2003)

Materials And Methods

All the materials and methods are described in Rousselle C et al, Improved Brain Uptake and Pharmacological Activity of Dalargin Using a Peptide-Vector-Mediated strategy (2003). *J Pharmacol Exp Ther.* **306**, 371-376.

Results

We measured the brain uptake of free and vectorised dalargin using the in situ brain perfusion in mice (Figure 3). The brain uptake of free dalargin was very low after 120 sec of perfusion (Vd = 16.7 +/- 1.2 µl/g) (Rousselle et al, 2003).

Interestingly, conjugation of dalargin to SynB3 via a disulfide linker (Dal-SS-SynB3) significantly enhanced its brain uptake (240 +/- 44.9 µl /g).

Free or conjugated dalargin were administered intravenously (iv) to mice and anti-nociception was determined using the Hot plate test, an assay known to be mediated by central receptors. This test measures the amount of time required for mice to react to standardized noxious

stimuli. Substances which increase the reaction time are described as displaying anti-nociceptive effects , which may be interpreted as a measure of analgesia.
The results show that iv administration of free dalargin to mice at 2 mg/kg in physiological saline exhibited only a small but non-significant analgesic response (Figure 4). In contrast, conjugation of dalargin to SynB3 led to a considerable enhancement of analgesic activity immediately (within 5 min, the first time point) after the iv injection (Rousselle et al, 2003).

3) Paclitaxel

Paclitaxel (PAX) has shown significant activity against human solid tumors, i.e., ovarian, head and neck, bladder, breast, and lung cancers. Paclitaxel has also been suggested to treat malignant glioma and brain metastases. However, brain tumours constitute a difficult problem and the therapeutic benefit of paclitaxel has been variable and low. This could be attributed to its limited entry into the central nervous system (CNS). We investigated the effect of vectorisation of paclitaxel with SynB3 vector linked each other by a succinate linkage. We demonstrate that this peptide vector enhances the solubility of paclitaxel and its brain uptake. We also show that the conjugated paclitaxel has a better efficacy in vivo than free paclitaxel.

Materials And Methods

The brain uptake studies were carried out as described in Blanc et al. Peptide-vector strategy bypasses P-glycoprotein efflux, and enhances brain transport and solubility of paclitaxel. (2004) *Anticancer Drugs.* **15**:947-954.

Results

BBB permeabilities of free and vectorised PAX were assessed using the in situ brain perfusion in mice (Figure 5). The brain uptake of free PAX was very low after 60 sec of perfusion (K_{in} = 0.53 ± 0.15 µl/s/g). Interestingly, conjugation of paclitaxel to SynB3 significantly enhanced its brain uptake. The transport coefficient K_{in} measured for PAX-OSUC-SynB3 was 11.8 ± 2.5 µl/s/g (Blanc et al, 2004).

The efficacy of Syn2001 in the rat glioblastoma model was assessed using intraperitoneal route of administration. Rats were implanted in the striatum with a glioma cell line (9L cells) at day 0 and were then administered intraperitonealy with either free paclitaxel (PAX) or vectorised paclitaxel (PAX-SynB3). The two groups were treated with 10 mg/kg.eq (mg base of Pax) every day for 5 consecutive days. As a control, one group received the vehicle alone. Animals treated with either the vehicle or free paclitaxel started dying on day 20 and all the animals were dead on day 25-28. Animals treated with vectorised paclitaxel had an increase in survival rate and all the animals were alive at day 35 (Figure 6).

4) Inhibitor Of DPIV

Dipeptidyl peptidase IV (DPIV) is a serine protease, which cleaves N-terminal dipeptides from a peptide chain containing, preferably, a proline residue in the penultimate position. Although the biological role of DPIV in mammalian systems has not been completely established, it is believed to play an important role in neuropeptide and hormone metabolism, T-cell activation, and the entry of HIV into lymphoid cells.

There are a lot of dipeptidyl peptidase IV inhibitors known in the art, but none of them are described to be capable of crossing the blood-brain-barrier in mammals and reaching the central nervous system (CNS) in a therapeutically effective amount for the treatment of CNS diseases.

Materials And Methods

The brain uptake was measured as described earlier.

Animals

Experiment – intraperitoneal application

90 Lewis rats, 10 per dose and test group

Female inbred Lewis rats were obtained from Charles River (Bad Sulzfeld, Germany).

Study compounds and treatment groups

ip application once daily from days 5-15 post immunization

Group 1 (Control): Vehicle (Saline, 100µl ip)

Group 2 (Inhibitor:Ile-Thia): L-*threo*-isoleucyl thiazolidine fumarate (120 µmol/kg = 31 mg/kg)

Group 3 (Inhibitor-Syn/24): (12 µmol/kg ~ 24mg/kg)

Group 4 (Inhibitor-SynB3/80): (40 µmol/kg ~ 80 mg/kg)

Group 5 (Inhibitor-SynB3/240): (106 µmol/kg ~ 240 mg/kg)

Group 6 (Inhibitor-SynB8/15): (12 µmol/kg ~ 15 mg/kg)

Group 7 (Inhibitor-SynB8/50): (40 µmol/kg ~ 50 mg/kg)

Group 8 (Inhibitor-SynB8/150): (120 µmol/kg ~ 150 mg/kg)

Group 9 (Rolip/15): Rolipram (15 mg/kg) (Positive control)

Experimental Procedures

Animals and Induction of EAE

Guinea pig MBP (50 mg/rat) is emulsified in Complete Freund's adjuvant (CFA) containing heat-killed Mycobacterium tuberculosis (H37Ra; 225 mg/rat) and injected s.c. at the base of the tail in a total volume of 100 µl (12). CFA (Sigma) and heat-killed *Mycobacterium tuberculosis* (H37Ra) were purchased from Life Technologies, Inc. (Rockville, MD). Clinical disease is scored on the following scale:

0.5: partial loss of tail tone;

1.0: complete tail atony;

1.5: complete tail atony and weakness of one hind limb;

2.0: weakness of both hind limbs;

2.5: hind limb weakness and paralysis of one hind leg;

3.0: paralysis of both hind legs;

3.5: limb paralysis of three legs;

4.0: quadriplegia and moribund status;

5.0: death due to EAE.

Experiments were terminated on day 16 post immunization (p.i.) and organs brain, spinal cord, plasma were collected for further analysis. Result of this further analysis will presented in a separate report.

For treatment, animals receive a volume of 200µl ip once daily on day 5-16 pi. Route of application was over 5s intraperitoneal (i.p.) in ml/kg BW (i.e. a 200g rat receive 200 µl). Treatment was once daily on days 5-16 p.i.

Results

We compared the brain uptake of free and vectorised DPIV inhibitors using intraperitoneal administration. The compounds were administered to mice at a dose of 5 mg/kg.eq by intraperitoneal route. The animals were sacrificed at various times and the total radioactivity within the brain was measured.

Figure 7 shows that the vectorised inhibitor (either with the vector SynB3 or SynB8) has a higher concentrations in the brain (AUC 120 and 150 min*nmol/g, respectively) compare to free inhibitor (AUC: 60min*nmol/g).

Clinical course and changes in body weight

Analysis of the primary data on clinical score by ANOVA for repeated measures on days 6-15 p.i. revealed a significant interaction between the factors "Treatment" x "Clinical score" with $F(7;63)=6.3;p<0.0001$.

Table 1: Mean clinical scores (day 6 - 15)

Group	n	Mean±SEM
Control (SHAM)	10	1.20±.10
Ile-Thia	10	1.25±.14
Inhibitor-SynB3/24	10	0.68±.09*
Inhibitor-SynB3/80	9	0.69±.10*
Inhibitor-SynB3/240	n.d.	n.d.
Inhibitor-SynB8/15	9	0.76±.12*
Inhibitor-SynB8/50	10	1.26±.14
Inhibitor-SynB8/150	10	0.76±.11*
Rolip/15	10	0.72±.08*

*= significant difference vs. SHAM with $p<0.05$

As revealed by posthoc comparisons, analysis of mean clinical scores (Table 1) illustrates protective effects in Group 3 (Inhibitor-SynB3/24), Group 4 (Inhibitor-SynB3/80), Group 6 (Inhibitor-SynB8/15), Group 8 (Inhibitor-SynB8/150), and Group 9 (Rolip/15). Inhibitor-SynB3/24 and Inhibitor-SynB3/80 were as effective or even slightly more effective as the positive control Rolipram. The free inhibitor Ile-Thia was not effective since it displays a similar score as the control.

The compound Inhibitor-SynB8 at 15 and 150 mg was well tolerated and as effective as Rolipram.

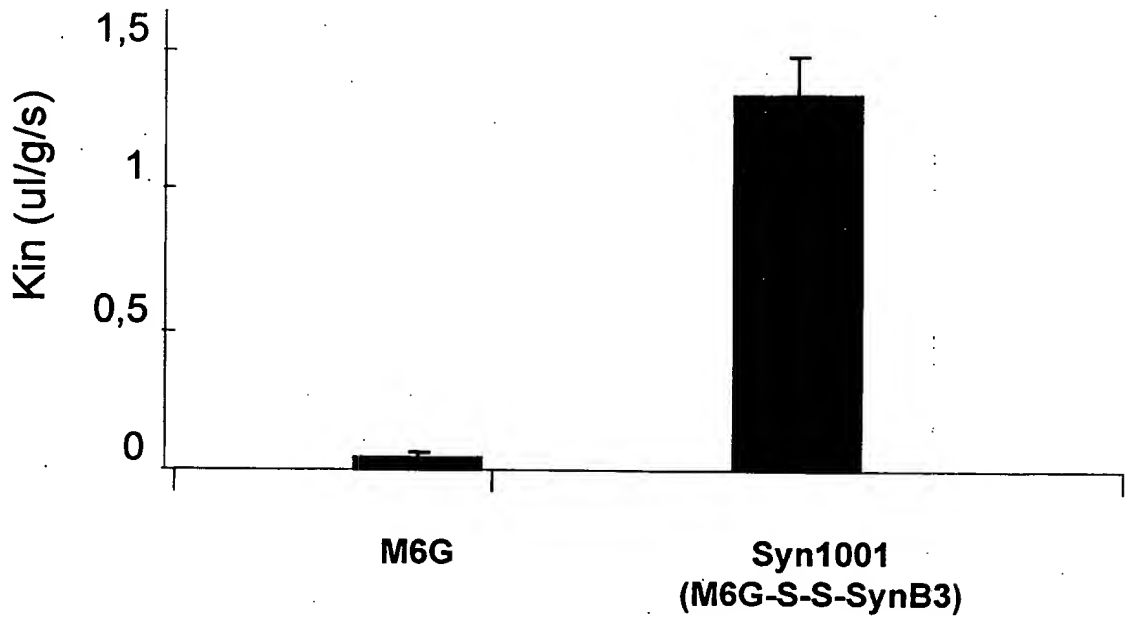

Figure 1: Brain transport coefficients (K_{in}) for [^{14}C] free and vectorised M6G uptake in right hemisphere of mouse rat brain after 60 s perfusion with buffer. Values are mean ± SEM (n= 3-5 animals). ***P< 0.001 .

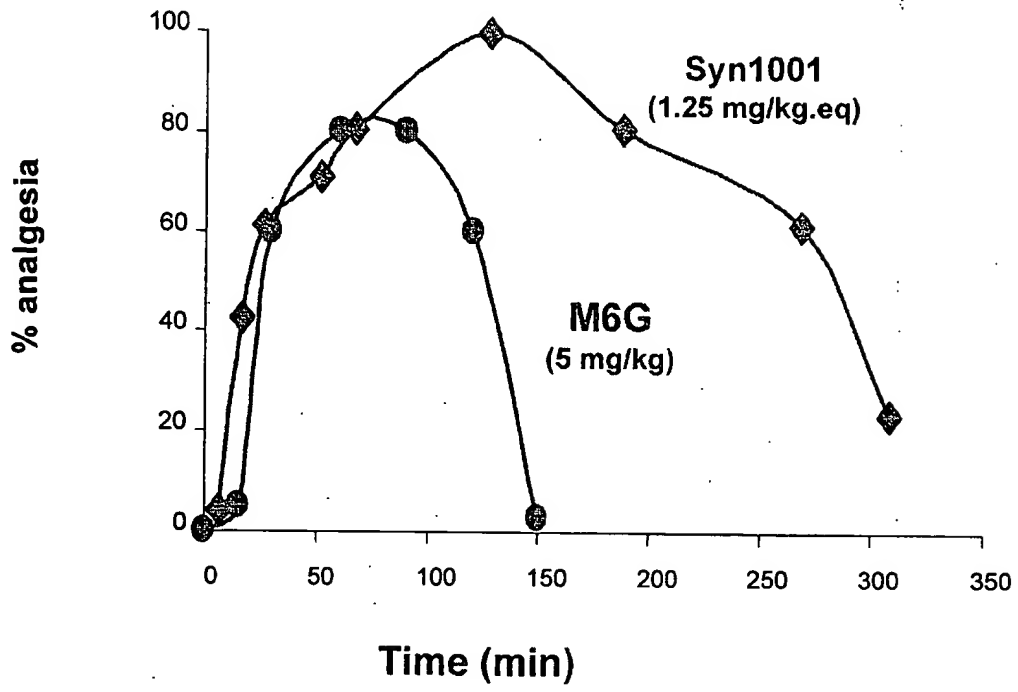

Figure 2: Antinociceptive activity of subcutaneous free and vectorised M6G in the tail flick in mice (n=10 per group) at the ED50 dose (M6G: 5 mg/kg; Syn1001: 1.25 mg/kg.eq). The antinociceptive effect was measured at 15, 30, 60, 90, 120, 150, 180, 240 and 300 min post-administration and is expressed as a percentage of analgesia.

Note
Figure 2 & 3 is missing Dal-SS-SynB1 data in graph

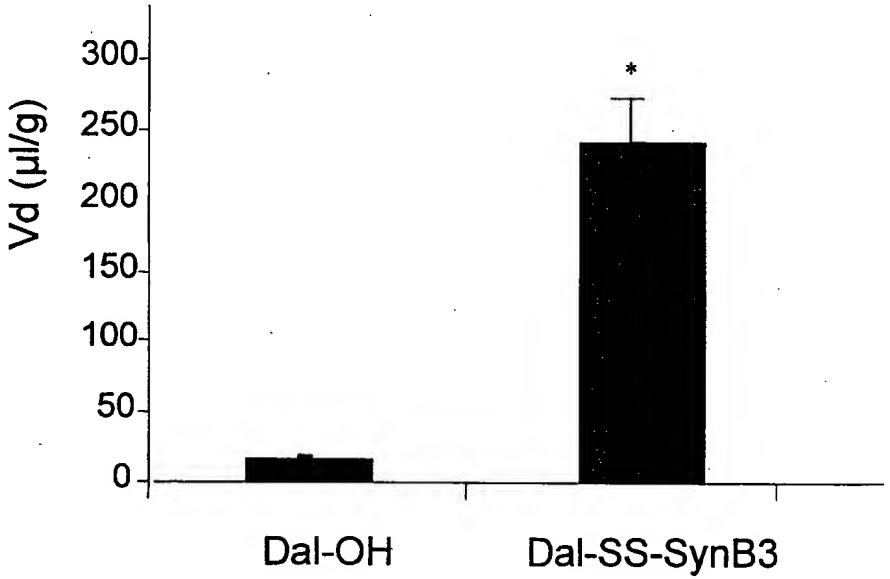

Figure 3:Distribution volume (V_d) for [^{14}C]Dal, [^{14}C]Dal-SS-SynB1, and [^{14}C]Dal-SS-SynB3 uptake in right hemisphere of mouse brain after 120 sec perfusion with buffer. Values are means +/- SEM(n= 4-6 mice). *p<0.05 versus free Dal.

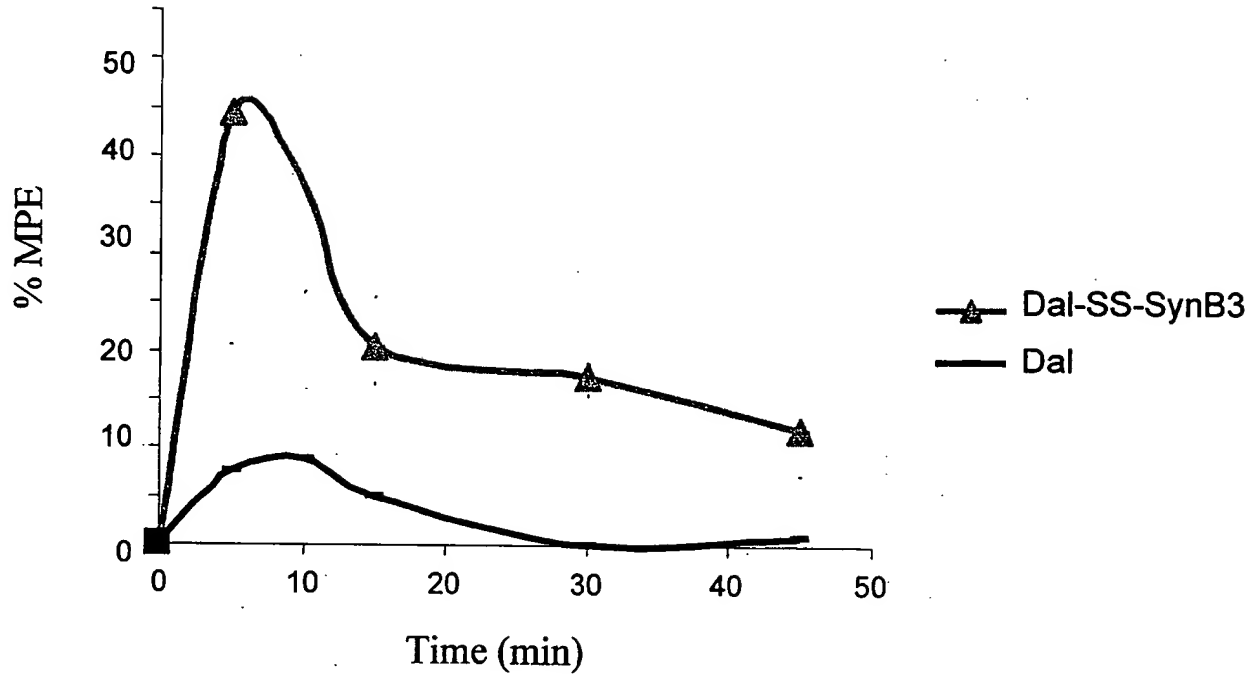

Figure 4: Analgesic activity after intravenous injection in mice of free dalargin (Dal) and vectorised dalargin as measured using the hot plate model. Values are means +/- SEM (n=15 mice).

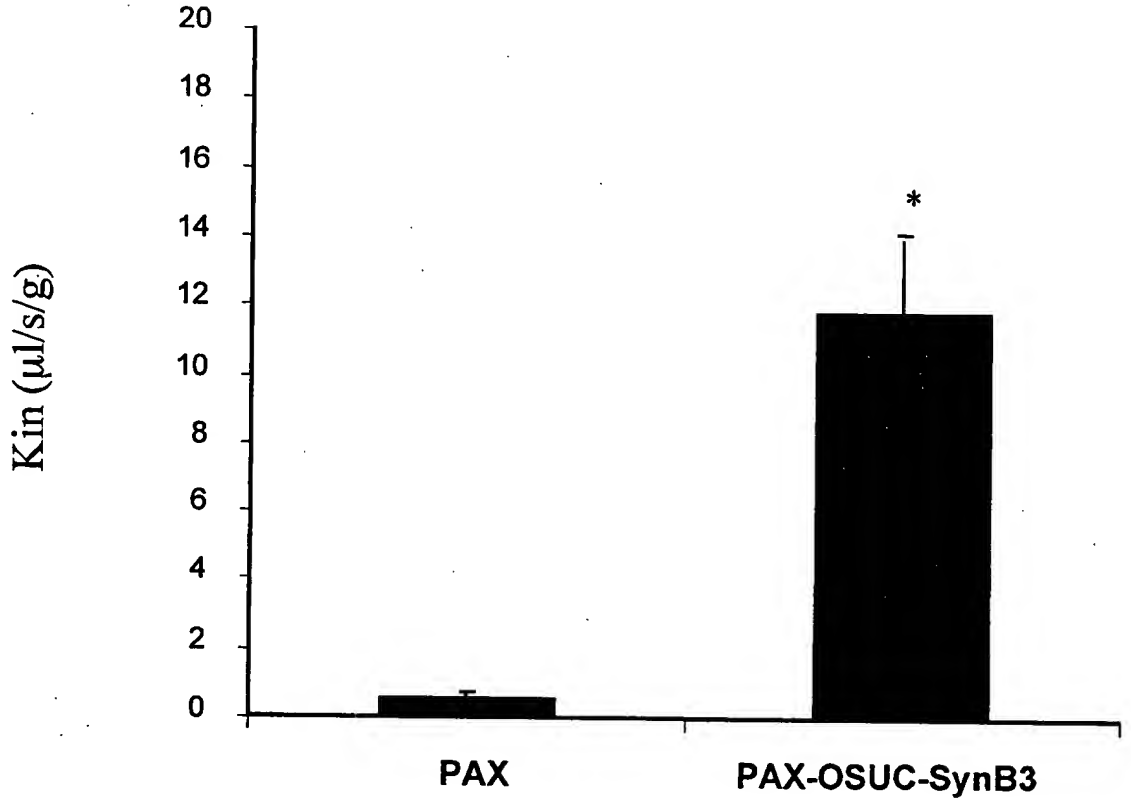

Figure 5: Brain transport coefficients (K_{in}) for [^{14}C] free and vectorised paclitaxel uptake in right hemisphere of mouse rat brain after 60 s perfusion with buffer. The mice were perfused with 0.007 mmol/ml of PAX or 0.002 mmol/ml of PAX-OSUC-SynB3. Values are mean ± SEM (n= 3-5 animals). *P< 0.05 .

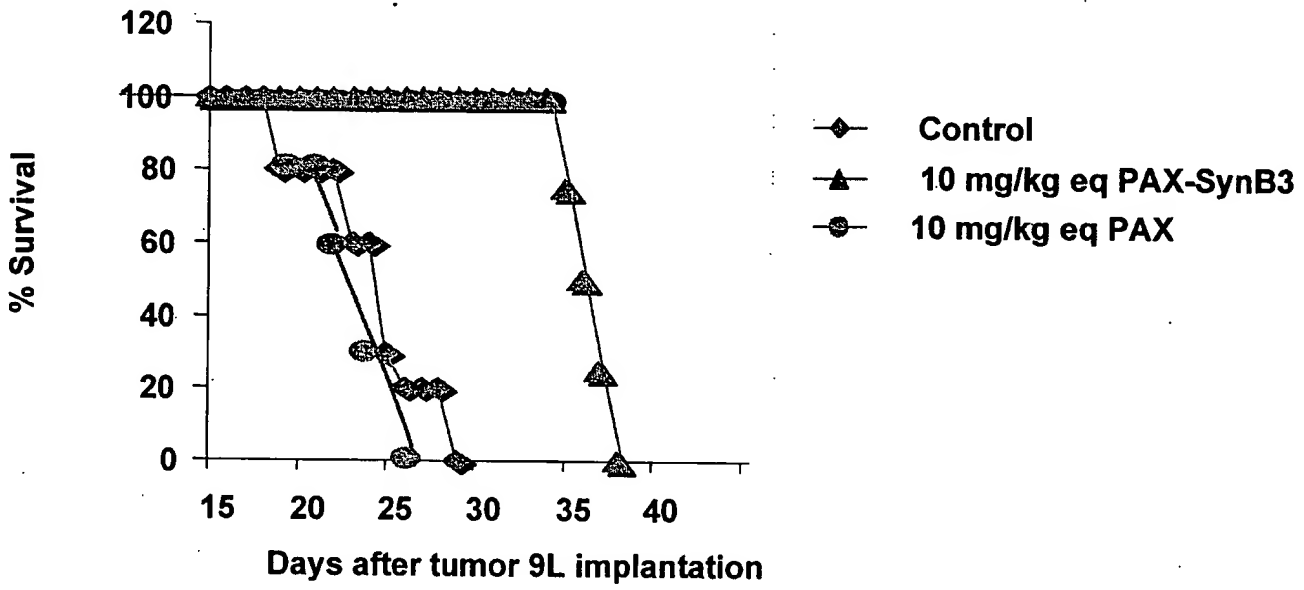

Figure 6: Survival rate of rats implanted with 9L cells and treated with either free or vectorised paclitaxel by ip route.

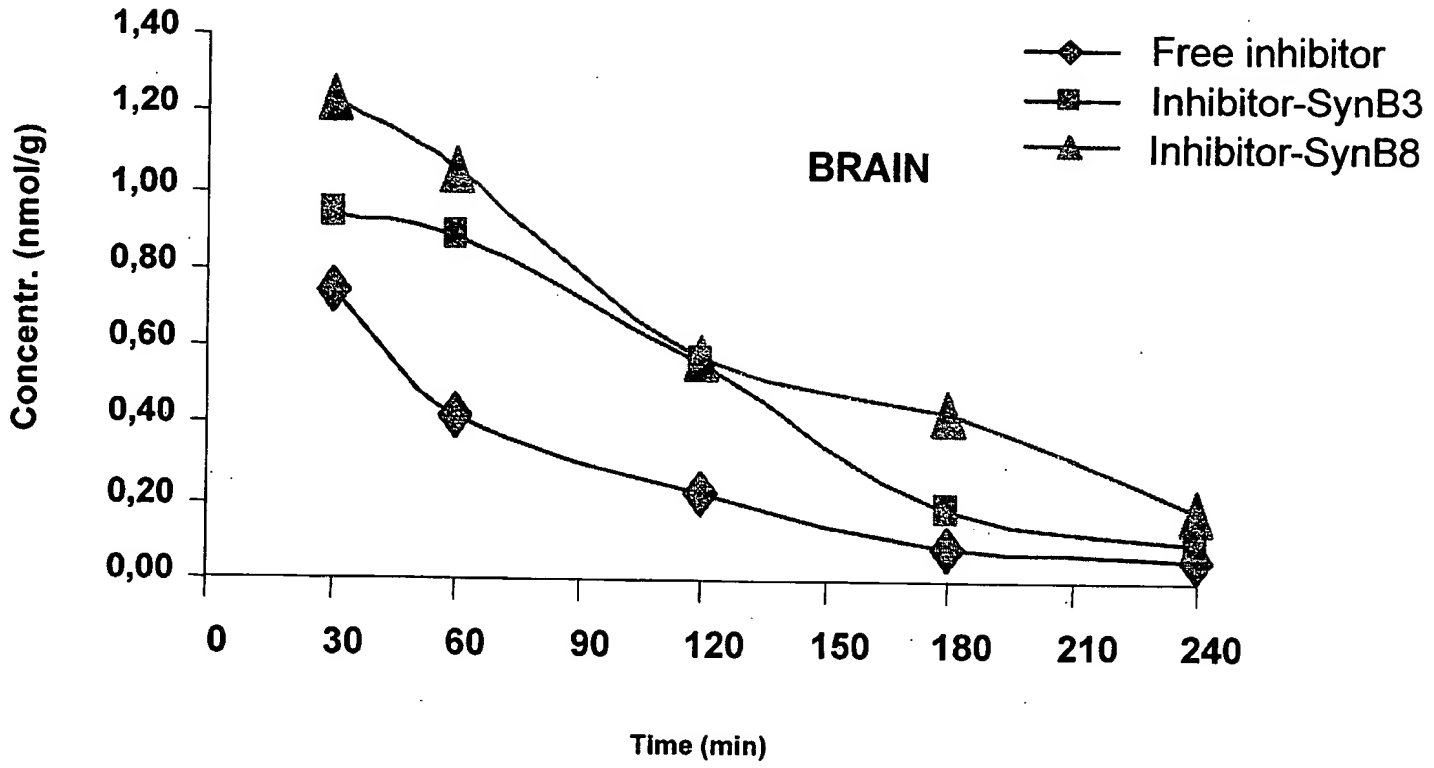

Figure 7: Brain uptake of free and vectorised DPIV inhibitors. The compounds were administered to mice at a dose of 5 mg/kg.eq by intraperitoneal route. The animals were sacrificed at various times and the total radioactivity within the brain was measured.

References Cited

Temsamani, Jamal et al., "Improved Brain Uptake and Pharmacological Activity Profile of Morphine-6-Glucuronide Using a Peptide-Vector-Mediated Strategy", *J. Pharmacol. Exp. Ther.*, 313:712-719 (2005).

Rousselle, C. et al., "Improved Brain Uptake and Pharmacological Activity of Dalargin Using a Peptide-Vector-Mediated Strategy", *J. Pharmacol. Exp. Ther.*, 306:371-376 (2003).

Blanc, et al., "Peptide-Vector Strategy Bypasses P-Glycoprotein Efflux, and Enhances Brain Transport and Solubility of Paclitaxel", *Anticancer Drugs.* 15:947-954 (2004).

Improved Brain Uptake and Pharmacological Activity Profile of Morphine-6-Glucuronide Using a Peptide-Vector-Mediated Strategy

ABSTRACT

Morphine-6-glucuronide (M6G), an active metabolite of morphine, has been shown to have significantly attenuated brain penetration relative to that of morphine. Recently, we have demonstrated that conjugation of various drugs to peptide vectors significantly enhances their brain uptake. In this study, we have conjugated morphine-6-glucuronide to a peptide vector SynB3 in order to enhance its brain uptake and its analgesic potency after systemic administration. We show by *in situ* brain perfusion that vectorisation of M6G (Syn1001) markedly enhances the brain uptake of M6G. This enhancement results in a significant improvement in the pharmacological activity of M6G in several models of nociception. Syn1001 was about 4 times more potent than free M6G (ED50 of 1.87 μmol/kg *versus* 8.74 μmol/kg). Syn1001 showed also a prolonged duration of action compared to free M6G (300 min and 120 min, respectively). Furthermore, the conjugation of M6G results in a lowered respiratory depression, as measured in a rat model. Taken together, these data strongly support the utility of peptide-mediated strategies for improving the efficacy of drugs such as M6G for the treatment of pain.

INTRODUCTION

The main metabolism pathway of morphine includes liver glucuronidation to morphine-6-glucuronide (M6G) and morphine-3-glucuronide (M3G). M6G is thought to contribute to the pharmacological effects of the parent drug (Abbott and Palmour, 1988; Paul et al., 1989; Frances et al., 1992), and various clinical trials have used M6G as the therapeutic drug in preference to morphine (Hanna et al., 1990; Thompson et al., 1995; Grace and Fee, 1996; Lötsch et al., 1997; Motamed et al., 2000; Penson et al., 2000). Antinociception studies in experimental animals have demonstrated that, although M6G and morphine are almost equally potent after systemic administration, the analgesic potency of M6G is more than 100-fold higher than morphine after intracerebroventricular injection, a route of administration that bypasses the blood-brain barrier (BBB) *in vivo* (Abbott and Palmour, 1988; Paul et al., 1989; Frances et al., 1992). These pharmacological data suggest that the brain penetration of M6G is significantly attenuated relative to that of morphine, probably due to the presence of the glucuronide moiety of M6G, conferring a higher hydrophilic character. Recently, a weak capacity and bi-directional transport by GLUT-1 and by a digoxin sensitive transporter, which could be oatp2, was reported to be involved in the transport of M6G through the mouse BBB (Bourasset et al., 2003). However, several studies have shown that morphine has a better BBB permeability than M6G after intravenous injection (Bickel et al., 1996; Wu et al., 1997). Thus, enhancing the brain uptake of M6G would be expected to result in an improvement in its analgesic activity.

Brain delivery is still one of the major challenges for the pharmaceutical industry since many therapeutic drugs are unable to penetrate the BBB, a complex endothelial interface in vertebrates that separates the blood compartment from the extracellular fluid compartment of the brain parenchyma. The capillaries in the brain parenchyma possess a high electrical

resistance due to tight junctions between the endothelial cells, and they also lack pores. Thus, the brain capillary endothelium behaves like a continuous lipid bilayer and diffusion through this BBB layer is largely dependent on the lipid solubility of the drug (Abbott and Romero, 1996). Various strategies have been developed to enhance the brain uptake of therapeutic drugs but most of these methods have been of limited use (Pardridge, 1998; Temsamani et al., 2001). Recently, we have shown that small peptide-vectors can be used to enhance brain uptake of various drugs without opening the tight junctions (Rousselle et al., 2000; 2001; 2002). The potential of this approach as an effective delivery system for transporting drugs across the blood-brain barrier has been demonstrated in a number of animal models (Rousselle et al., 2000; 2001; 2002).

In order to assess this strategy as a brain delivery method for M6G, we have conjugated M6G to a 10-amino acid peptide SynB3 via a disulfide linker and measured its brain uptake and pharmacological effect in mice. We also measured its effect on respiratory depression in rats.

METHODS

Animals

Adult OF1 mice (30-40g, 6-8 weeks old) and OFA rats (200-220g) were obtained from Iffa-Credo (L'Arbresle, France). Eight-week-old male Swiss mice were obtained from Janvier [Le Genest-Saint-Isle, France]. Animals were maintained under standard conditions of temperature and lighting and had free access to food and water. The research adhered to the ethical rules of the French Ministry of Agriculture for experimentation with laboratory animals (Law N° 87-848).

Preparation and Characterization of Peptide Conjugates

Synthesis of Syn1001

Synthesis of the peptide SynB3: The peptide SynB3 (H-RRLSYSRRRF-NH2, molecular mass, 1395 Da) was assembled on a carboxamide resin by conventional automated solid phase chemistry using a 9-fluorenylmethoxycarbonyl/tertiobutyl-protection scheme (Atherton and Sheppard, 1989). After trifluoroacetic acid (TFA) cleavage/deprotection, the crude peptide was purified on preparative C18 reverse phase HPLC (Waters LC40). Purity of the lyophilized products was assessed by C18 reverse phase analytical HPLC (Dunn and Pennington, 1994), and the molecular weight was checked by Matrix-Assisted Laser Desorption-Ionisation Time-of-Flight Mass Spectrometry (MALDI-TOF, Elite-DE-RP Perseptive Biosystems). MALDI TOF spectra were recorded in linear mode, using the matrix 2'-(4-Hydroxyphenylazo) benzoïc acid (HABA, Fluka).

Addition of the CyA-3MP linker: CyA-3MP-SynB3 was obtained in a two-steps one-pot reaction: One molar equivalent of SynB3, 6TFA was dissolved in dry DMF

(dimethylformamide, peptide synthesis grade), and mixed with 1 equivalent of SPDP (N-succinimidyl 3-(2-pyridyldithio)propionate, Fluka). Then 4-6 equivalents of DIEA (N,N,diisopropyletylamine) were added to start the reaction. The resulting product S-pyridyl-3-mercaptopropionyl-SynB3 was monitored by HPLC and MALDI-TOF and was not isolated. Five Equivalents of cysteamine hydrochloride (Fluka) dissolved in $H0_2$/DMF 50% were then added, with enough DIEA to maintain alkaline conditions in the reaction mixture. The resulting CyA-3MP-SynB3 (1821 Da) was purified on preparative C18 reverse phase HPLC, and lyophilized.

Coupling of the active principle Morphine-6-Glucuronide: One molar equivalent of CyA-3MP-SynB3, 6TFA was dissolved in DMF. 1.2 molar equivalents of morphine-6-glucuronide di-hydrate were resuspended in DMF using ultrasound. Four to six-equivalents of DIEA were added to the M6G suspension, followed by 1.5 equivalent of benzotriazol-1-yl-oxopyrrolidinephosphonium hexafluorophosphate (PyBop, Novabiochem) dissolved in DMF. After 5 min, the peptide CyA-3MP-SynB3 dissolved in DMF was added to the reaction mixture and left a further 20 min for coupling of the PyBOP activated M6G. Purification, lyophilisation and assessment of the conjugate Syn1001 (M6G-CyA-3MP-SynB3, 2002.33 Da) were performed as described above.

Radiolabelled compounds: Preparations were performed as described above, except that 17-[^{14}CH3]M6G (Biodynamics, U.K. custom synthesis, 28.7 Ci/mol) was kept limiting by raising the stoichiometry of peptide, to 1.5 eq in the coupling reactions. The resulting products were analyzed as described above, and the radiochemical purity was assessed by an HPLC fitted with a liquid scintillation counting detector (Flow One Packard). After isotopic dilution with the unlabelled conjugate, the specific activity of the compound was 14.3 μCi/mg.

Receptor binding assay

Radio-receptor assays were carried out in which competition between labeled opioid ligands and the cold test compound was measured using an opioid receptor-containing membrane preparation as described previously (Cotton et al., 1985; Kinouchi and Pasternak, 1991; Yoburn et al., 1991). The concentration of the test compounds ranged from 10^{-12} to 10^{-5} M. For opiate *mu* receptor, membrane homogenates of rat cerebral cortex (200 μg of protein) were incubated for 60 min at 22°C with 1 nM [^{3}H]DAMGO in the absence or presence of the test compound in a buffer containing 50 mM Tris-HCl [pH 7.7]. For delta receptor, membrane homogenates of guinea-pig cerebral cortex (300 μg of protein) were incubated for 120 min at 22°C with 1.5 nM [^{3}H]DPDPE in the absence or presence of the test compound in a buffer containing 50 mM Tris-HCl [pH 7.4], 5 mM $MgCl_2$ and 30 nM DAMGO. For *kappa* receptor, membrane homogenates of guinea-pig cerebellum (250 μg of protein) were incubated for 80 min at 22°C with 0.7 nM [^{3}H]U 69593 in the absence or presence of the test compound in a buffer containing 50 mM Tris-HCl [pH 7.4], 10 mM $MgCl_2$ and 1 mM EDTA. Nonspecific binding was determined in the presence of naloxone (1 μM for mu-receptor and 10 μM for kappa receptor) and naltrexone (10 μM) for the delta receptor.

Following incubation, the samples were filtered rapidly under vacuum through glass-fiber filters (GF/B, Packard) presoaked with 0.3% PEI and rinsed several times with ice-cold 50 mM Tris-HCl using a 96-sample cell harvester (Unifilter, Packard). The filters were dried then counted for radioactivity in a scintillation counter (Topcount, Packard) using a scintillation cocktail (Microscint O, Packard). IC_{50} values (concentration causing a half-maximal inhibition of control specific binding) and Hill coefficients (nH) were determined by non-linear regression analysis of the competitive curves. These parameters were obtained by Hill equation curve fitting. The inhibition constants (K_i) were calculated from the Cheng

Prusoff equation ($K_i = IC_{50} / (1+L/K_D)$, where L= concentration of radioligand in the assay, and K_D = affinity of the radioligand for the receptor). Ki values were determined using GraphPad Prism, (San Diego, CA). The data were fit by 1-site binding model.

***In situ* mouse brain perfusion study**

Surgical procedure: The uptake of [^{14}C]M6G and [^{14}C]Syn1001 (vectorised M6G) to the luminal side of six-week-old OF1 mouse brain capillaries was measured using the *in situ* brain perfusion method previously adapted in our laboratory for the study of drug uptake in the mouse brain (Dagenais et al., 2000; Rousselle et al., 2003). Briefly, the right common carotid artery of ketamine/xylazine (140/8 mg/kg, i.p) anesthetized mice was exposed and ligated at the heart side. The common carotid artery was catheterized rostrally with polyethylene tubing (0.30 mm i.d. x 0.70 mm o.d., Biotrol Diagnostic, Chennevrières-les-Louvres, France) filled with heparin (25 U/mL) and mounted on a 26G needle. The syringe containing the perfusion fluid was placed in an infusion pump (Harvard pump PHD 2000; Harvard Apparatus, Holliston, MA) and connected to the catheter. Brains of anesthetized mice were perfused for 60 sec at a flow rate of 2.5 mL/min. At the end of the perfusion time, the mouse was decapitated and the brain removed. Brain and perfusion samples were then digested for 2 hours in 1 ml of Solvable (Packard, Rungis, France) at 50°C and mixed with 9 ml of Ultima Gold XR scintillation cocktail (Packard). Total [^{14}C] and [^{3}H] were determined simultaneously in a Packard Tri-Carb Model 1900 TR Liquid Scintillation

The perfusate consisted of a Krebs-bicarbonate buffer, in mM: 128 NaCl, 24 $NaHCO_3$, 4.2 KCl, 2.4 NaH_2PO_4, 1.5 $CaCl_2$, 0.22 $MgSO_4$ and 9 D-glucose added before infusion. The solution was gassed with 95% O_2 and 5% CO_2 for pH control (=7.4) and warmed at 37°C in a water bath. Tracers were added to perfusate at concentrations of 0.3 µCi/ml for free M6G,

0.1 μCi/ml for Syn1001 and 0.3 μCi/ml for [^{3}H]sucrose, the latter being a vascular marker with poor BBB penetration.

Drug uptake was expressed as a single time point unidirectional transfer constant (Kin). Briefly, calculations were accomplished as described previously (Smith, 1996), from the following relationship:

Kin= (Qtot - Vv.Cpf) / (T.Cpf),

where Qtot is the measured quantity of [^{14}C] free or vectorised drug in brain ([^{14}C]tracer per gram of right brain hemisphere) at the end of the experiment, Vv is the cerebral vascular volume (microliters per gram), Cpf is the perfusion fluid concentration of [^{14}C] free of vectorised drug (disintegrations per minute per microliter), and T is the perfusion time in seconds. Vv was evaluated by the sucrose space and calculated by the ratio between radioactivity of [^{3}H]sucrose (expressed in dpm of sucrose per gram of brain) and the perfusate sucrose concentration.

Measurement of the Antinociceptive Effect

Tail flick: Responsiveness to radiant heat was determined using a modification of the procedure of D'Amour and Smith (1984) and Ling and Pasternak (1983). Naïve mice (OF1; 6-8 weeks old) were restrained in a paper handkerchief with the hand. A constant heat intensity (hot lamp) was applied to the ventral of the mice tail and when the animal flicked its tail in response to the noxious thermal stimulus, both the heat source and the timer stopped automatically. The stimulus intensity was adjusted so that the base-line tail-flick latencies ranged between 2 to 3 sec. Mice not responding after 10 sec were removed from the apparatus and assigned a latency of 10 sec in order to minimize tissue damage to the animal's tail. Base-line latencies were determined just before drug administration and again at the indicated times. The compounds were

administered by subcutaneous route in saline solution (volume of injection: 5 ml/kg). The antinociceptive effect was measured various times (30, 60, 180 and 300 min) after compound administration. At each time point two measurements (in a different place of the tail) were performed and the mean was calculated.

To correct for individual differences in base-line latencies, the antinociceptive data (latencies) were converted to percentage maximum possible effect (% MPE) using the following formula (Brady and Holtzman, 1982):

$$\% \text{ MPE} = \frac{(\text{Postdrug latency}) - (\text{Predrug latency})}{(\text{Maximum latency}) - (\text{Predrug latency})} \times 100$$

Maximum latencies were 30 min and 10 sec for the hot plate and tail flick latency tests, respectively.

The ED50 was calculated with non-linear regression equation using Sigma Plot® v.2.0.

Antagonism of Syn1001 antinociception by opiate antagonists was determined by pre-administration of naloxone (1 mg/kg; sc) and 3-methoxynaltrexone (0.2 mg/kg; sc) 15 min before administration of the drug. The antagonists Nor-Binaltorphimine (6 mg/kg) and Beta-funaltrexamine (10 mg/kg) were administered to mice subcutaneously 3 hours and 23 hours before administration of Syn1001, respectively (Pick et al, 1991; Paul et al, 1991).

Hot plate: In the hot-plate assay, naïve 6-8 weeks old OF1 mice (n=15) were placed on a 54°C surface (Harvard Apparatus, Holliston, MA) and the time to lick one of the paws or escape jump was recorded as the response latency. Pre-dosing latency was determined before administration of the compounds and was 4.6 ± 1.6 sec. The compounds (Syn1001 and M6G:

2.2 μmol/kg and morphine 2.6 μmol/kg) were administered intravenously (into the tail vain, volume of injection: 2 ml/kg). The hot plate latency was determined at various times (5, 10, 15, 30, 45, 90, 120 and 180 min) after compound administration. A maximal cutoff time of the heat was 30 sec to prevent tissue damage. To correct for individual differences in base-line latencies, the antinociceptive data (latencies) were converted to percentage maximum possible effect (% MPE) as described above.

Formalin test: Naïve eight-week-old male Swiss mice (n=10 per group) were injected subcutaneously (5 ml/kg) with either the vehicle (saline solution) or test compounds (2.18, 5.46 and 10.9 μmol/kg) 45 min before receiving a 10 μl intraplantar injection of 2% formalin solution (Sigma, France) into the right hind paw. The amount of time that the mice licked the injected paw was monitored. Both the acute and chronic phases were examined. The incidence of licking was measured during the first 7 min (acute phase) and in 2 min periods at 5 min intervals for 60 min (chronic phase). The observations were carried out for a period of one hour after the formalin injection.

Results are expressed as the mean ± the standard error of the mean (s.e.m). A global analysis of the data was performed using one factor or repeated measures analysis of variance (ANOVA). A Dunnett's test was used when the ANOVA indicated a significant difference. The level of significance was set at $p<0.05$.

Respiratory depression

The respiratory depression was measured in naïve OFA rats (200-220 g) as described by Ling *et al.* (1989). Animals were anaesthetized with valium/ketamine (8/50 mg/kg; ip). Vinyl cannulae were inserted in the femoral artery 24 hours before drug administration to obtain arterial blood samples and in the femoral vein to infuse drugs. All lines were tunneled subcutaneously to the back of the neck where they were exteriorized and were kept patent with heparinized

saline (50 U/ml). The compounds were given by subcutaneous route (43 μmol/kg for Syn1001 and M6G and 65 μmol/kg for morphine). During the respiratory depression studies, all animals remained unrestrained, were housed individually and were not handled. Blood pO_2, pCO2 and pH were measured using a Blood Gas Analyzer from arterial blood samples (0.2 ml).

RESULTS

Receptor binding assay

The affinity of M6G and vectorised M6G (Syn1001) to the main opioid receptors was investigated in radioligand competition binding assays. The data shows that Syn1001 binds to *mu* receptors with a higher affinity than free M6G (0.1 versus 3.8 nM). The *delta* receptor binding was similar for both Syn1001 and M6G (19 nM and 23 nM, respectively). Surprisingly, vectorisation of M6G exhibited a high affinity for the *kappa* receptor not shown by free M6G (1.1 nM for Syn1001 and 1860 nM for M6G). This increase in affinity to the *kappa* receptor was not related to the free peptide since we did not observe any *kappa* affinity for free SynB3 (Ki >10 μM).

BBB permeability

We measured the brain uptake of free M6G and Syn1001 using the *in situ* brain perfusion technique in mice. To assess the integrity of the BBB, [^{3}H]-sucrose was used as a marker of brain vascular volume since it does not measurably penetrate the BBB during brief periods of perfusion (e.g. 60-120 sec) (Dagenais et al, 2000). When M6G or Syn1001 were perfused, the distribution volume of [^{3}H]-sucrose into the right cerebral hemisphere was less than 20 μl/g indicating that the permeability of the BBB has not been altered. BBB permeabilities of M6G and Syn1001 were then assessed after 60 sec perfusion. The brain uptake of free M6G was very low after 60 sec of perfusion (Kin = 0.024 +/- 0.02 μl/g/sec). In contrast, conjugation of M6G to the SynB3 vector significantly enhanced its brain uptake, giving a Kin of 1.27 +/- 0.5 μl /g/sec.

Antinociceptive activity

First, we measured the effect of Syn1001, administered subcutaneously, in mice using the tail flick assay at different doses ranging from 1 to 4.24 μmol/kg. . Figures 1 A and B show that the effect of Syn1001 is dose-dependent and lasts for about 300 min. The calculated ED50 from this experiment was 3.6 mg/kg (1.87 μmol/kg) (Figure 1B). During the course of our studies, the ED50 varied from 1.87 to 3.2 μmol/kg. A similar experiment with free M6G (Figure 1C) showed that the ED50 of this compound is 4 mg/kg (8.74 μmol/kg). We then compared the effect of free M6G and Syn1001 by subcutaneous route at an equimolar dosing of 3.2 μmole/kg (1.5 mg/kg M6G and 6 mg/kg Syn1001). Figure 2 shows that Syn1001 is more potent, on a molar basis, than free M6G by subcutaneous route in the tail-flick assay. Interestingly, time-course studies with Syn1001 revealed a longer duration of action compared to M6G. The effect of Syn1001 lasted about 300 min while the effect of M6G was for 120 min. We also measured the antinociceptive effect of Syn1001 in the hot plate model in comparison with free M6G and morphine at equimolar dosing (2.2 μmol/kg for M6G and 2.6 μmol/kg for morphine) by the intravenous route in mice. Syn1001 displayed a significant analgesic effect compared to morphine or M6G (Figure 3).

Antagonism of Syn1001 antinociception by opiate antagonists.

Naloxone, a non-selective *mu* antagonist, administered subcutaneously immediately before Syn1001 reversed significantly its analgesic effect (Figure 4A). Interestingly, the analgesic activity of Syn1001 was also reversed by the antagonist 3-methoxynaltrexone (3-MTNX) (Figure 4A). Since Syn1001 displays a higher *kappa* affinity *in vitro* compared to free M6G, the contribution of *kappa* activity to the antinociception was assessed using the *kappa* selective antagonist Nor-Binaltorphimine (Nor-BNI). The *mu* antagonist, Beta-funaltrexamine (β-FNA), was used as a control. As expected, antinociception produced by Syn1001 was

inhibited by the *mu* antagonist but no inhibition was observed in the presence of the *kappa* antagonist (Figure 4B). This suggests that the analgesic effect observed with Syn1001 is mediated by the *mu* opioid receptor.

Formalin assay

To see whether the enhanced analgesic activity of Syn1001 over either M6G or morphine was also observed in a different nociceptive pain model, we assessed their relative activities in the formalin mouse pain model. Mice were subcutaneously administered with Syn1001, morphine, or M6G. Morphine and M6G were both administered at 1, 2.5 and 5 mg/kg while Syn1001 was administered at 4, 10 and 20 mg/kg in order to have an equivalent molar concentration of M6G (2.18, 5.46 and 10.9 μmol/kg, respectively). At all doses studied, administration of Syn1001 decreased the licking time both in the acute (1-7 min) and in the chronic (7-60 min) phases, compared to M6G or morphine-treated animals. This decrease in licking time was dose-dependent. At 2.18 μmol/kg, the total paw licking time for Syn1001 was about 50% in the chronic phase and at 10.9 μmol/kg, it was reduced almost to 0%. Figure 5 shows a comparison of the three compounds at equimolar dosing of 10.9 μmol/kg. In the acute phase, although animals treated with Syn1001 displayed less difference in paw-licking time compared to other groups, this difference was not statistically significant. However, a significant difference was observed in the chronic phase. The total paw licking time in this phase was about 25%, 30% and 0% for morphine, M6G and Syn1001, respectively.

Respiratory depression

We compared the effects of M6G and Syn1001 on respiratory depression in a rat model. Rats were administered with the compounds by the subcutaneous route at an equimolar dosing of

43 µmol/kg for M6G and Syn1001 (20 mg/kg M6G and 80 mg/kg Syn1001). Morphine was also administered as a control at a dose of 25 mg/kg (65 µmol/kg). The side effects observed in animals were usually scabbing at the injection site, subdued behavior and straub tail. Respiratory depression in the rat injected with free M6G and morphine is typically reflected in an initial increase in pCO_2. The levels of $pC0_2$ increased from 38 mmHg before administration to 62 mmHg at one hour post-administration, for both M6G and morphine (Figure 6). This increase in $pC0_2$ was accompanied by a decrease in pO_2 levels (data not shown). Interestingly, no significant increase in $pC0_2$ levels was observed with vectorised M6G (Figure 6). Measurement of blood pH showed a decrease in pH levels after M6G and morphine administration while no significant effect was obtained with Syn1001 administration. These preliminary data point out to a significant decrease in respiratory depression after vectorisation of M6G.

DISCUSSION

Our results confirm our previous reports that vectorisation of drugs with SynB vectors results in an enhancement of brain uptake and pharmacological activity (Rousselle et al., 2000; 2001; 2002). In the present study, our rationale was to attach M6G to the SynB3 peptide-vector in order to enhance its brain uptake. M6G was chosen because it has been reported to be more potent than morphine after central administration (Abbott and Palmour, 1988; Paul et al., 1989; Frances et al., 1992). As the affinity of both substances for the *mu* receptor has been reported to be similar, a possible explanation for this observation could involve differences in the permeability of the blood-brain barrier to M6G. In fact, several reports have indicated a significant lower BBB permeability to M6G by systemic administration, in comparison to morphine (Bickel et al., 1996; Wu et al., 1997). Therefore, a peptide vector that would enhance the BBB permeability of M6G would most likely enhance its pharmacological activity.

Our study shows that SynB3 enhances significantly the brain uptake of M6G as measured by the *in situ* brain perfusion in mice. The mechanism whereby vectorised M6G crosses the BBB is not yet clear but could involve adsorptive-mediated endocytosis, a mechanism previously proposed for doxorubicin vectorised with SynB3 (Rousselle et al., 2001). The SynB3 vector used in this study is positively charged (five arginines) and this net positive charge is likely to play a major role in electrostatic interactions between the peptide vector and the negative surface charges of the endothelial cells composing the BBB.

Vectorisation of M6G with the SynB3 vector resulted in a significant enhancement in the analgesic effect of M6G. We show by the tail flick assay in mice that the effect of Syn1001 is dose-dependent. We then compared the antinociceptive activity of M6G,

morphine and Syn1001 in various tests using the tail flick and hot plate tests. This comparison was useful because the rank order of potency of opioids may vary with the nature and/or the intensity of the nociceptive stimulus (Porreca et al., 1987; Millan, 1990, South and Smith, 1998). In fact, South and Smith (1998) have shown that systemic administration of M6G resulted in high levels of antinociception using the tail flick whereas no significant antinociception was detected using the hot plate test. In our study, Syn1001 was more potent than free M6G or morphine in the different tests used. The ratio of the antinociceptive ED50 of M6G over Syn1001 was approximately 4 on a molar basis. This indicates that vectorisation leads not only to improvement of brain uptake but also to an enhancement in the antinociceptive activity of M6G. This enhancement was due to the vectorisation of M6G since free peptide (SynB3) had no antinociceptive effect and no affinity for the opioid receptors. The enhanced analgesic activity of Syn1001 over M6G can also be obtained in another animal nociceptive pain model: the formalin pain model. At all doses studied, administration of Syn1001 decreased the licking time both in the acute and in the chronic phases. A significant difference was observed in the chronic phase compared to M6G and morphine. The almost total abolition of a chronic phase response with Syn1001 supports the conclusion that vectorisation of M6G leads to a significant enhancement of its antinociceptive effect.

The mechanism of action of Syn1001 was further explored by receptor binding studies both *in vitro* and *in vivo*. Using a radioligand-binding assay, Syn1001 was demonstrated to bind with higher affinity than M6G to the *mu* receptor *in vitro*. Surprisingly, it was noted that in the presence of the SynB3 vector, M6G exhibited a high affinity for the *kappa* receptor that it is not shown by free M6G or SynB3 vector. *In vivo*, the analgesic effect of Syn1001 was reversed easily by naloxone and β-funaltrexamine, confirming the opioid nature of the antinociception. Since no inhibition was obtained with the *kappa* antagonist Nor-BNI, it was

clear that the *mu* opioid receptor was mediating the analgesic effect of Syn1001. Interestingly, the analgesic effect was also antagonized by 3-methoxynaltrexone. This antagonist has been described to antagonize the action of M6G and heroin at a dose, which is inactive against morphine (Brown et al., 1997). These observations led to the hypothesis of the presence of a novel receptor, which is responsible for M6G and heroin analgesia (Brown et al., 1997). Since this antagonist also acts on the action of Syn1001, this points towards the action of Syn1001 being mediated by the same receptors as M6G and heroin.

The fact that vectorised M6G binds to the *mu* receptor *in vitro* indicates that free M6G does not need to be cleaved from the vector in order to have a pharmacological effect. M6G was conjugated to the SynB3 vector via a linker containing a disulfide bond. The disulfide-based linker system has been shown to be stable in plasma for several hours though labile in brain (Letvin et al., 1986). It is not clear yet in which form Syn1001 binds to its opioid receptors *in vivo*. Further studies are needed to assess the mechanism and rate of cleavage of vectorised M6G within the brain.

As demonstrated in this study and by others, M6G has been shown to have a slightly longer antinociceptive effect compared to morphine (150 min and 90 min, respectively) (Paul et al., 1989; Frances et al., 1990). This longer action is probably the result of a slower rate of elimination of M6G from the brain and its entrapment in the extracellular fluid (Frances et al., 1992; Van Crugten et al., 1997; Stain-Texier et al., 1999). The fact that Syn1001 induces a longer duration of action could be due to the enhancement of the bioavailability of the vectorised M6G in the extracellular fluid, thereby increasing its availability to bind to the *mu* receptors. Further investigations are needed to measure the concentrations of Syn1001 and M6G within the brain.

Respiratory depression is one of the most disturbing side effects associated with opioid drugs. Case reports have implicated M6G in respiratory depression (Osborne et al., 1986) and have reported on the respiratory depressant properties of M6G after cerebroventricular administration to dogs (Pelligrino et al. 1989) and rats (Gong et al., 1991). In one study in humans, M6G was shown to produce fewer respiratory effects than morphine (Peat et al., 1991; Thompson et al., 1995). However, this study was not compatible with the other observations where respiratory depression was observed after intrathecal administration of M6G in human subjects (Grace and Fee, 1996). In the present study, rats that received a high dose of M6G exhibited a significant increase in the pCO_2. Respiratory depression occurred at 30-60 min post-administration. On the other hand, no significant effect on respiratory depression was seen after Syn1001 administration. The difference in the respiratory effect between M6G and Syn1001 is not clear yet but a likely explanation may be the combined affinity of Syn1001 at the *mu* and *kappa* receptors. Several lines of evidence support this hypothesis. First, the respiratory depression effect has been shown to be associated with *mu* receptors, and that the predictability of the degree of respiratory depression of an opioid appears to decrease with its selectivity for *mu* opioid receptors (Stott and Pleuvry, 1991). Secondly, activation of *mu* and *kappa* opioid receptors leads to functionally opposite effects. Verborgh *et al.*, (1997) have shown that combination of *mu* and *kappa* receptor agonists can be additive with respect to antinociception with additionally less risk for respiratory side effects. It will be interesting to see whether the *kappa* binding seen with Syn1001 is agonist or antagonist and to measure the effect of respiratory depression in the presence of *kappa* antagonists.

In conclusion, our results show that vectorisation of M6G enhances its brain delivery. This enhancement in brain uptake results in a significant improvement in the analgesic activity of M6G and reduces respiratory depression. This study supports the usefulness of

peptide-mediated strategies for improving the efficacy and safety of M6G for the treatment of pain.

REFERENCES

Abbott FV and Palmour, RM (1988) Morphine-6-glucuronide: analgesic effects and receptor binding profile in rats. *Life Sci.* **43**:1685-1695 .

Abbott NJ and Romero IS (1996) Transporting therapeutics across the blood-brain barrier. *Mol. Med. Today.* **2**:106-113.

Atherton E and Sheppard RC (1989) Solid Phase Peptide Synthesis: A practical Approach. IRL Press at Oxford University Press, Oxford, England.

Bickel U, Schumacher OP, Kang YS and Voigt K (1996) Poor permeability of morphine 3-glucuronide and morphine 6-glucuronide through the blood-brain barrier in the rat. *J Pharmacol Exp Ther.* **278**:107-113.

Bourasset F, Cisternino S, Temsamani J and Scherrmann JM (2003) Evidence for an active transport of morphine-6-beta-d-glucuronide but not P-glycoprotein-mediated at the blood-brain barrier. *J Neurochem.* **86**:1564-1567.

Brady LS and Holtzman SG (1982) Analgesic effects of intraventricular morphine and enkephalins in nondependent and morphine-dependent rats. *J Pharmacol Exp Ther.* **222**:190-197.

Brown GP, Yang K, King MA, Rossi GC, Leventhal L, Chang A and Pasternak GW (1997) 3-Methoxynaltrexone, a selective heroin/morphine-6beta-glucuronide antagonist. *FEBS Lett.* **412**:35-38.

Cotton R, Kosterlitz HW, Paterson SJ, Rance MJ and Traynor JR. (1985) The use of [3H]-[D-Pen2,D-Pen5]enkephalin as a highly selective ligand for the delta-binding site. *Br J Pharmacol.* **84**:927-932.

D'Amour FE and Smith DL (1984) method for determining loss of pain sensation. *J Pharmacol Exp Ther.* **72**:74-79.

Dagenais C, Rousselle C, Pollack GM and Scherrmann JM (2000) Development of an in situ mouse brain perfusion model and its application to mdr1a P-glycoprotein-deficient mice. *J Cereb Blood Flow Metab.* **20**:381-386.

Dunn BN and Pennington MW. Eds. (1994) Methods in molecular biology Vol **36**. Peptide analysis protocols.

Frances B, Gout R, Campistron G, Panconi E and Cros J (1990) Morphine-6-glucuronide is more mu-selective and potent in analgesic tests than morphine. *Prog Clin Biol Res.* **328**:477-480.

Frances B, Gout R, Monsarrat B, Cros J and Zajac JM (1992) Further evidence that morphine-6 beta-glucuronide is a more potent opioid agonist than morphine. *J Pharmacol Exp Ther.* **262**:25-31.

Gong QL, Hedner T, Hedner J, Bjorkman R and Nordberg G (1991) Antinociceptive and ventilatory effects of the morphine metabolites: morphine-6-glucuronide and morphine-3-glucuronide. *Eur J Pharmacol.* **193**:47-56.

Grace D and Fee JP (1996) A comparison of intrathecal morphine-6-glucuronide and intrathecal morphine sulfate as analgesics for total hip replacement. *Anesth Analg.* **83**:1055-1059.

Hanna MH, Peat SJ, Woodham M, Knibb A, Fung C. (1990) Analgesic efficacy and CSF pharmacokinetics of intrathecal morphine-6-glucuronide: comparison with morphine. Br J Anaesth. **64**:547-50.

Kinouchi K and Pasternak GW (1991) Evidence for kappa 1 opioid receptor multiplicity in the guinea pig cerebellum. *Eur J Pharmacol.* **207**:135-141.

Letvin NL, Goldmacher VS, Ritz J, Yetz JM, Schlossman, SF and Lambert JM (1986) In vivo administration of lymphocyte-specific monoclonal antibodies in nonhuman primates. In vivo stability of disulfide-linked immunotoxin conjugates. *J Clin Invest.* **77**:977-984.

Ling GS and Pasternak GW (1983) Spinal and supraspinal opioid analgesia in the mouse: the role of subpopulations of opioid binding sites. *Brain Res.* **271**:152-156.

Ling GS, Paul D, Simantov R and Pasternak GW (1989) Differential development of acute tolerance to analgesia, respiratory depression, gastrointestinal transit and hormone release in a morphine infusion model. *Life Sci.* **45**:1627-1636 .

Lotsch J, Kobal G, Stockmann A, Brune K, Geisslinger G. (1997) Lack of analgesic activity of morphine-6-glucuronide after short-term intravenous administration in healthy volunteers. Anesthesiology. **87**:1348-58.

Millan MJ (1990) Kappa-opioid receptors and analgesia. *Trends Pharmacol Sci.* **11** : 70-76.

Motamed C, Mazoit X, Ghanouchi K, Guirimand F, Abhay K, Lieutaud T, Bensaid S, Fernandez C, Duvaldestin P. (2000) Preemptive intravenous morphine-6-glucuronide is ineffective for postoperative pain relief. *Anesthesiology.* **92**:355-60.

Osborne RJ, Joel SP and Slevin ML (1986) Morphine intoxication in renal failure: the role of morphine-6-glucuronide. *Br Med J.* **292**:1548-1549.

Pardridge WM (1998) CNS drug design based on principles of blood-brain barrier transport. *J Neurochem.* **70**:1781-1792.

Paul D, Standifer KM, Inturrisi CE and Pasternak GW (1989) Pharmacological characterization of morphine-6 beta-glucuronide, a very potent morphine metabolite. *J Pharmacol Exp Ther.* **251**:477-483.

Paul D, Pick CG, Tive LA, Pasternak GW. (1991) Pharmacological characterization of nalorphine, a kappa 3 analgesic. *J Pharmacol Exp Ther.* **257**:1-7.

Peat SJ, Hanna MH, Woodham M, Knibb AA and Ponte J (1991) Morphine-6-glucuronide: effects on ventilation in normal volunteers. *Pain.* **45**:101-104.

Pelligrino DA, Peterson RD, Henderson, SK and Albrecht RF (1989) Comparative ventilatory effects of intravenous versus fourth cerebroventricular infusions of morphine sulfate in the unanesthetized dog. *Anesthesiology.* **71**:250-259.

Penson RT, Joel SP, Bakhshi K, Clark SJ, Langford RM, Slevin ML. (2000) Randomized placebo-controlled trial of the activity of the morphine glucuronides. Clin Pharmacol Ther. 68:667-76.

Pick CG, Paul D, Pasternak GW. Comparison of naloxonazine and beta-funaltrexamine antagonism of mu 1 and mu 2 opioid actions (1991) *Life Sci.* **48**:2005-2011.

Porreca F, Heyman JS, Mosberg HI, Omnaas JR and Vaught JL (1987) Role of mu and delta receptors in the supraspinal and spinal analgesic effects of [D-Pen2, D-Pen5]enkephalin in the mouse. *J Pharmacol Exp Ther.* **241**:393-400.

Rousselle C, Clair P, Lefauconnier JM, Kaczorek M, Scherrmann JM and Temsamani J (2000) New advances in the transport of doxorubicin through the blood-brain barrier by a peptide vector-mediated strategy. *Mol Pharmacol.* **157**:679-686.

Rousselle C, Smirnova M, Clair P, Lefauconnier JM, Chavanieu A, Calas B, Scherrmann, JM and Temsamani J (2001) Enhanced delivery of doxorubicin into the brain via a peptide-vector-mediated strategy: saturation kinetics and specificity. *J Pharmacol Exp Ther.* **296**:124-131.

Rousselle C, Clair P, Temsamani J and Scherrmann JM (2002) Improved brain delivery of benzylpenicillin with a peptide-vector-mediated strategy. *J Drug Target.* **10** :309-315.

Rousselle C, Clair P, Smirnova M, Kolesnikov Y, Pasternak GW, Gac-Breton S, Rees AR, Scherrmann JM and Temsamani J (2003) Improved brain uptake and pharmacological activity of dalargin using a peptide-vector-mediated strategy. *J Pharmacol Exp Ther.* **306**:371-376.

Smith QR (1996) Brain perfusion systems for studies of drug uptake and metabolism in the central nervous system. *Pharm.Biotechnol.* **8**:285-307.

South SM, Smith MT. (1998) Apparent insensitivity of the hotplate latency test for detection of antinociception following intraperitoneal, intravenous or intracerebroventricular M6G administration to rats. *J Pharmacol Exp Ther.* **286**:1326-1332.

Stain-Texier F, Boschi G, Sandouk P and Scherrmann, JM (1999) Elevated concentrations of morphine 6-beta-D-glucuronide in brain extracellular fluid despite low blood-brain barrier permeability. *Br J Pharmacol.* **128**:917-924.

Stott DG and Pleuvry BJ (1991) Relationship between analgesia and respiratory depression for mu opioid receptor agonists in mice. *Br J Anaesth.* **67**:603-607.

Temsamani J, Rousselle C, Rees AR and Scherrmann JM (2001) Vector-mediated drug delivery to the brain. *Expert Opin Biol Ther.* **1**:773-782.

Thompson PI, Joel SP, John L, Wedzicha JA, Maclean M, Slevin ML (1995) Respiratory depression following morphine and morphine-6-glucuronide in normal subjects. *Br J Clin Pharmacol.* **40**:145-52 .

Van Crugten JT, Somogyi AA, Nation RL, Reynolds G (1997) Concentration-effect relationships of morphine and morphine-6 beta-glucuronide in the rat. *Clin Exp Pharmacol Physiol.* **24** :359-364.

Verborgh CM, Camu F and Meert TF (1997) Interaction between sufentanil and U-50488H with respect to antinociception and respiratory depression in rats. *Acta Anaesthesiol Scand.* **41**:895-902 .

Wu D, Kang YS, Bickel U and Pardridge WM (1997) Blood-brain barrier permeability to morphine-6-glucuronide is markedly reduced compared with morphine. *Drug Metab Dispos.* **25**:768-771.

Yoburn BC, Lutfy K and Candido J (1991) Species differences in mu- and delta-opioid receptors. *Eur J Pharmacol.* **193**:105-108.

FIGURES LEGEND

Figure 1: **A**: Antinociceptive activity of subcutaneous Syn1001 in the tail flick in mice (n=8 per group) at different doses (1.06; 2.1; 3.2 and 4.24 μmol/kg). The antinociceptive effect was measured at 30, 60, 180 and 300 min post-administration and is expressed as a percentage of the maximum possible effect (% MPE) *versus* time.

B and **C**: Dose-dependent antinociceptive activity of subcutaneous Syn1001 and M6G in the tail flick in mice. The effect was measured at 60 min. Values are means ± sem

Figure 2: Antinociceptive activity of subcutaneous M6G and Syn1001 in the tail flick in mice at a dose of 3.2 μmol/kg) (n=10 per group). The antinociceptive effect was measured at 30, 60, 120 and 240 min post-administration and was expressed as a percentage of the maximum possible effect (% MPE) *versus* time. Values are means ± sem . The effect seen with Syn1001 was significantly different from the response observed with M6 (* $P< 0.05$; ** $P<0.01$).

Figure 3: Antinociceptive activity of intravenous Syn1001, M6G and morphine in the hot plate in mice (n=15 per group) at a dose of 2.6 μmol/kg for morphine and 2.2 μmol/kg for M6G and Syn1001. The antinociceptive effect was measured at 5, 10, 15, 30, 45, 90, 120 and 180 min post-administration and was expressed as a percentage of the maximum possible effect (% MPE) *versus* time. Values are means ± sem. The effect seen with Syn1001 was significantly different from the response observed with M6 (* $P<0.01$).

Figure 4: Antagonism of Syn1001 analgesia. Mice (10 per group) were injected subcutaneously with Syn1001 (2.8 μmol/kg in panel A and 4.2 μmol/kg in panel B). The

different antagonists were administered to mice subcutaneously before administration of Syn1001 as described in Methods. The antinociceptive effect was measured using the tail flick assay and was expressed as a percentage of the maximum possible effect (% MPE) *versus* time. Values are means ± sem. *P<0.01.

Figure 5: Formalin test. Comparison of paw-licking time in acute and chronic phase after subcutaneous administration of either the vehicle or the test compounds at 10.9 μmol/kg to mice (n=15 per group). Values are means ± sem. *P<0.05, ****P<0.001.

Figure 6: Effect of Syn1001, M6G and morphine on arterial blood gases (**A**: pCO_2; **B**: pO_2) and pH (**C**). Femoral arterial lines were placed and arterial blood gases were taken 30, 60 and 90 min after sc administration of the compounds to rats at a dose of 43 μmol/kg for M6G and Syn1001 and 65 μmol/kg for morphine.

Figure 1A

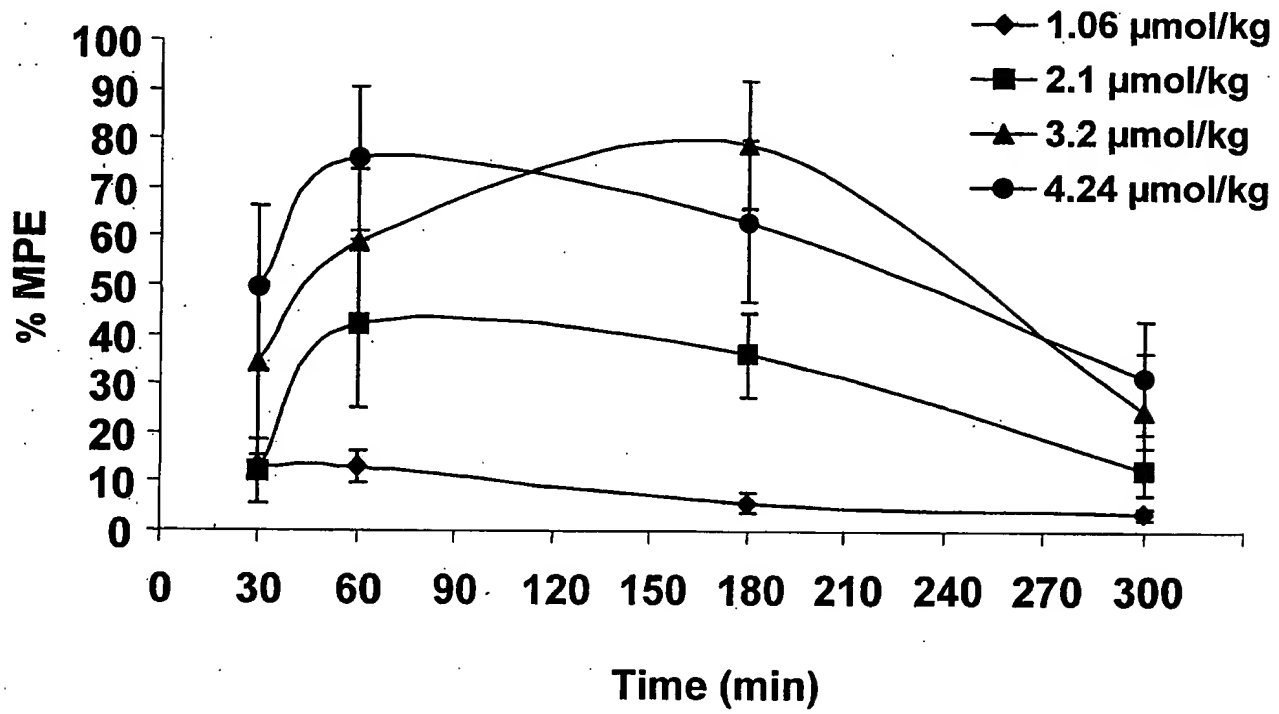
1.06 µmol/kg
2.1 µmol/kg
3.2 µmol/kg
4.24 µmol/kg
% MPE
100
90
80
70
60
50
40
30
20
10
0
0
30
60
90
120
150
180
210
240
270
300
Time (min)

Figure 1 B & C

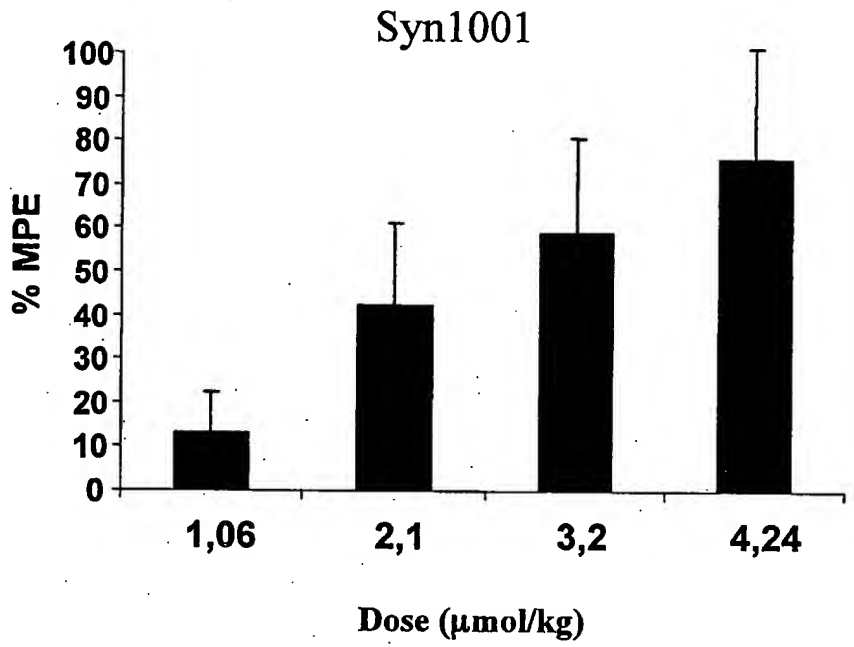
Syn1001
% MPE
100
90
80
70
60
50
40
30
20
10
0
1,06
2,1
3,2
4,24
Dose (µmol/kg)

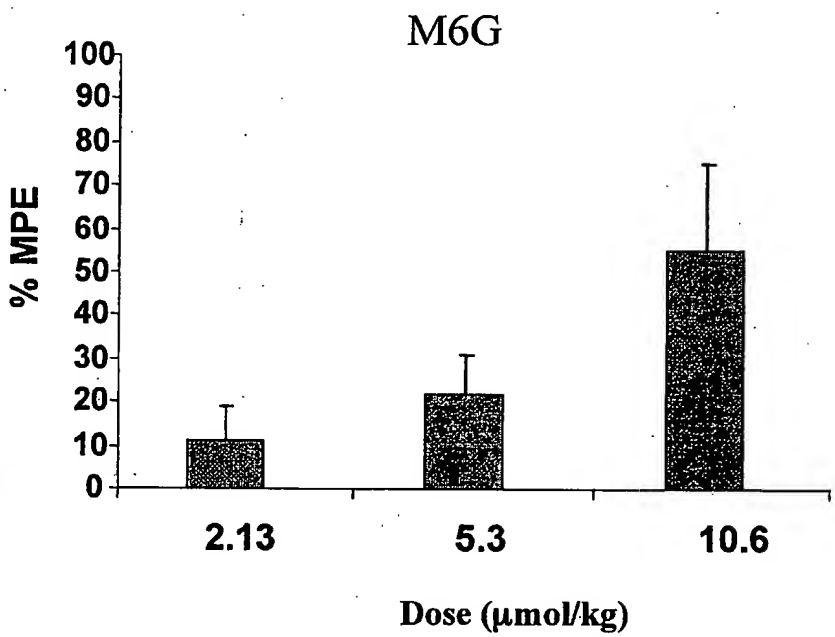
M6G
% MPE
100
90
80
70
60
50
40
30
20
10
0
2.13
5.3
10.6
Dose (µmol/kg)

Figure 2

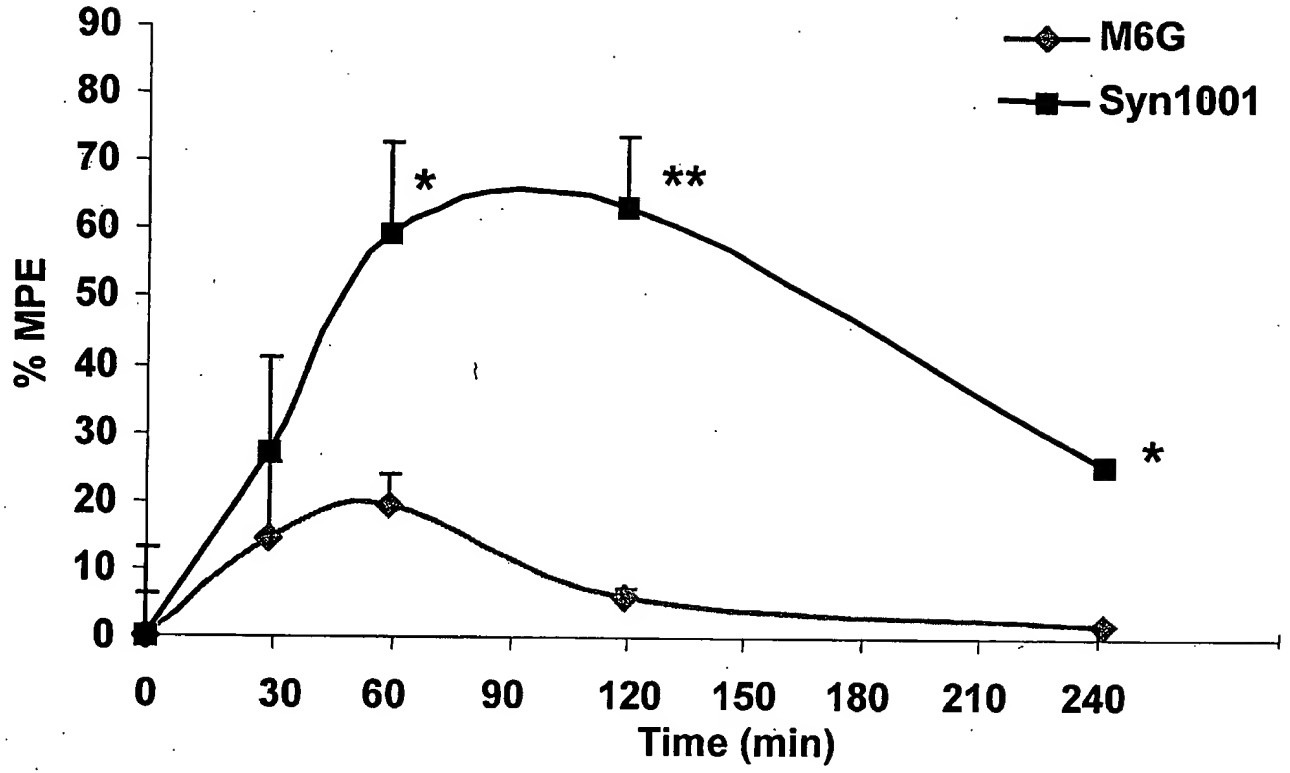
90
80
70
60
50
40
30
20
10
0
% MPE
M6G
Syn1001
*
**
*
0
30
60
90
120
150
180
210
240
Time (min)

Figure 3

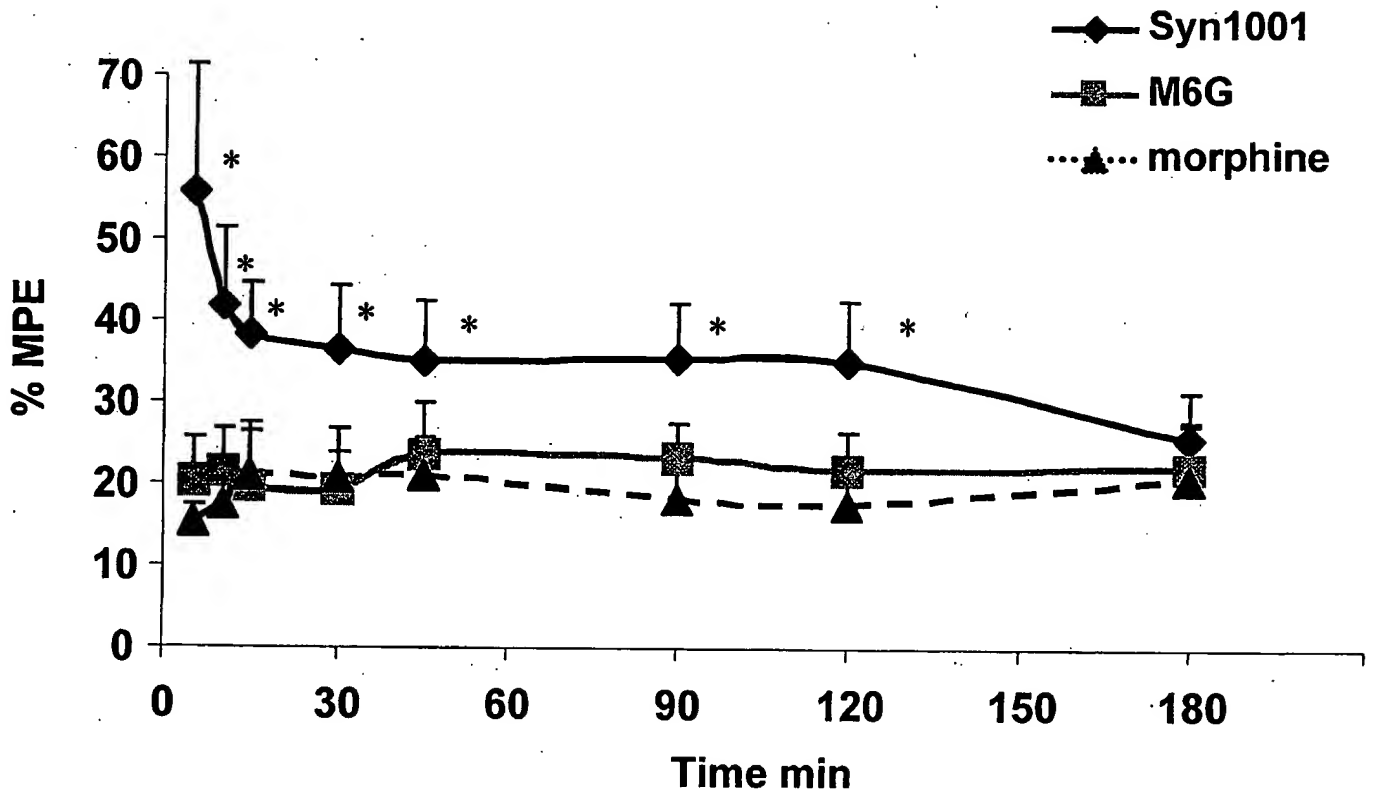
Syn1001
M6G
morphine
% MPE
70
60
50
40
30
20
10
0
0
30
60
90
120
150
180
Time min
*
*
*
*
*
*
*

Figure 4

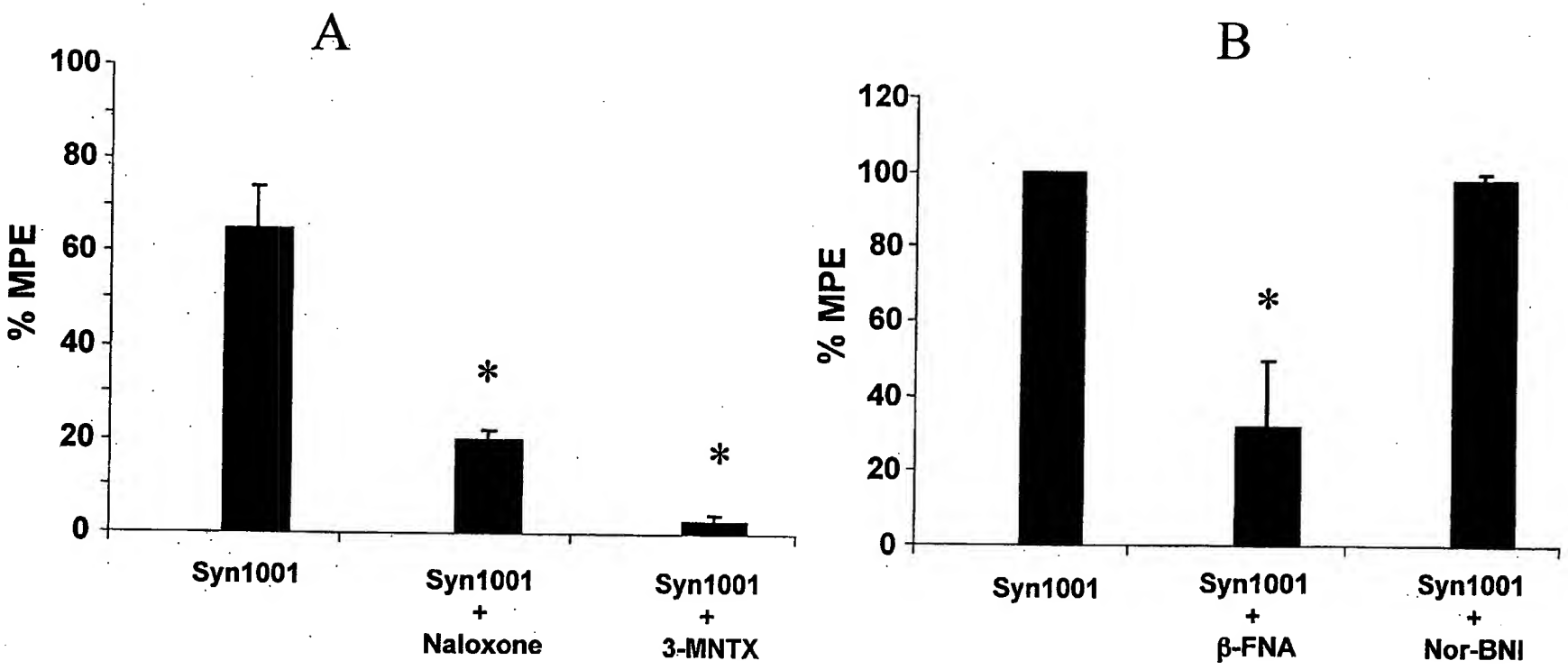
A
100
80
60
40
20
0
% MPE
*
*
Syn1001
Syn1001 + Naloxone
Syn1001 + 3-MNTX
B
120
100
80
60
40
20
0
% MPE
*
Syn1001
Syn1001 + β-FNA
Syn1001 + Nor-BNI

Figure 6A

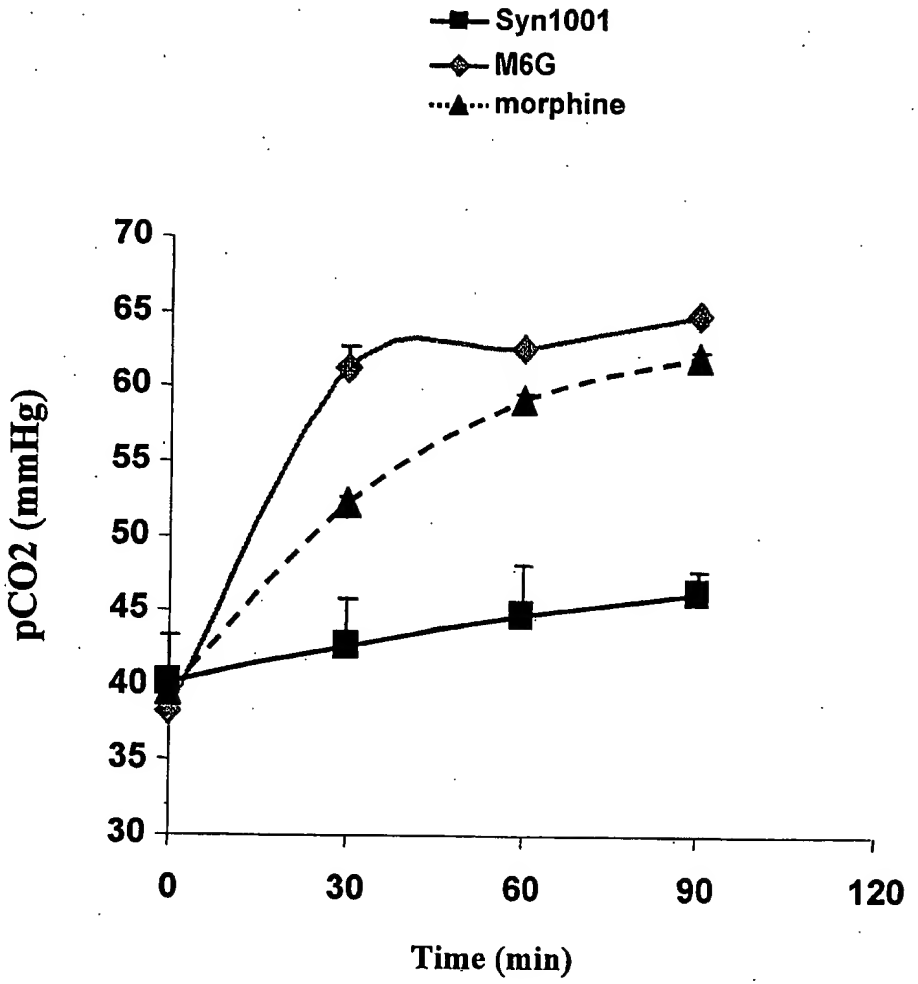
Syn1001
M6G
morphine
70
65
60
55
50
45
40
35
30
pCO2 (mmHg)
0
30
60
90
120
Time (min)

Figure 6B

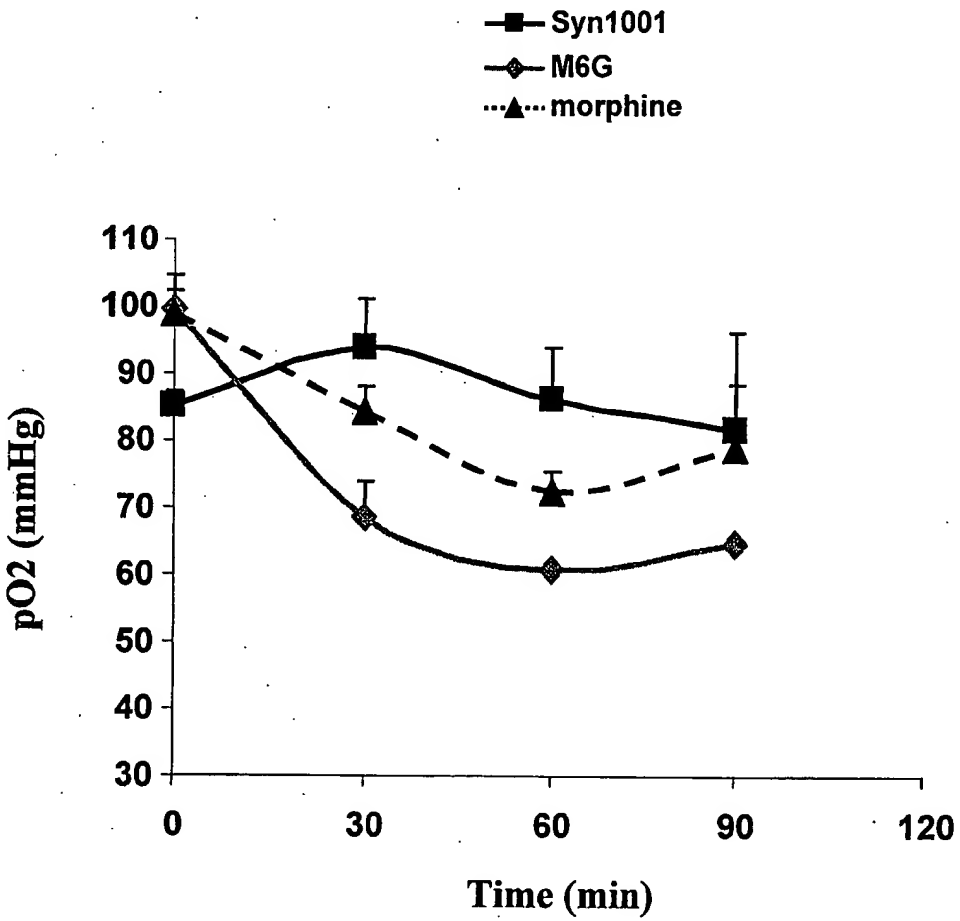
Syn1001
M6G
morphine
110
100
90
80
70
60
50
40
30
pO2 (mmHg)
0
30
60
90
120
Time (min)

Figure 6C